

A Thesis Submitted for the Degree of PhD at the University of Warwick

Permanent WRAP URL:

<http://wrap.warwick.ac.uk/173485>

Copyright and reuse:

This thesis is made available online and is protected by original copyright.

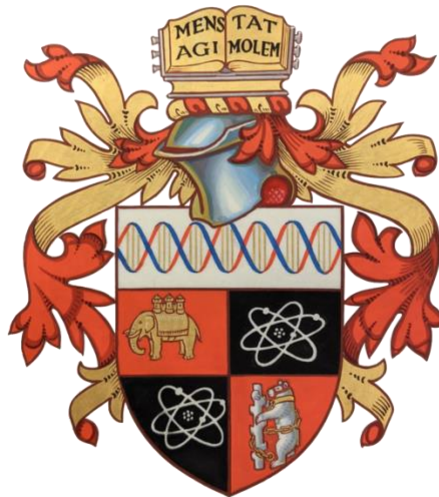
Please scroll down to view the document itself.

Please refer to the repository record for this item for information to help you to cite it.

Our policy information is available from the repository home page.

For more information, please contact the WRAP Team at: wrap@warwick.ac.uk

**A Novel Hyaluronic Acid Hydrogel as an Extracellular
Matrix to Improve Graft Survival in Autologous Adipose
Tissue Transfer**



Janak Ashwin Bechar
MB ChB BMedSc(Hons) MRCS

A thesis submitted for the degree of
Doctor of Philosophy in Medicine
To be awarded by Warwick Medical School, University of Warwick

Supervisors: Professor Joseph Hardwicke, Dr Claire Bastie and
Professor Shervanthi Homer-Vanniasinkam

June 2022

Table of Contents

TABLE OF CONTENTS	2
ACKNOWLEDGEMENTS	6
DECLARATION	9
ABSTRACT	10
LIST OF ABBREVIATIONS	11
LIST OF FIGURES	14
LIST OF TABLES	18
LIST OF EQUATIONS	18
CHAPTER ONE: GENERAL INTRODUCTION	19
1.1 INTRODUCTION	20
1.2 ADIPOSE TISSUE	21
1.2.1 <i>Adipose tissue types: white versus brown</i>	22
1.2.2 <i>Other adipose tissue types</i>	26
1.2.3 <i>Adipose tissue distribution</i>	26
1.2.4 <i>Adipose tissue hormones, adipokines, cytokines and chemokines</i>	28
1.2.5 <i>Adipose tissue origin and lineage differentiation</i>	31
1.2.5.1 Transcriptional regulation of adipocyte differentiation	32
1.2.5.2 Signal transduction and hormonal regulation of adipogenesis	39
1.2.6 <i>Adipose tissue growth</i>	40
1.3 ADIPOSE TISSUE TRANSFER OVERVIEW	41
1.3.1 <i>Adipose tissue transfer procedure overview</i>	42
1.3.2 <i>Adipose tissue harvest</i>	43
1.3.3 <i>Adipose tissue processing</i>	45
1.3.4 <i>Adipose tissue injection</i>	47
1.4 TISSUE ENGINEERING IN RECONSTRUCTIVE SURGERY	47
1.4.1 <i>The extracellular environment</i>	48
1.4.2 <i>Function of the extracellular environment</i>	49
1.4.3 <i>Hyaluronic acid (HA)</i>	50
1.4.4 <i>Hyaluronic acid hydrogels</i>	51
1.4.5 <i>Selection of hyaluronic acid as a matrix in adipose tissue transfer</i>	51
1.5 AIMS OF THE STUDY	56
1.5.1 <i>Synthesis and modification of hyaluronic acid</i>	57
1.5.2 <i>Characterisation of hyaluronic acid gel toxicity in vitro</i>	57
1.5.3 <i>Characterisation of hyaluronic acid gel toxicity in vivo</i>	58
CHAPTER TWO: GENERAL MATERIALS AND METHODS	59
2.1 CHEMICALS AND REAGENTS	60
2.1.1 <i>Cell line chemicals</i>	60
2.1.2 <i>Media formulations</i>	60
2.1.2.1 General media for MCF-7, 3T3-L1 and primary human pre-adipocytes	60
2.1.2.2 Induction media for 3T3-L1 and primary human pre-adipocytes	61
2.1.2.3 Maintenance media for 3T3-L1 and primary human pre-adipocytes	61
2.1.3 <i>Chemicals for hyaluronic acid functionalisation</i>	61
2.1.4 <i>Cell lines</i>	61
2.1.5 <i>Gene expression analyses</i>	62
2.1.5.1 Human and mouse gene expression assays	62
2.1.5.2 Quantitative polymerase chain reaction (qPCR), isolation kits and other reagents	63
2.1.6 <i>Miscellaneous</i>	63
2.2 EQUIPMENT	64

2.2.1	<i>Nuclear Magnetic Resonance (NMR) spectroscopy for hyaluronic acid functionalisation characterisation</i>	64
2.2.2	<i>Rheometer for hyaluronic acid hydrogel characterisation</i>	65
2.2.3	<i>Equipment for cell culture</i>	65
2.2.4	<i>Microscopy and imaging</i>	65
2.2.5	<i>Image analysis program</i>	65
2.2.6	<i>Miscellaneous equipment</i>	65
2.3	METHODS	66
2.3.1	<i>Functionalisation of hyaluronic acid</i>	66
2.3.1.1	Hyaluronic acid functionalised with hydrazine groups	66
2.3.1.2	Hyaluronic acid functionalised with aldehyde groups	66
2.3.2	<i>Hydrogel concentrations</i>	67
2.3.3	<i>NMR spectroscopy protocols and yield calculations</i>	67
2.3.4	<i>Rheology</i>	68
2.3.5	<i>Gel characterisation</i>	70
2.3.5.1	Gel fraction	70
2.3.5.2	Gel equilibrium water content	70
2.3.5.3	Gel swelling and degradation	71
2.3.5.4	Gel healing	71
2.3.6	<i>Mammalian cell culture</i>	73
2.3.6.1	MCF-7.....	73
2.3.6.1.1	MCF-7 retrieval	73
2.3.6.1.2	MCF-7 subculture	73
2.3.6.1.3	MCF-7 cryopreservation	74
2.3.6.2	3T3-L1 cells	74
2.3.6.2.1	Retrieval and subculture	75
2.3.6.2.2	Induction	75
2.3.6.2.3	Maintenance	76
2.3.6.3	Construction of <i>Per2-dLuc</i> expressing 3T3-L1 cells	76
2.3.6.4	Primary murine pre-adipocytes from FVB-Tg (CAG-luc-eGFP) mice.....	78
2.3.6.4.1	Adipose tissue harvest, processing, and primary cell isolation.....	79
2.3.6.4.2	Subculture, induction, and maintenance	82
2.3.6.5	Primary human pre-adipocytes.....	83
2.3.6.5.1	Liposuction, processing, and primary cell isolation.....	83
2.3.6.5.2	Primary cell isolation, subculture, induction, and maintenance	84
2.3.7	<i>Oil Red O staining</i>	87
2.3.8	<i>Per2-dLuc 3T3-L1 and CAG-luc-eGFP primary mouse pre-adipocyte imaging</i>	87
2.3.9	<i>FIJI programme image analysis</i>	88
2.3.10	<i>qPCR analyses</i>	88
2.3.10.1	RNA isolation.....	89
2.3.10.2	Reverse transcription.....	89
2.3.10.3	Polymerase chain reaction	90
2.3.11	<i>Murine in vivo experiments</i>	92
2.3.12	<i>Statistical analysis</i>	92

CHAPTER THREE: SYNTHESIS AND MECHANICAL PROPERTIES OF THE NOVEL HYALURONIC ACID HYDROGEL.....94

3.1	INTRODUCTION AND SELECTION OF HYALURONIC ACID FOR MODIFICATION.....	95
3.1.1	<i>Chapter aims</i>	96
3.2	HYALURONIC ACID SYNTHESIS WITH HYDRAZINE AND ALDEHYDE GROUPS	97
3.2.1	<i>Nuclear magnetic resonance (NMR) spectroscopy yields of synthesized products</i> 99	
3.3	CHARACTERISATION OF GEL WITH RHEOLOGY AND TERMINOLOGY	101
3.3.1	<i>Rheology methods</i>	105
3.3.2	<i>Rheology results</i>	108
3.4	CHARACTERISATION OF GEL PROPERTIES.....	121
3.4.1	<i>Gel fraction</i>	121
3.4.2	<i>Gel equilibrium water content</i>	122

3.4.3	<i>Gel swelling and degradation</i>	122
3.4.4	<i>Gel healing</i>	130
3.5	CONCLUSION.....	132
CHAPTER FOUR: <i>IN VITRO</i> EFFECTS OF HA HYDROGEL ON 3T3-L1, PRIMARY MURINE AND PRIMARY HUMAN ADIPOCYTES		133
4.1	INTRODUCTION	134
4.2	CHAPTER AIMS AND SELECTION OF CELL TYPES FOR EXPERIMENTATION	135
4.3	SELECTION OF GEL FOR <i>IN VITRO</i> CHARACTERISATION	137
4.4	EFFECTS OF 6% HA HYDROGEL ON MCF-7 CELL MORPHOLOGY	138
4.5	EFFECTS OF HA HYDROGEL ON <i>PER2-DLUC</i> 3T3-L1 ADIPOCYTES: PROLIFERATION AND DIFFERENTIATION.....	141
4.5.1	<i>Cell line characterisation and optimisation of data analyses</i>	141
4.5.1.1	Characterisation of <i>Per2-dLuc</i> 3T3-L1 cells	142
4.5.1.2	Analysis using a novel automated macro	144
4.5.2	<i>Results and discussion</i>	147
4.5.2.1	Layering HA hydrogel with <i>Per2-dLuc</i> 3T3-L1 adipocytes: cellular viability and differentiation	147
4.5.2.1.1	Cellular viability assessed using photon emission in <i>Per2-dLuc</i> 3T3-L1 cells grown on top of HA hydrogel.....	149
4.5.2.1.2	Cellular viability assessed using photon emission and characterisation of mature adipocyte gene markers of <i>Per2-dLuc</i> 3T3-L1 cells grown under a layer of HA hydrogel.....	153
4.6	PRIMARY CAG-LUC-EGFP MURINE ADIPOCYTE VIABILITY USING PHOTON EMISSION AND CHARACTERISATION OF MATURE ADIPOCYTE GENE MARKERS IN CELLS GROWN ON HA HYDROGEL AND CELLS ENCAPSULATED WITHIN HA HYDROGEL	160
4.7	MATURE ADIPOCYTE GENE MARKER CHARACTERISATION OF PRIMARY HUMAN ADIPOCYTES GROWN UNDER A LAYER OF HA HYDROGEL	167
4.8	CONCLUSION.....	169
CHAPTER FIVE: <i>IN VIVO</i> EFFECTS OF HA HYDROGEL ON INJECTED ADIPOCYTES IN A MURINE MODEL		171
5.1	INTRODUCTION	172
5.1.1	<i>Selection of the in vivo model</i>	172
5.2	CHAPTER AIMS	173
5.3	PILOT MURINE STUDY: DESIGN OPTIMISATION	174
5.3.1	<i>Methods</i>	174
5.3.1.1	Whole body luciferase expressing (CAG-luc-eGFP) mice.....	174
5.3.1.2	Experimental design	174
5.3.1.3	Data acquisition and processing.....	177
5.3.2	<i>Pilot results, discussion and improvements to design</i>	179
5.4	MAIN MURINE STUDY	183
5.4.1	<i>Methods</i>	183
5.4.2	<i>Results and discussion</i>	186
5.4.2.1	Cellular viability of injected CAG-luc-eGFP murine adipose tissue with gel <i>in vivo</i>	186
5.4.2.2	Gene expression of injected CAG-luc-eGFP murine adipose tissue with gel <i>in vivo</i>	189
5.5	CONCLUSION.....	191
CHAPTER SIX: GENERAL DISCUSSION		192
6.1	INTRODUCTION	193
6.2	MECHANICAL CHARACTERISTICS: GENERAL COMMENTS	194
6.2.1	<i>Synthesis of HA hydrogel modified with aldehyde and hydrazine groups</i>	194
6.2.2	<i>Characterisation of gel with rheology</i>	194
6.2.3	<i>HA hydrogel swelling, degradation, and healing</i>	197
6.3	HA HYDROGEL <i>IN VITRO</i> : GENERAL COMMENTS.....	200
6.3.1	<i>Analysis of images taken using a novel automated macro</i>	200
6.3.2	<i>Per2-dLuc 3T3-L1 cell survival on and under HA hydrogel</i>	201

6.3.3	<i>CAG-luc-eGFP primary murine adipocyte viability on and encapsulated within HA hydrogel.....</i>	205
6.3.4	<i>Mature adipocyte gene expression of primary human cells under HA hydrogel..</i>	206
6.4	HA HYDROGEL <i>IN VIVO</i> : GENERAL COMMENTS.....	207
6.4.1	<i>Main murine study photon emission and cell survival</i>	207
6.4.2	<i>Gene expression of in vivo murine experiments.....</i>	209
6.5	FUTURE DIRECTIONS.....	210
	ANNEX A.....	212
	ANNEX B.....	213
	ANNEX C.....	215
	PUBLISHED WORKS	215
	BIBLIOGRAPHY	216

Acknowledgements

It is perhaps folly to suggest that a project like this is the sole effort of an individual, given the following acknowledgements of key individuals and organisations that have supported and shaped my research. I have been exceptionally privileged to have had the opportunity to be able to pursue a project that I have found intellectually stimulating and rewarding. I am also deeply grateful for the financial and emotional support that I have received throughout my academic career to date.

I would primarily like to thank my supervisors, Professor Joseph Hardwicke and Dr. Claire Bastie. I am grateful to have received a decade of mentoring and clinical pedagogy from Joe, who cultivated and nurtured my interest in plastic surgery and research as a young medical student to the present day. I would also like to convey my deep gratitude and appreciation for the laboratory supervision I received from Claire, who adopted me as a PhD student in the first year of my research, during a time of project turmoil. Claire's general counsel and tolerance of my ambitious project plans (often out of hours), is a testament to her enthusiasm and exceptional dedication to her students. A special thank you is also reserved for Dr. Robert Dallmann, who was a supervisor for this project in all but name. Robert's insight, direction and support was invaluable during the course of this project and I am deeply grateful for his time and guidance. My thanks also goes to Professor Shervanthi Homer-Vanniasinkam for her ongoing support.

I would also like to convey my profound gratitude to Professor Andrew Dove and his post-doctoral fellows Dr Maria Perez-Madrigal, Dr Chiara Arno and Dr Joshua Worch for their help with the hyaluronic acid synthesis and characterisation part of the project. Their steadfast vision and enthusiasm for the project and help in this specialist field was invaluable and very much appreciated.

Components of this project would not have been possible without the expert help and guidance of Clinical Sciences Research Laboratory members Professor Harpal Randeva, Dr Soofiyah Ayaani, Sean James and importantly, Vanlata Patel and Suresh Kumar. I thank them all.

A special thank you is also reserved for Dr Kiran Shabir and Dr Seley Gharanei for their role in qPCR analysis. Of particular note is Dr Erin Greaves' generosity, along with Dr Kavita Panir and Priya Dhami, without whom the *in vivo* part of this project would not have been achievable. Dr Laura Cooper, part of the CAMDU team, provided invaluable expertise with FIJI, for which I am deeply grateful.

I would also like to thank the plastic surgery consultants at University Hospitals Coventry and Warwickshire for their generosity and patience (in particular Ms Joanna Skillman and Ms Katy Wallis), and for their tireless tolerance of my pursuit in attaining suitable human adipose tissue samples.

I would also like to thank the Medical Life Sciences Research Fund, the Wellcome Trust and the National Health Service Research Development Fund for their financial support, without which this project would not have been possible. I look forward to the hopeful day in the future, when I am able to repay their financial generosity in funding young researchers at their time of need.

A special thank you is also reserved for the patients who kindly and charitably consented for a sample of their adipose tissue to be used in this project. Of specific poignance is my deep gratitude to the mice that sacrificed their lives for the benefit of my research, and in particular to Charlotte (a resident of cage one) whose attempts to bite me never quite reached fruition. And to Jamie and Gadsden, (residents of cage four) whose pleasant disposition in being handled was always appreciated.

Having had to pause my PhD for just under six months to return to clinical medicine to help with the pandemic effort, I would also like to thank COVID-19. During this dark time I found resilience, acceptance of events beyond my control, and a reminder of the value and sanctity of life.

Lasty and most importantly, I would like to thank my parents, whose past and present sacrifices in leaving South Africa to afford me better opportunities have, I hope, borne fruition. This thesis is dedicated to them.

Declaration

This thesis is submitted in partial requirement to the University of Warwick in support for the award of Doctor of Philosophy. Unless explicitly mentioned in the text, all composition was performed by the author and is the candidates own work. I hereby confirm that no material from this thesis has been previously published, nor has any material been submitted for a degree at another University.

Abstract

Introduction

Adipose tissue transfer is used for correcting breast defects after cancer surgery and reconstruction after trauma or congenital defects. Graft survival can be as poor as 15%. Modified hyaluronic acid (HA) hydrogels can be used to suspend adipocytes to aid survival. The study aims were to synthesise a HA hydrogel with robust mechanical properties to support injection, and to assess adipocyte viability with HA hydrogel *in vitro* and *in vivo*.

Methods

A HA hydrogel with cross-linked aldehyde and hydrazine groups allowing self-healing around cells was engineered, with rheology and degradation properties characterised. *Per2*-dLuc 3T3-L1 murine pre-adipocytes expressing luciferase, CAG-luc-eGFP murine and human adipocytes were grown under, on, and encapsulated within HA hydrogel, with cell survival and gene expression investigated. A murine animal model underwent subcutaneous injection of primary murine adipocytes mixed with HA hydrogel, with cell survival and gene expression of mature adipocyte markers investigated.

Results

HA hydrogel can be degraded by tissue hyaluronidases in 4-5 days. Self-healing occurred in 30 minutes and is robust enough to resist deformation forces.

Per2-dLuc 3T3-L1 and CAG-luc-eGFP murine adipocytes were encapsulated within HA hydrogel and showed a <15% reduction in photon emission compared to control. Mature adipocyte markers gene expression levels in HA hydrogel encapsulated murine and human cells were similar to those of control (no HA hydrogel) cells. Primary murine adipocytes injected subcutaneously with HA hydrogel in wild type mice showed no difference in survival at higher gel volumes compared to control. Gene expression markers of differentiation in injected primary adipocytes mixed with HA hydrogel showed no difference compared to control cells.

Conclusion

The novel engineered HA hydrogel has suitable mechanical characteristics for injection and can support adipocyte survival *in vitro* and *in vivo*. A human pilot trial may be the next step in development of the novel HA hydrogel.

List of Abbreviations

Abbreviation	Unabbreviated
ACBP	Acyl-coenzyme A-binding protein
ADD1	Adducin 1
ALD	Aldehyde
AMP	Adenosine monophosphate
aP2	Adipocyte-specific fatty acid binding protein
ATB	Arden Tissue Bank
ATCC	American Type Culture Collection
ATP	Adenosine triphosphate
BAT	Brown adipose tissue
<i>bmal1</i>	Brain and muscle Arnt like protein 1
BMP	Bone morphogenic protein
Bsd	Blasticidin
cAMP	Cyclic adenosine monophosphate
CAMDU	Computer-advanced microscopy development unit
CD	Cluster of differentiation
cDNA	Complimentary deoxyribonucleic acid
C/EBP α	CCAAT/enhancer binding protein alpha
<i>cry</i>	Cryptochrome
DEPC	Diethyl pyrocarbonate
Dex	Dexamethasone
DIEP	Deep inferior epigastric artery flap
DMEM	Dulbecco's modified eagle medium
DMSO	Dimethyl sulfoxide
DNA	Deoxyribonucleic acid
ECACC	European Collection of Cell Cultures
ECM	Extracellular matrix
EDC	<i>N</i> -(3-Dimethylaminopropyl)- <i>N'</i> -ethylcarbodiimide hydrochloride

EDTA	Ethylendiaminetetraacetic acid
EGFP	Enhanced green fluorescent protein
ER	Endoplasmic reticulum
EWC	Equilibrium water content
FABP4	Fatty acid binding protein 4
FBS	Foetal bovine serum
FCS	Foetal calf serum
FDA	Food and drug administration
FGF	Fibroblast growth factor
FIJI	FIJI is just Image J
GAPDH	Glyceraldehyde-3-phosphate dehydrogenase
GF	Gel fraction
GPR81	G Protein-coupled receptor 81
HA	Hyaluronic Acid
HABP	Hyaluronic acid binding protein
HOBT	Hydroxybenzotriazole
HYD	Hydrazine
IBMX	3-isobutyl-1-methylxantine
ICAM-1	Intercellular adhesion molecule 1
IL-6	Interleukin-6
LPL	Lipoprotein lipase
Luc	Luciferase
MAPK	Mitogen-activated protein kinase
MCP-1	Monocyte chemoattractant protein1
MES	2-(N-morpholino)ethanesulfonic acid
miRNA	Micro ribonucleic acid
MKK	Mitogen-activated protein (MAP) kinase kinase
MMP	Metalloproteinases
MT1	Membrane type 1

mRNA	Messenger ribonucleic acid
MSC	Mesenchymal stem cells
Myf5	Myogenic factor 5
MyoD	Myoblast determination protein 1
NMR	Nuclear magnetic resonance
ORO	Oil Red O
Osx	Osterix
PBS	Phosphate buffer saline
PCK1	Phosphoenolpyruvate carboxykinase 1
<i>per2</i>	Period 2
PKA	Protein kinase A
PPAR- γ	Peroxisome proliferation-activated receptor gamma
qPCR	Quantitative polymerase chain reaction
RHAMM	Receptor for HA-mediated motility
ROI	Region of interest
RPL7	Ribosomal protein L7
RT	Real time
Runx2	Runt-related transcription factor 2
SHN2	Schnurri 2
SMAD	Suppressor of mothers against decapentaplegic homolog
SRC3	Steroid receptor co-activator 3
SREBP1	Sterol regulatory element-binding protein 1
SVF	Stroma vascular fraction
TAK	Transforming growth factor-beta activated kinase
TGF- β	Transforming growth factors-beta
TNF α	Tumour necrosis factor alpha
TRAM	Transverse rectus abdominus myocutaneous flap
UCP1	Uncoupling protein 1
UHCW	University Hospitals Coventry and Warwickshire
WAT	White adipose tissue

List of Figures

Figure	Description	Page
1.1	Distribution of white and brown adipose tissue. Adipose tissues are found throughout the body and perform different roles.	25
1.2	Differentiation of white and brown adipose tissue. Mesenchymal lineages share common progenitor cells. Mature white adipocytes can transdifferentiate into brown adipose tissue cells.	33
1.3	Development of mesenchymal derivatives. Schematic of key positive and negative transcription factors in pluripotent mesenchymal cell differentiation.	34
1.4	Stages of differentiation. Multipotent stem cells have the capacity to differentiate into myoblast, osteoblast and chondroblast lineages as well as adipocytes.	38
1.5	Three layers of lipo-aspirate after centrifugation.	46
1.6	A monomer of hyaluronic acid. This monomer unit may be repeated thousands of times to constitute varying molecular weights of hyaluronic acid.	54
1.9	Functionalisation of hyaluronic acid. Schematic of hydrazine-modified hyaluronic acid (in blue- HA-HYD) and aldehyde-modified hyaluronic acid (in red- HA-ALD).	55
2.1	Anatomy schematic of a mouse after laparotomy. Perigonadal adipose tissue.	80
2.2	Representative images of murine gonadal adipose tissue isolation. Abdominal view post laparotomy, gonadal adipose tissue after excision, minced adipose tissue before centrifugation, adipose tissue after digestion.	81
2.3	Schematic of the Filtron Tissu-Trans System.	85

2.4	Two 10 mL Luer lock syringes of processed lipo-aspirate. Lipo-aspirated adipose tissue is less than 2 mm in size after passed through one stage of purification.	86
2.5	Three way tap mixing system.	93
3.1	Synthesis schematic of HA-HYD and HA-ALD. HA-HYD is synthesised through amidation between carboxyl of HA and hydrazines of adipic acid dihydrazide via the solvent solution EDC/MES.	98
3.2	NMR spectroscopy plot of HA-HYD.	100
3.3	Illustration of phase angle calculation. For calculation of rheology.	104
3.4	Representative images of 1.5 % and 6% HA-HYD:HA-ALD 1:1 ratio gels.	106
3.5	Frequency sweep of 1.5%, 3% and 6% concentrations of HA hydrogel in a HA-ALD:HA-HYD 1:1 ratio, showing storage (G') and loss modulus (G'') with increasing frequency.	109
3.6	Mean frequency sweep values for storage modulus, loss modulus and loss factor for 6% concentration HA hydrogel for various HA-ALD:HA-HYD ratios and frequency sweep mean storage modulus values for all gel ratios.	112
3.7	Mean amplitude sweep values for storage modulus and loss modulus for 6% concentration HA hydrogel of varying HA-ALD:HA-HYD ratios and mean amplitude sweep storage modulus values for all gel ratios.	116
3.8	Mean time sweep values for storage modulus and loss modulus for 6% concentration HA hydrogel of varying HA-ALD:HA-HYD ratios and mean time sweep storage modulus values for all gel ratios.	120

3.9	Equilibrium water content for 3% and 6% HA hydrogel.	123
3.10	Gel swelling and degradation characterisation for 3% gel HA-ALD:HA-HYD 1:1 ratio in various solutions.	125
3.11	Gel swelling and degradation characterisation for 6% gel HA-ALD:HA-HYD 1:1 ratio in various solutions. Solutions used for degradation were PBS, culture media and three concentrations of hyaluronidase solution.	126
3.12	Gel swelling and degradation characterisation for 6% gel for varying HA-ALD:HA-HYD ratios in PBS solution. Gel ratios examined for degradation in PBS were 1.5:1, 1:1.5, 2:1 and 1:2.	128
3.13	Gel swelling and degradation characterisation for 6% gel in a 1:2 HA-ALD:HA-HYD ratio in two solutions. Degradation solutions were PBS and E3.	129
3.14	The self-healing ability of HA hydrogels.	131
4.1	MCF-7 cell morphology in 6% HA hydrogel. Representative images.	140
4.2	Oscillations of <i>Per2</i> and <i>Bmal1</i> d-Luc 3T3-L1 adipocytes. LumiCycle luminometer traces.	143
4.3	Bespoke macro code for image analysis in FIJI. Code used to analyse Alligator images of experiments using <i>Per2-dLuc</i> 3T3-L1 and CAG-luc-eGFP primary mouse pre-adipocytes.	147
4.4	Schematic representation of two experimental conditions. <i>Per2-dLuc</i> 3T3-L1 cells under a layer of HA hydrogel, and on a layer of HA hydrogel.	149
4.5	Time course quantification of photons emitted by <i>Per2-dLuc</i> 3T3-L1 cells grown on top of a layer of HA hydrogel. Mean photon emission by <i>Per2-dLuc</i> 3T3-L1 control cells and <i>Per2-dLuc</i> 3T3-L1 cells grown on a layer of HA hydrogel.	152

4.6	Time course quantification of photons emitted by <i>Per2-dLuc</i> 3T3-L1 cells grown beneath a layer of HA hydrogel. Mean photon emission by <i>Per2-dLuc</i> 3T3-L1 control cells and <i>Per2-dLuc</i> 3T3-L1 cells grown beneath a layer of HA hydrogel.	158
4.7	Mean expression of PPAR-γ normalised to RPL7 in 3T3-L1 cells. Control and HA hydrogel-covered cells.	160
4.8	Schematic representation of three experimental conditions. CAG-luc-eGFP adipocytes on HA hydrogel, cells and HA hydrogel mix and control.	164
4.9	Mean photon emission of CAG-luc-eGFP adipocytes on top of HA hydrogel, mixed within HA hydrogel and control cells.	165
4.10	Primary murine pre-adipocytes mean expression of PPAR-γ and CD36. Normalised to RPL7.	166
4.11	Primary murine pre-adipocyte morphology grown on HA gel at Day 5 compared to control.	167
4.12	Mean expression of adipocyte genes (PPAR-γ, CD36 and aP2) normalised to housekeeping genes GAPDH and RPL-7 in primary human adipocytes.	169
5.1	Photon density emitted from mice in the PhotonImager Optima.	179
5.2	Representative images of mice and regions of interest on Day 12 post injection.	181
5.3	Pilot time course of photon emission determined by whole mouse ROIs.	182
5.4	Main study mouse weights over time.	186
5.5	Photon emission of murine groups (main study).	189
5.6	Group 1 and 2 gene expression of mature adipocyte markers. Normalised to GAPDH.	191

List of Tables

Table	Description	Page
1.1	Summary of differences between white and brown adipose tissue.	24
2.1	Concentrations and ratios of hyaluronic acid hydrogel compositions.	69
2.2	Additives for induction and maintenance media for adipocyte differentiation.	77
2.3	TaqMan assay references for mouse adipocyte and housekeeping genes and human adipocyte and housekeeping genes.	91
3.1	HA-HYD:HA-ALD ratios based on 6% gel composition for rheology.	107
5.1	Summary of the subcutaneous injections of adipose tissue and HA hydrogel (pilot).	177
5.2	Summary of main study experimental conditions.	185

List of Equations

Equation	Description	Page
2.1	Formulae for gel fraction, equilibrium water content and swelling factor.	72
3.1	Shear stress, shear strain and viscosity equations.	102
3.2	Storage and loss moduli equations.	103

Chapter One: General Introduction

1.1 Introduction

Reconstruction of soft tissue defects presents a major challenge in the context of patients suffering after trauma or after cancer resection. Breast cancer is the most common malignancy in the UK, accounting for 31% of all new cancers, with 16 000 patients undergoing mastectomy each year (CRUK, 2020). Breast reconstruction is offered for these patients to improve their cosmetic and health-related quality of life (Harcourt and Rumsey, 2001). Autologous adipose tissue transfer is commonly used in breast reconstruction and can be used alone or with other surgical techniques. The technique entails harvesting adipose tissue from where there is an excess via liposuction, adipose tissue purification and injection of adipose tissue into a defect. Adipose tissue take in recipient sites is highly variable, however. Adipose tissue graft survival is typically 53% (Kim et al., 2018). A systematic review of 16 clinical studies revealed that adipose tissue graft survival after injection at the recipient site can be as poor as 15% of the original volume transferred from 6 months to 3.7 years follow up (Yu et al., 2015). This leads to repeated adipose tissue transfer procedures under general anaesthetic for a desired volume of reconstruction and outcome.

Recent literature has explored the role of synthetic and natural polymers such as collagen gels in adipocyte tissue engineering. However, these materials have been suboptimal for use in adipocyte proliferation (Borzacchiello et al., 2007). Hyaluronic acid (HA) is a natural stromal compound that exists in the extracellular matrix and has important ligands for regulation of migration, growth and angiogenesis (Agren et al., 2000). HA has been of more interest recently, with HA hydrogel systems being used in commercial applications such as dermal fillers in aesthetic surgery (Patrick Jr et al., 1999). The prospect of augmenting adipose tissue transfer using HA hydrogel to support adipose tissue has been of interest to reduce the number of procedures during reconstruction and achieve a better patient experience.

1.2 Adipose tissue

Adipose tissue is a specialised connective tissue, with numerous important functions, such as a major store for adipocytes rich in triglyceride (Megías M, 2019). In the mid-1980s, secretory functions of adipose tissue started to be elucidated with serine protease adipsin (also named complement factor D), which was reported to be reduced in obese murine mouse models compared to wild-type littermates (Cook et al., 1987). Adipsin was thought to be implicated in lipid storage (Saleh et al., 2011). Other secretory functions include the production of exosomes which transport micro ribonucleic acid (miRNA) between cells locally and systemically, which have been found to have a role in glucose metabolism and adipose tissue distribution differences between human males and females (Santamaria-Martos et al., 2020). Adipose tissue is also a key metabolic organ and is thought to secrete numerous endocrine hormones. The most important of these is thought to be the discovery of leptin which is secreted by adipocytes (Zhang et al., 1994). Leptin acts by signalling brain centres to modulate food intake, but also has effects on immune system function and metabolism (Chlouverakis, 1972, La Cava and Matarese, 2004).

Adipose tissue is also a key regulator of blood glucose levels and is very sensitive to insulin which stimulates adipocytes to take up glucose, increasing the synthesis of lipid and decreasing the breakdown of triglycerides in adipocytes (Carobbio et al., 2017). Disruption of any one of the key roles of adipose tissue (triglyceride storage, secretory and endocrine function, and insulin sensitivity) may have marked effects in obesity-related diseases such as type 2 diabetes mellitus (Carobbio et al., 2017).

1.2.1 Adipose tissue types: white versus brown

Historically, two primary types of adipose tissue are found in humans distinguishable based on tissue colour, with different functions and morphologies. White adipose tissue (WAT) generally contains unilocular adipocytes with large lipid droplets, pushing their organelles to the periphery of the cell, whilst brown adipose tissue (BAT) is multilocular and has many small lipid droplets and has been shown to be inducible at lower temperatures in adults. This ability to be induced is more evident in lean, rather than obese individuals (Drake, 2009). BAT are smaller than WAT, growing 15 to 50 μm and 100 μm in diameter respectively (Cinti, 2012). BAT is also more ellipsoidal in cell shape and is enriched with iron-rich mitochondria, giving a brown appearance (Richard et al., 2020).

As well as morphological differences, BAT and WAT differ on a molecular level, summarised in Table 1.1 and discussed in this Chapter. WAT and BAT comprise physiological differences which result in further specialised tissue functions. WAT's role is primarily as an energy store, is insulin sensitive, has an endocrine communication role and comprises the largest adipose volume in humans (Hausman et al., 2001). WAT can range from 3% to 70% in underweight and obese adults, respectively (Hausman et al., 2001).

Heterogenous tissue containing large, mature adipocytes with lipid droplets and stromal cells (such as fibroblasts, adipocyte progenitors, endothelial cells, pericytes and immune cells) are hallmarks of WAT (Gesta et al., 2007). Stromal cells and adipocytes are suspended in an extracellular matrix (ECM) comprised of collagen types I, III, IV, V and VI as well as other important proteins such as hyaluronic acid and glycosaminoglycans (Flynn et al., 2006). Metabolically, WAT stores surplus energy in the form of triacylglycerol, which further serves as a heat insulator and provides mechanical protection by absorbing and dissipating external forces, thereby protecting sensitive structures such as organs (Frühbeck et al., 2009).

By contrast, BAT was thought to only be present in infants, with recent imaging revealing that BAT is active in the thoracic and supra-clavicular regions in mature adults (Nedergaard et al., 2007) as shown in Figure 1.1. There is a difference in BAT distribution in human male and females, with females having increased BAT activity and mass (Cypess et al., 2009). An inverse relationship exists between BAT and age/ body weight (Cypess et al., 2009). BAT activity is also more pronounced in winter and lessened in summer. The mechanism for this has yet to be elucidated but is thought to be related to temperature or light exposure (Au-Yong et al., 2009).

Adipogenesis of BAT is also promoted by pharmacological agents causing stimulation of beta adrenergic receptors (Yoneshiro et al., 2013). Some studies have also suggested that immune cells (such as eosinophils), type two cytokines and active macrophages increase BAT activity energy expenditure (Qiu et al., 2014, Vargovic et al., 2016, Shan et al., 2017).

Releasing energy as heat, BAT is important in non-shivering thermogenesis in infants and adult humans (Chondronikola et al., 2016). Heat is produced by uncoupling fatty acid oxidation from adenosine tri-phosphate (ATP) by uncoupling protein 1 (UCP1) present in mitochondrial membranes from brown adipocytes (Frühbeck et al., 2009). BAT effectively utilises fatty acids and also releases fatty acids from WAT during non-shivering thermogenesis (Frontini and Cinti, 2010).

Characteristic	WAT	BAT
Function		
Involvement in physiological processes related to energy homeostasis	Important energy storage capacity in the form of triacylglycerols	Relevant participation in thermogenesis, mitochondrial biogenesis and oxidative phosphorylation
	Fatty acid and glycerol release; Lipolysis and lipogenesis	Relative lower adipose tissue storage capacity
	Adipogenesis	Low secretory activity of adipokines and other adipose-derived factors and growth factors
	Extraordinarily high secretory activity of adipokines and growth factors	
Macroscopic features		
Main depot location	Subcutaneous abdominal, perirenal, inguinal, gonadal and retroperitoneal	Interscapular, paravertebral, axillary and perineal
Colour	White (highly variable, ranging from light ivory to strong yellow hue)	Brown (variable from light pink to dark red tone)
Vascularization	Adequately vascularized (++)	Extraordinarily profuse vascularisation both in terms of blood flow and number of vessels (++++)
Innervation	Mainly sympathetic (++) but also evidence of parasympathetic (+)	Sympathetic nervous system (++++)
Tissue organization	Small lobules of densely packed cells	Lobular gland-like structure
Microscopic features		
Adipocyte Shape	Variable from polyhedral to spherical	Mainly polygonal
Size	Highly variable, ranging from ~25µm up to 200µm (increasing their volume by up to 1000x)	Comparatively much smaller (between 15–60µm)
Nucleus	Peripheral semilunar, flattened or cup-shaped occupying only 2–3% of the cell volume	Centrally located, with mainly round or oval shape
Lipid droplets	Predominantly unilocular with one single large lipid droplet that occupies 90% of the cell volume	Multilocular with abundant small lipid droplets
Cytoplasm	Thinly stretched into a scant peripheral rim	Considerable volume uniformly stretched around the cell
Mitochondria	Few, small, elongated	Abundant, large, round
Endoplasmic reticulum (ER)	Sparse cisternae of rough ER, few tubules of smooth ER	Poorly developed ER
Multicellularity	High presence of other cell types (++++), such as fibroblasts, immune cells	Low presence of other cell types (+/-)
Main molecular features		
Cytochrome c	Low (+)	High (+++)
Hox genes	A1 (-), C4 (-)	A1 (+++), C4 (+++)
Leptin	High (+++)	Present at birth, not in adulthood

Table 1.1 Summary of differences between white and brown adipose tissue. Adapted from Frühbeck et al., 2009.

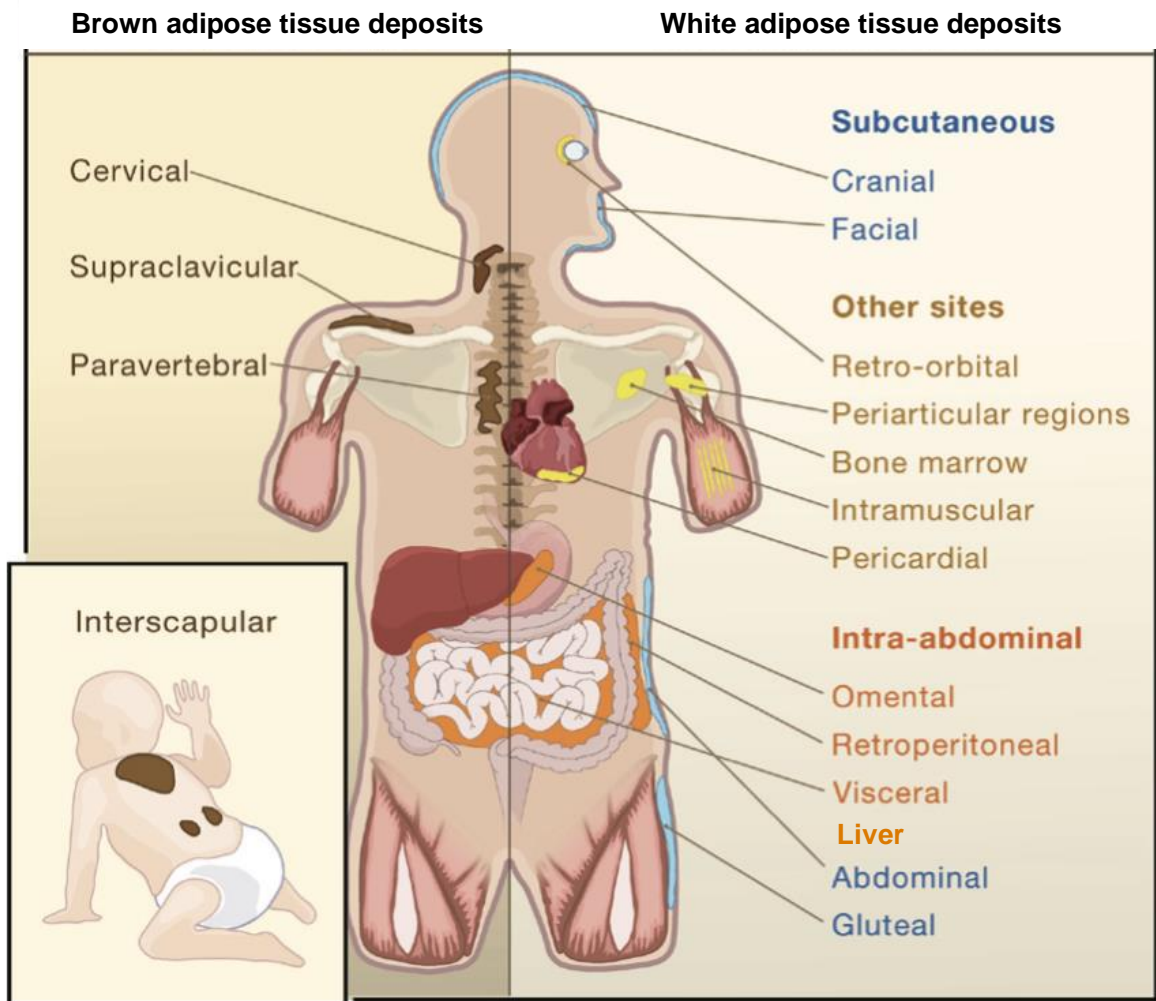


Figure 1.1 **Distribution of white and brown adipose tissue.** Adipose tissues are found throughout the body and play different roles (Gesta et al., 2007).

1.2.2 Other adipose tissue types

Two further types of adipose tissue in addition to WAT and BAT have been described as beige and pink adipocytes. Beige adipose tissue exhibits characteristics of both WAT and BAT and are thought to develop within WAT as a pre-adipocyte subset (Wu et al., 2012) or differentiation of white adipocytes (Barbatelli et al., 2010). Beige adipose tissue can be promoted by a variety of conditions such as cold exposure (Barbatelli et al., 2010), variations in diet/exercise (Wang et al., 2019), post-biotics/ pharmaceutical agents (Reynés et al., 2019) and various adipokines (Kaisanlahti and Glumoff, 2019). Induction of beige adipose tissue occurs in humans as well as mice, but the effect is seen to a greater degree in mice (Ikeda et al., 2018).

Pink adipocytes are the most recent discovery of adipose tissue type and also arise from WAT in mice during pregnancy (Giordano et al., 2014). Derived from WAT, they are epithelial cell-like and form alveoli for milk secretion with a pink hue in mice (Giordano et al., 2014). Whilst present in lactating rodents and exhibiting reversible trans-differentiation, it is debatable whether pink adipose tissue is present in humans (Cinti, 2018). Adipose tissue subtypes are of particular relevance as adipocyte plasticity may offer a therapeutic target to combat pathology such as obesity and cancer (Apostoli et al., 2014).

1.2.3 Adipose tissue distribution

Adipose tissue exists in a variety of locations around the human body. Subcutaneous WAT is the largest proportionate, contributing 80% of all adipose tissue (Reddy et al., 2019). As described in Section 1.2.2, WAT acts as a store of excess energy and also acts as a physiological buffer during limited energy expenditure. Lipid may start accumulating in ectopic sites such as the liver, if subcutaneous storage capacity is exceeded via the actions of adipocyte hyperplasia or hypertrophy (Freedland, 2004). Subcutaneous WAT is also the

prime insulator preventing loss of heat and also acts as a shock absorber against external forces (Kwok et al., 2016). Increasing evidence exists that pre-adipocytes that form subcutaneous WAT are a distinct population from pre-adipocytes that form ectopic adipose tissue (Gesta et al., 2006).

Research has shown that pre-adipocytes isolated from human and mouse specimens express developmental genes prior to WAT development in a pattern that persists throughout adulthood, suggesting that cells exhibit autonomous function and a strong inheritable link for adipose tissue distribution (Baker et al., 2005, Gesta et al., 2006). Of particular note and relevance to reconstructive surgery is the macroscopic deposit locations of these adipose tissue types.

Large deposits of WAT residing in the subcutaneous abdominal plane, are particularly easy to harvest for adipose tissue transfer. Harvesting visceral adipose tissue stores for adipose tissue grafting presents practical difficulties. As the adipose tissue is within the peritoneum, the proximity of sensitive structures (such as all intra-abdominal organs) leads to a high risk of damaging these structures, with life-threatening sequelae (Coronado-Malagón and Tauffer-Carrion, 2012). As such, the risk of harvesting visceral adipose tissue outweighs the benefits of harvesting subcutaneous adipose tissue stores that are relatively low-risk.

Visceral adipose tissue is located in the retroperitoneal space, omentum and mesentery (Björntorp, 1990). Typically, lean individuals do not have large volumes of visceral adipose tissue which is marked metabolically active, persistently releasing free fatty acids into the circulation via the portal vein (Björntorp, 1990). Large amounts of visceral adipose tissue is associated with metabolic syndromes and promotes hyperlipidaemia, insulin resistance and atherosclerosis.

In contrast, high proportionate accumulation of subcutaneous adipose tissue appears to be protective against the deleterious effects of the metabolic syndrome than accumulation of visceral adipose tissue. Obese and older individuals with a high ratio of subcutaneous adipose tissues present fewer sequelae of the metabolic syndrome, such as type 2 diabetes and cardiovascular disease (Björntorp, 1990, Krssak et al., 1999).

As described in this Section, ectopic and excessive adipose tissue promotes inflammation and insulin resistance (Gustafson et al., 2015). However, adipose tissue expansion via newly differentiated adipocytes rather than hypertrophy reduces insulin resistance and inflammation (Ghaben and Scherer, 2019).

Most studies investigating the adipose tissue extracellular matrix (ECM) focussed on scaffold forming collagen that constrains adipose tissue expansion from mechanical stress, with new research suggesting that targeting excessive ECM production may improve the metabolic syndrome (Khan et al., 2009, Spencer et al., 2011). Subcutaneous adipose tissue also secretes ECM proteins to a greater degree than visceral adipose tissue, with subcutaneous adipose tissue secreting collagen types 1a1, 3a1 and 5a1 to a proportionately higher degree than visceral adipose tissue (Mori et al., 2014). ECM is associated with an increased ectopic accumulation of adipose tissue in other organs and also restricts the size of adipocytes (Chun, 2012). However, despite more ECM being secreted by subcutaneous adipose tissue, subcutaneous adipose tissue is still more beneficial than visceral adipose tissue in reducing the risk of metabolic disease (Khan et al., 2009, Spencer et al., 2011).

1.2.4 Adipose tissue hormones, adipokines, cytokines and chemokines

In addition to being an energy storage organ, adipose tissue actively secretes adipokines, cytokines, chemokines and growth factors in its role as a

key endocrine organ. Adipokines mediate metabolic processes such as fatty acid oxidation, lipogenesis, insulin sensitivity, glucose metabolism and synthesis, and used as an energy source in metabolically active tissues such as muscle and the brain and are of particular importance in adipose tissue distribution (Ahima and Lazar, 2008).

Over 200 adipokines have been described to date (Friedman, 2016). Three of the most described are leptin, adiponectin and omentin. Leptin deficient mice (*ob/ob*) grow to be markedly obese, as this adipokine is vital for appetite suppression and regulation, with action in the hypothalamus, hippocampus and neocortex (Funahashi et al., 2003, Friedman, 2016). In lean and obese humans, blood leptin concentrations correlate with WAT volumes (Boden et al., 1996, Hube et al., 1996). Adiponectin in contrast to leptin, is inversely proportional to adipose tissue volume, and has a greater effect regarding volume on subcutaneous WAT compared to visceral WAT (Samaras et al., 2010). Adiponectin is also highly expressed in skeletal muscle and the liver, leading to increased glucose synthesis and increased fatty acid oxidation (Fang and Judd, 2018). Omentin levels are reduced in metabolic disease such as obesity and type 2 diabetes mellitus (de Souza Batista et al., 2007, Pan et al., 2010). The examples of adipokines as described above demonstrate their importance in regulating whole body metabolism.

Increased adiposity in obesity increases circulating blood concentrations of the cytokines interleukin-6 (IL-6) and tumour necrosis factor alpha (TNF α), which decrease as adipose tissue volume falls (Bastard et al., 2000). Along with monocyte chemoattractant protein-1 (MCP-1), adipose tissue is a marked source of these cytokines, which is crucial for inflammatory cell recruitment (e.g., macrophages), being secreted by expanding adipose tissue. IL-6 and TNF α recruit other immune cells (e.g., T cells). These immune cells can represent up to 60% of adipose tissue mass in morbidly obese individuals and is characterised by a low-grade inflammatory state in obesity, which increases apoptosis in

adipose tissue (Cancello and Clement, 2006, Han et al., 2010). This inflammatory state leads to lipids being accumulated in non-adipose tissues (such as the liver and muscle ectopically). This accumulation promotes insulin resistance, and thus a vicious cycle of inflammatory sequelae (Heilbronn and Campbell, 2008). Cytokines and chemokine production is more limited in lean adipose tissue and thus contributes less to excess adipose tissue-related metabolic diseases (Han et al., 2010). Studies have more recently begun to predict the development of glucose tolerance or type 2 diabetes based on adiponectin, TNF α , complement C3 and interleukin-6 (Pradhan et al., 2001, Freeman et al., 2002, Samaras et al., 2010).

However, the role of differing adipokine profiles produced by subcutaneous versus visceral adipose tissue in the role of metabolic disease has just begun to be elucidated. Visceral adipose tissue expresses significantly higher proportions of inflammatory regulators (TNF α , macrophage inflammatory protein, IL-8, IL-6) and early adipogenesis factors (cAMP response element-binding protein and cAMP response element-binding protein-3). Adiponectin expression is equivocal between visceral and subcutaneous adipose tissues (Samaras et al., 2010). Subcutaneous adipose tissue had higher adiponectin, leptin and nuclear factor κ B mRNA expression (Samaras et al., 2010).

There is increasing evidence that adipose tissue adipokine expression adapts to the actions of exercise and weight loss. Subcutaneous adipose tissue upregulates adiponectin receptor expression (R1 and R2) after one month of aerobic training (Blüher et al., 2007). One year post gastric bypass surgery, adiponectin gene expression increased by 15 times in subcutaneous adipose tissue, with a decrease in IL-6 expression after 15 weeks in patients who underwent a weight-loss regime (Bruun et al., 2006, Coughlin et al., 2007).

1.2.5 Adipose tissue origin and lineage differentiation

Subcutaneous adipose tissue is of mesenchymal origin (Unamuno et al., 2018, Megías M, 2019). Each discrete adipose tissue depot has a unique developmental origin and genetic fingerprint and adipokine profile (Unamuno et al., 2018). During gastrulation, paraxial mesodermal stem cells express myogenic transcription factor Myf5, becoming brown adipocytes or myocytes. Mesenchymal stem cells of the lateral mesoderm by contrast, do not express Myf5 and differentiate into white adipocytes or pericytes associated with blood vessels (Figure 1.2). Multipotent stem cells that give rise to the adipocyte lineage are derived from a population of cells that also differentiate into other mesenchymal cell types such as chondrocytes, myocytes and osteoblasts (Konieczny and Emerson Jr, 1984, Gregoire, 1998).

Adipoblasts are the first cell type that are unipotent in the adipogenic lineage from mesodermal stem cells and become pre-adipocytes. In an appropriate micro-environment, pre-adipocytes differentiate into mature adipocytes that exhibit lipid synthesis and storage capacity (Katz et al., 1999). The potential for new adipocyte generation from adipocyte precursors is exhibited throughout life in white adipose tissue (Miller Jr et al., 1984, Prins and O'rahilly, 1997).

Whilst later molecular pathways in adipogenesis have been elucidated, early molecular events that lead to commitment of precursor cells have yet to be fully elucidated (Gregoire, 2001). Cell cultures that are from primary white adipose tissues are at different stages of differentiation/ development can't be interrogated and controlled as effectively as pre-adipocyte cell lines, but reflect the tissue environment *in vivo* to a greater degree (Butterwith, 1994).

Proliferating pre-adipocyte cells and primary cultures of adipose precursor cells phenotypically resemble fibroblasts (Butterwith, 1994). Induction of

differentiation of these cells at confluence triggers these cells to change in shape from a spindle-like fibroblastic phenotype to a spherical shape with accumulation of lipid and adopting the characteristics of a mature adipocyte (Butterwith, 1994).

A variety of adipocyte differentiation protocols have been devised for pre-adipocytes from various sources, with the inducing agents and results varying widely in mature adipocyte yield (Grégoire et al., 1992). Spontaneous differentiation to mature adipocytes may result from pre-adipocytes exposed to foetal calf serum (FCS), with the amount of serum in the growth medium being proportional to the degree of differentiation (Gregoire, 2001).

1.2.5.1 Transcriptional regulation of adipocyte differentiation

Pluripotent mesenchymal stem cells (MSCs), as well as differentiating down an adipocyte lineage, can also differentiate down a bone or muscle pathway. Bone morphogenic proteins (BMPs), some transforming growth factors (e.g. TGF- β) play an important role in influencing MSCs down a bone lineage and therefore regulating adipogenesis (Unamuno et al., 2018). BMP-2 and BMP-4 phosphorylates mothers against decapentaplegic homolog 1 protein (SMAD-1), SMAD-5 and SMAD-8 which forms complexes with SMAD-4. These complexes move into the nucleus and provides further adipogenesis regulation (Miyazono et al., 2005).

Pathways independent of SMAD which regulate adipogenesis and osteogenesis include the MKK3.p38 MAPK and TAK1 signalling pathways which regulate BMP genes. A myriad of other pathways also negatively regulate adipogenesis, such as the hedgehog family and Wnt10b/Wnt3a (Gesta et al., 2007). Figure 1.3 describes some of the most understood pathways.

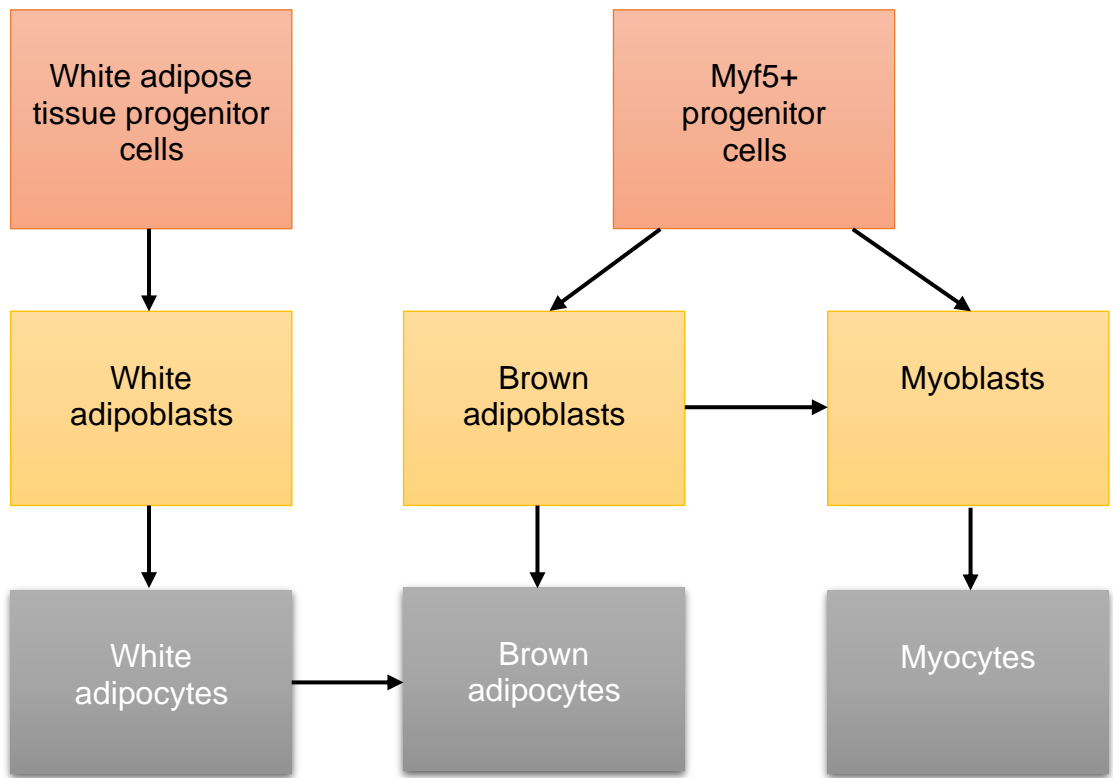


Figure 1.2 **Differentiation of white and brown adipose tissue.** Mesenchymal lineages share common progenitor cells. Mature white adipocytes can transdifferentiate into brown adipose tissue cells (Saely et al., 2012).

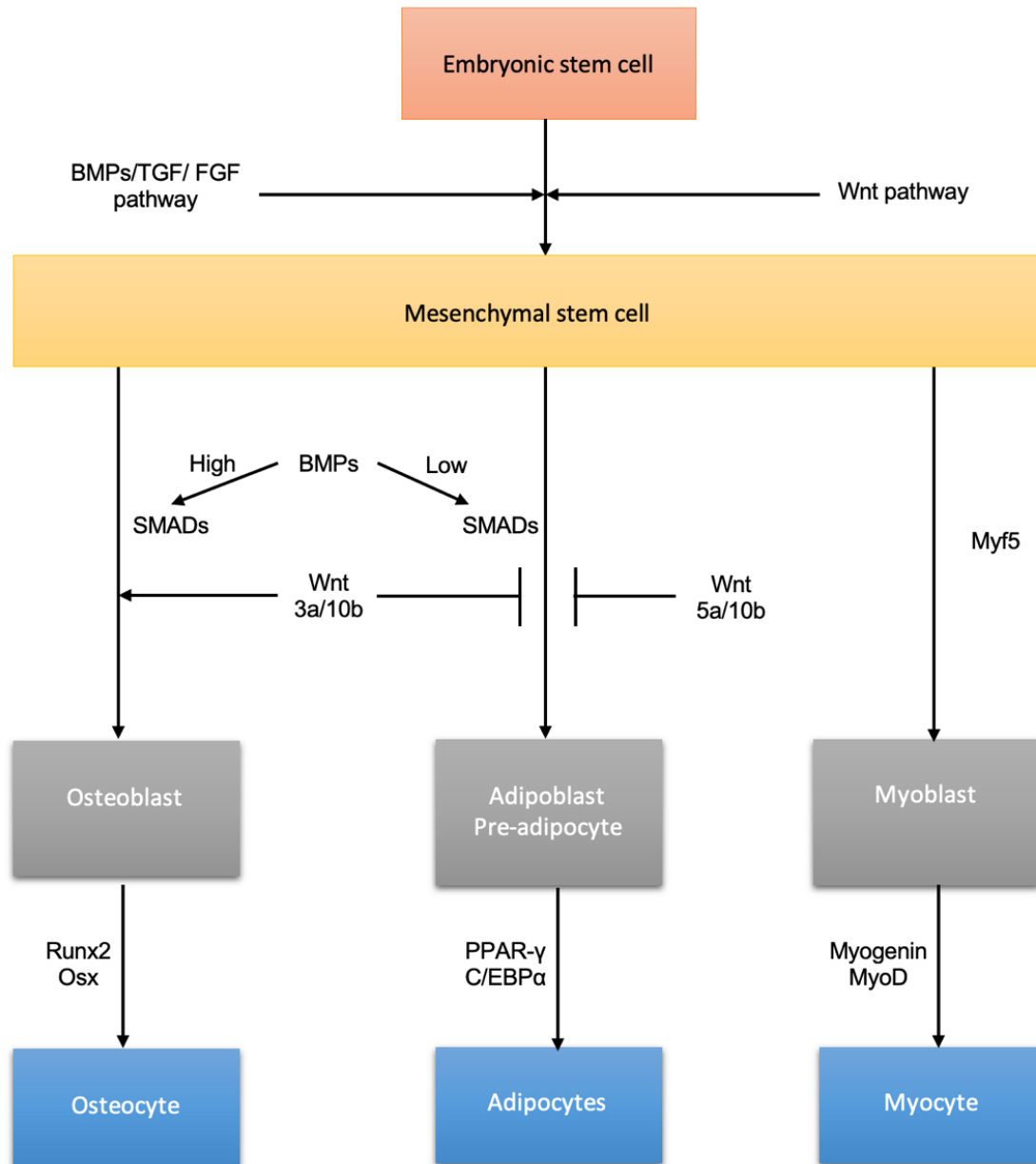


Figure 1.3 **Development of mesenchymal derivatives.** Schematic of key positive and negative transcription factors in pluripotent mesenchymal cell differentiation (Gesta et al., 2007).

White pre-adipocytes which are committed to mature adipocytes exit the cell cycle before terminal differentiation. This is most often by contact inhibition as proliferating pre-adipocytes reach confluence (Fajas, 2003). Differentiation of progenitor cells into adipocytes is typified by a sequential expression of specific genes that result in a mature adipocyte phenotype (Figure 1.4). These changes occur mainly at transcription, and result in early, mid and later mRNA, along with protein markers and terminally, triglyceride accumulation (MacDougald and Lane, 1995). Adipocyte differentiation from pre- adipocytes has been mainly described in mouse 3T3-L1, primary human and primary mouse adipocytes (Rosen and Spiegelman, 2000, Rosen et al., 2000, Gesta et al., 2007).

Two transcription factors have been identified that are critical in adipocyte differentiation regulation. Peroxisome proliferation-activated receptor gamma (PPAR- γ) and CCAAT/enhancer binding protein alpha (C/EBP α) activate adipocyte-specific genes and promote exit from cell cycle (growth arrest). Both PPAR- γ and C/EBP α mutually induce each other as they have responsive elements in their respective promoters (Mandrup and Lane, 1997).

The most selective and specific transcription factor for adipocyte differentiation is PPAR- γ and is induced at the start of differentiation, under the control of C/EBP α (Gregoire, 1998). Activated PPAR- γ increases energy delivery to the differentiating cells, activating a large array of adipocyte differentiation genes and exits the cell from the cell cycle (Fajas et al., 1998). Before triggering exit from the cell cycle, PPAR- γ targets genes responsible for lipid transport (e.g. fatty acid binding protein (FABP4)), uptake of fatty acids (e.g. lipoprotein lipase (LPL) or cluster of differentiation 36 (CD36)), recycling of fatty acids residing within the cell (e.g. phosphoenolpyruvate carboxykinase 1 (PCK1)) and lipolysis (e.g., G protein-coupled receptor 81 (GPR81)) (Graves et al., 1992, Spiegelman et al., 1993).

The transcription factor C/EBP α is expressed slightly before other adipocyte transcription factors. PPAR- γ has binding regions for the C/EBP family on its promoter region (Zhu et al., 1995, Mandrup and Lane, 1997). Cyclic AMP response element binding protein (CREB) acts early in the differentiation process by upregulating PPAR- γ and C/EBP α , whilst other adipocyte transcription factors such as GATA2/3 and SMAD3 interact with C/EBP α to inhibit transcription of the PPAR- γ promoter (Rosen et al., 2000).

A further early transcription factor in adipocyte differentiation is adipocyte determination-and differentiation-dependent factor-1/sterol regulatory element binding protein-1 (ADD-1/SREBP-1). ADD-1/SREBP-1 also stimulates genetic expression of lipogenesis mechanisms (Kim and Spiegelman, 1996, Ericsson et al., 1997) and along with C/EBP expression, induces and adds to the expression of PPAR- γ , the primary coordinator of adipocyte differentiation (Fajas et al., 1998, Saladin et al., 1999). Steroid receptor co-activator-3 (SRC-3) also has a strong pro-adipogenic action, with a synergistic action with transcription factors C-EBP and PPAR- γ expression (Louet et al., 2006). Bone morphogenetic protein-2 (BMP2) also promotes early adipogenesis by stimulating intra-nuclear localisation of Schnurri-2 (SHN2), SMAD1 and C/EBP α . Lipoprotein lipase (LPL) whilst not a transcription factor, peaks mid-way in differentiation at day four to five (MacDougald and Lane, 1995). LPL acts as a catalyst for the hydrolysis of triglycerides with particular respect to endothelial cells and is highly expressed in WAT and is secreted by mature adipocytes (MacDougald and Lane, 1995).

Negative regulation of early adipogenesis results by activation of β -catenin signalling by Wnt proteins and androgens. TGF β acts by phosphorylating SMAD3 resulting in adipogenesis inhibition. Pre-adipocyte factor-1 (pref-1) expression also inhibits early adipogenesis *in vivo* (Wang et al., 2006).

Various other late phase markers are produced by differentiating adipocytes such as leptin, angiotensinogen II or adipsin (MacDougald and Lane, 1995, Gregoire, 2001). Acyl-coenzyme A (CoA)-binding protein (ACBP) is also another late marker of adipogenesis, with acyl-CoA performing metabolic and regulatory roles during late differentiation (Mandrup et al., 1998).

Although PPAR- γ and C/EBP α are involved in early phase regulation of adipogenesis, as they increase factors including aP2, leptin and CD36, they are considered the orchestrators of adipocyte differentiation (Spiegelman et al., 1993, Hollenberg et al., 1997, Gregoire, 2001). Late phase adipocyte differentiation (in which adipocyte-specific fatty acid binding protein (aP2) plays a role) is marked by increased lipogenesis and increasing insulin sensitivity, with increased expression of mRNAs for proteins responsible for triglyceride synthesis such as fatty acid synthase and glycerol-3-phosphate dehydrogenase. Adenosine triphosphate (ATP) also increases for synthesis of triglycerides (Spiegelman and Ginty, 1983, Bernlohr et al., 1984, Katz et al., 1999).

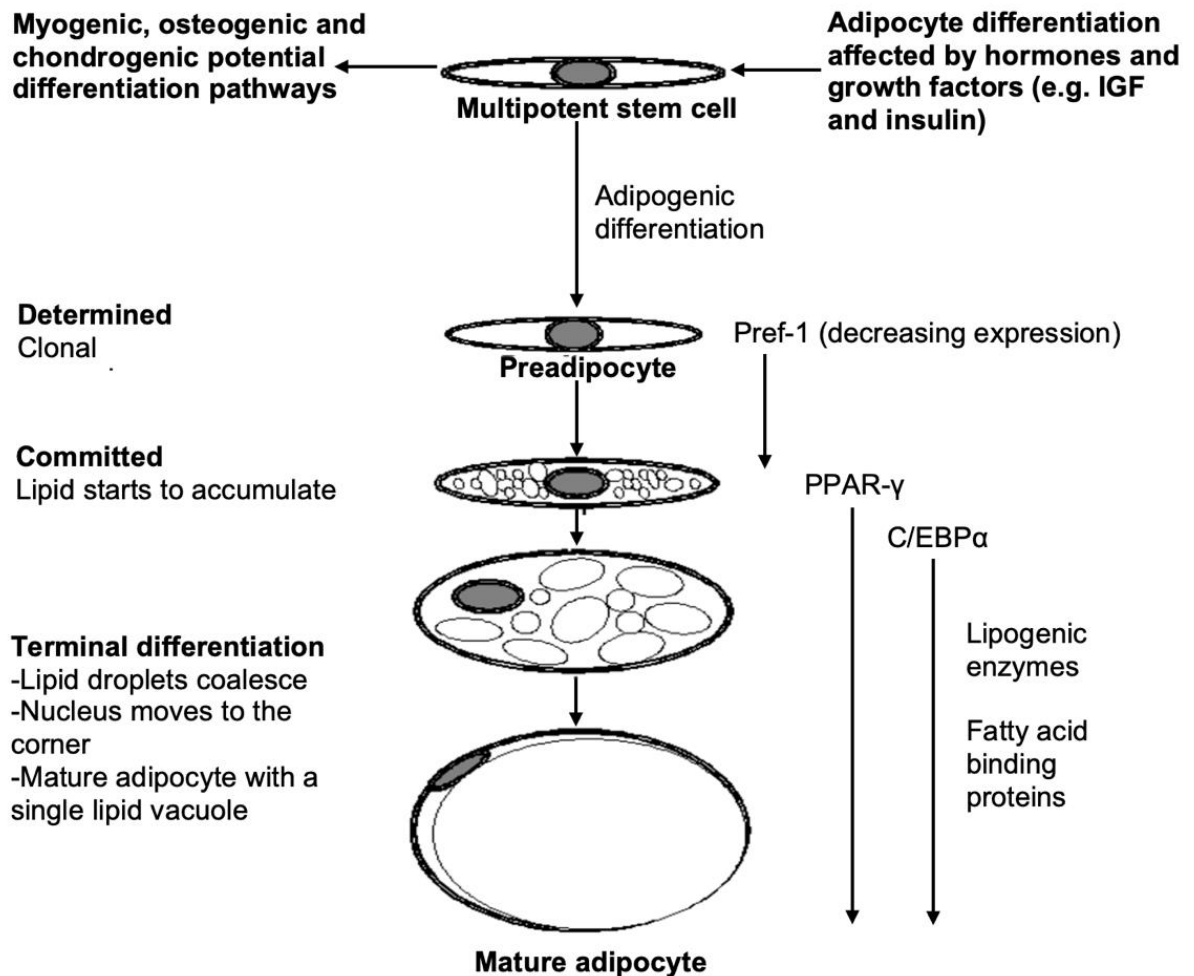


Figure 1.4 Stages of differentiation. Multipotent stem cells have the capacity to differentiate into myoblast, osteoblast and chondroblast lineages as well as adipocytes. On exposure to the appropriate micro-environment, sequential gene expression of transcription factors results in clonal expansion and terminal adipocyte differentiation, with cells accumulating lipid droplets that coalesce to fill the cell volume in white adipose tissue. Gene expression events are on the right, with arrows conferring the duration of effects (Niemelä et al., 2007).

1.2.5.2 Signal transduction and hormonal regulation of adipogenesis

Chemicals have been used to augment differentiation to mature white adipocytes, such as the addition of dexamethasone to growth media which stimulates the glucocorticoid receptor pathway (Reusch et al., 2000, Rosen and Spiegelman, 2000). Stimulation of the cAMP pathway can also be used to induce adipogenesis by the addition of 3-isobutyl-1-methylxanthine (IBMX) to cell media with high concentrations of insulin. The involvement of glucocorticoid, cAMP signalling and insulin/insulin-like growth factor pathways in differentiation to mature white adipocytes is well established (Ntambi and Young-Cheul, 2000, Gregoire, 2001).

Specific receptors mediate adipocyte differentiation via the effects of hormones and growth factors leading to a cascade of intra-cellular events. Insulin growth factor-1 (IGF-1) and insulin are a key regulator of adipogenesis (Girard et al., 1994). Insulin activates the IGF-1 receptor in pre-adipocytes as it is expressed to a higher degree than the insulin receptor in white adipose tissue, activating numerous signal transduction pathways which mediate adipocyte differentiation (Gregoire, 1998, Boucher et al., 2014). However, different cells with adipogenic potential may respond to insulin stimulation to a varying degree. This effect is most pronounced in bone marrow-derived stem cells being able to differentiate to adipocytes without the need for insulin (Laharrague et al., 1998). In mature adipocytes, insulin binds to the insulin receptor to a greater degree (rather than the IGF-1 receptor) and is very important in white adipose tissue for terminal differentiation (Boucher et al., 2014). However, both IGF-1 and insulin receptors are important for terminal differentiation in brown adipose tissue (Guerra et al., 2001, Tseng et al., 2004).

Dexamethasone activating the nuclear glucocorticoid receptor (which acts in a similar mechanism to PPAR- γ) has also been used to induce differentiation of pre-adipocyte cell lines and primary pre-adipocytes (Rosen and Spiegelman, 2000). By stimulating the C/EBP pathway and reducing pref-1 (a negative regulator of adipogenesis), dexamethasone is a potent promoter of adipogenesis (Smas et al., 1999, Wu et al., 1996). IBMX is pro-adipogenic and may work through the accumulation of cAMP, inducing the C/EBP transcription family and subsequently PPAR- γ . cAMP is an activator of protein kinase A (PKA), which is required for PPAR- γ expression. cAMP phosphorylates transcription factors such as cAMP response element binding protein (CREB) which increases insulin sensitivity (Cao et al., 1991, Reusch et al., 2000).

Sex hormones have also been found to have a role in adipogenesis. Oestrogen has been shown to increase clonal expansion of pre-adipocytes, whilst progesterone has increased adipogenesis in 3T3-L1 cells *in vitro* (Hauner and Löffler, 1987, Rondinone et al., 1992, Anwar et al., 2001), although these hormones are rarely used in common protocols.

1.2.6 Adipose tissue growth

Adipose tissue expands via hyperplasia (cell number increase) and hypertrophy (cell size increase) (Sun et al., 2011). Adipocyte total number seems to be controlled with the rate of new adipocytes being regulated by adipocyte death (Unamuno et al., 2018). Small increases in adipocyte number in adulthood have been suggested, contrary to a steady state of adipocytes (Unamuno et al., 2018). This suggests that adipocytes have a potential to regenerate after surgical procedures to harvest subcutaneous adipose tissue and expands in line with body habitus (Rosen and Spiegelman, 2000).

1.3 Adipose tissue transfer overview

Soft tissue reconstruction is most often required after cancer resection or after major trauma. Current reconstruction is reliant on autologous tissue transfer with or without an artificial implant (for example in breast cancer reconstruction) (Al Sufyani et al., 2016).

Autologous adipose tissue transfer is a common procedure performed by reconstructive surgeons. The procedure enables a defect of varying sizes to be filled with a conforming and natural feeling substance (adipose tissue), taken from a different area of the body such as the thigh or abdomen. First described by Neuber (Neuber, 1910), adipose tissue transfer was initially used to fill small defects. More recently, adipose tissue transfer has been used in a variety of applications such as correcting breast contour defects after cancer surgery and lower limb defects after major trauma. In all applications, adipose tissue transfer confers a minimally invasive surgical option to restore the physical form of a patient (Benjamin et al., 2015, Agha et al., 2016).

Autologous adipose tissue transfer can be used alone or with other surgical techniques. Briefly, post-mastectomy reconstructive strategies can be divided into vascularised and non-vascularised techniques. Vascularized flaps constitute a large mass of adipose tissue/muscle/skin transferred with its blood supply maintaining a pedicle (Harcourt and Rumsey, 2001). Examples of these flaps are the deep inferior epigastric artery flap (DIEP) and transverse rectus abdominus myocutaneous flap (TRAM). However, as with any large flap, donor site morbidity may be significant (Tachi and Yamada, 2005). Non-vascularized alternatives such as silicone implants have long term complications such as implant rupture, capsular contracture and breast implant associated anaplastic large cell-lymphoma, a form of cancer (Beahm and Walton, 2009). Implant based breast reconstruction can have an early complication rate of up to 15% post operatively (infection and flap necrosis), compared to less than 3% for autologous

reconstruction (Crowe Jr et al., 2004, Stolier et al., 2008, Beahm and Walton, 2009). Capsular contracture which is a feature of implant based reconstruction affects up to 30% of women after reconstruction and is the most common complication, leading to painful breasts and even implant rupture with repeated surgery to correct (Adams Jr, 2009). Since 2008, the incidence of women with anaplastic large cell lymphoma after implant based breast reconstruction has increased, with an estimated 1 in 6920 women with a breast implant reported to have anaplastic large cell lymphoma in a population of Dutch women (de Boer et al., 2018), suggesting a move to other methods of breast augmentation such as adipose tissue transfer.

1.3.1 Adipose tissue transfer procedure overview

Various techniques of adipose tissue harvest and transfer have been described, the most common of which is the Coleman adipose tissue transfer technique, first described in 1987 (Egro et al.). The technique described four steps: infiltration, harvesting, adipose tissue processing and implantation in a multi-planar manner (i.e., more than one plane). This technique remains the benchmark for adipose tissue transfer due to its higher adipose tissue graft survival of 80% volume verses 10-50% for preceding methods and has changed minimally in recent years (Markey and Glogau, 2000, Joyce et al., 2015).

Ideal areas for adipose tissue harvest have yet to be defined (Ferlay et al., 2015). Most commonly used donor sites are usually the anterior abdominal wall, outer thigh or flank as adipose tissue stores here are found reliably and are typically non-fibrous (Markey and Glogau, 2000). Harvesting involves the aspiration of an adipose tissue solution from a given donor site, through a metal cannula. The aspirate contains both adipocytes and adipocyte-derived mesenchymal stem cells which increase regenerative potential through proliferation and differentiation and vascularisation through release of local chemokines and cytokines of the graft (Pu et al., 2008, Pallua et al., 2009). This

aspirate is then processed to attain a high concentration of cells, eliminating tumescence solution, free fatty acids, debris and blood (Pu et al., 2005, Condé-Green et al., 2010). This is usually achieved via the action of a centrifuge or gravity, with the adipocyte fraction having the highest density (Kurita et al., 2008). The adipocyte fraction has been demonstrated to have higher concentrations of growth factors and increased adipose tissue survivability compared with the adipocyte fraction remaining with blood and other debris (Canizares et al., 2009, Pallua et al., 2009). Research has demonstrated that centrifugation to separate the adipocyte fraction at 1,200 g resulted in enhanced graft uptake compared with no processing and whole lipo-aspirate injection, with 3,000 g centrifuge separation resulting in significant damage to adipose stem cells (Kurita et al., 2008).

Lastly, implantation confers the process of introducing the adipose tissue graft to the donor site in a 3D, multi-level manner using a metal cannula. The graft receives nutrition via diffusion over the first 48 hours, followed by the growth of blood vessels into the graft to support further growth (neovascularisation). Adipose tissue deposits should not exceed 2 mm to avoid necrosis, with a key strategy being the formation of micro-ribbons in the tissue (Sherman et al., 2010, Khouri et al., 2014b). Introduction of too much adipose tissue can lead to increased interstitial pressure and a collapse of capillaries, leading to hypoxia and graft loss (Khouri et al., 2014a). However, the success of adipose tissue graft take is highly variable. Adipose tissue graft survival is typically 53% (Kim et al., 2018). However, adipose tissue graft survival at the recipient site can be as poor as 15% of the original volume transferred (Yu et al., 2015).

1.3.2 Adipose tissue harvest

Adipose tissue harvest that is less traumatic increases adipocyte survival and durability (Simonacci et al., 2017). Several techniques have been proposed for adipose tissue grafting. For example, Fagrell et al. (Fagrell et al., 1996)

proposed a 'adipose tissue cylinder graft' comprised of adipose tissue cores, avoiding damage to adipocytes whilst maintaining graft architecture. A high aspiration pressure has also been found to impair adipocyte function, with a low aspiration pressure yielding better adipocyte function and more adipocytes (Pu et al., 2005). High aspiration pressures may disrupt adipocyte structural integrity by up to 90% (Pu et al., 2008).

Cannula size may also have an effect on adipocyte survival, with an inverse relationship between cannula size and cellular damage (Campbell et al., 1987). Coleman et al (Coleman, 2006) described the gold standard technique for adipose tissue harvest with a blunt two-holed three-millimetre cannula connected to a 10 mL syringe with adipose tissue suctioned by hand using a plunger. The negative pressure created by hand coupled with a curette-type action of the cannula allows discrete parcels of fat to be aspirated into the syringe for centrifugation.

Adipose tissue harvest body sites are varied and patient specific. The abdominal wall is the most common site for adipose tissue harvest, followed by the lateral thigh and medial thigh/knee area (Crawford et al., 2010). Adipose tissue can be harvested using the "wet" or "dry" method (Illouz et al., 1989, Klein, 1993). The "wet" method, pioneered in 1993, describes infiltration of a donor site using a Klein's solution (0.9% saline, adrenaline, and local anaesthetic). The infiltration expands the adipose tissue-layer via hydro-dissection, increasing ease of aspiration and minimising post-operative pain and bruising (Dasiou-Plakida, 2003). A low shear force has been demonstrated to improve graft survival (Dasiou-Plakida, 2003). The "dry" method of lipoaspiration is without Klein's solution and may lead to higher post-operative analgesic requirements (Klein, 1993). More recently, micro and nano grafts have been used in delicate areas (e.g., face and eyelids) with a harvest cannula of 0.7 mm in diameter (Dasiou-Plakida, 2003). Micro grafts harvested using a 1 mm cannula showed normal cell architecture, although nano adipose tissue grafts contained no adipocytes. Both

micro and nano adipose tissue grafts contained adipose derived stem cells, with clinical cases reporting improved skin quality at six months after the procedure (Gause et al., 2014).

1.3.3 Adipose tissue processing

Freshly harvested adipose tissue is heterogenous and requires several steps to purify the adipocyte content (Simonacci et al., 2017). Lipo-aspirate contains blood and immune cells as well as other debris which need to be excluded by sedimentation, filtering, washing and centrifugation (Simonacci et al., 2017). Not purifying the lipoaspirate increases inflammation and can lead to degradation of the graft and a false sense of volume (Sommer and Sattler, 2000, Mojallal and Foyatier, 2004). A study by Strong et al (Strong et al., 2015) demonstrated more favourable outcomes when using centrifugation rather than gravity separation. Other studies showed no difference in adipose tissue retention with centrifugation, washing or filtration (Khater et al., 2009).

Centrifugation at speeds of more than 50 g caused mechanical damage to adipocytes leading to cell death (Khater et al., 2009). Moreover, high centrifugation forces result in decreased neovascularisation potential of adipose tissue grafts and adipocyte progenitor cell differentiation ability (Ferraro et al., 2011). Cell death during high centrifugation also leads to a higher oil portion, which decreases the viable adipocyte proportion (Ferraro et al., 2011). The gold standard for adipose tissue processing is the Coleman method, whereby lipo-aspirate is centrifuged at 3,000 rpm for three minutes to isolate the adipocyte portion. After this step, three layers become apparent (Figure 1.5). The top layer contains free lipids, which are discarded by pouring. The middle layer contains the adipose tissue. The bottom layer is an aggregate of interstitial fluid, blood and infiltration fluid (Coleman, 2006).

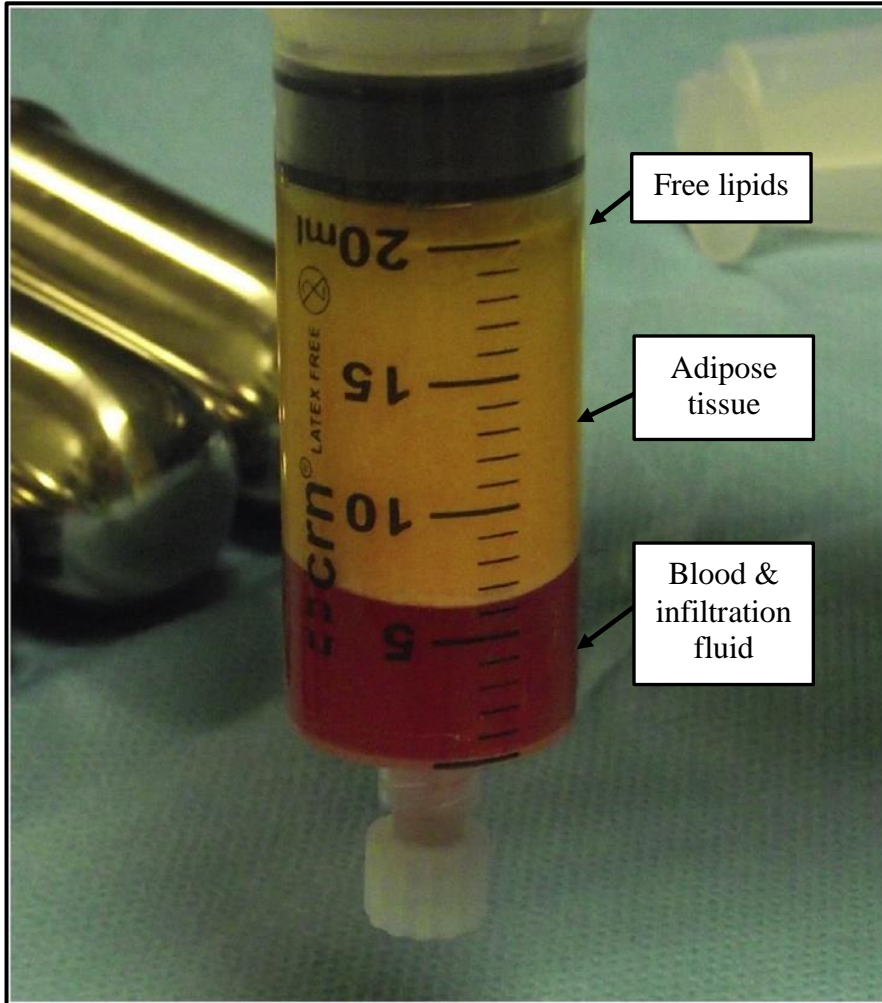


Figure 1.5 Three layers of lipo-aspirate after centrifugation (Simonacci et al., 2017).

1.3.4 Adipose tissue injection

A wide variety of techniques have been described in the literature for adipose tissue injection to increase longevity of results, but there is no consensus for an optimal technique. A cannula is inserted into the desired area through a cutaneous incision. A small cannula has been demonstrated to show less tissue trauma and reduce the chance of recipient complications such as bleeding or haematoma formation and impaired vascularity (Kakagia and Pallua, 2014).

The injected adipose tissue graft is usually dispersed within the recipient in a multi-planar (fanning out) pattern. Adipose tissue grafts are delivered in small aliquots (small beads of 1-2 mm size) at various depths to limit both increased interstitial pressure within the tissues and cell death (Kakagia and Pallua, 2014).

The major theory of adipose tissue graft was first described by Peer (Peer, 1950) and supported by Coleman. The authors demonstrated that on day one, transferred adipocytes survive and continue to develop. There is also a recruitment of inflammatory cells such as macrophages for debris phagocytosis. On day four, neovascularisation begins, starting at the periphery, with central adipose tissue therefore undergoing more prolonged ischaemia. Central adipose tissue only vascularises if the adipose tissue beads are small (Peer, 1950).

1.4 Tissue engineering in reconstructive surgery

More recently, efforts have been made to increase the proportion of adipose tissue volume survival by using grafts suspended in platelet-rich plasma (Salgarello et al., 2011) and the use of a standardised stem cell enrichment process (Peltoniemi et al., 2013). Neither process has demonstrated significant benefit, with efforts turning to tissue engineering for possible solutions to improve cell survival described in this Section.

As well as flap reconstructive options and adipose tissue transfer, non-vascularised and acellular alternatives have also begun to be used in soft tissue reconstruction. Prosthetic reconstructive options have often had long term complications such as implant rupture and capsular contracture (Beahm and Walton, 2009).

The Food and Drug Administration (FDA) in the United States has continued to search for other materials for soft tissue reconstruction, exploring extracellular matrices, oils and other synthetic polymers (Patrick Jr, 2001, Lavik and Langer, 2004, Levenberg and Langer, 2004). These novel materials tend to lose volume over time, leading to a change in shape and volume with a loss of mechanical integrity. This may lead to a poor aesthetic result and reconstructive failure (Levenberg and Langer, 2004).

Collagen and HA hydrogels are used as temporary fillers for subcutaneous injection and are approved by the FDA. Such hydrogels and fillers can be used to suspend adipose tissue cells in a homogenous matrix. Fillers alone usually last for three to four months and diminish due to the effects of endogenous enzymatic degradation (Clark et al., 1989). To date, the use of a modified HA hydrogel being used in adipose tissue transfer to improve clinical outcomes has yet to be described in the literature.

1.4.1 The extracellular environment

Changing in nature, the extracellular matrix (ECM) is a complex structure that is dynamic. The ECM constitutes a wide range of cells such as fibroblasts, adipocyte progenitors, endothelial cells, pericytes and immune cells (Flynn et al., 2006). The ECM is also composed of a rich mixture of secreted proteins, glycoproteins and proteoglycans. This mix surrounds stromal cells and adipocytes, and also contains collagen types I, III, IV, V and VI as well as hyaluronic acid (Flynn et al., 2006, Gesta et al., 2007)

1.4.2 Function of the extracellular environment

The role of the ECM is varied and includes cell maintenance and tissue support, including organ morphogenesis and wound healing (Flynn et al., 2006). Engineered decellularized ECM (through a process of chemical, enzymatic and mechanical means of removing cells leaving just the ECM) has been shown to influence cells for improved infiltration and integration, a reduction of pathological scar development and modulating immune responses (Schmidt and Baier, 2000). Notably, ECM has been demonstrated to be degraded and remodelled within tissues, promoting regeneration of damaged or deficient tissues (Flynn et al., 2006)

The ECM is also critically important in the differentiation and maintenance of adipocytes. Flynn *et al* (Flynn et al., 2006) demonstrated a protocol to decellularize human placenta using existing vasculature. *In vitro* cell culture showed that placental decellular matrix could facilitate the adhesion of primary human adipose precursor cells. During adipocyte differentiation, marked changes occur to the ECM. The first change to the ECM is the deposition of collagen, most markedly at the interface between the cell and ECM, followed by thickening of the basement membrane (Napolitano, 1965). Further changes in the composition of the ECM have been demonstrated during adipogenesis which induce morphological changes to cells (Fukai et al., 1993, Spiegelman and Ginty, 1983). These alterations in ECM may lead to changes in adhesion characteristics and cellular reorganisation, leading to the expression of adipogenic genes (Gregoire, 1998).

As pre-adipocytes lose their fibroblastic phenotype, the expression of collagen type 1 and III decreases, whilst collagen type IV, laminin, glycosaminoglycans and entactin increase throughout differentiation (Aratani and Kitagawa, 1988, Weiner et al., 1989, Ono et al., 1990). During differentiation, intra-cellular and peri-cellular of fibronectin also declines (Antras et al., 1989).

Research has also shown that inhibition of collagen arrests adipocyte differentiation, suggesting that it is an important factor in adipogenesis (Ibrahimi et al., 1992).

Boudreau and Weaver (Boudreau and Weaver, 2006) further demonstrated the importance of the extracellular environment when differentiating adipocytes using matrix metalloproteinases (MMP). The ECM is vitally important in the ability of a tissue to sense forces placed on it and its environment. It impacts signalling and gene expression, regulating synthesis and maturation in adipocytes. Membrane type 1-matrix metalloproteinase (MT1-MMP) null pre-adipocytes failed to differentiate in MT1-MMP null mice. However, they grew in a simulated extracellular environment using a 2D rigid matrix. When imbedded in a 3D matrix, they did not differentiate until the expression of ectopic MT1-MMP (Boudreau and Weaver, 2006). This presents a good example of the importance of MMPs within the ECM contributing to adipocyte differentiation.

Choi *et al* (Choi et al., 2010) have presented key requirements for the development of new tissue engineered reconstructive alternatives. The alternative soft tissue replacement must have a minimal immune response after implantation and have host-suitable degradation characteristics. It must be bioactive, helping to generate functional adipose tissue and incorporate a vascular supply.

1.4.3 Hyaluronic acid (HA)

A non-sulfonated anionic glycosaminoglycan, HA is a natural material that exists in the mammalian extracellular matrix. It is a polysaccharide with a high molecular weight which regulates several tissue functions *in vivo* (Patrick Jr et al., 1999). HA is a polymer- being of various molecular sizes, depending on the number of monomer units forming the chain molecule (Figure 1.6). As well as cell signalling roles, HA has viscoelastic properties and contributes to the mechanical

properties and lubrication of tissues (Mow et al., 1984, Ambrosio et al., 1999). HA also interacts with cluster of differentiation 44 (CD44), receptor for HA-mediated motility (RHAMM) and intercellular adhesion molecule-1 (ICAM-1), important ligands for regulation of migration and growth which gives HA specific biological importance during development, wound healing and in the structure and function of tissues and organs (Agren et al., 2000, Highley et al., 2016a).

1.4.4 Hyaluronic acid hydrogels

Hydrogels are hydrated polymer networks with a range of properties and characteristics. Their use ranges from cell and therapeutic delivery to creating unique cellular micro-environments with a high-water content for cell migration, proliferation and differentiation *in vivo* (Highley et al., 2016b, Wang et al., 2018a).

The biopolymer HA can be altered to comply to permit specific cell interactions such as motility, fate and phenotype (Wang et al., 2018a). A range of applications to date have been described, such as dermal fillers in cosmetics (Andre, 2004), intra-articular injections (Jha et al., 2010), matrices for corneal repair (Inoue and Katakami, 1993) and for post-surgical cessation of adhesion (Burns et al., 1995, Highley et al., 2016b).

1.4.5 Selection of hyaluronic acid as a matrix in adipose tissue transfer

Recent literature has explored the role of synthetic and natural polymers in adipocyte tissue engineering (Borzacchiello et al., 2007). The literature has focussed on the use of poly(lacto-co-glycolic) acid, poly(glycolic acid) fibre matrices, polytetrafluoroethylene scaffolds, collagen gels and gelatine microspheres (Patrick Jr et al., 1999, Kral and Crandall, 1999, Huss and Kratz, 2001, Kimura et al., 2003, Choi et al., 2010). However, these materials have been suboptimal for use in adipocyte proliferation (Borzacchiello et al., 2007).

Over recent years, the development of HA as a useful extracellular matrix in adipogenesis has been hampered by its high hydrophilic nature and its comparatively poor handling and processing (Patrick Jr et al., 1999). HA interacts with a large number of HA-binding proteins (HABPs), which may lend to the unique properties, such as augmenting cellular signalling and improved solubility (Turley, 1982, Knudson and Knudson, 1993). HABPs include CD44, RHAMM, hyaluronectin and tumour necrosis factor- α stimulated gene 6 (TSG-6) (Stern et al., 2006). CD44 is highly conserved and spans the plasma membrane of cells (Stern et al., 2006). Given the ability of HA as a CD44 ligand and its ability to degrade predictably via oxidation and hyaluronidases, HA has been of more interest recently (Dicker et al., 2014). Several HA hydrogel systems have already reached commercial uses such as dermal fillers in aesthetic surgery (Patrick Jr et al., 1999).

For use in injection (for example in an adipocyte suspension), there are several considerations for design. Firstly, the modified HA needs to be of a low enough viscosity to permit extrusion, but also to gelate once extruded through a delivery cannula or needle to form a stable gel. The gel must be stable enough to resist deformative natural tissue forces and maintain its shape to preserve cell viability. A gel with a high viscosity may subject adipocytes to high shear forces whilst being extruded, reducing overall cell viability. A gel with fewer cross-links may therefore be less viscous and also allow for diffusion of nutrients to metabolically active cells (Tirella et al., 2012, Malda et al., 2013).

Self-healing and shear-thinning are also useful qualities in gels. Shear thinning refers to the mechanical breaking apart of cross-links when extruded through a delivery cannula, with self-healing upon cessation of the force (Wang et al., 2018b). To this end, Wang et al (Wang et al., 2018a) explored the use of dynamic covalent bonds in hydrogels. These dynamic bonds are covalent in nature and are stronger than physical bonds but are in an equilibrium of being bound and unbound. This equilibrium of bonds allows cells to move more easily

within these hydrogels than traditional fixed covalent bond constructs (McKinnon et al., 2014, Wang et al., 2018b).

A number of functional side chain candidates have been elucidated that exhibit these transient covalent bonds including acetals, oximes, imines, hydrazones and aldehydes. Wang et al (Wang et al., 2018a) modified HA hydrogels using the hydrazone bond- a dynamic covalent bond between nucleophilic hydrazine ($R-NHNH_2$) and electrophilic aldehyde ($R-CHO_2$) (Figure 1.7). Variants of these bonds in hydrogels have been previously interrogated for their self-healing and shear -thinning characteristics (Yeo et al., 2006, Ito et al., 2007). These gels have also been shown to offer protection of cells during extrusion (Ma et al., 2020). However, the long term sequelae in terms of cell viability and sustainability of adipocytes in an extracellular construct has yet to be determined fully (Choi et al., 2010).

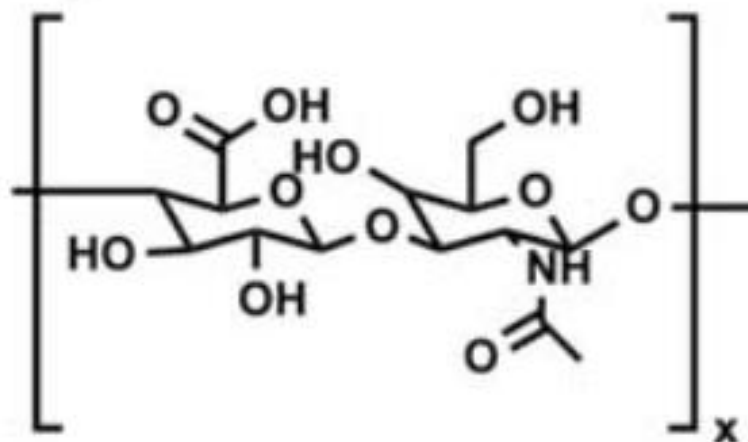


Figure 1.6 A monomer of hyaluronic acid. This monomer unit may be repeated x times to constitute varying molecular weights of hyaluronic acid (Wang et al., 2018a).

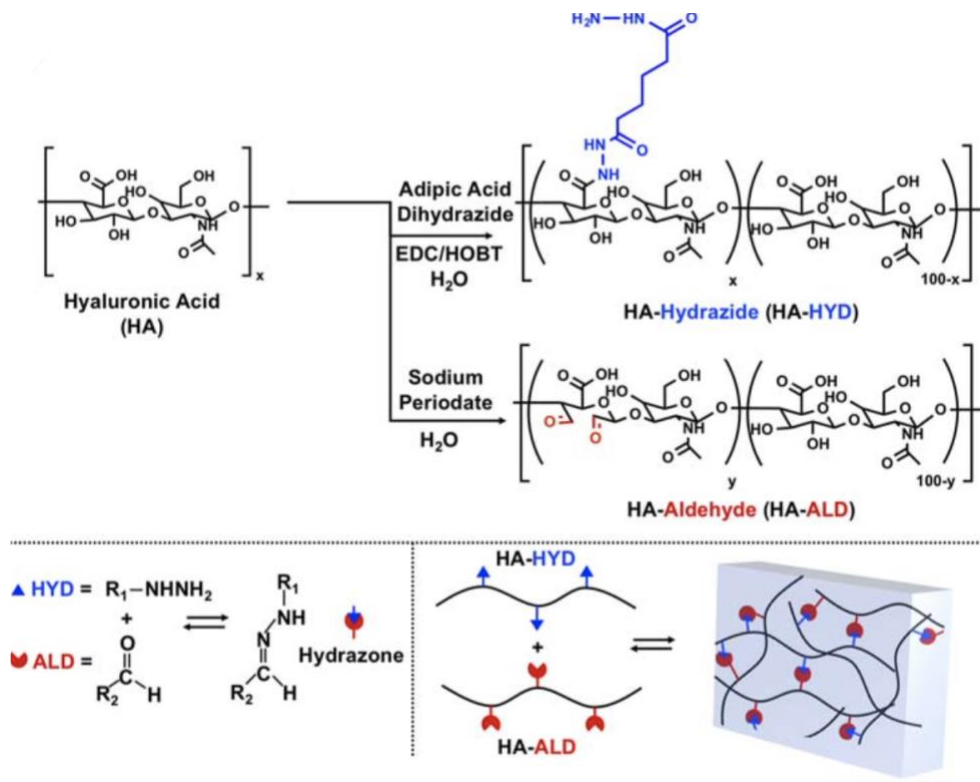


Figure 1.7 Functionalisation of hyaluronic acid. Schematic of hydrazine-modified hyaluronic acid (in blue- HA-HYD) and aldehyde-modified hyaluronic acid (in red- HA-ALD) via amidation between hyaluronic acid carboxyl groups and hydrazines of adipic acid dihydrazide and oxidation of hyaluronic acid by sodium periodate, respectively (Wang et al., 2018a).

1.5 Aims of the study

The aim of this study is to determine the potential of a novel hyaluronic acid (HA) hydrogel for the augmentation of adipocyte transfer. Hyaluronic acid functionalised with hydrazine and aldehyde groups is known to demonstrate positive mechanical characteristics.

I hypothesised that the use of such a hydrogel as an extracellular support may lead to improved adipose tissue retention in a more predictable manner. This may be through a number of mechanisms: hydrogels may be critical in providing cellular support over the first 48 hours where diffusion of nutrients to adipocytes is key, before neovascularisation occurs. These hydrogels may also provide support for neovascularisation from surrounding tissues after 48 hours.

Hydrogels may also facilitate dispersal and delivery of adipocytes in a more homogenous manner, increasing the chance of adipose tissue globules being less than 1 mm, and reducing the chance of cellular hypoxia and necrosis of globules over 2 mm.

The novel hydrogel is temporary. At resorption of the hydrogel, remaining adipocytes should provide a permanent filler in a greater volume. The introduction of a hybrid hyaluronic acid/adipose tissue cell hydrogel filler may allow for greater long-term volume, leading to fewer patients requiring repeated adipose tissue transfer procedures.

The below aims and objectives have been derived from the areas needing further exploration.

1.5.1 Synthesis and modification of hyaluronic acid

The first aim was to develop a protocol for reliable synthesis of a functionalised HA hydrogel made from a combination of HA aldehyde (HA-ALD) and HA hydrazine (HA-HYD) and to characterise the synthesised HA-ALD and HA-HYD using nuclear magnetic resonance (NMR) spectroscopy. Viscoelastic properties and stiffness of gel was then interrogated by rheology for varying gel concentrations and gel degradation and swelling characteristics in phosphate buffer saline (PBS), culture medium and various tissue-mimicking endogenous hyaluronidase concentrations attained.

1.5.2 Characterisation of hyaluronic acid gel toxicity *in vitro*

The toxicity profile of the gel on adipocytes *in vitro* was investigated. Murine pre-adipocytes (3T3-L1 cell line and primary murine adipocytes) were used to elucidate the effects of HA hydrogel on cell proliferation and differentiation. 3T3-L1 cells were transfected to exhibit expression of luciferase (under the *per2* promoter) and adipocytes harvested from luciferase expressing mice (directed by the CAG promoter) and grown within HA hydrogel. Growth curves were generated for intensity of light emitted as a proxy for cell number. A macro programme was written using FIJI to analyse serial images taken using a hypersensitive camera to track cell growth over time. mRNA expression levels of adipose differentiation marker mRNAs were quantified using quantitative polymerase chain reaction (qPCR).

Human adipocytes were obtained from lipoaspirate that was superfluous to clinical need from patients consented for inclusion in this study, under ethical approval granted to the Arden Tissue Bank at University Hospital Coventry and Warwick. Human adipocytes were then cultured in an adipogenic medium as control, and adipocytes dispersed in a gel augmented adipogenic medium as a

comparator. Gene expression in adipose tissue cells from both conditions were characterised using qPCR.

1.5.3 Characterisation of hyaluronic acid gel toxicity *in vivo*

The toxicity profile of HA hydrogel on adipocytes was investigated *in vivo*, by harvesting adipose tissue from bioluminescent mice and injecting it into the sub-cutaneous plane of wild type mice mixed with varying amounts of gel. Growth curves were generated for intensity of light emitted as a proxy for cell number. At the end of the experiment, the mice were sacrificed, and the grafted adipose tissue was excised and characterised for histology, and qPCR performed.

Chapter Two: General Materials and Methods

2.1 Chemicals and reagents

2.1.1 Cell line chemicals

Amphotericin B (Sigma-Aldrich, Haverhill, United Kingdom)

Biotin (Sigma-Aldrich, Haverhill, United Kingdom)

Bovine serum albumin (Fisher Scientific, Loughborough, United Kingdom)

Dexamethasone (DEX) (Sigma-Aldrich, Haverhill, United Kingdom)

Dimethyl sulfoxide (DMSO) (Sigma-Aldrich, Haverhill, United Kingdom)

D Luciferin salt (VWR International, Lutterworth, United Kingdom)

Foetal bovine serum (FBS) (Gibco™, Fisher Scientific, Loughborough, United Kingdom)

Insulin (Gibco™, Fisher Scientific, Loughborough, United Kingdom)

3-Isobutyl-1-methylxanthine (IBMX) (Sigma-Aldrich, Haverhill, United Kingdom)

Liberase TL research grade (Merck Life Science UK LTD, Gillingham, United Kingdom)

Penicillin/Streptomycin 100X (Gibco™, Fisher Scientific, Loughborough, United Kingdom)

Red cell lysis buffer (Fisher Scientific, Loughborough, United Kingdom)

Rosiglitazone (Cayman Chemical, Cambridge, United Kingdom)

Trypsin-EDTA solution 1X (Sigma-Aldrich, Haverhill, United Kingdom)

Trypan blue solution 0.4% (Sigma-Aldrich, Haverhill, United Kingdom)

2.1.2 Media formulations

2.1.2.1 General media for MCF-7, 3T3-L1 and primary human pre-adipocytes

Dulbecco's Modified Eagle's Medium 'DMEM'/F12 with 10% FBS and 1% penicillin/streptomycin.

2.1.2.2 Induction media for 3T3-L1 and primary human pre-adipocytes

Dulbecco's Modified Eagle's Medium/F12 (DMEM/F12) with 10% FBS and 1% penicillin/streptomycin, insulin 1 µg/mL, 0.5 mM 3-Isobutyl-1-methylxanthine (IBMX) and 0.5 µM dexamethasone (DEX).

2.1.2.3 Maintenance media for 3T3-L1 and primary human pre-adipocytes

Dulbecco's Modified Eagle's Medium/F12 (DMEM/F12) with 10% FBS and 1% penicillin/streptomycin, insulin 1 µg/mL and 5 µM rosiglitazone.

2.1.3 Chemicals for hyaluronic acid functionalisation

Adipic dihydrazide 'adipic acid' (TCI Chemicals, Eschborn, Germany)

Ethylene glycol (Sigma Aldrich, Darmstadt, Germany)

Hyaluronic acid sodium salt 50 kDa (Carbosynth, Newbury, United Kingdom)

Hyaluronic acid sodium salt 1-2 million Da (Carbosynth, Newbury, United Kingdom)

N-(3-Dimethylaminopropyl)-*N'*-ethylcarbodiimide hydrochloride 'EDC' (Sigma Aldrich, Darmstadt, Germany)

2-(*N*-morpholino)ethanesulfonic acid 'MES' (Sigma Aldrich, Darmstadt, Germany)

Sodium (meta)periodate (Sigma Aldrich, Darmstadt, Germany)

2.1.4 Cell lines

MCF-7 (European Collection of Authenticated Cell Cultures, Salisbury, United Kingdom)

3T3-L1 (American Type Culture Collection (ATCC), Virginia, United States of America)- these cells were maintained in the Bastie laboratory (Medical School, Warwick University, United Kingdom) after receipt and optimised for differentiation efficiency. They were discarded after five passages.

2.1.5 Gene expression analyses

2.1.5.1 Human and mouse gene expression assays

Human Taqman gene expression assay RPL7: Hs02596927_g1 (Thermo Fisher Scientific, Waltham, MA)

Human Taqman gene expression assay AP2 (AP2A1): Hs00900330_m1 (Thermo Fisher Scientific, Waltham, MA)

Human Taqman gene expression assay PPARG: Hs01115513_m1 (Thermo Fisher Scientific, Waltham, MA)

Human Taqman gene expression assay CD36: Hs00354519_m1 (Thermo Fisher Scientific, Waltham, MA)

Human Taqman gene expression assay GAPDH: Hs_02758991_g1 (Thermo Fisher Scientific, Waltham, MA)

Mouse Taqman gene expression assay RPL7: Mm02342562_gH (Thermo Fisher Scientific, Waltham, MA)

Mouse Taqman gene expression assay FABP4: Mm00445878_m1 (Thermo Fisher Scientific, Waltham, MA)

Mouse Taqman gene expression assay PPARG: Mm00440940_m1 (Thermo Fisher Scientific, Waltham, MA)

Mouse Taqman gene expression assay CD36: Mm00432403_m1 (Thermo Fisher Scientific, Waltham, MA)

Mouse Taqman gene expression assay GAPDH: Mm99999915_g1 (Thermo Fisher Scientific, Waltham, MA)

2.1.5.2 Quantitative polymerase chain reaction (qPCR), isolation kits and other reagents

RNeasy Plus Mini Kit (Qiagen, Düsseldorf, Germany)

RNeasy Plus Micro Kit (Qiagen, Düsseldorf, Germany)

Applied Biosystems High-Capacity cDNA Reverse Transcription Kit. Includes: 1 x 1mL of 10X RT Buffer; 1 x 1mL of 10X RT Random Primers; 1 x 0.2mL of 25X dNTP Mix (100mM); 1 x 0.2mL of MultiScribe Reverse Transcriptase (50U/uL) (Thermo Fisher Scientific, Waltham, MA)

RNAse free 1.5mL Eppendorf (Fisher Scientific, Loughborough, United Kingdom)

MicroAmp EnduraPlate Optical 96-Well Fast Clear Reaction Plates (ABI Applied Biosystems, Waltham, MA)

Applied Biosystems RNase Inhibitor (Thermo Fisher Scientific, Waltham, MA)

TaqMan Fast Advanced Master Mix (ABI Applied Biosystems, Waltham, MA)

2.1.6 Miscellaneous

T75 cell culture flask (VWR International, Lutterworth, United Kingdom)

Chloroform (Sigma-Aldrich, Haverhill, United Kingdom)

Corning® Primaria™ 24 Well Flat Bottom Surface Modified Multiwell Cell Culture Plate (Appleton Woods, Birmingham, United Kingdom)

Corning® Primaria™ 24 Well Flat Black Bottom Surface Modified Multiwell Cell Culture Plate (Appleton Woods, Birmingham, United Kingdom)

Diethyl pyrocarbonate (DEPC) treated water (Scientific Laboratory Supplies Ltd., Nottingham, United Kingdom)

Ethanol (Sigma-Aldrich, Haverhill, United Kingdom)

Falcon® 48 Well Clear Flat Bottom TC-Treated Cell Culture Plate (Appleton Woods, Birmingham, United Kingdom)

Haemocytometer with cover slip (Fisher Scientific, Loughborough, United Kingdom)

Hyaluronidase from bovine testes (Sigma-Aldrich, Haverhill, United Kingdom)
Isoflurane (Merk Scientific, New Jersey, USA)
Isopropanol (Fisher Scientific, Loughborough, United Kingdom)
 β mercaptoethanol (Sigma-Aldrich, Haverhill, United Kingdom)
Mr Frosty™ cryofreezing container (VWR International, Lutterworth, United Kingdom)
Neutral formalin (Scientific Laboratory Supplies Ltd., Nottingham, United Kingdom)
Nuclease-free water (Fisher Scientific, Loughborough, United Kingdom)
Oil Red O (Sigma-Aldrich, Haverhill, United Kingdom)
Phosphate buffer saline (Fisher Scientific, Loughborough, United Kingdom)
Red food colouring (Sainsbury's, London, United Kingdom)
0.2 μ M syringe filter Luer lock (Scientific Laboratory Supplies Ltd., Nottingham, United Kingdom)
Tissue Strainers 250 μ m nylon mesh (Fisher Scientific, Loughborough, United Kingdom)
TRizol™ reagent (Fisher Scientific, Loughborough, United Kingdom)
Whatman filter paper size 1 (GE Healthcare, New York, NY)

2.2 Equipment

2.2.1 Nuclear Magnetic Resonance (NMR) spectroscopy for hyaluronic acid functionalisation characterisation

400 Mhz NMR with 5 mm BBFO smart probe (Bruker, Billerica, MA).

2.2.2 Rheometer for hyaluronic acid hydrogel characterisation

MCR 302 (Anton Paar, London, United Kingdom)

2.2.3 Equipment for cell culture

Biological safety cabinet HR1200 (Haier, Qingdao, China)

Carbon dioxide incubator MCO-170AICD (PHCBI, Tokyo, Japan)

Water bath 1259123 (Grant Instruments, Shepreth, United Kingdom)

2.2.4 Microscopy and imaging

Alligator Luminescence System (Cairn, Faversham, United Kingdom)

EVOS FL auto imaging system (Thermo Fisher Scientific, Waltham, MA)

Light microscope 521 230 (Leica, Wetzlar, Germany)

PhotonImager Optima (Biospace Lab, Ateliers Laumonier, France)

2.2.5 Image analysis program

FIJI v2.1.0/1.53c build 5f23140693 (Schindelin et al., 2012)

Micro-Manager 1.4.22 (Edelstein et al., 2014)

M3Vision Optima (Biospace Lab, Ateliers Laumonier, France)

2.2.6 Miscellaneous equipment

FreeZone 2.5 Litre Benchtop Freeze Dry System (Labconco, Kansas City, MO)

Shaker-incubator Model ES-20 (Grant Instruments, Cambridge, United Kingdom)

Sorvall Legend RT centrifuge (Thermo Fisher Scientific, Waltham, MA)

2.3 Methods

This Section provides a description of general methods used throughout the study. Specific methods are described in each given Chapter.

2.3.1 Functionalisation of hyaluronic acid

The addition of hydrazine and aldehyde functional groups methodology is based on Wang et al., 2018. Modifications of the original method are described in Chapter 3.2.

2.3.1.1 Hyaluronic acid functionalised with hydrazine groups

A 2-(N-morpholino)-ethanesulfonic acid (MES) solution was made by dissolving 15 g of MES in 500 mL of distilled water (dH₂O) with gentle agitation at room temperature. 13 g of adipic acid was then dissolved in 200 mL of MES solution with gentle agitation. 1 g of hyaluronic acid (MW 50 kDa) was then dissolved in the resulting solution, being gently heated to 37°C.

N-(3-Dimethylaminopropyl)-*N'*-ethylcarbodiimide hydrochloride (EDC) 1.9 g was dissolved in 50 mL MES. The resulting EDC solution was added drop-wise to the adipic acid/MES solution and left to react overnight at room temperature. The solution was dialysed against dH₂O (3500 molecular weight dialysis membrane) for 5 days with dH₂O changes twice daily. The product was lyophilised and stored at -20°C until use.

2.3.1.2 Hyaluronic acid functionalised with aldehyde groups

1 g of hyaluronic acid was dissolved in 75 mL of dH₂O at 37°C and agitated. A solution of sodium periodate (0.515 g sodium periodate dissolved in 25 mL

dH₂O) was added and the reaction stirred for two hours in darkness. The reaction was quenched with 10 mL of ethylene glycol.

The resulting reaction was dialysed for five days against dH₂O (14 000 molecular weight dialysis membrane) and lyophilised. The product was stored at -20°C for use.

2.3.2 Hydrogel concentrations

A hyaluronic acid hydrogel was made by dissolving pre-determined amounts of hyaluronic acid functionalised with hydrazine (HA-HYD) and hyaluronic acid functionalised with aldehyde (HA-ALD) in PBS, separately. Gelation involved mixing the HA-HYD and HA-ALD solutions, allowing gelation to occur for 30 minutes before use. An exemplar is given below:

1 mL of 1.5% hyaluronic acid hydrogel in a 1:1 HA-HYD:HA-ALD ratio was made by dissolving 7.6 mg HA-HYD in 0.5mL PBS. 7.6 mg HA-ALD was dissolved in 0.5 mL of PBS. The HA-HYD and HA-ALD solutions were mixed together and left to gelate at room temperature for 30 minutes. Further gel ratios and concentrations are shown in Table 2.1.

2.3.3 NMR spectroscopy protocols and yield calculations

Characterisation using NMR spectroscopy was performed according to manufacturer's guidelines using a 400 Mhz NMR with 5 mm BBFO smart probe (Bruker, Massachusetts, United States of America) for HA-HYD.

2.3.4 Rheology

Hydrogels were made by the methods described in Section 2.3.2. A 50 mm flat geometry plate was used for all time, amplitude and frequency sweeps with a 0.8 mm gap between plates and at 21°C. Further details of time, amplitude and frequency sweeps are described in Section 3.3.

Time sweeps were performed in triplicate over ten minutes with gelation *in situ* on the 50 mm plate. The storage modulus and loss modulus were recorded at one second intervals with a set amplitude at 0.5% and frequency 10 rad/s. Section 3.3 further describes the storage and loss modulus.

Frequency sweeps were also performed in triplicate for each gel composition, with angular frequencies from 100 rad/s to 0.1 rad/s with storage modulus being recorded for each of 16 time points. Amplitude was set at 0.5% for all time points

Amplitude sweeps were performed in triplicate for shear strain values from 0.01 – 100% for a fixed frequency of 10 rad/s. Storage modulus and loss modulus values were recorded for each shear strain value over 25 points.

		HA-HYD concentrations		
		1.5% (7.5 mg)	3% (15.2 mg)	6% (30.4 mg)
HA-ALD concentrations	1.5% (7.5 mg)	1:1	1:2	1:4
	3% (15.2 mg)	2:1	1:1	1:2
	6% (30.4 mg)	4:1	2:1	1:1

Table 2.1 Concentrations and ratios of hyaluronic acid hydrogel compositions. The HA hydrogel is made out of two constituents: carrying amounts of HA-HYD and HA-ALD dissolved separated in 0.5 mL of PBS and then mixed together to gelate. This table displays the varying amounts of HA-HYD and HA-ALD used to construct gels of different constitutions.

2.3.5 Gel characterisation

A number of methods were used to interrogate the physical properties for selected hydrogels fabricated (Table 2.1). Each method below was performed in triplicate for all gel constituents except 4:1 and 1:4. The rationale for exclusion of these gels is given in Chapter 3.

2.3.5.1 Gel fraction

The gel fraction is used to determine the proportion of gel that is unreacted and not polymerised, i.e., the weight percentage of dried polymer (cross-linked) before and after washing with a solvent.

To determine the gel fraction (GF), the weights (W_g) of lyophilised gels were recorded. The lyophilised hydrogels were washed with PBS and allowed to swell for three days, with frequent changing of PBS to extract any non cross-linked or unreacted precursors. After 72 hours, the hydrogels were lyophilised and their weight recorded again (W_r). The expression for GF is described in Equation 2.1A.

2.3.5.2 Gel equilibrium water content

The equilibrium water content is a useful method of describing the water content of a given hydrogel. To determine the gel equilibrium water content (EWC), hydrogels were left in PBS and allowed to swell for 24 hours, after which their weight was recorded (W_s). The hydrogels were then lyophilised, and weights recorded again (W_d) (Equation 2.1B).

2.3.5.3 Gel swelling and degradation

Hydrogels were exposed to each of three corresponding solutions: PBS, DMEM/F12 media, and three hyaluronidase solutions (100 U/mL, 50 U/mL or 10 U/mL in PBS).

Once in solution, the hydrogels were kept at 37°C with a shaking speed of 80 rpm. The swelling solution was replaced daily to remove any unreacted precursors and to prevent the build-up of solute concentration. At specific time points, the hydrogels were removed from solution, gently balloted dry and weighed. Hydrogel swelling and degradation to destruction was described as a percentage weight of the hydrogel at the start of the experiment (W_0) compared to the time point weight (W_t).

2.3.5.4 Gel healing

The hallmark of dynamic covalent bonds between hydrazine and aldehyde side chains of functionalised hyaluronic acid results in these bonds being able to be broken and reformed easily. As such, this gives the ability of these hydrogels to self-heal.

A 6% concentration of 1:1 HA-ALD:HA-HYD ratio hydrogel was gelled into 1 mL cylinders with two duplicates (Section 2.3.2). The second duplicate was made from PBS dyed with a drop of red food colouring. The non-dyed and dyed duplicates were halved, and a non-dyed half applied to the cut surface of a dyed half. The hybrid gels were left at room temperature for one hour, and colour diffusion noted (if any) was recorded.

$$\text{Gel Fraction (\%)} = \frac{W_r}{W_g} \times 100 \% \quad (\text{A})$$

$$\text{EWC (\%)} = \frac{W_s - W_d}{W_d} \times 100\% \quad (\text{B})$$

$$\text{Swelling Factor (\%)} = \frac{W_t}{W_0} \times 100\% \quad (\text{C})$$

Equation 2.1. **Formulae for gel fraction (A), equilibrium water content (B) and swelling factor (C).** (W_g) lyophilised gel weight at the start of the experiment; (W_r) lyophilised gel weight after three days of PBS washing; (W_s) weight after swelling in PBS for 24 hours; (W_d) weight after lyophilisation; (W_0) weight at the start of the experiment; (W_t) weight at a specific time point.

2.3.6 Mammalian cell culture

Four main cell types were used for the duration of the study: 1) murine pre-adipocytes 3T3-L1 cells, 2) primary murine adipocytes 3) primary human adipocytes and 4) MCF-7 human breast cancer cells.

2.3.6.1 MCF-7

The MCF-7 epithelial-like breast cell line was established in 1973 by the Michigan Cancer Foundation. The cells were harvested from the pleural effusion of a 69 year old Caucasian woman and immortalised (Holliday and Speirs, 2011). All MCF-7 cells were at passage 15 (P15) when received and were stored in liquid nitrogen until needed. Experiments were performed using passages P16 to P20 inclusive.

2.3.6.1.1 MCF-7 retrieval

A vial of frozen MCF-7 cells from liquid nitrogen stores was partially thawed (sides thawed but centre of vial frozen). The partially frozen cells were transferred gently into a 100 mm tissue culture plate and 12 mL of warm media (DMEM/F12 with 1% penicillin/ streptomycin and 10% FBS, Section 2.1.2) added dropwise onto the cells to thaw them fully. Media was changed the following day after the cells became adherent to plastic.

2.3.6.1.2 MCF-7 subculture

MCF-7 cell population density was maintained at 75% confluence to ensure cells continued to grow in their exponential growth phase. Once 75% confluence had been reached, the cells were split (typically 1:3). To split the cells, the plate was washed twice with 5 mL PBS warmed to 37°C to eliminate any FBS. The cells were lifted from plastic by using 2 mL trypsin-EDTA and incubated till

cell detachment (5% CO₂, 37°C). 10 mL of media was added to quench the trypsin, and a pipette used to aspirate the cells repeatedly to insure maximal detachment. The cells were then diluted 1:3 and seeded into new 100 mm culture plates with media.

2.3.6.1.3 MCF-7 cryopreservation

Each 100 mm plate (with cells at 75% confluence) were frozen in 2 mL of freezing media (DMEM/12 with 1% penicillin and 10% FBS with 10% DMSO).

The cells were trypsinised as described in Section 2.3.6.1.2, and centrifuged at 1,000 rpm at 4°C for five minutes. The supernatant was discarded and the pellet resuspended using 2 mL of freezing media. 1 mL of the resulting cell suspension was pipetted into a cryovial which was placed in a Mr Frosty for 12 hours at -20°C. The cells (in the Mr Frosty box) were then placed in a -80°C freezer for further gradual cooling, and vials were transferred into liquid nitrogen for long term storage.

2.3.6.2 3T3-L1 cells

The cell line 3T3-L1 are murine in origin and were first established as a cell line by the American Type Culture Collection (ATCC) in 1974 with limited details such as passage number (Zebisch et al., 2012). More recently, the European Collection of Cell Cultures (ECACC) has provided researchers with 3T3-L1 cells and is currently working on a few lines of these cells. Cells were obtained from existing stocks in the Bastie laboratory and were previously tested for differentiation. Cells were used for not more than five passages after thawing.

2.3.6.2.1 Retrieval and subculture

The retrieval and subculture procedures were the same as MCF-7 cells described in Section 2.3.6.1.1 and 2.3.6.1.2. The only difference compared to MCF-7 cells, is that 3T3-L1 cells are maintained in subculture at a lower confluence than MCF-7 cells.

2.3.6.2.2 Induction

Pre-adipocytes retain their proliferative abilities whilst undifferentiated. Mature adipocytes on the other hand, lose their ability to divide. For the duration of this study, pre-adipocytes were grown until they reached nearly confluence and kept at confluence before being induced to differentiate into mature differentiated adipocytes. The differentiation process was divided into two phases: an induction phase that triggers the early events of adipose differentiation and a maintenance phase that allows lipids to accumulate into forming mature adipocytes. The two phases are described below.

Working stock solutions of insulin, IBMX and dexamethasone were established: 0.17 nM insulin, 0.25 μ M dexamethasone and 0.5 mM IBMX. Media mixes of these stock solutions are displayed in Table 2.2 to give induction and maintenance differentiation media. For the induction phase of the adipocyte differentiation, the cells were maintained at confluence for 48 hours. This allowed the cells to exit their proliferative phase of cell growth, making them more sensitive to the differentiation process. After 48 hours at confluence, the cells were exposed to the induction media for four days (day zero to day four). Induction media was changed every 48 hours. Insulin is an anabolic hormone that induces adipogenesis and increases lipogenesis later in differentiation (Carobbio et al., 2017). Dexamethasone acts synergistically with insulin and also promotes adipogenesis via glucocorticoid receptors (Reusch et al., 2000, Rosen and Spiegelman, 2000). IBMX induces adipogenesis by inhibiting

phosphodiesterases by increasing intra-cellular cAMP (Reusch et al., 2000, Rosen and Spiegelman, 2000). Lastly, rosiglitazone (a member of the thiazolidinedione drug family) stimulates adipogenesis via activation of peroxisome proliferator-activated receptor gamma (PPAR γ) (Crossno et al., 2006) (Figures 1.3 and 1.4).

2.3.6.2.3 Maintenance

At the end of the induction phase, cells were switched to maintenance media (Table 2.2) with a change of media every 48 hours until day 12 when fully mature adipocytes were used for experimental purposes (Chapter 4).

2.3.6.3 Construction of *Per2-dLuc* expressing 3T3-L1 cells

Per2-dLuc 3T3-L1 cells were used in this study. Bioluminescence produced from these cells was used as a proxy for cell survival within HA hydrogels. Specific methods for the use of these *Per2-dLuc* 3T3-L1 cells are described in Chapter 4. The construction of a *Per2-dLuc* reporter line followed a protocol adapted from Ramanathan et al., 2012. The plasmids described were a kind gift from Professor Andrew Liu (University of Florida). Professor Andrew Liu (University of Florida) described a recombinant based methods for generating a P(*Per2*)-*dLuc* Lentiviral reporter gene where firefly *luciferase* (*dLuc*) is under the control of the mouse promoter Period 2 (*Per2*) (Liu et al., 2007). Stably expressed cell lines were generated in collaboration with Dr Robert Dallmann (University of Warwick).

Additive	Induction media (10 mL volume)	Maintenance media (10 mL volume)
<i>Insulin (1 µg/ mL)</i>	1 µL	1 µL
<i>IBMX (0.5 mM)</i>	10 µL	-
<i>Dexamethasone (0.25 µ)</i>	2.5 µL	-
<i>Rosiglitazone (5 µM)</i>	-	5 µL

Table 2.2 Additives for induction and maintenance media for adipocyte differentiation.

Luciferases from the North American firefly (*Photinus pyralis*) emit photons in a two-step process, using D-luciferin as their substrate and the co-factors Mg⁺⁺, adenosine triphosphate (ATP) and O₂ to produce luciferyl adenylate and by-product pyrophosphates. Luciferyl adenylate then reacts with O₂ to produce oxyluciferin, adenosine monophosphate (AMP) and photons of light of wavelengths 550 nm to 620 nm (Ugarova, 1989, Fraga et al., 2006, Mezzanotte et al., 2017).

The 3T3-L1 cells were grown in 100 mm culture plates and infected with the lentiviral supernatant produced. Once confluent, the cells were split again and incubated overnight until adhesion. Blasticidin (the selection antibiotic) was added to DMEM/F12 media at 10 µg/ml for five days (changing media every 2-3 days) to select for stably transduced cells. At Day 5, the cell media was changed to standard DMEM/F12 media. For experimental cells and the visualisation of luciferase expression, cells were incubated in the presence of 1 mM luciferin and incubated in a LumiCycle luminometer, and light emission was recorded over three days.

2.3.6.4 Primary murine pre-adipocytes from FVB-Tg (CAG-luc-eGFP) mice

All experiments were conducted with license approval from the Home Office, UK, and approved by the Animal Welfare and Ethical Review Body at the University of Warwick. Mice were provided food and water *ad libitum*. Ambient humidity and temperature were kept at 50% and 21°C, respectively.

Primary adipocytes from mice constitutively expressing firefly luciferase directed by the human cytomegalovirus immediate early promoter enhancer with chicken beta-actin/ rabbit beta-globin hybrid promoter (CAG) (Cao et al., 2004, Sheikh et al., 2007) were acquired surplus to need as a kind gift from Dr Erin Greaves (University of Warwick). These FVB-Tg (CAG-luc-eGFP)L2G85Chco/J mice were initially purchased from The Jackson Laboratory, Farmington, CT (JAX

stock number 008450). The mice were bred and maintained in specific pathogen free facilities at the University of Warwick, UK. Wild-type FVB/N mice were purchased from Charles River (Wilmington, MA) and were used as recipients of CAG-luc-eGFP adipose tissue and HA hydrogel (see Chapter 5).

Adults male and female CAG-luc-eGFP mice aged 12 weeks old were used. All mice were culled using a Schedule 1 method, i.e., carbon dioxide poisoning.

2.3.6.4.1 Adipose tissue harvest, processing, and primary cell isolation

CAG-luc-eGFP were sacrificed and sprayed with 100% ethanol to neutralise pathogens on the fur of the animals. The abdominal cavity was opened using a pair of sterile scissors and gonadal adipose tissue was dissected (Figure 2.1 and Figure 2.2A) using a second pair of sterile scissors.

A 1 g aliquot of dissected adipose tissue was placed in a 100 mm tissue culture plate with 10 mL of PBS supplemented with 1% penicillin/ streptomycin (Figure 2.2B). Macroscopically, small blood vessels were removed by eye using two sterile pairs of forceps. The tissue was then transferred into a fresh 100 mm plate with 10 mL of fresh PBS with 1% penicillin/ streptomycin, before being minced into 2-3 mm pieces. The pieces were then transferred into a 50 mL sample tube with PBS. The pieces in PBS were then centrifuged at 500 g for 30 seconds and the supernatant removed to reduce the number of red cells in the tissue (Figure 2.2C). The adipose tissue was re-suspended in a further 10 mL of PBS with 1% penicillin/ streptomycin. Tissue centrifugation and supernatant aspiration was repeated twice more to ensure a cleaner tissue.

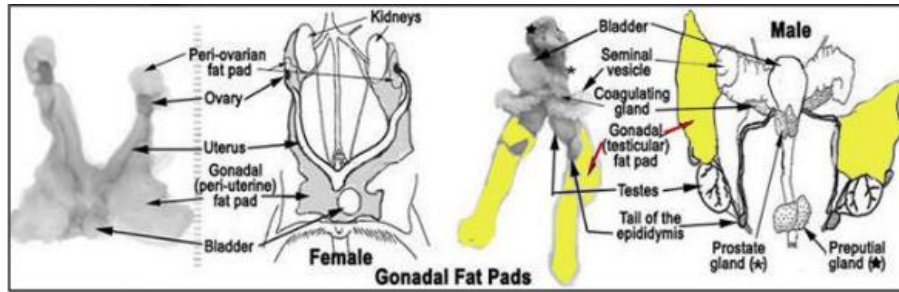


Figure 2.1 Anatomy schematic of a mouse after laparotomy. Peri-gonadal adipose tissue is highlighted in yellow for male and female mice for dissection (Cook M et al.,1965).

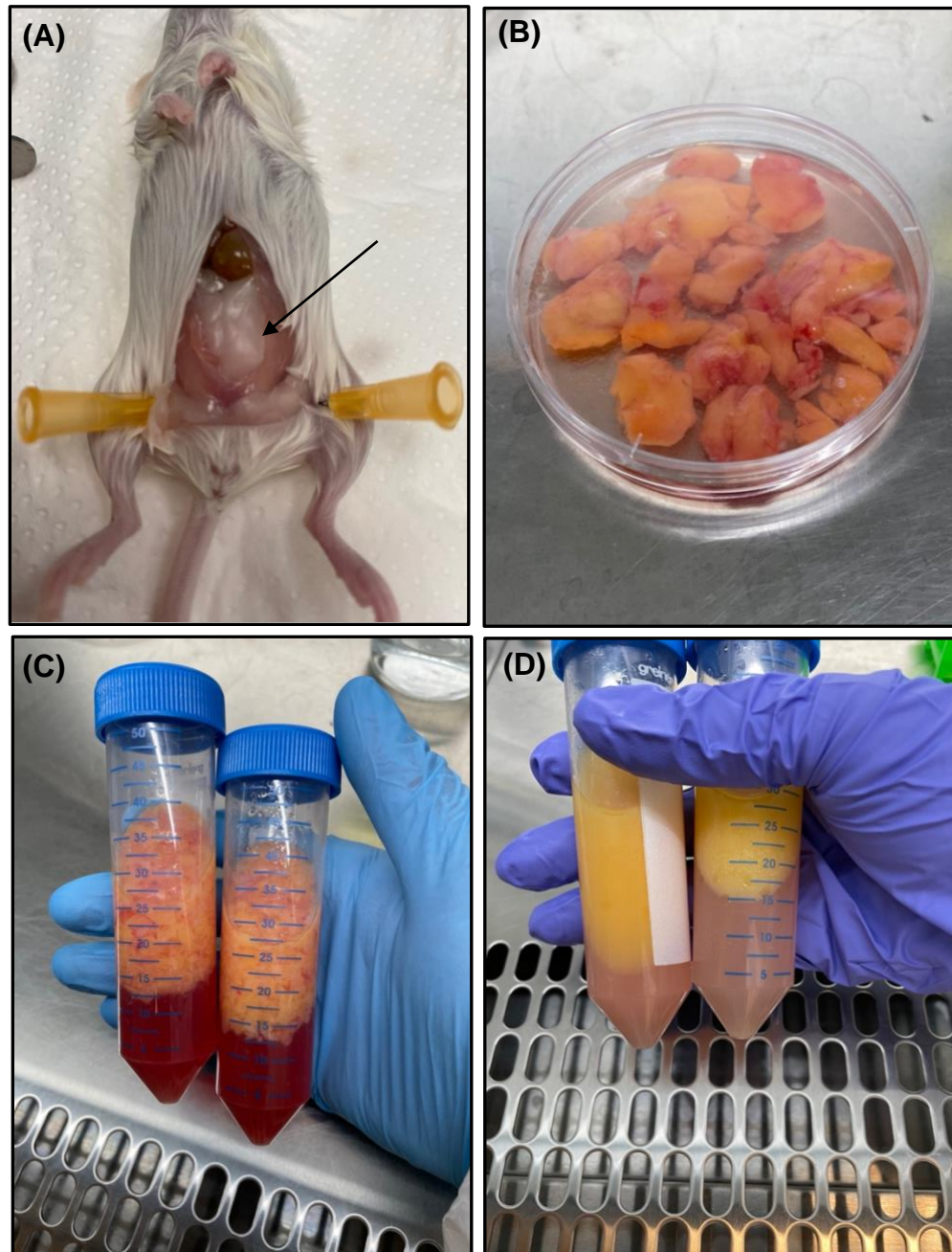


Figure 2.2 Representative images of murine gonadal adipose tissue isolation. **(A)** Abdominal view post laparotomy, with gonadal adipose tissue labelled. **(B)** Gonadal adipose tissue after excision from numerous mice in 10 mL PBS. **(C)** Minced adipose tissue with blood-tinged PBS (lower phase) before centrifugation. **(D)** Adipose tissue after digestion.

The tissue was transferred into a fresh 50 mL sample tube and 100 μ L Liberase (1 μ g/100 μ L) was added to the tissue along with 250 μ g of bovine serum albumin. The resulting suspension was digested by incubating at 37°C under agitation for 30 minutes (Figure 2.2D). After digestion, the resulting suspension was passed through 250 μ m nylon mesh into a fresh 50 mL sample tube, with intermittent washing of the mesh with 5 mL warmed PBS to ensure maximum cell retention.

The suspension was then centrifuged at 2,500 rpm for ten minutes to form a pellet that contains stroma vascular fraction (SVF). The supernatant constituted two discrete phases: an upper ring with free lipids and a middle phase with mature adipocytes. Both phases of the supernatant were discarded. The SVF was resuspended in red cell lysis buffer for five minutes and centrifuged again at 2500 rpm for ten minutes to remove red blood cells. The resulting pellet was resuspended in 10 mL DMEM/12 with 1% penicillin and 10% FBS and plated in a 10 cm culture plate on day zero.

2.3.6.4.2 Subculture, induction, and maintenance

The 100 mm plate media with cells attached to the plastic was changed on day one post isolation. Once cells reached 70% confluence, they were split (typically 1:3). To split the cells, the plate was washed twice with 5 mL PBS warmed to 37°C to eliminate any FBS.

The cells were lifted from plastic by using 2 mL trypsin-EDTA and incubated till cell detachment (5% CO₂, 37°C). 10 mL of media was added to quench the trypsin, and a pipette used to aspirate the cells repeatedly to insure maximal detachment. The cells were then diluted 1:3 and seeded into new 100 mm culture plates with media.

2.3.6.5 Primary human pre-adipocytes

Primary human pre-adipocytes were harvested from patients (surplus to clinical need). Research consent was attained from patients who were due to undergo liposuction and autologous adipose tissue transfer for breast reconstruction at University Hospitals Coventry and Warwickshire (UHCW) as per good clinical practice guidelines set out by the Home Office (ethics reference 18/SC/0180).

The Arden Tissue Bank (ATB) based at UHCW received lipoaspirate from theatre and were responsible for sample record keeping and issue of the sample for research.

2.3.6.5.1 Liposuction, processing, and primary cell isolation

In theatre, after general anaesthetic, a solution of 500 mL saline with 0.5 mL of 1:1000 adrenaline was infiltrated into anterior abdominal wall adipose tissue in a multiplanar manner. The purpose of the infiltration solution was to expand the adipose tissue subcutaneous plane, making harvest easier and to limit blood loss via the action of adrenaline constricting blood vessels.

Lipoaspirate was attained by a low suction (20 mmHg) 3 mm metal cannula through small abdominal incisions from the previously infiltrated anterior abdominal wall adipose tissue after 10 minutes. The lipoaspirate was processed via the Filtron Tissue-Trans system (Ideal Medical Solutions, Epsom, UK).

The system constituted a fine mesh-lined receptacle through which freshly lipo-sucked adipose tissue passes. Adipose tissue globules are retained within the mesh chamber, and infiltration fluid and blood were suctioned out of the chamber (Figure 2.3). When the abdominal adipose tissue subcutaneous compartment was emptied, the suction was turned off, and the processed lipoaspirate extracted from the Filtron Tissue-Trans system into 10 mL Luer lock syringes (Figure 2.4).

2.3.6.5.2 Primary cell isolation, subculture, induction, and maintenance

Isolation of primary human pre-adipocytes using processed lipoaspirate was identical to the protocol described for murine primary pre-adipocytes in 2.3.6.4.1. The only difference of note is the non-requirement to mince the adipose tissue into 1-2 mm pieces as the processed adipose tissue from the Filtron Tissue-Trans system is less than 2 mm in size (Figure 2.4).

Subculture, induction and maintenance of primary human pre-adipocytes was also identical to the protocols used for murine primary pre-adipocytes, described in Section 2.3.6.4.2.



Figure 2.3 Schematic of the Filtron Tissu-Trans System. Adipose tissue harvested using a 3 mm metal cannula under low suction (20 mmHg) entered the System and passed through a fine mesh located within the cannister. Adipose tissue globules were retained within the mesh bag and waste exited the cannister (IdealMedicalSolutions, 2021).



Figure 2.4 Two 10 mL Luer lock syringes of processed lipo-aspirate. Lipo-aspirated adipose tissue is less than 2 mm in size and has already passed through one stage of purification in the Filtron Tissue-Trans system.

2.3.7 Oil Red O staining

Cells with intra-cellular lipid droplets can be better visualised microscopically and for semi-quantification by staining with Oil Red O (ORO). ORO is a lysochrome which stains lipids an orange-red colour.

A 0.5% stock solution was prepared by dissolving 500 g ORO powder in 100 mL isopropanol by constant vortex for ten minutes. The solution was allowed to sit for ten minutes and vortexed once more for 15 minutes. A working solution was made using three parts ORO stock solution and two parts distilled water. The resulting solution was mixed and allowed to rest for 15 minutes before being filtered through Whatman paper number one (GE Healthcare, New York, NY).

To fix, the cells were washed twice in warmed PBS. The PBS was discarded and 1 mL of formalin was added to each well in a given six well plate to just cover the cells and incubated for one hour. Formalin was aspirated and the wells washed twice in room temperature distilled water. To stain the cells, a 60% isopropanol solution in distilled water was prepared and 2 mL added to each well and incubated for ten minutes at 37°C and aspirated. The ORO working solution was added (1.5 mL per well) and incubated at room temperature for 30 minutes. The ORO solution was carefully removed, and the cells washed in distilled water several times until no excess stain was seen.

2.3.8 *Per2-dLuc* 3T3-L1 and CAG-luc-eGFP primary mouse pre-adipocyte imaging

Representative and routine light microscopy of given cells were undertaken using the Leica light microscope and EVOS phased/ brightfield microscope (Leica, Wetzlar, Germany).

Per2-dLuc 3T3-L1 and CAG-luc-eGFP primary mouse pre-adipocytes (2.3.6.3 and 2.3.6.4) produced light after D-luciferin (1 mM) was added to the media.

Photons were measured in a reproducible way as a proxy for cell survival in the Alligator bioluminescence detector incubator. The incubator is a light-tight enclosure for sensitive optical recordings, allowing serial measurements over several days. The roof of the Alligator houses the hypersensitive camera (EM-CCD, Hamamatsu Photonics, Welwyn Garden City, UK). Micro-Manager, an open-source programme, runs the assembly. Images were taken at hourly intervals with a photon gain of 12. Total exposure per image was 60 minutes.

2.3.9 FIJI programme image analysis

Images taken by the Alligator system were analysed by FIJI in a reproducible and quantitative manner, allowing light intensity to be compared between tissue culture plates.

A bespoke macro programme was written to run on FIJI in the Computing and Advanced Microscopy Development Unit (CAMDU) based at Warwick Medical School. Development of this macro and image analysis of Alligator photographs is further described in Chapter 4.

2.3.10 qPCR analyses

Gene expression quantification was performed in cell populations after differentiation into mature adipocytes in varying concentrations of HA hydrogels (see Chapter 4.8). RNA was first isolated, then converted to cDNA by reverse transcription. Detection and quantification of the gene of interest was done by quantitative polymerase chain reaction (qPCR).

2.3.10.1 RNA isolation

Cells were collected and lysed in TRIzol (0.4 mL/ well in six well plates). 250 µL of chloroform /mL was added and samples were vortexed for 15 seconds. The samples were centrifuged for five minutes at 10,000 rpm which resulted in three layers. The clear RNA phase was then aspirated and 550 µL isopropanol/ 1mL TRIzol added and mixed. The sample was then centrifuged at 12,000 rpm in a refrigerated centrifuge set at 4°C for 20 minutes. The isopropanol supernatant was poured off and 1 mL 75% ethanol in DEPC treated water added. After mixing gently, the sample was centrifuged at 9,500 rpm for five minutes. The supernatant was poured off and the resulting pellet left to air dry. 30 µL of DEPC treated water was added to the pellet. The absorbance of the resulting RNA was then measured at 260 nm and 280 nm using a Nanodrop to assess the purity of the samples and only samples with a 260/280 ratio greater than 1.8 were used. A measurement at 230 nm was also performed to determine the presence of other contaminants.

2.3.10.2 Reverse transcription

Reverse transcription (RT) is the process of synthesising complimentary DNA using RNA isolated in 2.3.10.1 as a template using a RNA dependent DNA polymerase reverse transcriptase (RTase). This process is dependent on primers annealing to the isolated RNA, acting as a starting point for RTase to add complimentary nucleotides to form cDNA strands (Applied Biosystems High-Capacity cDNA Reverse Transcription Kit, Thermo Fisher Scientific, Waltham, MA).

For each specimen, 20 µL of nuclease free water was added to each isolated RNA sample tube and 4 µL of SuperScript™ IV VILO Master Mix. Samples were matched to a control without any RNA using 4 µL of SuperScript™ IV VILO Control. Primers were then annealed during incubation for ten minutes at 25°C. Reverse transcription by RTase resulted through incubation at 50°C for

ten minutes. The RTase enzyme was then inactivated by denaturation by incubation at 85°C for five minutes. Samples were stored at -20°C for up to one week or -70°C for long term storage.

2.3.10.3 Polymerase chain reaction

Real-time quantitative polymerase chain reaction (RT-qPCR) is a valuable method by which the magnitude of gene expression can be determined by a fluorescence mediated quantification of DNA.

Double stranded complimentary DNA synthesised from extracted RNA in Section 2.3.10.2 was denatured, allowing the double helix structure to separate into individual unpaired strands. The region of interest (specific genes) was identified by annealing primers to either end, flanking the region of interest. A DNA polymerase extends each primer from the 3' end using nucleotides for each corresponding DNA base acting as a template. Numerous cycles of this amplification are conducted, resulting in an exponential rise of DNA replicates. The resulting terminal amount of replicated DNA is proportional to the cDNA synthesised initially.

TaqMan (ABI Applied Biosystems, Waltham, MA) RT-qPCR was performed for quantification of mRNA for ribosomal protein L7 (RPL-7), glyceraldehyde-3-phosphate dehydrogenase (GAPDH), cluster of differentiation 36 (CD36), peroxisome proliferator-activated receptor gamma (PPAR γ), adipocyte protein 2 (aP2, in human cells) and fatty acid binding protein P4 (FABP4, in murine cells), as shown in Table 2.3. Further details are described in Chapter 4.

A

Gene Name	Reference
CD36	Mm00432403_m1
PPAR- γ	Mm00440940_m1
FABP4	Mm00445878_m1
GAPDH	Mm99999915_g1
RPL7	Mm02342562_gH

B

Gene Name	Reference
CD36	Hs00354519_m1
PPAR- γ	Hs01115513_m1
AP2	Hs00900330_m1
GAPDH	Hs_02758991_g1
RPL7	Hs02596927_g1

Table 2.3 TaqMan assay references for (A) mouse adipocyte and housekeeping genes and (B) human adipocyte and housekeeping genes. RPL 7 and GAPDH are housekeeping genes. CD36, PPAR- γ , FABP4 and AP2 are mature adipocyte gene markers.

2.3.11 Murine *in vivo* experiments

Minced CAG-luc-eGFP adipose tissue was injected in the subcutaneous plane into wild-type FVB/N strain mice under general anaesthesia using isofluorane (Merck Scientific, Kenilworth, NJ) with various volumes of HA hydrogel via 23-gauge sterile needles.

Mixing of HA hydrogel and adipose tissue was done in a closed sterile system using two 2 mL syringes (one with gel constituents and the other with CAG-luc-eGFP adipose tissue) and a three-way tap (Figure 2.5). To mix, via the action of the plunger, the contents of one syringe was pushed through the three-way tap and the process repeated. Specific methods are described in Chapter 5.

2.3.12 Statistical analysis

Statistical analysis was undertaken using Microsoft Excel (version 16.52, Microsoft, Richmond, VA) or GraphPad Prism (GraphPad Software, San Diego, CA). Data was compared using a one-way/ post hoc test ANOVA or ANOVA with repeated measures were appropriate, Student's t-test, followed by *ad hoc* two sample Mann Whitney U-test (non-parametric). Results were expressed as mean and standard error of the mean (s.e.m) with a *p* value <0.05 to attain significance.



Figure 2.5 Three way tap mixing system. HA hydrogel constituents were loaded in one syringe, and minced CAG-luc-eGFP adipose tissue in the other syringe. Materials were then transferred between each syringe via the action of the three-way tap (red dot) which mixed the materials until homogenised. The left Eppendorf shows 1 mL HA-ALD solution and the right, 1 mL HA-HYD solution before loading into the syringe.

Chapter Three: Synthesis and Mechanical Properties of the Novel Hyaluronic Acid Hydrogel

3.1 Introduction and selection of hyaluronic acid for modification

Breast cancer constitutes a significant burden on patients and the National Health Service, with over 16, 000 mastectomies each year (CRUK, 2020). Autologous adipose tissue transfer as a method for breast reconstruction is one of the most commonly used procedures for reconstruction, improving the health-related quality of life that patients receive (Harcourt and Rumsey, 2001). Autologous adipose grafting has variable take, with graft survival after three years being as poor as 15% of the original volume grafted (Yu et al., 2015).

To explore the hypothesis that a hydrogel can augment adipocyte survival, it was first necessary to select a hydrogel material that satisfied the selection criteria (described later in this Section). Selection was important to ensure biocompatibility, be Food and Drug Agency (FDA) approved, be safely modified to not be cell toxic, biodegradable by endogenous enzymes and to be form stable to resist deformative forces and robust enough to withstand injection.

Hyaluronic acid (HA) satisfied most of these criteria as a component of the extracellular matrix: it is easily synthesised and degraded by endogenous tissue hyaluronidases and naturally contributes to tissue mechanical and viscoelastic properties (Mow et al., 1984, Ambrosio et al., 1999). HA is also used in the commercial cosmetic industry for facial feature augmentation and has a proven clinical track record (Patrick Jr et al., 1999).

However, endogenous (unaltered) HA did not have the properties of being form stable and did not exhibit the qualities of being able to be injected through a needle without losing its mechanical properties by not being able to self-heal, needing modification to be clinically utilised (Wang et al., 2018a). The desired modified HA hydrogel needed to be of low enough viscosity to allow extrusion through a needle and following gelation, be mechanically more robust after being

delivered- resisting deformative natural tissue forces to preserve its shape. A gel with a high viscosity may subject adipocytes to high shear forces whilst being extruded, reducing overall cell viability (Tirella et al., 2012, Malda et al., 2013). A gel with fewer cross-links may therefore be less viscous and also allow for diffusion of nutrients to metabolically active cells (Tirella et al., 2012, Malda et al., 2013). Furthermore, the HA hydrogel needed to exhibit shear thinning; being able to break apart cross links during extrusion and self-healing with force cessation. To this end, the natural tissue HA needed to be modified to exhibit these properties described (Wang et al., 2018a).

Wang et al., 2018a modified HA hydrogels using the hydrazone bond- a dynamic covalent bond between nucleophilic hydrazine ($R-NHNH_2$) and electrophilic aldehyde ($R-CHO_2$) (Figure 1.6 and 1.7). Variants of these bonds in hydrogels have been previously interrogated for their self-healing and shear-thinning characteristics (Yeo et al., 2006, Ito et al., 2007). These gels have also been shown to offer protection of cells during extrusion (Ma et al., 2020). However, the long term sequelae in terms of cell viability and sustainability of adipocytes in an extracellular construct has yet to be determined fully (Choi et al., 2010).

3.1.1 Chapter aims

This Chapter outlined the development a protocol for reliable synthesis of a functionalised HA hydrogel made from a combination of HA aldehyde (HA-ALD) and HA hydrazine (HA-HYD). HA-ALD and HA-HYD was characterised using nuclear magnetic resonance (NMR) spectroscopy and the viscoelastic properties and stiffness of gel was attained by rheology for varying gel concentrations.

The gel degradation and swelling characteristics were ascertained in phosphate buffer saline (PBS), culture medium and various tissue-mimicking endogenous hyaluronidase concentrations.

3.2 Hyaluronic acid synthesis with hydrazine and aldehyde groups

Functionalisation of hyaluronic acid with hydrazine and aldehyde groups is described in Chapter 2 (Section 2.3.1). Synthesis of HA with hydrazine and aldehyde groups was based on previous literature Wang et al., 2018a. Minor alterations were made to improve yields of the synthesised HA products described below.

Chemicals and compounds for HA synthesis are described in Section 2.1.3. Functionalisation of HA with hydrazine and aldehyde groups are described in Section 2.3.1. For HA-HYD synthesis, the substitution in using MES solution rather than hydroxybenzotriazole dissolved in a DMSO/H₂O mixture as the primary reaction solvent was made as the hydrazine groups would have better affinity for hyaluronic acid side chains, thus increasing the yield of the product (Figure 3.1a). The increase in yield from 20% to ~77% is described in Section 3.2.1.

After synthesis of HA-HYD, the increased dialysis duration from three to five days was done to better eliminate unreacted toxic chemicals. The product was lyophilised and stored at -20°C for use. No changes were made to the synthesis protocol of HA-ALD described in 2.3.1.2 and figure 3.1b (Wang et al., 2018a).

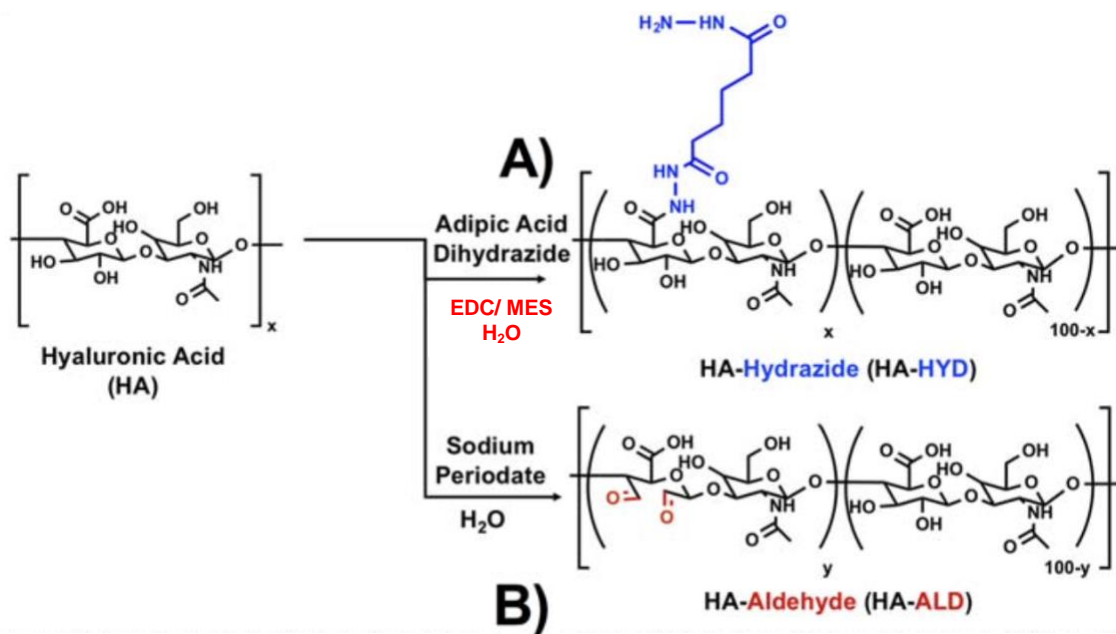


Figure 3.1 Synthesis schematic of A) HA-HYD and B) HA-ALD. HA-HYD is synthesised through amidation between carboxyl of HA and hydrazines of adipic acid dihydrazide via the solvent solution *N*-(3-Dimethylaminopropyl)-*N'*-ethylcarbodiimide hydrochloride (EDC)/ 2-(*N*-morpholino)ethanesulfonic acid (MES) rather than in hydroxybenzotriazole dissolved in a DMSO/H₂O mixture. Adapted from Wang et al., 2018.

3.2.1 Nuclear magnetic resonance (NMR) spectroscopy yields of synthesized products

As described in 2.3.3, the synthesised HA-HYD product was quantified and characterised using NMR spectroscopy. Wang et al., 2018a conferred a 30% functionalisation of HA disaccharide repeats with hydrazine groups and 20% modification of disaccharide repeats with aldehyde groups.

Hydrazide modification was quantified by NMR spectroscopy by integrating the butyl linker (8H, $\delta = 2.1-2.5$ ppm, 1.5-1.8 ppm) relative to the methyl of HA (3 H, $\delta = 2.0$ ppm) and determined to be ~77% of disaccharide repeats of HA, which is higher than the 20% functionalization described by Wang et al., 2018a (Figure 3.2). This may be due to EDC being dissolved in 50 mL MES rather than solution of hydroxybenzotriazole as used in Wang et al., 2018a.

Due to the COVID-19 pandemic, HA-ALD was not characterised due to the drastic reduction of key chemicals commercially available. The methods (Section 2.3.1.2) used to synthesize HA-ALD were identical to the protocol described by Wang et al., 2018a.

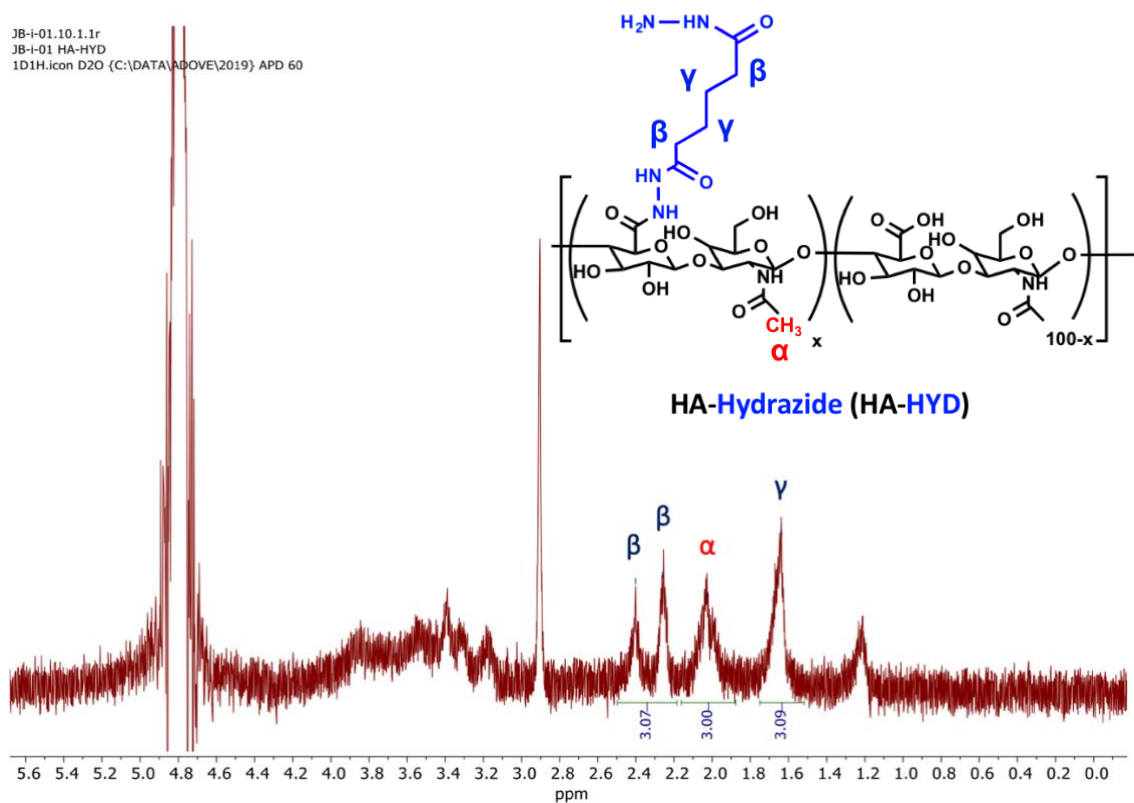


Figure 3.2 NMR spectrum of HA-HYD. Hydrazide modification was quantified integrating the butyl linker in (8H, 2.1-2.5 ppm, 1.5-1.8 ppm) relative to the methyl of HA in red α (3 H, 2.0 ppm). Corresponding hydrazine blue β and γ side chains were also apparent at 3.07ppm and 3.09ppm respectively. These were determined to be ~77% of disaccharide repeats of HA. Schematic of molecular chains (inset) (Wang et al., 2018).

3.3 Characterisation of gel with rheology and terminology

Rheology was performed to ascertain the mechanical behavioural characteristics of various concentrations and ratios of HA-HYD:HA-ALD hydrogels to reliability. Rheology was used specifically to determine the viscosity and elasticity of HA hydrogels rather than absolute strength of the material. Hydrogels, as crosslinked, swollen networks typically have a threshold over which they behave in a liquid manner as the limits of their viscosity and elasticity are reached (Rodell et al., 2013). These characteristics were described as shear stress and shear strain (analogous to shear rate). Viscosity (η) is a function of shear stress (σ) and shear strain (γ) shown in Equation 3.1.

Shear stress is the force applied to a gel or fluid to induce shear flow (failure) and is applied in a circular manner in a rheometer, where shear flow is the velocity gradient applied between surfaces that are moving, i.e., the relative movement of a hydrogel between the two plates of a rheometer. As seen in Equation 3.1, shear strain describes the rate of strain on the hydrogel system.

Shear stress and shear strain are of particular relevance as they are the functions used to describe the hydrogels behaviour and the identification of the point at which the hydrogel becomes a liquid with increasing forces applied. However, the relationship between the stress and strain of a given hydrogel system can be more accurately described by the storage modulus (G') and loss modulus (G''). These moduli factor the stress and strain, as well as the phase angle (δ) shown in Equation 3.2. The phase angle refers to the difference between two rheometer oscillating traces for each of strain and stress plotted on a graph where the x axis is time and the y axis amplitude (Figure 3.3). If the storage modulus is above the loss modulus for a given time during rheological examination, the substance can be said to be a gel. However, if the loss modulus is above the storage modulus, the substance can be said to have more properties of a liquid (Chambon et al., 1986).

$$\text{Shear stress } (\sigma) = \frac{\text{Force}}{\text{Surface area}} = \frac{F}{A}$$

$$\text{Shear strain } (\gamma) = \frac{\text{Velocity}}{\text{Distance}} = \frac{V}{h}$$

$$\text{Viscosity} = \frac{\text{Shear stress}}{\text{Shear strain}}$$

Equation 3.1 Shear stress, shear strain and viscosity equations.

Shear stress and shear strain were used to describe the mechanical characteristics of various concentrations and ratios of HA-HYD:HA-ALD hydrogels (Anton-Paar, 2021).

$$\text{Storage modulus } (G') = \frac{\sigma}{\gamma} \cos\delta$$

$$\text{Loss modulus } (G'') = \frac{\sigma}{\gamma} \sin\delta$$

Equation 3.2 **Storage and loss moduli equations.** Mechanical characteristics are used to describe the storage and loss moduli of a given hydrogel system. The substance can be said to be a gel if the storage modulus is above the loss modulus for a given time. The substance can be said to have more properties of a liquid if the loss modulus is above the storage modulus. Storage modulus (G'), loss modulus (G''), shear stress (σ), shear strain (γ) and phase angle (δ) (Anton-Paar, 2021).

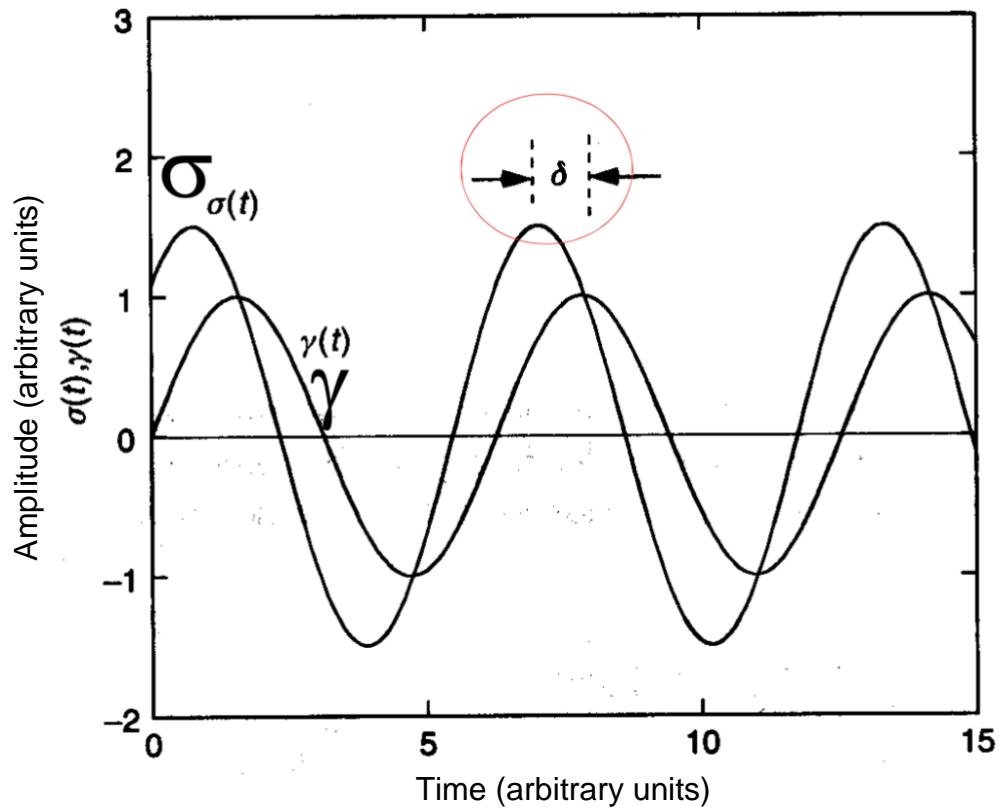


Figure 3.3 Illustration of phase angle calculation. The phase angle (δ) circled in red, refers to the difference between two rheometer oscillating traces for each of shear stress (σ) and shear strain (γ) plotted on a graph where the x axis is time and the y axis amplitude in arbitrary units (Ibarburu, 2006)

3.3.1 Rheology methods

Rheology was performed as described in Section 2.3.4 using various gel concentrations and ratios of HA-ALD:HA-HYD based on Table 2.1. Gels based on 1.5% and 3% concentrations compositions did not hold form after gelation, and were therefore not suitable for further interrogation of all HA-ALD:HA-HYD ratios, with only 1.5% 1:1 and 3% 1:1 ratios interrogated (Figure 3.4). Gel ratios based on 6% concentrations were therefore more suitable (Table 3.1), with all 6% ratios not exhibiting flow. Therefore, not all gel percentages and ratios were subjected to full rheological interrogation.

Time sweeps were performed in triplicate over ten minutes with gelation *in situ* on the 50 mm plate. The storage modulus and loss modulus were recorded at one second intervals (i.e., 600 time points over ten minutes) with a set amplitude at 0.5% and frequency 10 rad/s as standard. Time sweeps are performed to ascertain the gels' stability with a constant amplitude and frequency, and to measure the speed of gelation, when both HA-HYD and HA-ALD are added to the 50 mm rheology plate and the sweep started immediately.

Frequency sweeps were also performed in triplicate for each gel composition, with angular frequencies from 100 rad/s to 0.1 rad/s with storage modulus being recorded for each of 16 time points. Amplitude was set at 0.5% for all time points. This was performed to establish the point at which the gel failed with increasing frequency oscillation, with constant amplitude and over a set time.

Amplitude sweeps were performed in triplicate for shear strain values from 0.01 – 100% for a fixed frequency of 10 rad/s. Storage modulus and loss modulus values were recorded for each shear strain value over 25 points. This was performed to establish the point of failure where the gel behaved more as a liquid with increasing amplitudes of force with a constant frequency and over a set time.

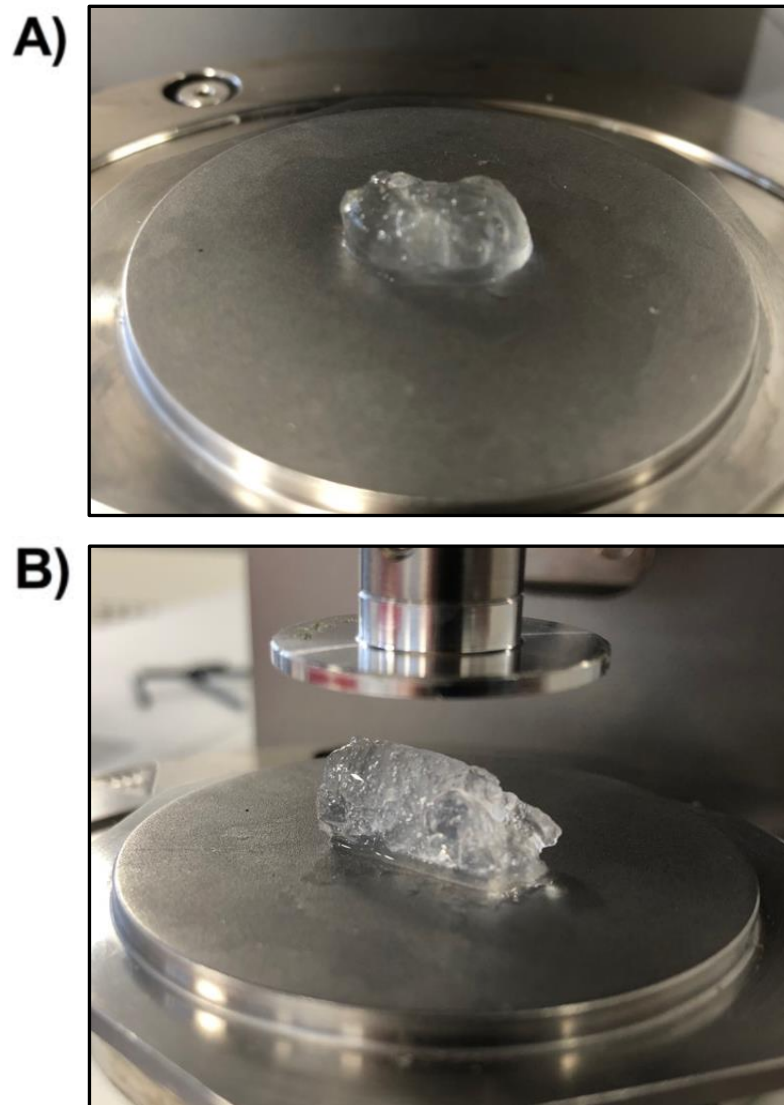


Figure 3.4 Representative images of (A) 1.5 % and (B) 6% HA-HYD:HA-ALD 1:1 ratio gels.

HA-ALD:HA-HYD ratios based on 6% concentration	Milligram weights for hydrogel after PBS reconstitution to make up 2 mL volume
1:1	30 mg:30 mg
1.5:1	45 mg:30 mg
1:1.5	30 mg:45 mg
2:1	60 mg:30 mg
1:2	30 mg:60 mg

Table 3.1 HA-HYD:HA-ALD ratios based on 6% gel composition for rheology. HA-ALD and HA-HYD constituents were dissolved separately in 1 mL PBS and then mixed together *in situ* on the rheometer plate.

3.3.2 Rheology results

A pilot frequency sweep of 1.5%, 3% and 6% gels in a 1:1 HA-ALD:HA-HYD ratio was performed as described in Section 2.3.4 and 3.3.1. The results are displayed in Figure 3.5. The purpose of this was to provide a direct comparator of 1:1 ratio gels of all three concentrations. This pilot sweep was used to calibrate the rheometer.

The 1.5% concentration gel (green trace) demonstrated the lowest values of G' and G'' compared to 3% and 6%. This suggested that the 1.5% gel is the least stiff of all three concentrations. G' and G'' values of the 3% gel were next stiff (grey traces), followed by 6% gel (red trace).

Of note, is that G' is above G'' for all three traces suggesting that all three concentrations are behaving as gels, up to the transection of G' and G'' where the gels are behaving more as liquids as the frequency approached 100 rad/s. This can be termed the transition from a viscoelastic solid to a viscoelastic liquid. Varying the frequency and keeping the amplitude and time points the same gives an indication of the interactions within a given material, giving rise to the various differences in stiffness and fluidity described above.

The gelation point is the transition point whereby $G' < G''$ before the gelation point and $G' > G''$ thereafter (i.e., a cross in the G' and G'' lines at the start of the graph at ~ 0.1 rad/s). As shown in Figure 3.5, all three G' and G'' traces were parallel from 0.1 rad/s to just after 10 rad/s indicating a stable gelation characteristic for 1.5%, 3% and 6% gel concentrations.

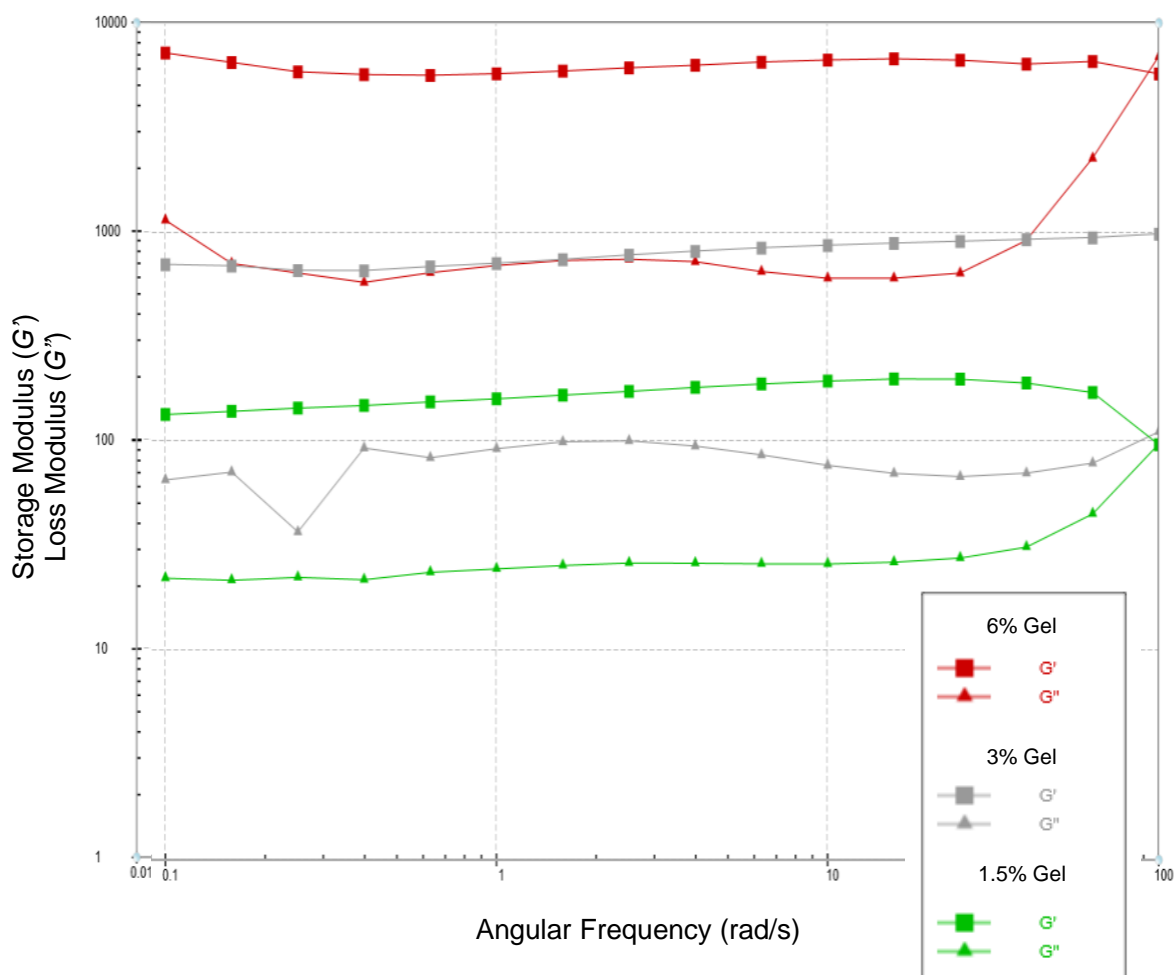


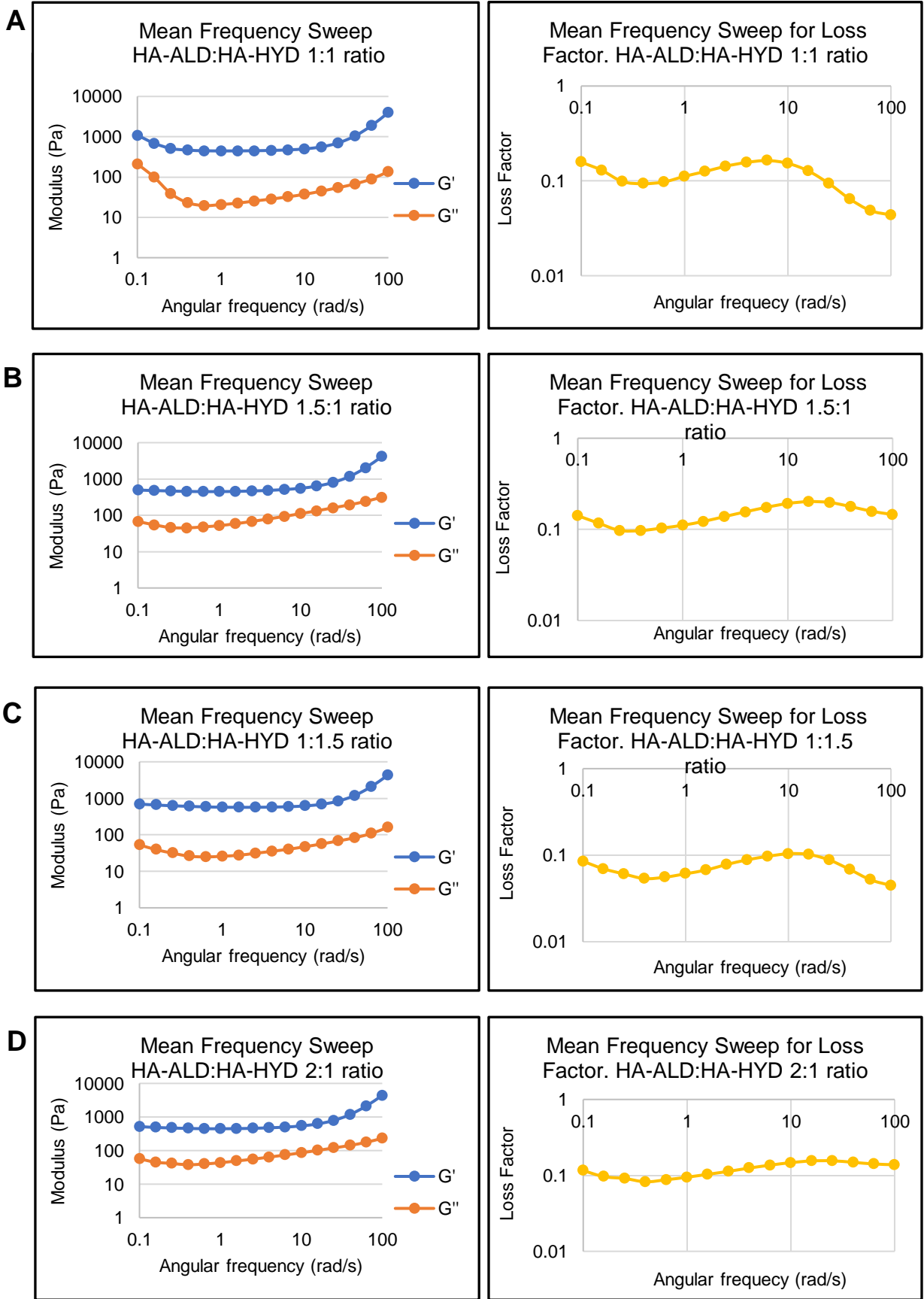
Figure 3.5 Frequency sweep of 1.5%, 3% and 6% concentrations of HA hydrogel in a HA-ALD:HA-HYD 1:1 ratio, showing storage (G') and loss modulus (G'') with increasing frequency. Square data points represent G' and triangle G'' . Insert: green data points describe 1.5%, grey data points 3% and red data points 6% gel concentrations ($n=3$ separate experiments for all displayed data).

Frequency, amplitude and time sweeps were undertaken in triplicate as described in 2.3.4 and 3.3.1 for a 6% HA hydrogel concentration for each of five HA-ALD:HA-HYD ratios described in Table 3.1

Figure 3.6, panels A-F shows the mean G' and G'' frequency sweep traces for 6% gel concentrations for the HA-ALD:HA-HYD ratios 1:1, 1.5:1, 1:1.5, 2:1 and 1:2. Here, the frequency force applied to the hydrogel is increasing, with constant amplitude and time points. Additionally, graphs of the loss factor in relation to increasing frequency are displayed. The loss factor is merely a function of the phase angle between G' and G'' (Figure 3.3). The loss factor ($\tan\delta$) is used to describe the liquid/gel transition point, also known as the gel point. It refers to the character of the sample, and the change from liquid to solid or vice versa. A liquid is ideally viscous if $\tan\delta$ is 100, whilst a solid is ideally elastic if $\tan\delta$ is 0.01 (Anton-Paar, 2021).

For each gel ratio using a 6% concentration, G' was consistently above G'' for all ratios, indicating gel characteristics (Figure 3.6, panels A-E). Of note, is that the gelation point for all ratios was not captured, with no transection of G' and G'' traces at the start of the frequency sweep. None of the ratios reached failure at 100 rad/s, retaining gel characteristics at the higher frequencies. The mean loss factors remained at ~ 0.1 for all gel values, indicating a similar gel character for all ratios (Figure 3.6, panels A-E).

Figure 3.6, panel F shows cumulative mean G' values for all 6% concentration gel ratios. All gel ratios followed a similar path throughout the frequency sweep, with an increase of G' after 10 rad/s. This suggests an ongoing maturation of covalent bonds between HA-ALD and HA-HYD, which results in a stiffer gel as the frequency progresses.



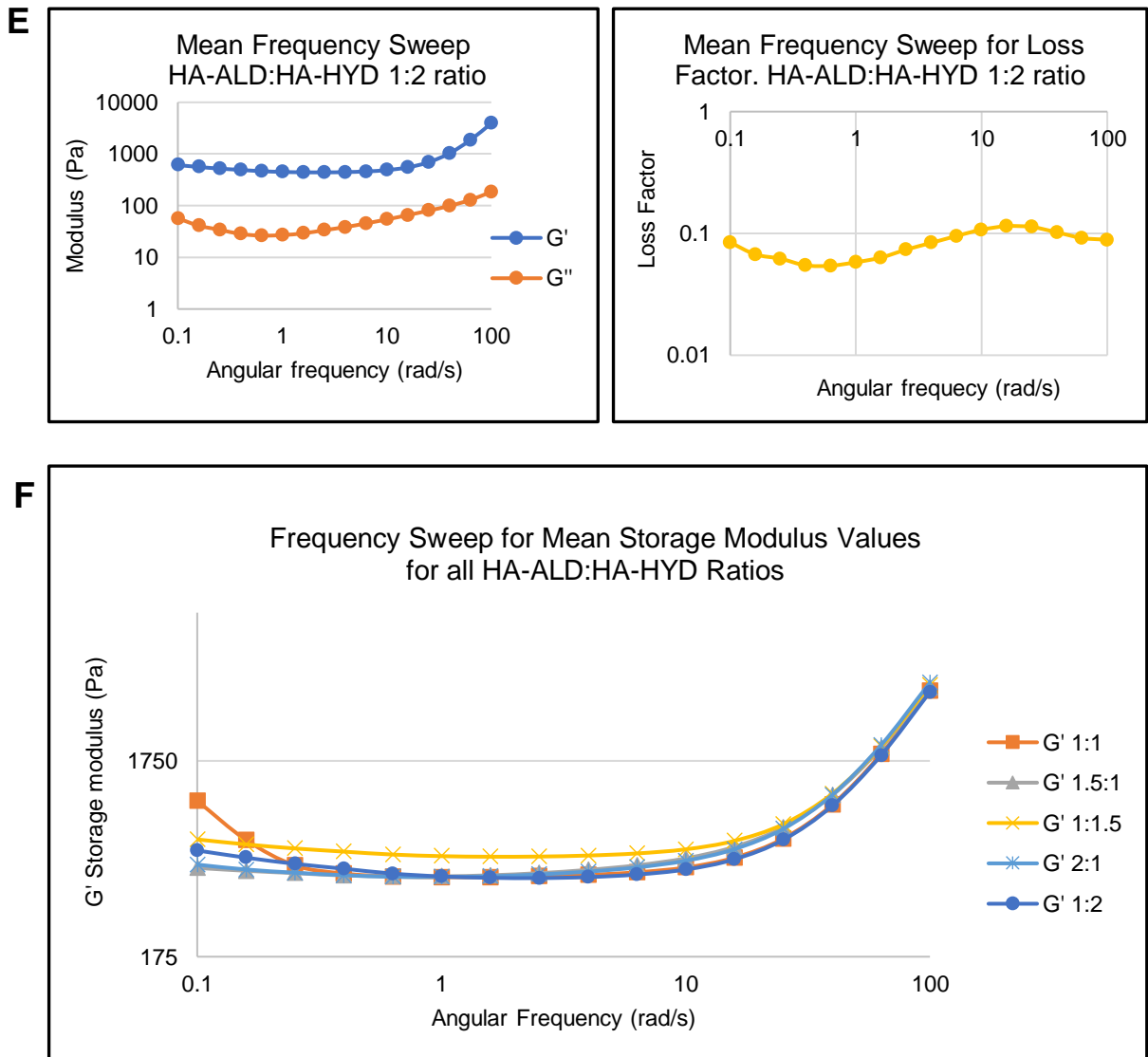
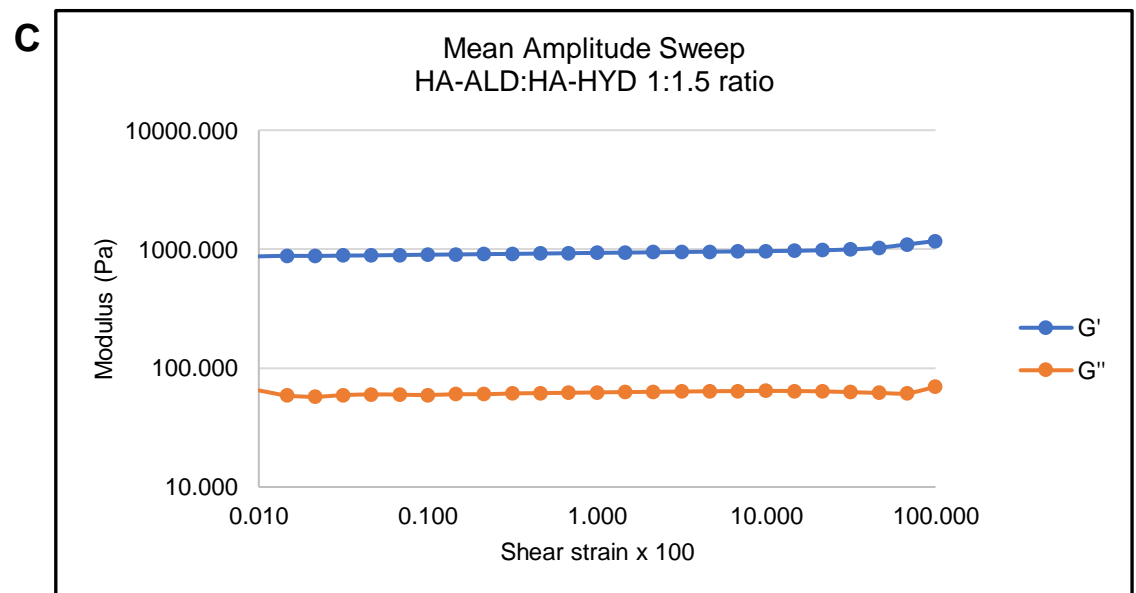
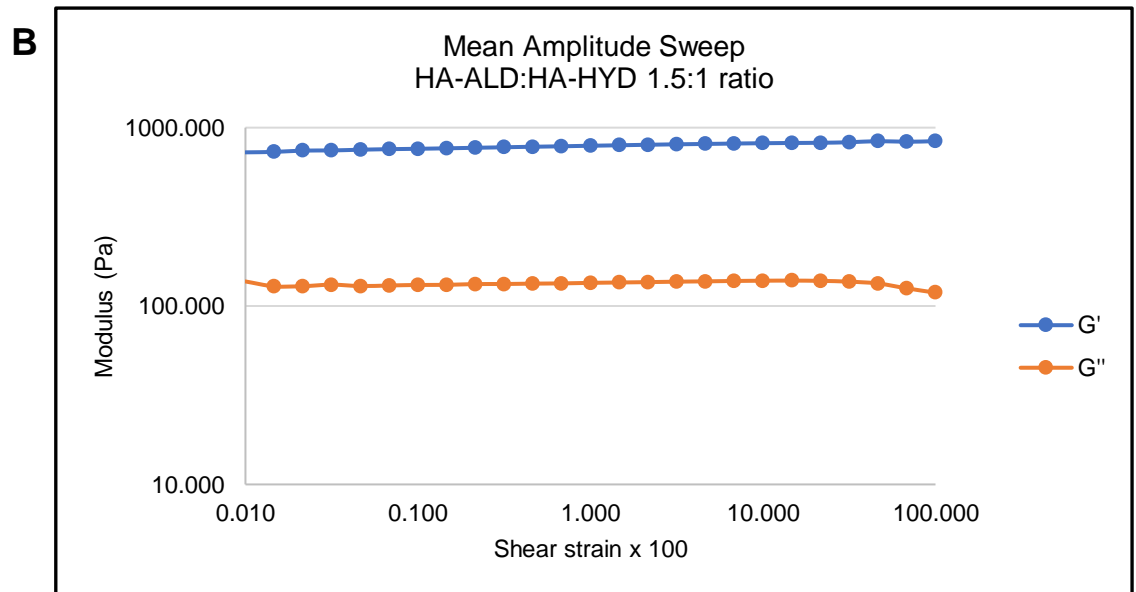
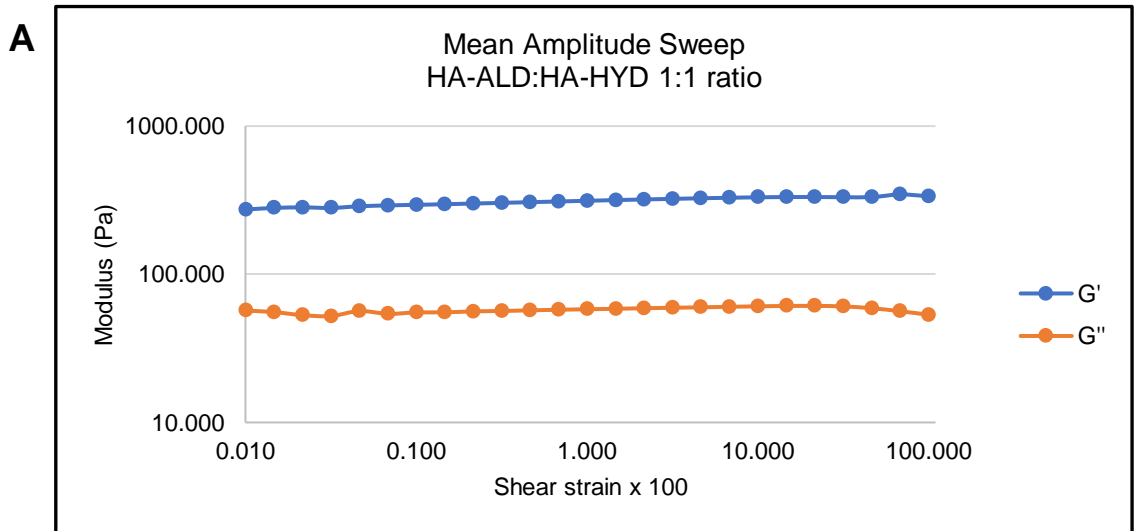


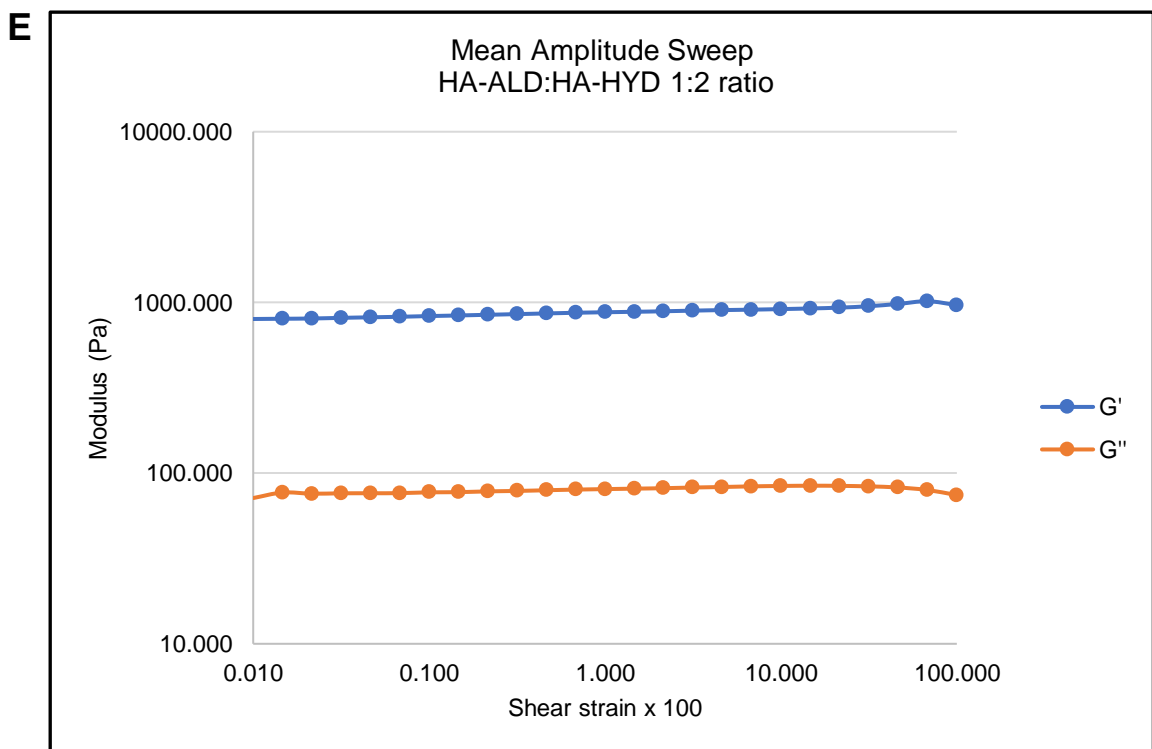
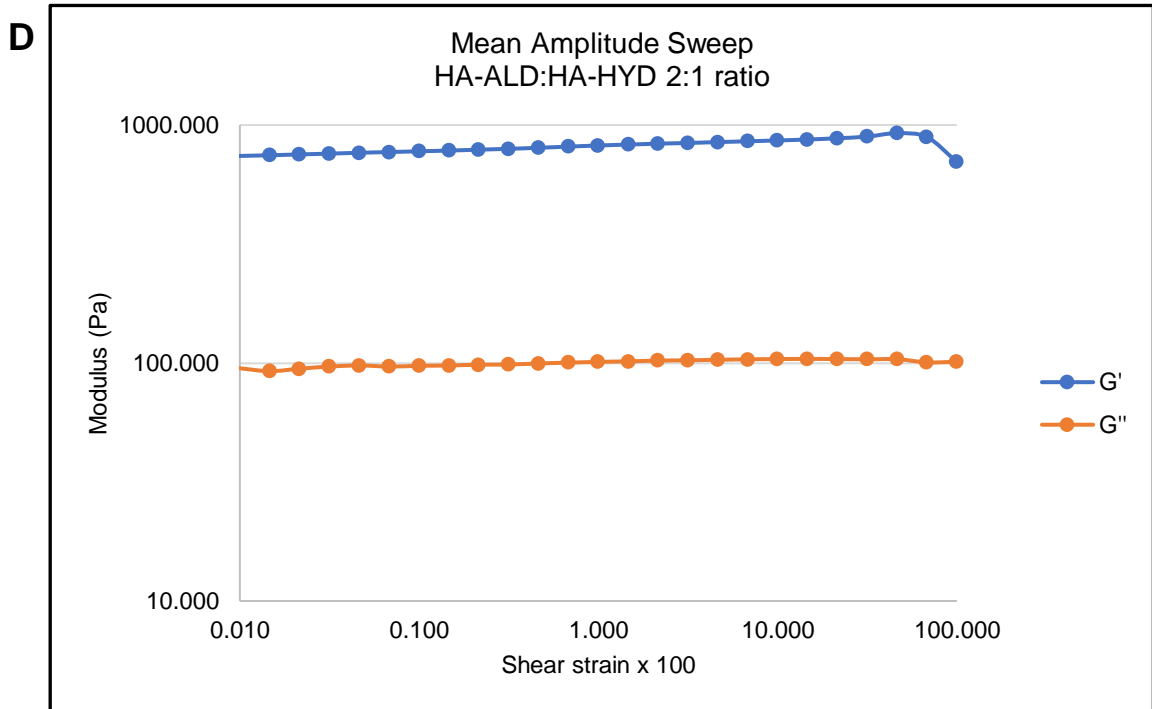
Figure 3.6 (A-E) Mean frequency sweep values for storage modulus, loss modulus and loss factor for 6% concentration HA hydrogel for various HA-ALD:HA-HYD ratios. Frequency sweeps were performed for each gel HA-ALD:HA-HYD ratio at a 6% concentration: (A) 1:1, (B) 1.5:1, (C) 1:1.5, (D) 2:1, (E) 1:2. Storage modulus (G' , blue), loss modulus (orange, G'') and loss factor (yellow). **(F) Frequency sweep mean storage modulus values for all gel ratios.** Storage modulus (G'). Gel ratios displayed 1:1 (orange), 1:1.5:1 (grey), 1:1.5 (yellow), 2:1 (light blue), 1:2 (dark blue) ($n=3$ separate experiments for all displayed data).

Amplitude sweeps are best suited to describing the deformation behaviours of materials in a non-destructive range. If the upper limit is observed, the material can behave in three ways- softening, exhibiting flow or fracturing if the material is sufficiently brittle.

As shown in Figure 3.7, panels A-E, G' is above G'' for all gel ratios indicating that gelation was completed before the start of the sweep. As also seen in Figure 3.6, no transections of G' and G'' lines occurred in Figure 3.7, either at the start of the sweep (gelation not observed) or at the end of the sweep (failure of the gel becoming a liquid). This is of particular importance, as the latter suggested that the gel is robust at higher amplitudes and throughout the entire range during the sweep. This suggests that the gel may be able to resist deformative forces of a high amplitude when used in a murine *in vivo* model or in patients, with the gel maintaining its shape in a given cavity needing reconstruction with external deformative forces.

In Figure 3.7, panel F shows G' cumulative mean values for all ratios. As seen, the 1:1 ratio had the lowest G' . Ratios with a higher proportion of HA-HYD tended to have a higher G' throughout the sweep (1:1.5 yellow followed by 1:2 grey traces). All five ratios showed a plateau with a slight upward trend until value ~ 80 shear strain $\times 100$. This suggested that the hydrogels were showing more solid characteristics as the amplitudes applied to them increased. Suggestions of gel failure were apparent for ratios 1:1.5, 1:2 and 2:1 HA-ALD:H-HYD, as the G' values started to deviate from their gentle upward trend. This is in keeping with a gel suffering rheological fatigue and demonstrates the start of failure of the gels' mechanical properties (Anton-Paar, 2021).





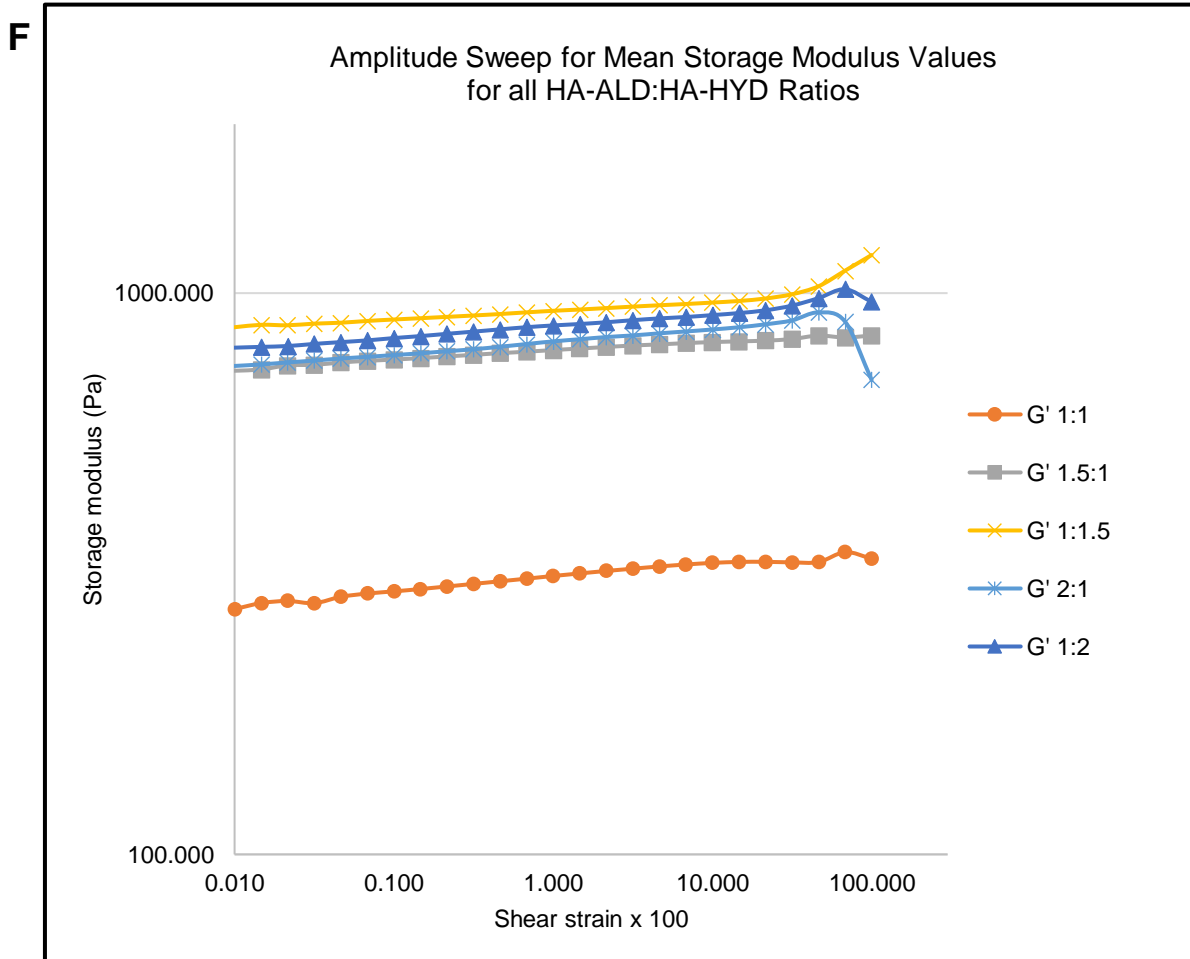


Figure 3.7

(A-E) Mean amplitude sweep values for storage modulus and loss modulus for 6% concentration HA hydrogel of varying HA-ALD:HA-HYD ratios. Amplitude sweeps were performed for each gel HA-ALD:HA-HYD ratio at a 6% concentration: (A) 1:1, (B) 1.5:1, (C) 1:1.5, (D) 2:1, (E) 1:2. Storage modulus (blue, G') and loss modulus (orange, G'').

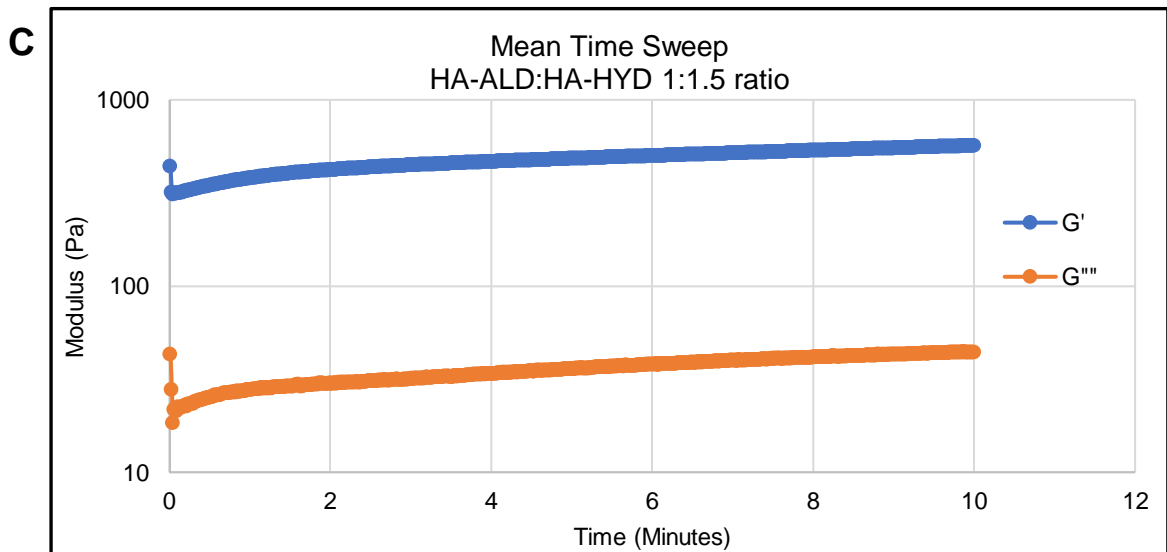
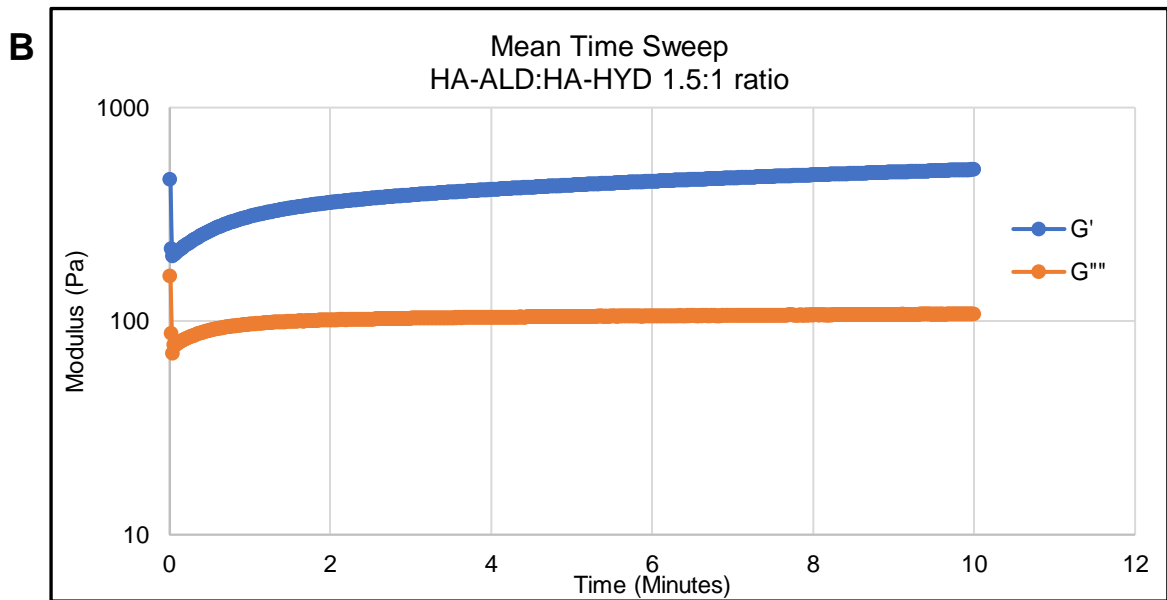
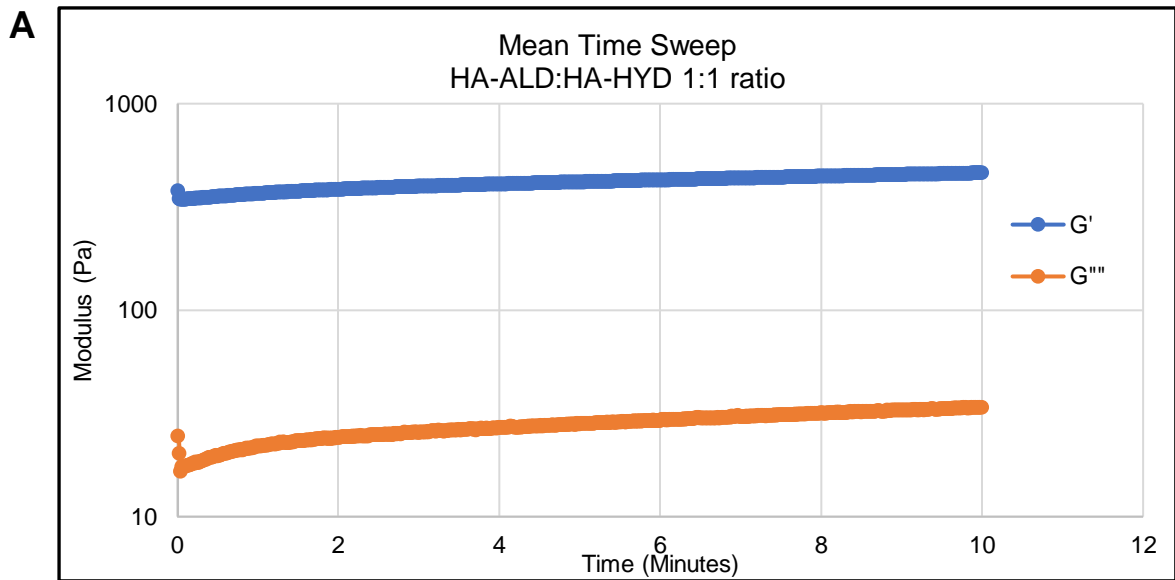
(F) Mean amplitude sweep storage modulus values for all gel ratios. Storage modulus (G'). Gel ratios displayed 1:1 (orange), 1.5:1 (grey), 1:1.5 (yellow), 2:1 (light blue), 1:2 (dark blue) (n=3 separate experiments for all displayed data).

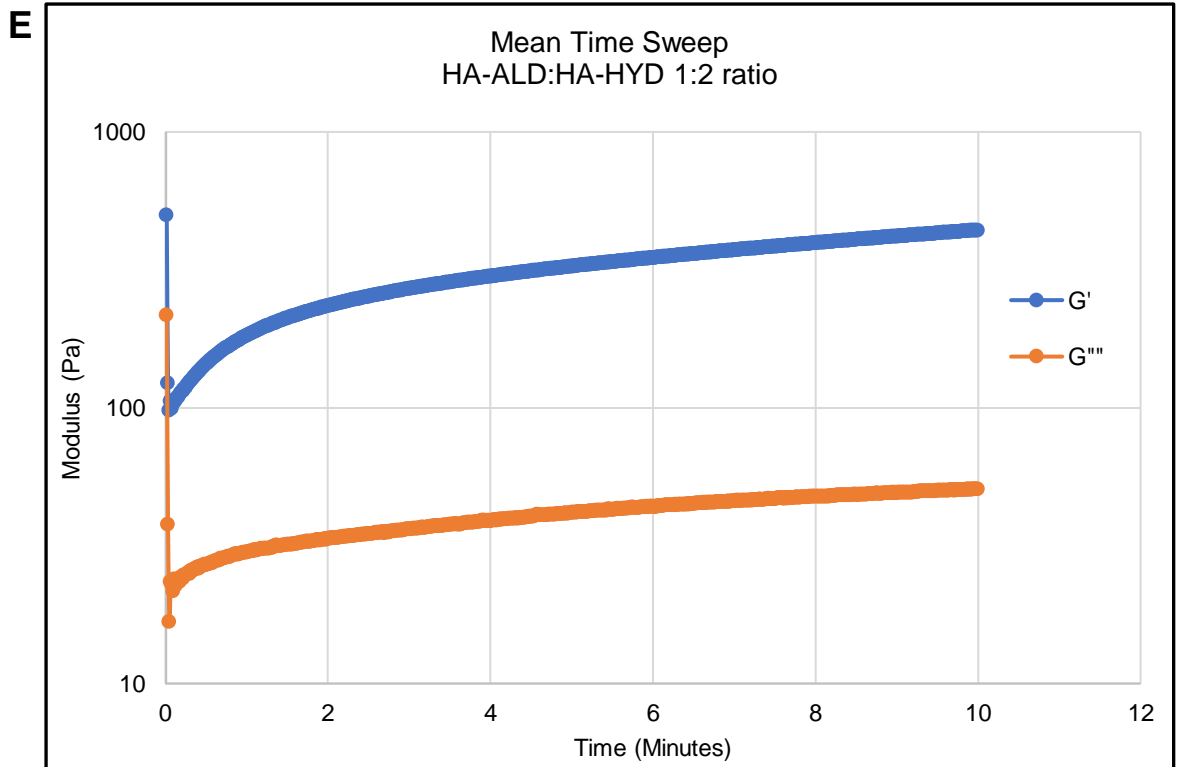
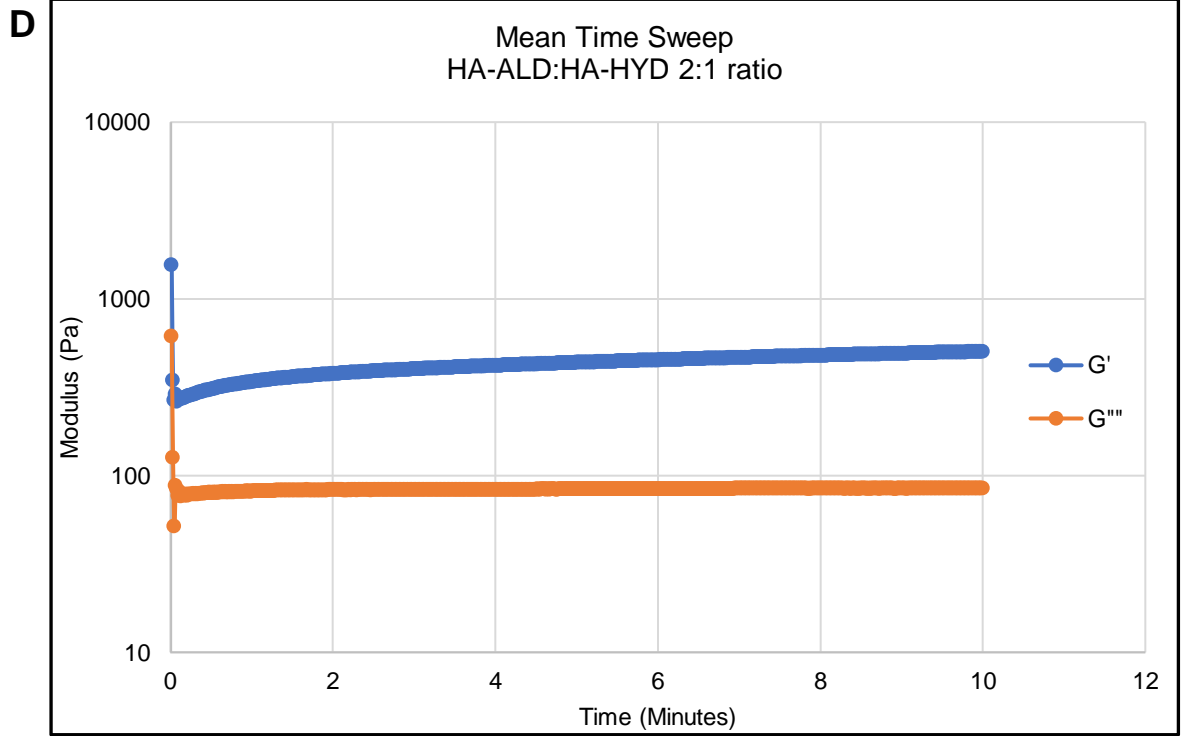
Time sweeps were performed to evaluate the time-dependent viscoelastic properties of HA hydrogels, with oscillatory sweeps performed with shearing under constant dynamic-mechanical conditions (i.e., constant frequency and amplitude).

As shown in Figure 3.8, panels A-E, all graphs showed G' above G'' for all ratios at a 6% concentration with mean values from triplicate repeats, suggesting a gel with consistent properties for the duration of the time sweep. This was in congruity with findings shown for frequency and amplitude sweeps (Figure 3.6 and Figure 3.7). However, upward inflections of G'' were seen all graphs (Figure 3.7, panels A-F) before two seconds, suggesting that the gelation point was less than two seconds after HA-ALD and HA-HYD were added together on the rheometer plate.

All graphs in Figure 3.8 also showed a more marked increase in inclination after two seconds and before one minute, which suggested a slower forming of dynamic covalent bonds between HA-ALD and HA-HYD after the gelation point. After one minute, the inclination of both G' and G'' slowed, suggesting a slower increase in dynamic covalent bonds.

As with Figure 3.7 panel F, Figure 3.8 panel F demonstrated a higher G' for ratios with a higher proportion of HA-HYD tending to have a higher G' throughout the sweep (1:1.5 ratio by 1:2 ratio traces), suggesting gels with a higher proportion of HA-HYD are more gel-like and viscous.





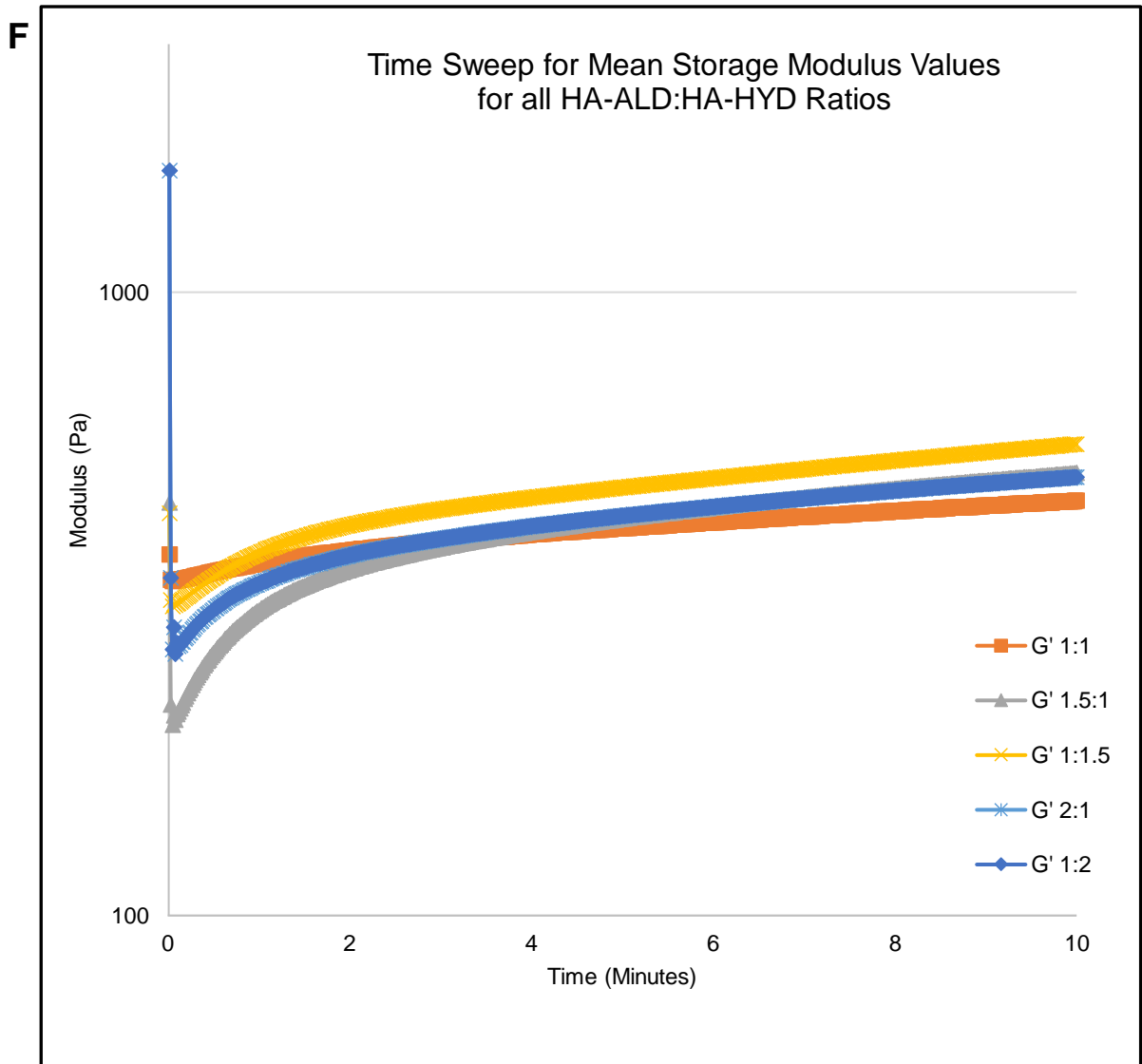


Figure 3.8

(A-E) Mean time sweep values for storage modulus and loss modulus for 6% concentration HA hydrogel of varying HA-ALD:HA-HYD ratios. Time sweeps were performed for each gel HA-ALD:HA-HYD ratio at a 6% concentration: (A) 1:1, (B) 1.5:1, (C) 1:1.5, (D) 2:1, (E) 1:2. Storage modulus (blue, G') and loss modulus (orange, G'').

(F) Mean time sweep storage modulus values for all gel ratios. Storage modulus (G'). Gel ratios displayed 1:1 (orange), 1.5:1 (grey), 1:1.5 (yellow), 2:1 (light blue), 1:2 (dark blue) (n=3 separate experiments for all displayed data).

3.4 Characterisation of gel properties

A number of processes were used to better define the HA hydrogels characteristics, particularly in ascertaining the unreacted chemicals present in the final lyophilised product, the amount of liquid held within a given HA hydrogel, and the profiles of which HA hydrogels degrade in various solutions.

3.4.1 Gel fraction

The gel fraction was used to determine the proportion of gel that is unreacted and not polymerised. i.e., the weight percentage of dried polymer (cross linked) before and after washing with a solvent. This was of particular relevance as some unreacted compounds are cell toxic, potentially reducing adipocyte viability (Kennedy Jr, 2002). To determine the gel fraction (GF), the weights (W_g) of lyophilised gels were recorded. The lyophilised hydrogels were washed with PBS and allowed to swell for three days, with frequent changing of the PBS solvent to extract any non-cross linked or unreacted precursors. At the end of three days, the hydrogels were lyophilised, and their weight recorded again (W_r). The expression for GF is described in Equation 2.1A.

Two gel concentrations were chosen for gel fraction interrogation: 3% and 6% in a 1:1 HA-ALD:HA-HYD ratio. No other ratios or concentrations were interrogated as the results for 3% and 6% concentrations were identical regarding residual un-reacted products during synthesis. Performed in triplicate, 0.5 mL of 3% gel was made using 7.6 mg of HA-ALD in 250 μ L PBS and 7.6 mg of HA-HYD in 250 μ L PBS mixed together and left to gelate as per Section 2.3.2. For the 6% gel, the same procedure was followed with 15.2 mg HA-ALD and HA-HYD. The hydrogels were then lyophilised and weighed, followed by three days of washing with PBS. After this step, the hydrogels were lyophilised again and weighed. There was less than 5% difference between the lyophilised products after

washing, showing a minimal unreacted product burden after mean of triplicate repeats for both 3% and 6% gel concentrations.

3.4.2 Gel equilibrium water content

To determine the gel equilibrium water content (EWC), hydrogels were left in PBS and allowed to swell for 24 hours, after which their weight was recorded (W_s). The hydrogels were then lyophilised, and weights recorded again (W_d) (Equation 2.1B). The equilibrium water content is a useful method of describing the water content of a given hydrogel, as described in 2.3.5.2. Hydrogels of 3% and 6% concentrations were made as described in 3.4.1 and 2.3.2. The EWC for 3% and 6% gels was $96.4\% \pm 0.04\%$ and $96.4\% \pm 0.76\%$ respectively as a mean of three triplicate repeats for each concentration (Figure 3.9). This suggested a high proportion of water present- confirming that the material was in fact a hydrogel, rather than a compound with a high hydration and high concentration of HA product.

3.4.3 Gel swelling and degradation

As described in 2.3.5.3, hydrogels were exposed to each of three corresponding solutions: PBS, DMEM/F12 media, and three hyaluronidase solutions (100 U/mL, 50 U/mL or 10 U/mL in PBS). The hyaluronidase solutions were to simulate the various tissue conditions in the human body. Hydrogels selected for swelling and degradation studies were 1:1 ratio of 3% and 6% gel, followed by 6% gels in HA-ALD:HA-HYD ratios 1:1.5, 1.5:1, 2:1 and 1:2. Once in a given solution, the hydrogels were kept at 37°C with a shaking speed of 80 rpm. The swelling solution was replaced daily to remove any unreacted precursors and to prevent the build-up of solute concentration. At specific time points, the hydrogels were removed from solution, gently balloted dry and weighed. Hydrogel swelling and degradation to destruction was described as a percentage weight of the hydrogel at the start of the experiment (W_0) compared to the time point weight (W_i).

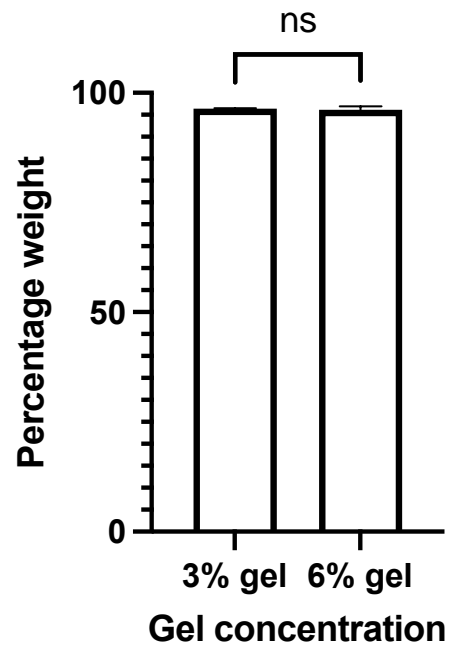


Figure 3.9 Equilibrium water content for 3% and 6% HA hydrogel. Equilibrium water content was determined as described in Section 2.3.5.2 for the 3% HA hydrogel (dark grey bars) and 6% HA hydrogel (light grey bars) (Mean \pm s.e.m. n=3 separate experiments. ns: not significant).

Gel swelling and degradation characteristics are shown in Figure 3.10 for mean values of triplicate repeats for 3% concentration gel in a HA-ALD:HA-HYD 1:1 ratio. As seen, all gel had perished by 264 h post exposure, with PBS and media degrading the gel at the slowest rate. Hyaluronidase solutions degraded the gel more rapidly, with the lowest concentration (E1- 10 U/mL) being the slowest (gel perished by 216 h). Both E2 (50 U/mL) and E3 (100 U/mL) degraded the gel fully by 168 h.

In Figure 3.11, gel swelling and degradation of mean values (three repeats per experiment) for 6% concentration gel in a HA-ALD:HA-HYD 1:1 ratio is shown. In contrast to 3% concentration degradation studies in Figure 3.10, 6% gels in all solutions increased in weight compared to baseline at 8 h. This may have been a result of the higher 6% concentration having greater concentrations of side chains and therefore capacity to hold liquid more effectively. Both PBS and E1 solution gels remained intact at the end of the study period at 264 hours. The fastest degradation of gel was in the media solution, followed by E3 and E2 hyaluronidase solutions. The E1 hyaluronidase solution gel showed the most resistance to degradation.

These results were unusual, as they did not follow the degradation trend predicted and established for 3% gel concentrations in Figure 3.10- whereby the highest concentration of hyaluronidase solution (E3) caused the most rapid degradation, followed by lower concentrations of hyaluronidase, media and finally PBS. This may be due to free HA-ALD and HA-HYD side chains, which have not formed dynamic covalent bonds yet, interacting with and binding to the active ingredients in each of the degradation solutions to lesser or greater degrees, lowering their degradation efficacy.

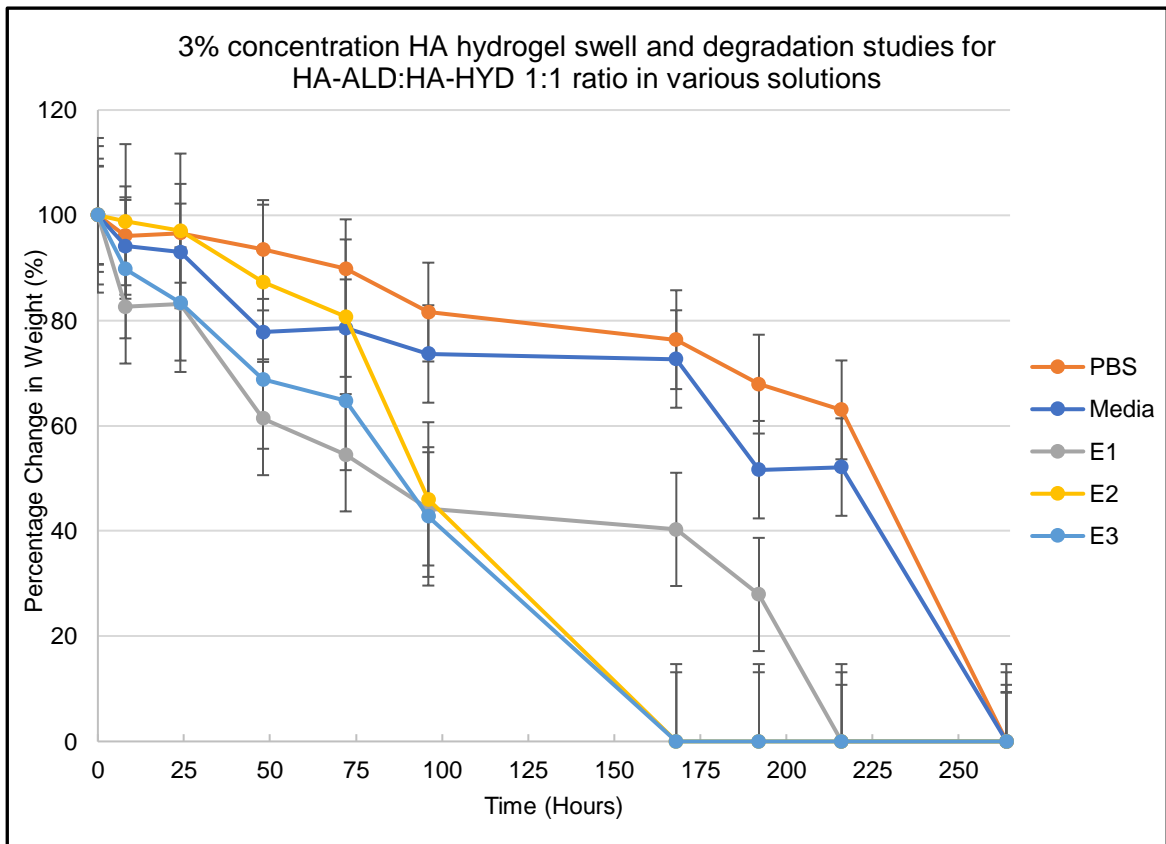


Figure 3.10 Gel swelling and degradation characterisation for 3% gel HA-ALD:HA-HYD 1:1 ratio in various solutions. Solutions used for degradation were PBS (orange), culture media (blue) and three concentrations of hyaluronidase solution (E1-E3, in grey, yellow and light blue, respectively) (mean \pm s.e.m and representative of n=3 experiments).

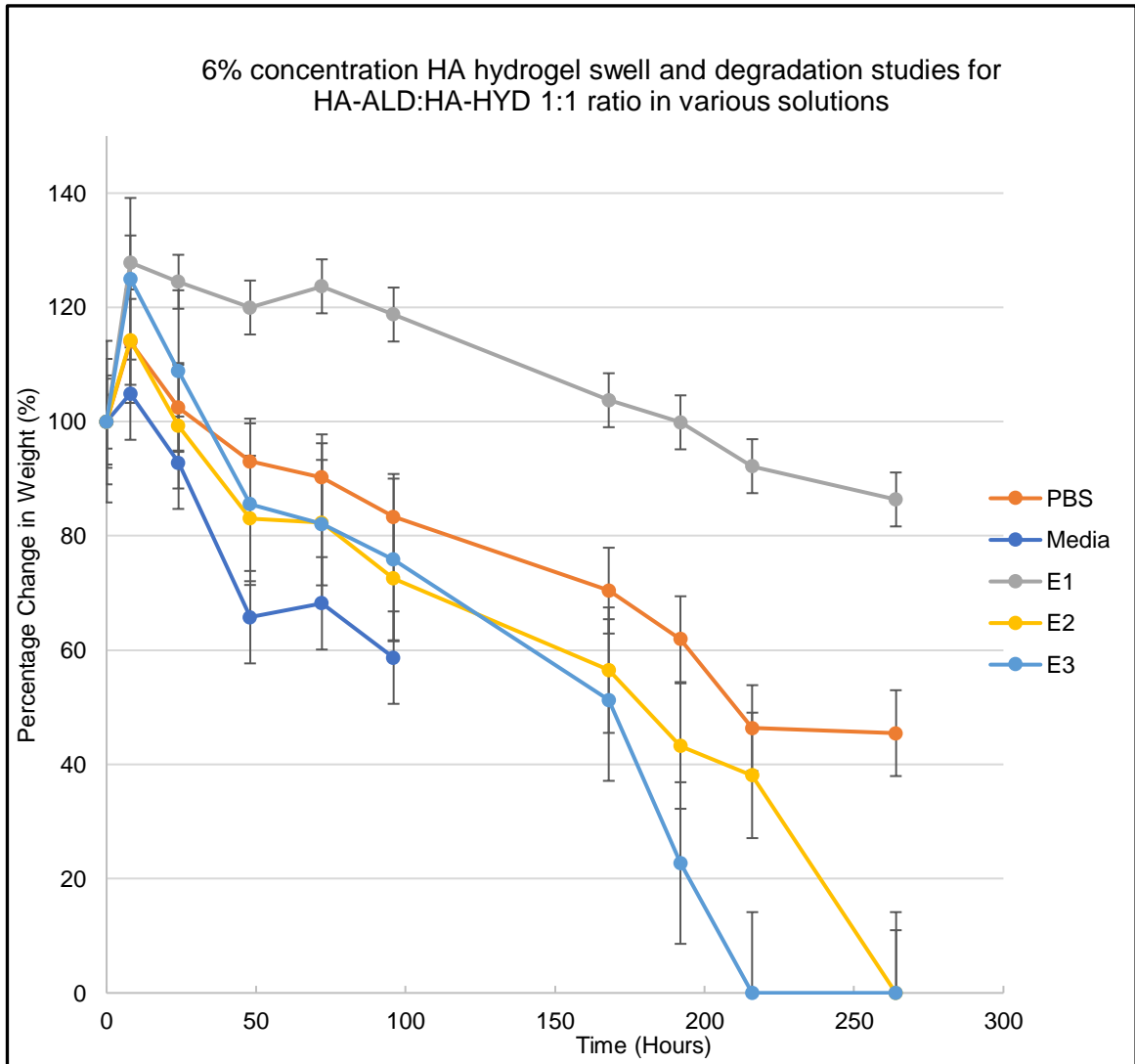


Figure 3.11 Gel swelling and degradation characterisation for 6% gel HA-ALD:HA-HYD 1:1 ratio in various solutions. Solutions used for degradation were PBS (orange), culture media (blue) and three concentrations of hyaluronidase solution (E1-E3, in grey, yellow and light blue, respectively) (mean \pm s.e.m and representative of n=3 experiments).

As shown in Figure 3.10 and Figure 3.11, all five degradation solutions degraded the 3% and 6% HA hydrogels in a HA-ALD:HA-HYD 1:1 ratio. To better understand the effect of differing ratios at a 6% gel concentration for 1.5:1, 1:1.5, 2:1 and 1:2 ratios, gels of these ratios were degraded with PBS over 48 h to elucidate any differences. PBS was used in the first instance, as 3% HA hydrogels in previous experiments were degraded slower in this condition, as shown in Figure 3.10 and similarly for the 6% gels (Figure 3.11). This allowed differences to be investigated in the most rapidly changing period of degradation of 48 h.

In Figure 3.12, mean values of triplicate repeats for various gel ratios at a 6% gel concentration (1.5:1, 1:1.5, 2:1 and 1:2 ratios). Gels with a higher proportion of HA-HYD (HA-ALD:HA-HYD 1:2 and 1:1.5 ratios) were more resistant to degradation from PBS. All four gel ratios swelled to past 100% of the original weight at 8 h, with ratios HA-ALD:HA-HYD 1:2 and 1:1.5 ratios exhibiting more swelling than ratios 1.5:1 and 2:1 with lower proportions of HA-HYD. This may be due to HA-HYD side chains being more able to withstand degradation and with an increased ability to be hydrated, compared to HA-ALD side chains. This would explain why gels with a higher proportion of HA-HYD demonstrating a higher swelling weight and also resistance to degradation in PBS.

The HA-ALD:HA-HYD 1:2 6% concentration hydrogel ratio was selected for long term degradation studies due to its resistance of degradation in PBS demonstrated in Figure 3.12. Figure 3.13 shows this mean data from triplicate repeats. As demonstrated, the 1:2 ratio gel maintained its weight till the end of the experiment at 20 days in PBS, demonstrating a transient increase in weight up to day two. Gel in E3 hyaluronidase solution showed a higher swelling weight at day two than gel in PBS solution, and was fully degraded at day five.

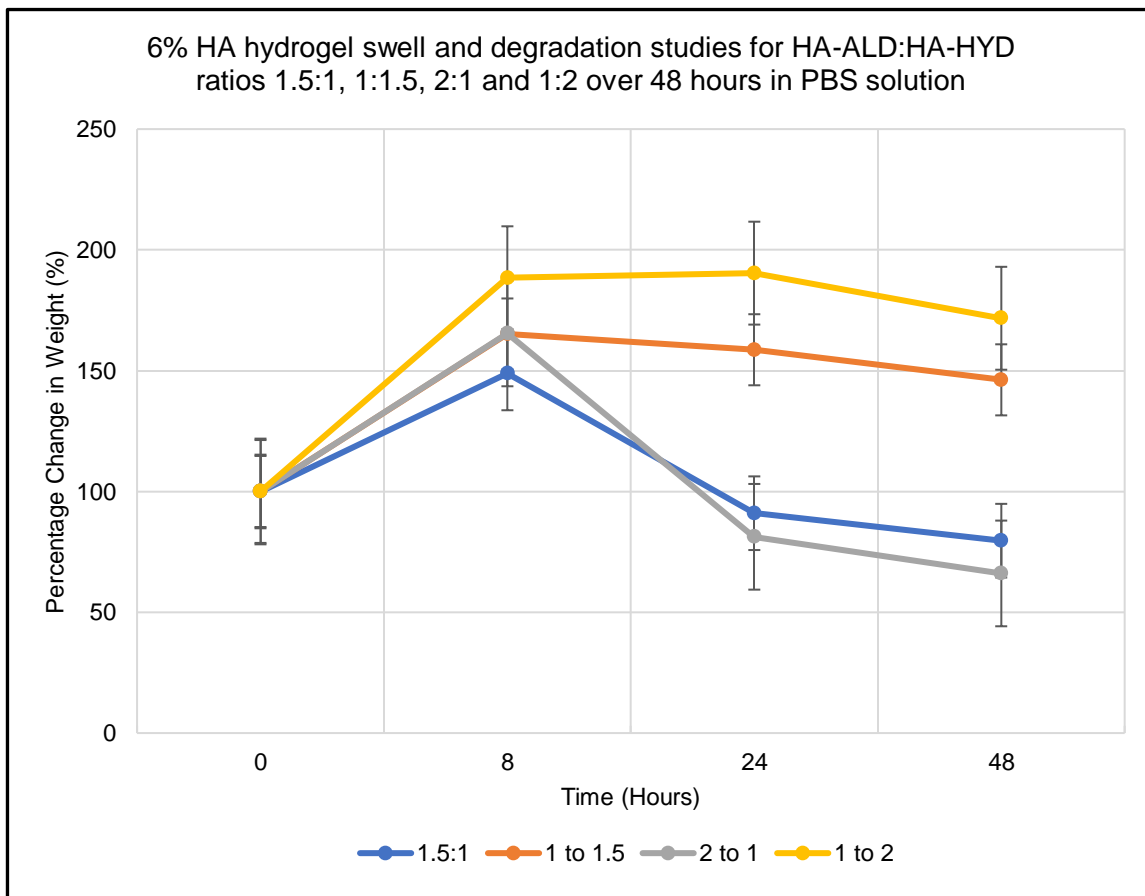


Figure 3.12 Gel swelling and degradation characterisation for 6% gel for varying HA-ALD:HA-HYD ratios in PBS solution. Gel ratios examined for degradation in PBS were 1.5:1 (blue), 1:1.5 (orange), 2:1 (grey) and 1:2 (yellow) (mean \pm s.e.m and representative of n=3 experiments).

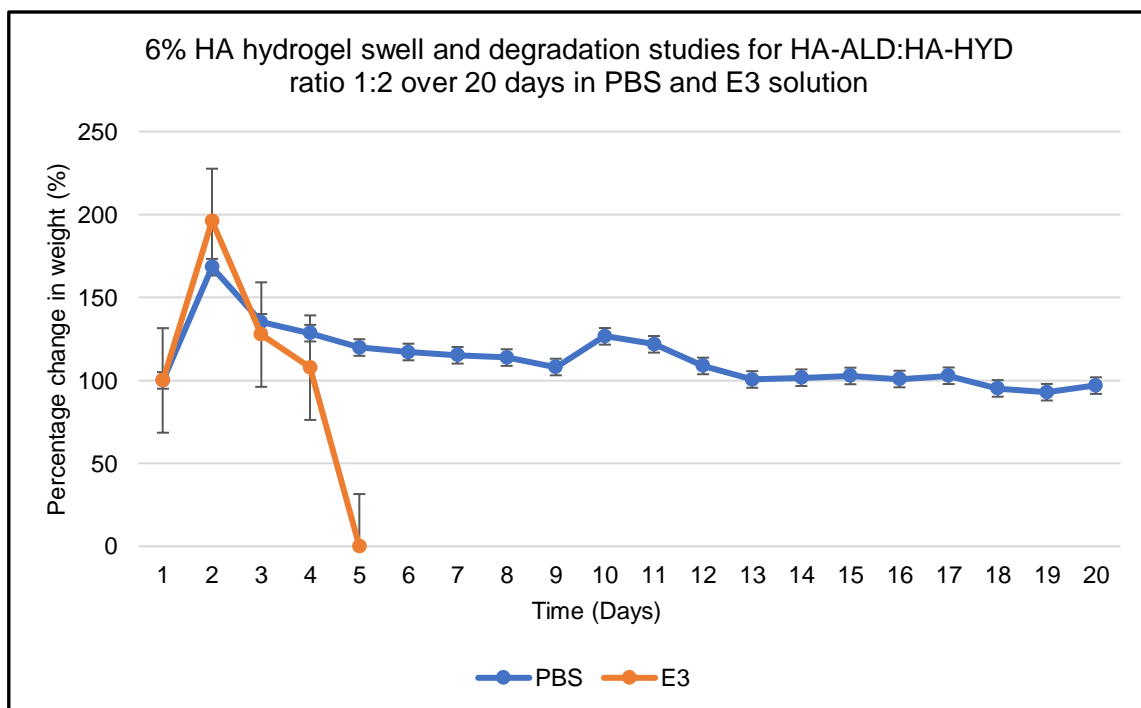


Figure 3.13 Gel swelling and degradation characterisation for 6% gel in a 1:2 HA-ALD:HA-HYD ratio in two solutions. Degradation solutions were PBS (blue) and E3 (orange) over 20 days (mean \pm s.e.m and representative of n=3 experiments).

3.4.4 Gel healing

The hallmark of dynamic covalent bonds between hydrazine and aldehyde side chains of functionalised hyaluronic acid results in these bonds being able to be broken and reformed easily. As such, this gives the ability of these hydrogels to self-heal. Self-healing is a critically important gel characteristic, as the gel will need to be robust to be injected into a patient and self-heal to fill a space in reconstruction.

The methods for interrogating gel self-healing are described in Section 2.3.5.4. Non-dyed and dyed 6% concentration 1:1 HA-ALD:HA-HYD ratio gel duplicates were halved, and a non-dyed half applied to the cut surface of a dyed half. The hybrid gels were left at room temperature for one hour, and colour diffusion noted (if any).

In Figure 3.14, the self-healing ability of HA hydrogels is shown. As seen, red food dye clearly diffused across the cut interface at room temperature after one hour. This suggests that the dynamic covalent bonds between branches of HA-ALD and HA-HYD have reformed, allowing dye diffusion.

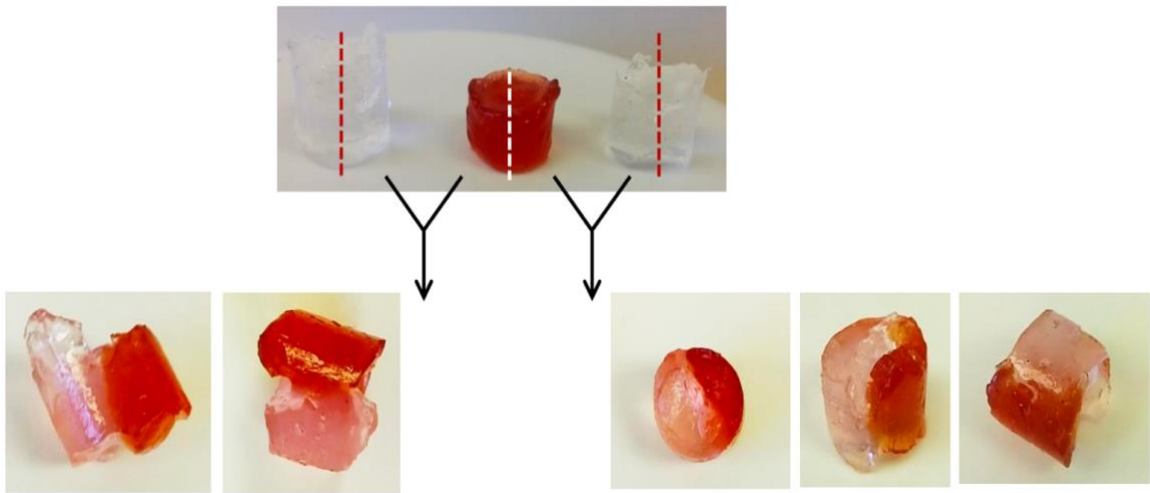


Figure 3.14 The self-healing ability of HA hydrogels. 6% concentration 1:1 HA-ALD:HA-HYD ratio gel duplicates were halved, and a non-dyed half applied to the cut surface of a dyed half and observed after one hour.

3.5 Conclusion

This Chapter aimed to develop a synthesis protocol for a novel HA hydrogel and to define the HA hydrogel's physical characteristics. Rheological studies showed that the gel formed quickly, with most of the dynamic covalent bonds formed within two seconds of mixing. The gel was found to be robust, with G' being above G'' throughout the end points of all frequency, amplitude and time sweeps for all gel concentrations and ratios.

Further rheological characterisations also revealed a more gradual increase in both G' and G'' for frequency, amplitude, and time sweeps, suggesting that there was a continued, albeit slower rate of dynamic covalent bond formation till the end of the experiments. This is consistent with the gelation time described by Wang et al., 2018, which suggested that the gelation time was less than two hours after mixing HA-ALD and HA-HYD components.

The swelling, degradation and healing characteristics of the gels were interrogated, which showed that the gel can be degraded under tissue-like conditions, using for example, hyaluronidase solutions. Furthermore, gel characteristics changed from 3% to 6% gel concentrations and differing HA-ALD:HA-HYD ratios in terms of rheology, gel swelling and degradation, which suggested that the gel can be fine-tuned for desired characteristics.

**Chapter Four: *In vitro* effects of HA hydrogel on
3T3-L1, primary murine and primary human
adipocytes**

4.1 Introduction

Soft tissue reconstruction is required after cancer resection or major trauma, with adipose tissue transfer being a common method of reconstruction. After adipose tissue harvest and processing, the lipoaspirate is injected into the area needing reconstruction (Section 1.3). The graft receives nutrition via diffusion over the first 48 hours, followed by the growth of blood vessels into the graft to support further growth (neovascularisation).

On day one post adipose tissue transfer, adipocytes survive and continue to develop, whilst pre-adipocytes proliferate and begin to differentiate. There is also a recruitment of inflammatory cells such as macrophages for debris phagocytosis (Mojallal and Foyatier, 2004). On day four, neovascularisation begins, starting at the periphery, with central adipose tissue therefore undergoing more prolonged ischaemia. Central adipose tissue only vascularises if the adipose tissue beads are small (Peer, 1950).

The extracellular matrix (ECM) surrounding pre-adipocytes and adipocytes is of critical importance for cell survival, proliferation and differentiation. The ECM has also been shown to affect tissue regeneration, remodelling and the maintenance and differentiation of pre-adipocytes to adipocytes (Flynn et al., 2006). The ECM is vitally important in the ability of a tissue to sense forces placed on it and its environment (Boudreau and Weaver, 2006). HA is a key constituent of the ECM, and has specific biological importance during development, wound healing and in the structure and function of tissues and organs (Agren et al., 2000, Highley et al., 2016a).

Given the importance of the ECM, the role of the novel HA hydrogel in pre-adipocyte cell survival, proliferation and differentiation into mature adipocytes needed to be interrogated.

4.2 Chapter aims and selection of cell types for experimentation

A pilot study was performed examining gel toxicity and proliferation using MCF-7 murine cells. These adherent cells are not known to be invasive or aggressive and have a low migratory potential once adhered onto plastic. MCF-7 cells accumulate lipid like adipocytes (but are not true adipocytes) (Chamras et al., 2002), which make them a good pilot cell type to investigate potential HA hydrogel toxicity. Furthermore, the aim is for HA hydrogel to be used for breast reconstruction after cancer surgery, with the gel being in contact with breast cells. Thus, adverse effects were important to investigate on MCF-7 cells in the first instance.

In order to investigate the effect of HA hydrogel on proliferation and differentiation on pre-adipocytes, 3T3-L1 pre-adipocytes were used. 3T3-L1 cells are murine in origin and were first established as a cell line by the American Type Culture Collection (ATCC) in 1974 with limited details such as passage number (Zebisch et al., 2012). 3T3-L1 cells have pre-adipocyte characteristics and can be differentiated into adipocytes reliably (Jessen and Stevens, 2002). 3T3-L1 cells were engineered to express luciferase under the control of the *Per2* promoter and emit photons after exposure to luciferin, the substrate for luciferase (described in Section 2.3.6.3 and Figure 4.2). These *Per2-dLuc* 3T3-L1 cells were used to demonstrate the objective that cells can proliferate and differentiate grown in the presence of HA hydrogel (Section 4.5).

To investigate proliferation within HA hydrogel, a reproducible methodology to visualise and track proliferation in a three-dimensional HA hydrogel construct using *Per2-dLuc* 3T3-L1 murine pre-adipocytes and CAG-luc-eGFP primary mouse pre-adipocytes was developed.

Serial photographs were attained to record photons emitted from these cell types. A large number of data points from images (over 100 per experiment) captured from these cell types needed to be analysed in an effective and reliable manner. An automated macro to analyse the intensity of photons released from these cells in HA hydrogel as a proxy for cell number and survival was therefore devised.

In order to investigate the effects of the HA hydrogel on cell differentiation, gene expression for specific adipocyte markers (i.e., cluster of differentiation 36 (CD36), peroxisome proliferator-activated receptor gamma (PPAR- γ) and adipocyte protein 2 (aP2)) were analysed in cells exposed to the HA hydrogel and compared to control cells that were maintained in culture without HA hydrogel.

Primary adipocytes are better at mimicking the cell populations that are harvested to produce a lipo-aspirate for adipose tissue transfer in reconstructive surgery applications (as described in Section 1.3), than 3T3-L1 pre-adipocytes. As a better physiological model of pre-adipocytes than 3T3-L1 cell lines, primary murine adipocytes were used to investigate proliferation and differentiation effects of HA hydrogel using the same construct of measuring cell viability as *Per2-dLuc* 3T3-L1 murine pre-adipocytes.

Primary murine pre-adipocytes and adipocytes were harvested from CAG-luc-eGFP mice. CAG-luc-eGFP primary mouse pre-adipocytes also express luciferase under the control of the *Per2* promoter (described in Section 2.3.6.4).

Luciferase is expressed in adipose tissue of CAG-luc-eGFP mice (Gassman et al., 2016). Isolated primary pre-adipocytes have fibroblast-like characteristics before differentiation. These cells were used to demonstrate the effect of HA hydrogel on primary cell proliferation and adipocyte differentiation (Section 4.6).

After characterisation of CAG-luc-eGFP primary mouse pre-adipocyte survival and differentiation with HA hydrogel, and confirmation that the cells behaved normally, primary human pre-adipocytes were used to investigate survival and differentiation with HA hydrogel. Using CAG-luc-eGFP primary mouse pre-adipocytes first before primary human pre-adipocytes allowed a safe test of the hypothesis that HA hydrogel did not harm cell survival or differentiation and reducing potential waste of human tissue samples.

Primary pre-adipocytes from human donors surplus to clinical requirement were collected to investigate cell proliferation and differentiation in HA hydrogel, as described in Section 2.3.6.5. Importantly, to remain as close as possible to clinical conditions, primary human cells were harvested in the same manner as used in human restorative surgery (described in Section 1.3). Gene expression for specific adipocyte markers (i.e., CD36, PPAR- γ and aP2) were analysed in primary human pre-adipocytes exposed to the HA hydrogel and compared to control cells that were maintained in culture without HA hydrogel.

4.3 Selection of gel for *in vitro* characterisation

As described in Chapter 3, HA hydrogel can be reconstituted in PBS at varying concentrations: 1.5%, 3% and 6%. In describing their form, gel at 1.5% did not hold its shape after gelation and was thus unsuitable for further characterisation (Section 3.3). Whilst the 3% HA hydrogel retained its shape, it was less robust than 6% gel, evidenced by lower G' values compared to 6%. In addition, the 3% concentration HA hydrogel was easily degraded in studies performed in PBS, media and when the gel was exposed to hyaluronidase enzyme (Section 3.4), which can be found in the ECM. As seen in Figure 3.10, 3% HA hydrogel in E1 hyaluronidase and PBS solutions was fully degraded after exposure for 216 hours in these solutions at the end of the experiment, whilst 6% HA hydrogel was intact for the same conditions at 264 hours (Figure 3.11).

Numerous ratios of 6% HA hydrogel were subjected to degradation studies (Section 3.4.3). Gels with higher ratios of HA-HYD were found to be more resilient to PBS solution. As seen in Figure 3.12, 6% concentration HA hydrogel at a HYA-ALD:HYD 1:2 ratio showed the least degradation to PBS solution at 48 hours. The HYA-ALD:HYD 1:2 ratio at 6% concentration was thus used in all *in vitro* and *in vivo* experiments unless otherwise specified. As such, 3% gels were excluded from the study.

4.4 Effects of 6% HA hydrogel on MCF-7 cell morphology

In order to investigate the effects of the HA hydrogel on cell morphology, MCF-7 cells were grown and differentiated in HA hydrogel at 6% concentration with a HA-ALD:HA-HYD ratio of 1:1 (Table 2.1). A 6% concentration gel was selected with desirable mechanical and degradation characteristics after rheological characterisation described in Section 3.3 and 3.4. Annex A (Figure A) also displays pilot gel toxicity using MCF-7 cells for gel concentrations 1.5% and 3%.

MCF-7 cells were seeded at 100,000 per well in F12/DMEM media (Day 0) in a 24-well plate (Corning® Primaria™ 24 Well Flat Black Bottom Surface Modified Multiwell Cell Culture Plate, Appleton Woods, Birmingham, United Kingdom). On Day 1, HA-ALD (50 µL) was carefully deposited onto the layer of confluent cells, followed by HA-HYD (50 µL). HA hydrogel constituents were synthesised at 6% concentrations in a HA-ALD:HA-HYD 1:1 ratio (Table 2.1).

On Day 1 when cells were confluent, representative baseline photographs of cells were taken (Figure 4.1). Cell media was then replaced with the induction media and cells maintained for 48 hours as described in Section 2.3.6.2.2 (in the same manner as 3T3-L1 differentiation media). Maintenance media was then introduced to the cells (described in Section 2.3.6.2.3) until Day 14, followed by

Oil Red O staining to better visualise the accumulation of lipid droplets within MCF-7 cells (described in Section 2.3.7). The results are displayed in Figure 4.1.

As apparent in Figure 4.1, the 80% confluent MCF-7 cell layer was not disturbed by the addition of the gel (Figure 4.1, left panel). MCF-7 cells continued to grow, albeit as an apparent slower rate since 100% confluency was never reached, even at Day 14 post HA hydrogel addition (Figure 4.1, right panel). However, there was a significant lipid accumulation in MCF-7 cells revealed by the Oil Red O staining at Day 14, strongly suggesting that there was no qualitative difference in cell number at Day 1 after exposure to 6% gel concentration or at Day 14.

MCF-7 cells in 6% HA gel

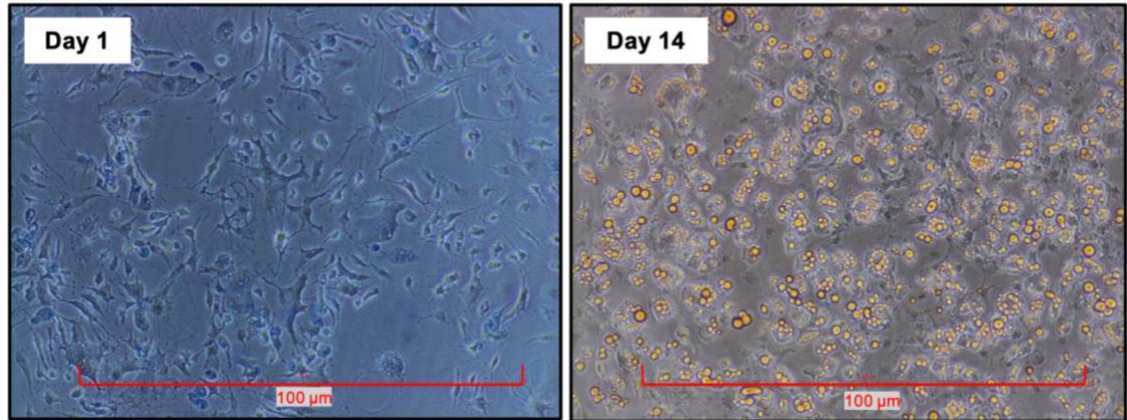


Figure 4.1 MCF-7 cell morphology under 6% HA hydrogel. Cells were grown to 80% confluence and 100 μ L of 6% HA hydrogel (HA-ALD:HA-HYD 1:1 ratio) was carefully added on top of the cell layer on Day 1. Cells were stained with Oil Red O on Day 14 after gel addition. Pictures are representative images of $n=3$ independent experiments performed in triplicates. Scale (red line) is 100 μ M.

4.5 Effects of HA hydrogel on *Per2-dLuc* 3T3-L1 adipocytes: proliferation and differentiation

4.5.1 Cell line characterisation and optimisation of data analyses

Having established, at least qualitatively, that HA hydrogel did not disrupt the morphology of the breast cell line MCF-7, nor their ability to accumulate lipids, investigations into the effects of the HA hydrogel (6% concentration) on adipocyte physiology were initiated. 3T3-L1 cells were used, as a murine model of adipocytes, to study the effects of HA hydrogel on adipocyte differentiation.

Mature adipocytes are only obtained after several days (13 to 21 days (Zebisch et al., 2012)) post confluence, following an induction phase where the adipose machinery (i.e., genes) are promoted. This is followed by a maintenance phase where lipids accumulate, giving rise to noticeable lipid droplets. Preliminary data (not shown) demonstrated significant variability in experiments where cell numbers were assessed at different days during the differentiation process. This was due to the gel embedding the cells and impairing the accurate and reproducible extraction and counting of cells. As such, a methodology to assess growth and cellular viability in the presence of the gel without the need to retrieve the cells was needed.

The cell line 3T3-L1 with an integrated luciferase reporter allowing luminescence recording of rhythmic clock gene expression such as *Per2* and *Bmal1* demonstrated that 3T3-L1 cells displayed bioluminescence rhythms (Ramanathan et al., 2014). Bioluminescence methodology allowed the quantification of photon emission, which indicated periodic expression of luciferase, and by extrapolation, suggested that cells remained viable. In addition, this method allowed for the recording of cell behaviour for several days, which was ideal for the purpose of the project.

4.5.1.1 Characterisation of *Per2-dLuc* 3T3-L1 cells

Lentiviral P(*Per2-dluc*) reporter vector was constructed (as described in Section 2.3.6.3), where the Period 2 promoter (*Per2*) controls the expression of luciferase and is used to generate the stable luciferase-expressing 3T3-L1 cells, *Per2-dLuc* 3T3-L1.

Two independent *Per2-dLuc* 3T3-L1 cell lines were generated and maintained in a DMEM media in the presence of luciferin (1 mM), the substrate for the luciferase, and incubated in a LumiCycle luminometer (as detailed in Section 2.3.6.3). Photon emission (bioluminescence) that parallels luciferase expression and therefore *Per2* promoter activity, was recorded for a short 2.5-day period. Representative data are presented in Figure 4.2. 3T3-L1 cells expressing luciferase under brain and muscle Arnt like protein 1 (*Bmal1*) promoter were run simultaneously. *Bmal1* and *Per2* have been demonstrated to have opposite patterns of oscillations (Aoyagi et al., 2005). *Bmal1* and *Per2* promoter 3T3-L1 cells have opposite rhythmic oscillations via the action of a feedback loop. *Bmal1* and *Clock* are two transcription factors that form a positive feedback loop of expression, forming a heterodimer and binding to the E-box on the regulatory region of genes including Period 1 (*Per1*) and cryptochrome (*cry*). After translation of *cry* and *Per1* which form a factor complex together, the factor complex inhibits gene expression in the cell nucleus for *Bmal1* and *Clock*. Concurrently, *Bmal1* is upregulated by *Per2* and the cycle is restarted once more (Aoyagi et al., 2005).

The purpose of having the *Bmal1*-expressing cells was to confirm that the bioluminescence seen with *Per2* cells was indeed rhythmic oscillations as the patterns were opposite to each other.

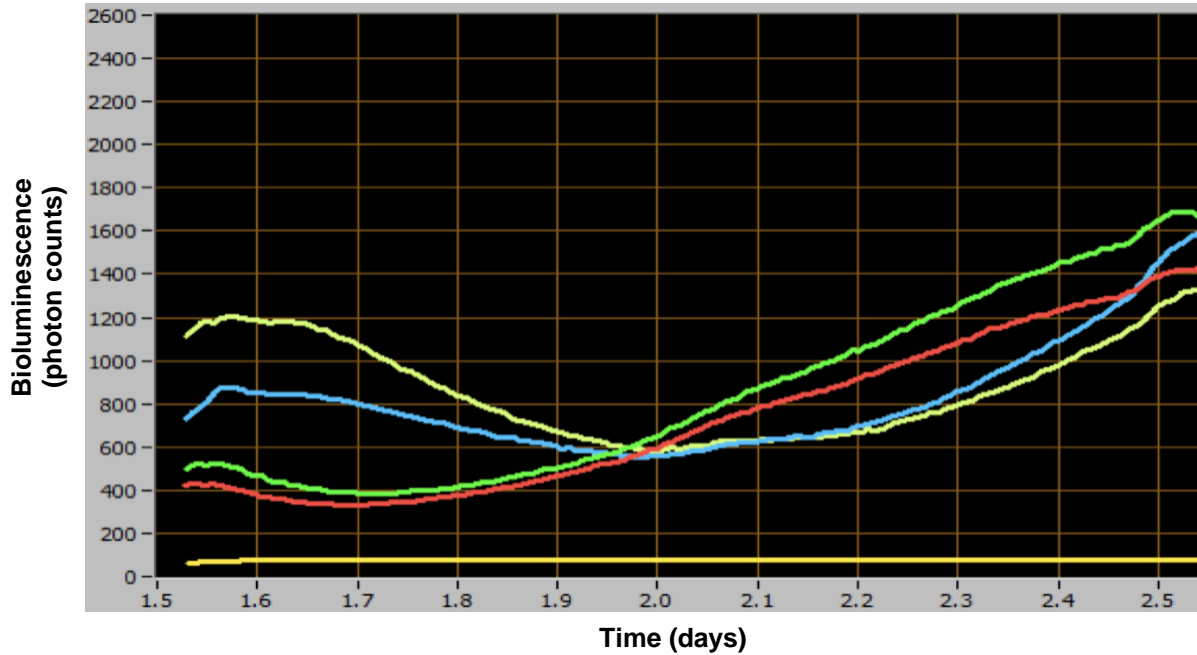


Figure 4.2 Oscillations of *Per2* and *Bmal1 d-Luc* 3T3-L1 cells. Photon output was measured for just over 2.5 days. Dark yellow line- background photon amplitude; Red/dark green- *bmal-luc* activity; blue/ light yellow- *per2-luc* activity (n=2 repeats for each promoter type).

4.5.1.2 Analysis using a novel automated macro

Images of experiments using *Per2-dLuc* 3T3-L1 and CAG-luc-eGFP primary mouse pre-adipocytes using the hypersensitive Alligator camera were taken hourly for the duration of the experiment. Most experiments lasted more than five days, with all experiments being performed in triplicate. This resulted in large number of images for each experiment needing to be analysed in a high throughput, but reliable manner.

Optimisation of the analytical technique described in this Section was performed on an experiment identical to that described in Section 4.5.2, whereby *Per2-dLuc* 3T3-L1 cells underwent proliferation and differentiation to adipocytes. A hypersensitive camera in the roof of the Alligator detected photons emitted.

Micro-Manager, an open-source programme, ran the assembly (Edelstein et al., 2014). Images were taken at hourly intervals with a photon gain of 12 which increased the sensitivity of the assembly for photon detection. Total exposure per image was 60 minutes.

Images taken of *Per2-dLuc* 3T3-L1 cells were analysed using FIJI (as described in Section 2.3.9). To analyse photons emitted from individual wells in a given image and to manage the large numbers of photographs of wells, a bespoke macro was written. Figure 4.3 displays the important parts of the 208-line macro code written for this project. Commands highlighted in green confer the task that section of the code is going to enact to the image and is further described below.

In order for the macro to accurately analyse a given image, a series of command codes need to be followed. Code line 22 and the block that follows it (Annex B) identifies wells in a given image and draws circles around them to form a region of interest (ROI). Huang thresholding (line 29) is then used to better identify areas of light compared to background, by minimising features of

fuzziness with a ROI (Huang and Wang, 1995). The background is then converted to black to better identify these areas (line 30 Annex B and Figure 4.3A). Rarely, the macro can detect noise close to a well and identify this as another well, perhaps due to reflection of photons against the walls of peripheral well. To mitigate this, code line 34 is a user-inputted failsafe to confirm the number of wells and rows in a given plate.

Code line 64 (Annex B) identifies the largest well and draws a circle around it to better define the ROIs and applies this to the other wells. Code line 96 measures the number of pixels in a given well and compares it to the known well diameter of 15.6 mm to ensure correct ROI circles have been drawn around each well. Finally, the other incorrect ROI circles are removed in code line 106. Next, rows of wells are grouped together in code line 128, as controls or experimental wells and the well intensity of light measured (Figure 4.3B).

Line code 137 outputs the data in a tabulated format, with triplicate well mean and standard deviation values. Line code 160 closes the given image and line codes 163 and 171 saves the tabulated single image data in a given location. Line codes 173 and 175 repeat the above coding to open the next image in the sequence before the macro starts again to analyse further images in the sequence till completion of the image set *usque in finem*.

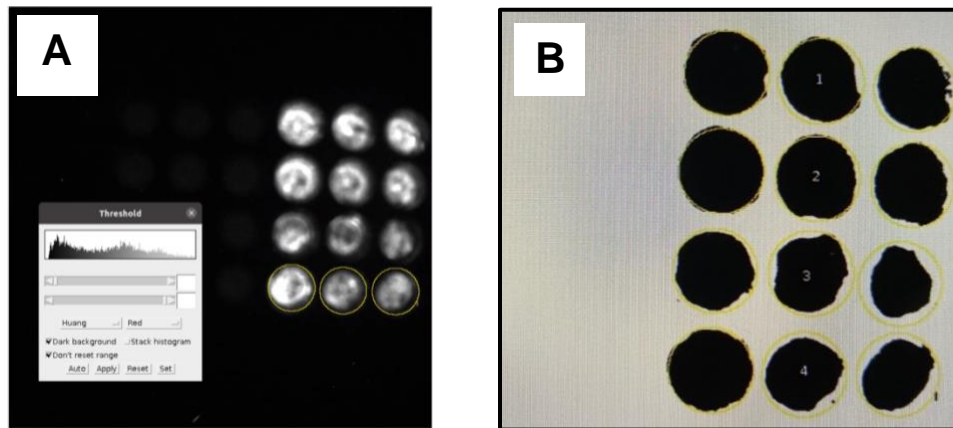


Figure 4.3 Bespoke macro code for image analysis in FIJI. Code used to analyse Alligator images of experiments using *Per2-dLuc* 3T3-L1 and CAG-luc-eGFP primary mouse pre-adipocytes. Panel (A) demonstrates regions of interest (wells) and the Huang thresholding method of line code 29 (Annex B). Inset panel (B) shows ROIs after noise and background interference have been negated of line code 128 (Annex B).

4.5.2 Results and discussion

4.5.2.1 Layering HA hydrogel with *Per2-dLuc* 3T3-L1 adipocytes: cellular viability and differentiation

Having generated and tested the macro for reliability in analysing Alligator images, I investigated the effects of HA hydrogel on *Per2-dLuc* 3T3-L1 cell viability in various conditions. This Section describes *Per2-dLuc* 3T3-L1 cell viability sitting on plastic, under a layer of HA hydrogel. As explained in Section 4.3, a 6% HA hydrogel with a HA-ALD:HA-HYD ratio of 1:2 was chosen for its mechanical and degradation characteristics.

The experimental conditions were to mimic the clinical conditions where patients received lipoaspirate encapsulated within HA hydrogel. The aim was for cells to thus be exposed to gel in a three-dimensional manner, and not just flat, on a one-dimensional surface. However, 3T3-L1 cells are typically grown in two-dimensions on plastic which has been demonstrated to elicit normal cell behaviour (Levine and Stockdale, 1984, Mandrup et al., 1998, Kramer et al., 2014). Therefore, I investigated i) whether 3T3-L1 adipocytes required adhesion to proliferate and differentiate on HA hydrogel (i.e., not plastic) and ii) the effects of how HA hydrogel impaired differentiation and diffusion of nutrients to the cells.

Two sets of experiments were performed in triplicate using *Per2-dLuc* 3T3-L1 cells: cell survival on top of a layer of HA hydrogel, and cell survival under a layer of HA hydrogel. A schematic of both experiments is shown in Figure 4.4.

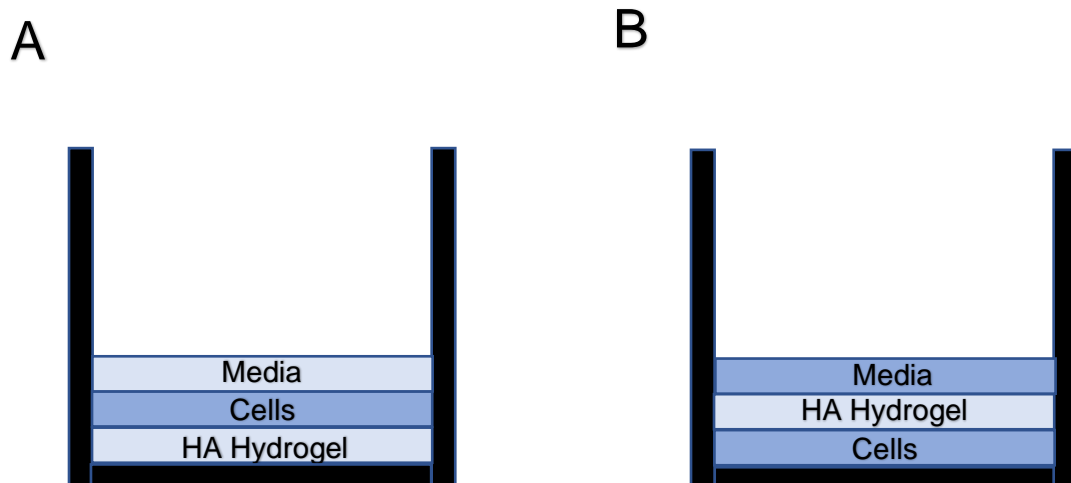


Figure 4.4 Schematic representation of two experimental conditions. (A) HA hydrogel was gelled (6% concentration, HA-ALD:HA-HYD 1:2 ratio) on the bottom of a 24 well plate for 30 minutes and *Per2-dLuc* 3T3-L1 cells were seeded (120,000 cells/well) on top of the HA hydrogel. **(B)** *Per2-dLuc* 3T3-L1 cells were seeded (120,000 cells/well) and HA hydrogel (6% concentration, HA-ALD:HA-HYD 1:2 ratio) carefully added to the well. In both conditions, cells were grown in the induction media for 48 hours, before being switched to maintenance media till the end of the experiment.

4.5.2.1.1 Cellular viability assessed using photon emission in *Per2-dLuc* 3T3-L1 cells grown on top of HA hydrogel

On Day 0, HA-ALD (50 μ L) was pipetted into wells of a 24 well plate, followed by HA-HYD (50 μ L) and allowed to gelate for 30 minutes. *Per2-dLuc* 3T3-L1 cells were seeded (120,000 density) in F12/DMEM media, supplemented with D-luciferin (1 mM) as shown in Figure 4.4A. The plate was incubated in the Alligator bioluminescence detector (Section 2.3.8) for longitudinal luciferase activity recording.

On Day 1, the 3T3-L1 adipocyte differentiation programme was initiated, and media was replaced with induction media (500 μ L) to each well, supplemented with D-luciferin (described in Section 2.3.6.2.2). The plate was returned to the Alligator bioluminescence detector and the induction media changed daily. On Day 3, the induction media was changed to maintenance media (500 μ L) supplemented with D-luciferin (described in Section 2.3.6.2.3) and returned to the Alligator bioluminescence detector, with a change of media every 48-72 hours. Notably, media was changed at the same time of day.

Control cells were seeded in the same conditions but maintained in culture media that followed the change to induction media (Day 1) and maintenance media (Day 3), described above. Image capture was ended after seven days (173 hours), where final data capture was performed, and mRNA extracted for adipocyte markers expression analysis (Section 4.5.2.1.2).

Figure 4.5 demonstrated that *Per2-dLuc* 3T3-L1 control cells that were maintained in media without HA hydrogel showed periodic luciferase expression, as evidenced by higher photon emission when luciferase was induced and low photon emission when luciferase was not expressed. This periodicity was ~24 hours, which has been reported in the literature (Ramanathan et al., 2012, Ramanathan et al., 2014) and was relatively constant throughout the seven-day experiment.

As seen in Figure 4.5A, the lack of oscillation between 85 and 130 hours may be due to decreased luciferin concentration in the media as changes in media were less frequent during this time period. Data presented are representative of n=3 independent experiments where the same pattern was observed. This is in line with the oscillations re-occurring with the same periodicity, when fresh media was provided at just past 130 hours. Oscillations were also observed in *Per2-dLuc* 3T3-L1 cells grown on a layer of HA hydrogel and paralleled the photon emission of control cells. Periodicities and patterns (including the lapse in oscillations between 85 and 130 hours) were similar in both conditions. Unexpectedly, however, considering that the cells behaved similarly in both conditions, the number of emitted photons was significantly and consistently lower (15.8%) in the cells grown on the HA hydrogel than in the control cells, at any time during the experiment (Figure 4.5B).

Surprisingly, at $t = 0$ (i.e., Day 0) where cells were seeded onto wells pre-coated with HA hydrogel, the difference in photon emission was readily significant. This was despite having the same cellular density (120,000 cells/well) in both conditions (control wells (no gel) and pre-coated wells). It was also interesting to note that the shift towards lower emission (in cells grown on HA hydrogel layer) remained typically of the same proportion during the entire experiment, suggesting that the HA hydrogel was intrinsically impairing photon emission (or the ability of the apparatus to record them) rather than affecting cell viability.

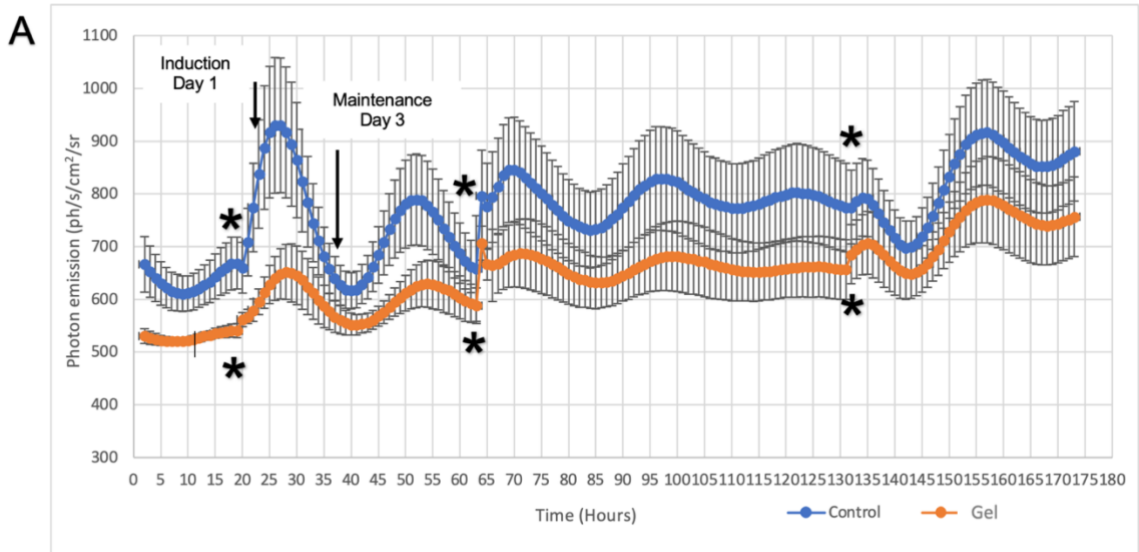
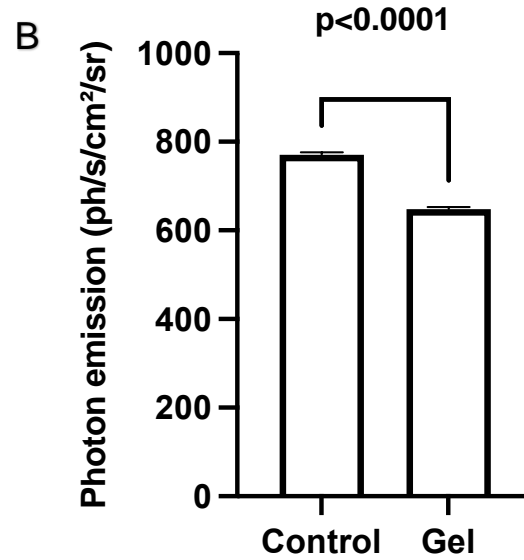


Figure 4.5 (A) Time course quantification of photons emitted by *Per2-dLuc* 3T3-L1 cells grown on top of a layer of HA hydrogel (6% concentration, HA-ALD:HA-HYD ratio 1:2). Cells were seeded in 24 well plates on HA hydrogel (orange line) or on plastic (blue line). The adipocyte differentiation process was induced by the addition of the induction media (Section 2.3.6.2.2) with luciferin (1 mM) to reveal luciferase expression via photon emission recorded using the Alligator bioluminescence detector. At Day 3, induction media was replaced by maintenance media with luciferin. Media changes are indicated by an arrow. Data was collected for five days following luciferin addition (data is mean \pm s.e.m, n=3 experiments).



(B) Mean photon emission by *Per2-dLuc* 3T3-L1 control cells and *Per2-dLuc* 3T3-L1 cells grown on a layer of HA hydrogel (6% concentration, HA-ALD:HA-HYD ratio 1:2). Control *Per2-dLuc* 3T3-L1 cells grown on plastic (dark grey bar). *Per2-dLuc* 3T3-L1 cells grown on HA hydrogel (light grey bar). (data is mean \pm s.e.m, n=3 experiments, unpaired student's t test ** p<0.0001).**

These effects were confirmed in the following experiment (see Section 4.5.2.1.2, Figure 4.6) where at $t=0$, cells were first seeded onto the plastic in the same conditions before the addition (or not) of HA hydrogel. At $t=0$, photon emission was identical in all conditions. The shift was only observed a few hours after the addition of the HA hydrogel. In any case, this data suggested that the presence of HA was not altering cell viability or growth and demonstrated that adipocytes, whose growth and differentiation are usually dependent on adherence, were not affected by the presence of HA hydrogel.

4.5.2.1.2 Cellular viability assessed using photon emission and characterisation of mature adipocyte gene markers of *Per2-dLuc* 3T3-L1 cells grown under a layer of HA hydrogel

Having examined the cellular viability of *Per2-dLuc* 3T3-L1 cells proliferating on HA hydrogel in Section 4.5.2.1.1, the next step was to investigate whether the HA hydrogel was permeable to nutrients present in media. Diffusion of nutrients through HA hydrogel to reach *Per2-dLuc* 3T3-L1 cells is a critically important in order to understand whether adipocytes can proliferate and differentiation whilst fully encapsulated within HA hydrogel, as will be the case in the true conditions that lipoaspirate would experience during adipose tissue transfer in humans for breast reconstruction (Section 1.3).

As seen in Section 4.5.2.1.1, 3T3-L1 cells demonstrated a number of emitted photons significantly and consistently lower (15.8%) in the cells grown on the HA hydrogel than in the control cells, at any time during the experiment (Figure 4.5B). The design of the experiment in this Section allowed both intervention and control-arm *Per2-dLuc* 3T3-L1 cells to adhere on plastic, with HA hydrogel in the intervention arm being added on the cells in a thin layer, thereby removing any effects the cells may feel growing on a non-plastic surface (such as HA hydrogel).

Cell characterisation in this Chapter was limited to cell survival in varying gel exposures using photon emission of *Per2-dLuc* 3T3-L1 adipocytes. In order to investigate whether HA hydrogel has any effects on adipocyte differentiation, markers of differentiation were examined at the end of the experiment. A number of candidates for mature adipocyte genetic expression are described in the literature (Dani et al., 1997, Maeda et al., 1997). As described in Section 1.2.5, a series of genes are upregulated and expressed to induce differentiation from pre-adipocytes to mature adipocytes. Three gene targets were used to interrogate mature adipocyte gene expression: CD36, peroxisome proliferator-activated receptor gamma (PPAR- γ) and fatty acid binding protein P4 (FABP4) in murine cells. As described in Section 1.2.5.1, PPAR- γ as a critical transcription factor in adipocyte differentiation, and is an early/mid regulator of adipogenesis, with FABP4 and CD36 having roles in the orchestration of a host of transcription factors resulting in adipocyte differentiation (Gregoire, 2001). The housekeeping gene RPL7 was used, as it maintained stable expression through differentiation (Dani et al., 1997, Maeda et al., 1997).

Per2-dLuc 3T3-L1 cells were seeded (120,000 cells per well). Cells reached 90% confluence on Day 1, and HA-ALD (50 μ L) was carefully added onto the surface of the cell layer, followed by HA-HYD (50 μ L) to allow gelation in situ. After gelation, induction media was added and supplemented with D-luciferin, and switched to maintenance differentiation media two days later. Recordings were ended on Day 5 (116 hours) in the Alligator detector, where final acquisition was performed. At the end of the experiment on Day 5, mRNAs were harvested, and gene expression levels were quantified using qPCR. Table 2.3 displays the references of Taqman essays for specific adipose differentiation markers.

Figure 4.6A showed both *Per2-dLuc* 3T3-L1 adipocytes in control conditions and under HA hydrogel exhibited periodicity. The periodicity displayed for both conditions was ~24 hours in duration and was reproducible over the course of the experiment. This mirrored the findings described in Figure 4.5A for *Per2-dLuc* 3T3-L1 adipocytes grown atop a layer of HA hydrogel.

There were also periods of low oscillation (between 45 to 63 hours and again between 85 and 105 hours) as seen in Figure 4.6A, which could be attributed to lower available luciferin present in the media due to less frequent media changes (signified by * in Figure 4.6A).

Periodicity was restored when the media was changed at 67 hours and 106 hours, when concentrations of available luciferin were restored, and photon emission resumed via the action of luciferase. Figure 4.6A demonstrates the same photon emission for control and intervention (cells under HA hydrogel) at $t = 0$ (i.e.; Day 0), when cells were seeded onto wells. The two traces took 2-3 days to diverge, suggesting an evolving condition that resulted in the divergence. This may be explained by the changing characteristics of HA hydrogel. As described in Section 3.4.3, HA hydrogel at 6% concentration and 1:2 HA-ALD:HA-HYD ratio swelled past its starting weight when exposed to degradation solutions (PBS, media and hyaluronidases) as seen in Figures 3.11, 3.12 and 3.13. This suggested that the gel was not fully hydrated prior to the start of the experiment (despite allowing gelation for 30 minutes). As such, the swelling of the HA hydrogel layer in wells may have resulted in mechanical movement of the gel, exerting shearing forces on the cells adhered to the bottom of the cells, possibly comprising their viability.

This would explain the divergence in photon emission between control and *Per2-dLuc* 3T3-L1 adipocytes after t=0 under HA hydrogel- a difference which was maintained till the end of the experiment. As shown in Figure 4.6B, this difference was 15.2%. Nonetheless, the data demonstrates that nutrients were able to diffuse through the HA hydrogel as the cells survived.

As shown in Figure 4.7, PPAR- γ gene expression was observed in control cells that were grown in media only. Of note, is that PPAR- γ was expressed in fully differentiated cells of mRNA isolated at Day 5, which is still early in the differentiation programme. There was no difference in PPAR- γ expression between *Per2-dLuc* 3T3-L1 cells differentiated under HA hydrogel compared to control. This data strongly suggests that the presence of HA hydrogel, whilst altering photon emission through an unclear mechanism, does not alter adipose tissue differentiation.

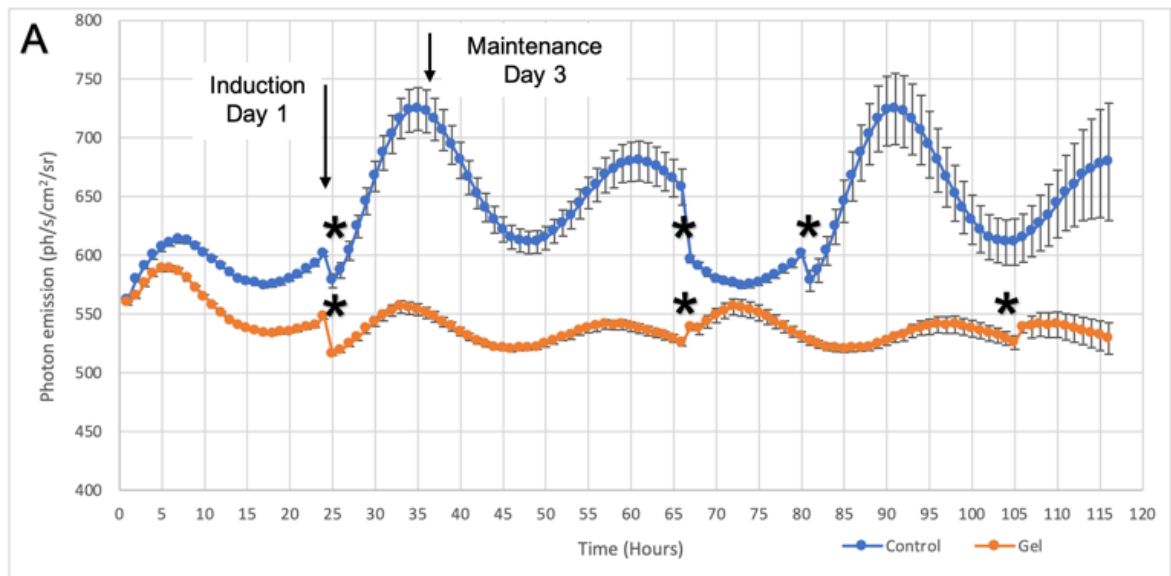
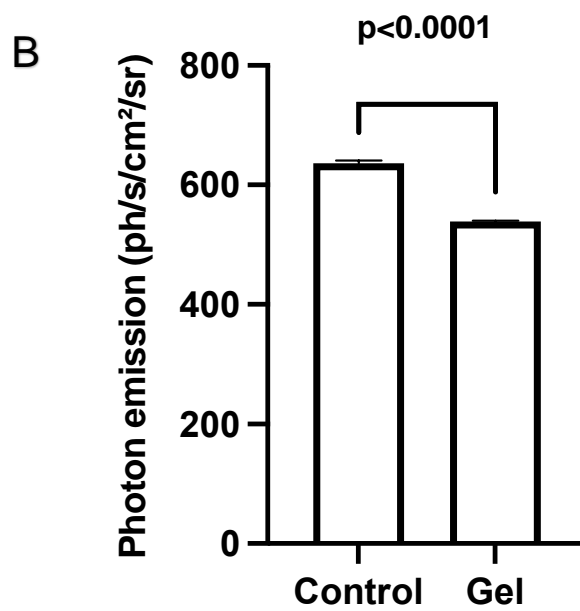


Figure 4.6 (A) Time course quantification of photons emitted by *Per2-dLuc* 3T3-L1 cells grown beneath a layer of HA hydrogel (6% concentration, HA-ALD:HA-HYD ratio 1:2). Cells were seeded in 24 well plates on HA hydrogel (orange line) or on plastic (blue line). The adipocyte differentiation process was induced by the addition of the induction media (Section 2.3.6.2.2) with luciferin (1 mM) to reveal luciferase expression via photon emission recorded using the Alligator bioluminescence detector. At Day 3, induction media was replaced by maintenance media with luciferin. Media changes are indicated by an arrow. Data was collected for five days following luciferin addition (data is mean \pm s.e.m, n=3 experiments).



(B) Mean photon emission by *Per2-dLuc* 3T3-L1 control cells and *Per2-dLuc* 3T3-L1 cells grown beneath a layer of HA hydrogel (6% concentration, HA-ALD:HA-HYD ratio 1:2). Control *Per2-dLuc* 3T3-L1 cells grown on plastic (dark grey bar). *Per2-dLuc* 3T3-L1 cells grown beneath HA hydrogel (light grey bar) (data is mean \pm s.e.m, n=3 experiments, unpaired student's t test **** p<0.0001).

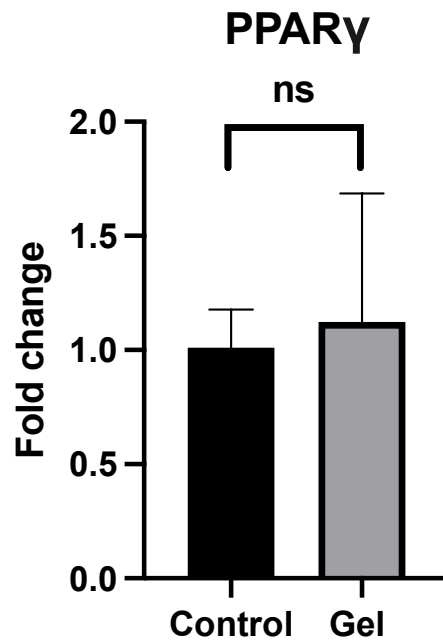


Figure 4.7 Mean expression of PPAR- γ normalised to RPL7 in 3T3-L1 cells. 3T3-L1 cells were seeded at 100,000 per well in 24-well plates. HA hydrogel was added onto 90% confluent cells. Control well contains cells only. Both control and HA hydrogel-covered cells were maintained in an induction media for two days and switched to a maintenance media on Day 3. On Day 5, cells were harvested and PPAR- γ mRNA expression levels were determined by qPCR (n= 3, students t test, ns=not significant. Mean \pm s.e.m).

4.6 Primary CAG-luc-eGFP murine adipocyte viability using photon emission and characterisation of mature adipocyte gene markers in cells grown on HA hydrogel and cells encapsulated within HA hydrogel

Sections 4.5.2.1.1 and 4.5.2.1.2 described cells grown on a layer of HA hydrogel and cells grown under a layer of HA hydrogel compared to control, respectively. They demonstrated that *Per2-dLuc* 3T3-L1 cells survived when exposed to HA hydrogel in this manner, with a ~15% reduction of photon emission for both experiments compared to control, without however, demonstrating any negative effects on gene expression of mature adipocyte markers. This strongly supported the fact that HA hydrogel did not impact adipocyte differentiation adversely, when grown under a layer of HA hydrogel.

However, cells grown under HA hydrogel are barely representative of the clinical conditions where adipocytes will be injected encapsulated within HA hydrogel to form beads in a three-dimensional manner. Thus, HA hydrogel encapsulation experiments in this Chapter were more physiological and closer to the true conditions that lipoaspirate would experience during adipose tissue transfer in humans for breast reconstruction (Section 1.3).

To investigate the effect of HA hydrogel on adipocytes encapsulated fully within the HA hydrogel, FVB-Tg (CAG-luc-eGFP)L2G85Chco/J homozygous mice were used. These are whole-body conventional luciferase-expressing mice and luciferase was detected in the animal's adipose tissues (Dr Greaves, unpublished data). Primary adipocytes were harvested, and their differentiation and viability tested in HA hydrogel as described above. Briefly, a combination of three-month old male and female mice were utilised. The mice were culled using carbon dioxide as per Home Office guidance and gonadal adipose tissue was harvested as described in Section 2.3.6.4.1. Having isolated adipocytes, three

experimental conditions were devised where primary cells were seeded at the same density i) without HA hydrogel (control), ii) on top of a layer of HA hydrogel and iii) cells were mixed with HA hydrogel in wells. For this experiment, the cells were seeded at a higher density compared to Section 4.5.2.1 (150,000 cells rather than 120,000), to empirically account for the increased cell surface area through mixing, i.e., suspended in three dimensions rather than in two dimensions that cells experience, being grown in a single plane on top of a layer of HA hydrogel or on plastic under HA hydrogel.

Primary murine CAG-luc-eGFP adipocyte culture is described in Section 2.3.6.4.2. On Day 0, HA-ALD (50 μ L) was pipetted into in a 24 well plate, followed by HA-HYD (50 μ L) and allowed to gelate for 30 minutes. CAG-luc-eGFP primary adipocytes were seeded (150,000 cells/well) into wells with F12/DMEM media supplemented with D-luciferin. On Day 1, media was replaced with of induction media, supplemented with luciferin (Section 2.3.6.2.2) and three wells mixed to disperse the cells within the gel in three-dimensional manner using a pipette tip. On Day 3, the induction media was changed to maintenance media supplemented with D-luciferin, with a change of maintenance media every 48 to 72 hours.

A diagram of the three experiment conditions is shown in Figure 4.8. Images were captured till Day 5 (103 hours). Importantly, all media was changed at the same time of day for consistency. Control cells were seeded in the same conditions but without HA hydrogel. On Day 5, recordings were stopped when the final acquisition was performed. mRNA was extracted for gene analysis and processed in the same manner as described in Section 2.3.10 and 4.5.2.1.2.

As seen in Figure 4.9, primary CAG-luc-eGFP adipocytes that were maintained in media supplemented with luciferin without HA hydrogel demonstrated bioluminescence, as shown by photon emission. Overall, there was a significant difference of all three groups, with control cells emitting the most photons, followed by cells mixed in with HA hydrogel and finally, cells on top of

HA hydrogel. However, the differences between these conditions are small. CAG-luc-eGFP adipocytes that were encapsulated within the HA hydrogel demonstrated better luminescence than cells grown on top of the HA hydrogel. This is reassuring, as primary CAG-luc-eGFP adipocyte luminescence was better when exposed to HA hydrogel in a more physiological condition i.e., that replicates lipoaspirate injected in reconstructive procedures where primary cells are in contact with HA hydrogel in three dimensions (mixed in) rather than in contact with only one surface (cells grown on HA hydrogel). CAG-luc-eGFP primary murine adipocyte gene expression was then investigated for each of the three cell conditions (cells mixed with HA hydrogel, on top of HA hydrogel and control without HA hydrogel). This was to establish whether the HA hydrogel conditions altered the adipocyte gene expression in these primary murine cells. The same gene targets used in previous experiments were interrogated to characterise differentiation: CD36 and PPAR- γ , normalised to RPL7.

As seen in Figure 4.10, control CAG-luc-eGFP primary murine adipocytes grown in media only expressed CD36 and PPAR- γ . Importantly, there was no significant difference in CD36 or PPAR- γ mRNA levels between control, CAG-luc-eGFP primary murine adipocytes grown on top of HA hydrogel and mixed with HA hydrogel; strongly suggesting that the HA hydrogel did not affect primary murine adipocyte differentiation.

Figure 4.11 shows CAG-luc-eGFP primary murine adipocyte morphology seeded at (150,000 cells/well) on top of the HA hydrogel at the end of the experiment at Day 5 (Figure 4.8A) at 4x and 20x magnification. As seen, there was no observable difference in cell morphology of CAG-luc-eGFP primary murine adipocytes on top of gel compared to control.

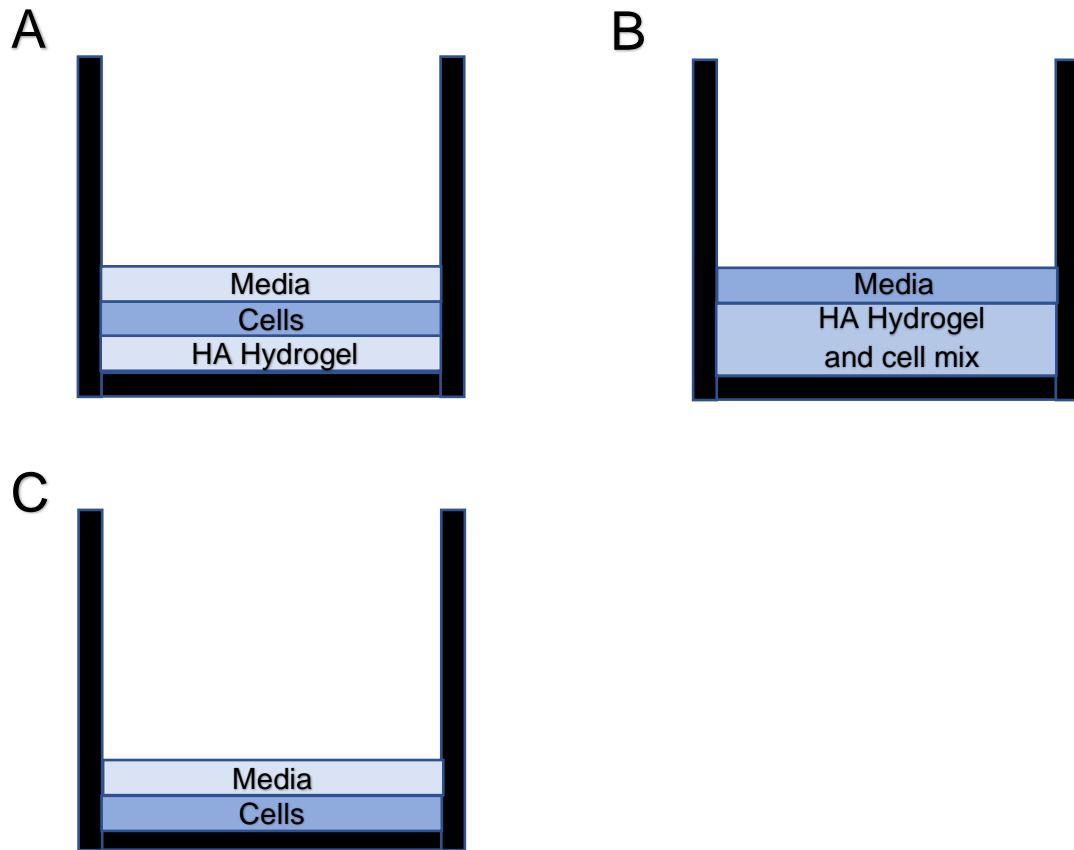


Figure 4.8

Schematic representation of three experimental conditions. **(A)** HA hydrogel was gelled (6% concentration, HA-ALD:HA-HYD 1:2 ratio) on the bottom of a 24 well plate for 30 minutes and CAG-luc-eGFP adipocytes were seeded (150,000 cells/well) on top of the HA hydrogel. **(B)** HA hydrogel (6% concentration, HA-ALD:HA-HYD 1:2 ratio) and CAG-luc-eGFP adipocytes were seeded (150,000 cells/well) in wells and mixed to allow gelation, with cells suspended within the HA hydrogel. **(C)** CAG-luc-eGFP adipocytes were seeded (150,000 cells/well) in wells without HA hydrogel as control. All cell conditions were maintained in an induction media for two days and switched to maintenance media on Day 3. On Day 5 image capture was stopped.

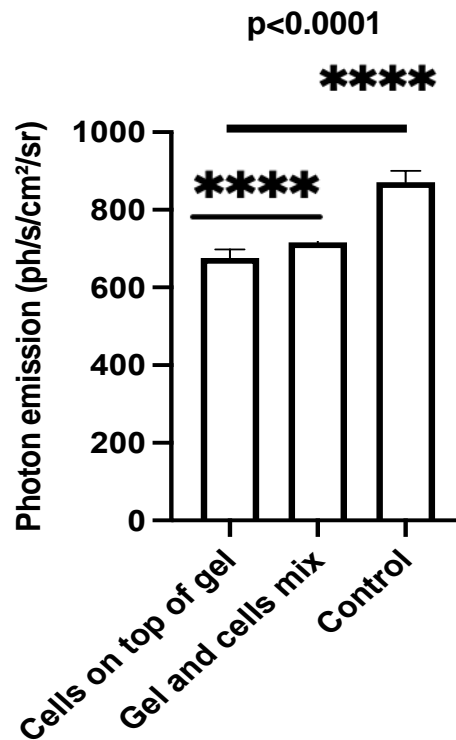


Figure 4.9 Mean photon emission of CAG-luc-eGFP adipocytes (seeded at 150,000 cells/ well) on top of HA hydrogel (dark grey, left bar), mixed within HA hydrogel (light grey, middle bar) and control cells (intermediate grey, right bar). The HA hydrogel used was at 6% concentration and a HA-ALD:HA-HYD ratio of 1:2. Control wells contained cells only. All cell conditions were maintained in an induction media for two days and switched to maintenance media on Day 3. On Day 5 image capture was stopped (n=3 independent experiments. Mean \pm s.e.m, one sample t test, **** p<0.0001).

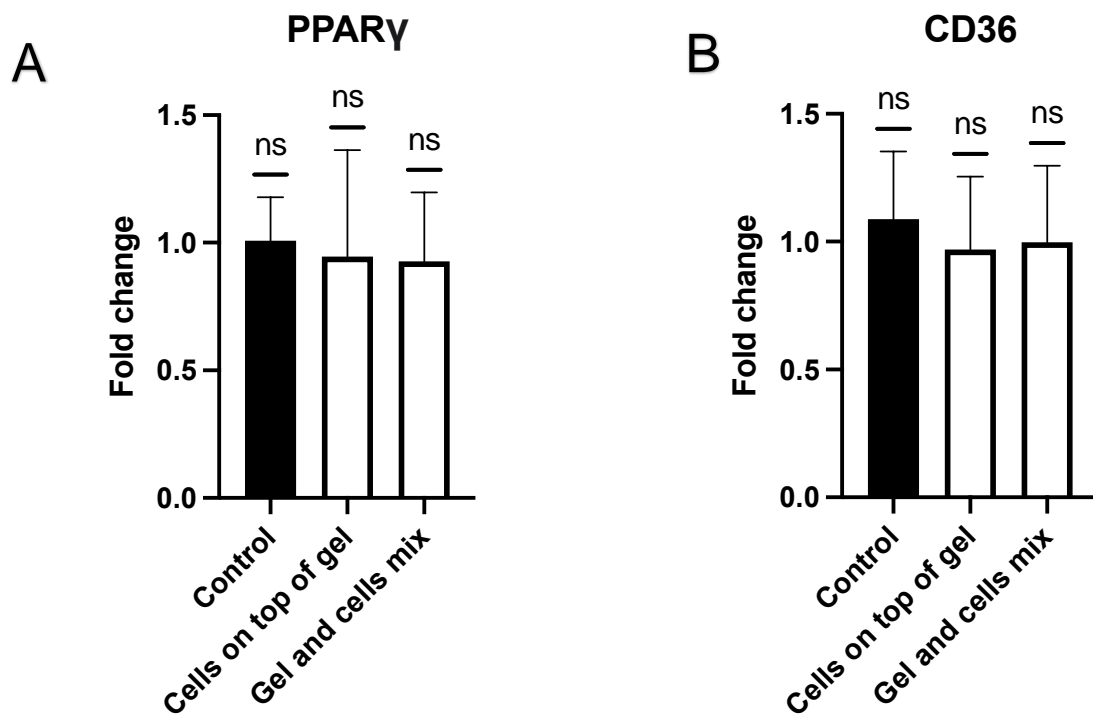


Figure 4.10 (A) Primary murine pre-adipocytes mean expression of PPAR γ . (B) Primary murine pre-adipocytes mean expression of CD36. Normalised to RPL7. Primary murine pre-adipocytes were seeded at 150,000 cells per well in 24-well plates on top of HA hydrogel. Control wells were cells only. For the mixed condition on Day 1, HA hydrogel and cells were mixed, and all wells were maintained in an induction media for two days and switched to a maintenance media on Day 3. On Day 5, cells were harvested and PPAR γ and CD36 mRNA expression levels were determined by qPCR (n= 3, one-way ANOVA, ns- non-significant. Error bars one standard deviation).

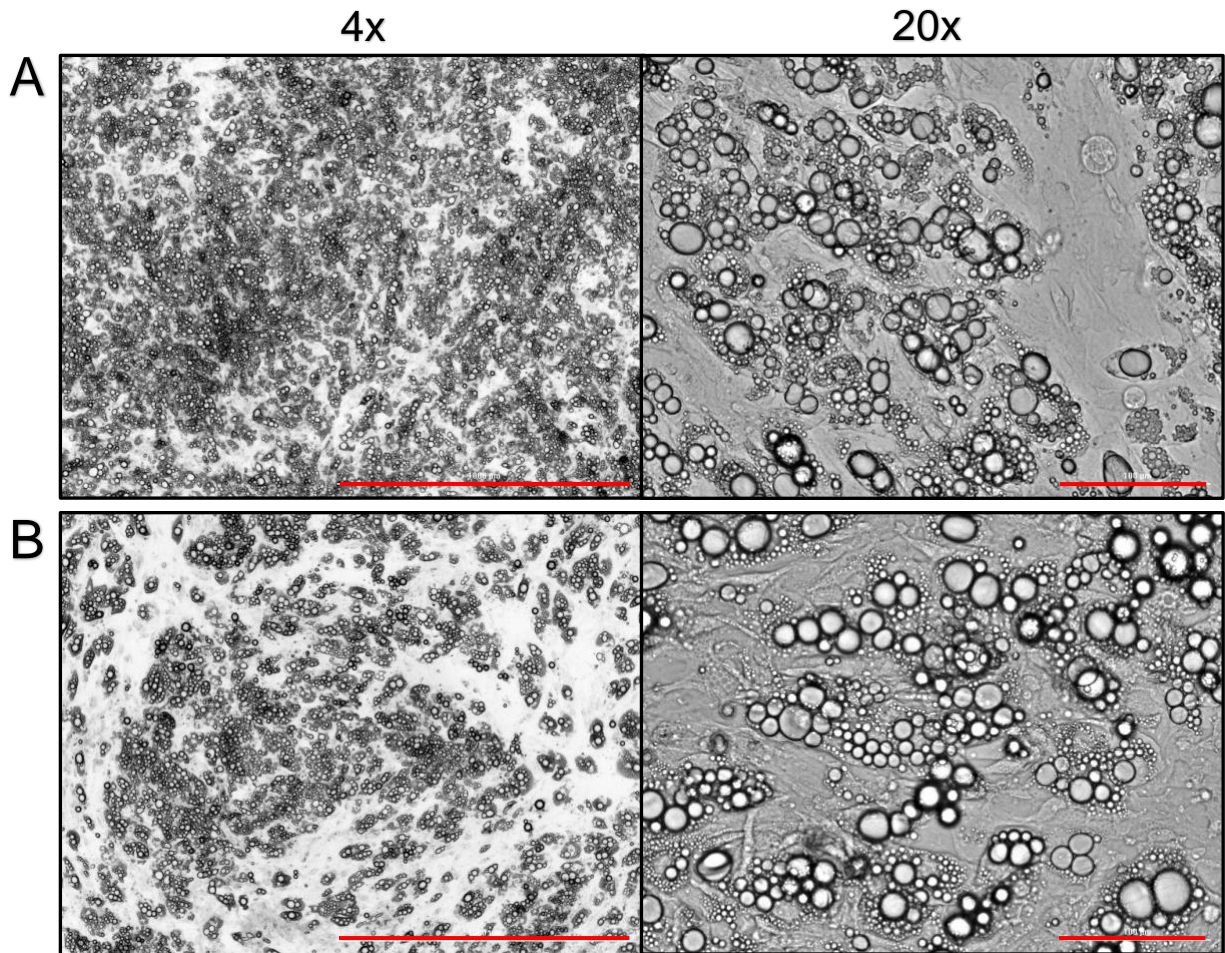


Figure 4.11 Primary murine pre-adipocyte morphology grown on HA gel at Day 5 compared to control. (A) Primary murine pre-adipocytes were seeded at 150,000 cells per well in 24-well plates on top of HA hydrogel (6% concentration, HA-ALD:HA-HYD 1:2 ratio). **(B)** Control wells were cells only. On Day 5, cells were photographed at 4x and 20x using the EVOS FL auto imaging system (Thermo Fisher Scientific, Waltham, MA). Pictures are representative images of n=3 independent experiments performed in triplicates. Scale (red line) 1000 μm and 100 μm for 4x and 20x magnification, respectively.

4.7 Mature adipocyte gene marker characterisation of primary human adipocytes grown under a layer of HA hydrogel

In addition to cells of murine origin, human primary pre-adipocytes were differentiated in the presence of gel and gene markers of differentiation were examined. Human primary pre-adipocytes were used as they are a constituent of primary adipose tissue transfer reconstructive procedures described in Chapter 1.3. In this Section, three gene targets were used to interrogate mature adipocyte gene expression: CD36, peroxisome proliferator-activated receptor gamma (PPAR- γ) and adipocyte protein 2 (aP2) in human cells, normalised to RPL7, as previously described.

Primary human adipocyte harvest and subculture is described in Section 2.3.6.5. Briefly, on Day 0, primary human adipocytes were seeded (120 000 cells per well) in a 24-well plate in F12/DMEM. Cells reached 90% confluence on Day 1, and HA-ALD (50 μ L) was carefully added onto the surface of the cell layer, followed by HA-HYD (50 μ L) to allow gelation *in situ*. The gel concentration used was 6% in a HA-ALD:HA-HYD 1:2 ratio. Wells with cells only were defined as control wells. After gelation, induction media was added to each well (described in Section 2.3.6.2.2). On Day 3, the induction media was changed to maintenance differentiation. Control cells were seeded in the same conditions but maintained in culture media (induction of Day 1 and maintenance on Day 3) only. At the end of the experiment, mRNAs were extracted, and gene expression levels were quantified using qPCR.

Figure 4.12 shows that CD36, PPAR- γ and aP2 gene expression was observed in control primary murine adipocytes. Remarkably, there was no difference in CD36, PPAR- γ or aP2 gene expression levels between control and cells grown under HA hydrogel (normalised to RPL7), showing that HA hydrogel may be used in the context of primary human adipocytes.

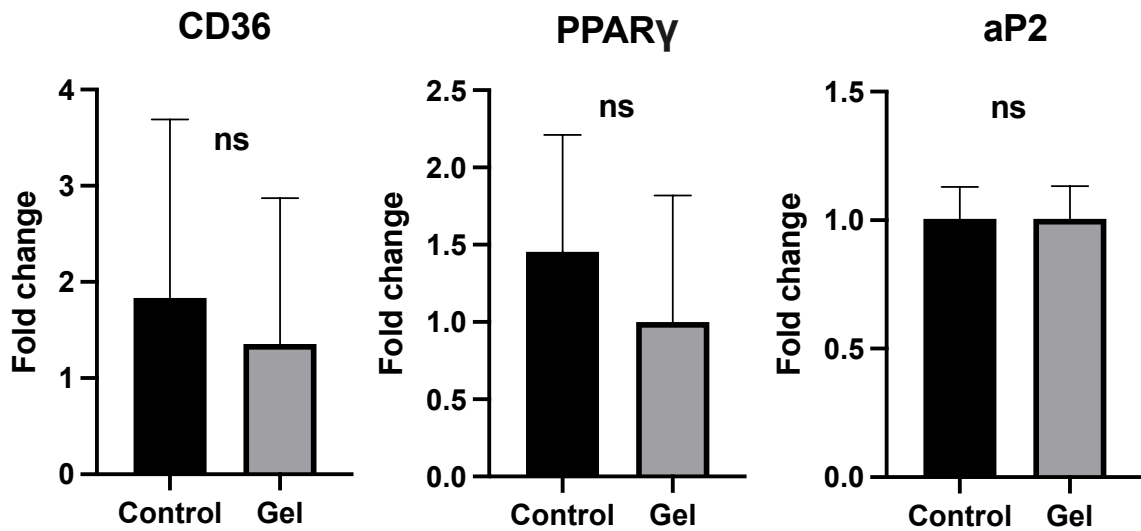


Figure 4.12 Mean expression of adipocyte genes normalised to the housekeeping gene RPL-7 in primary human adipocytes. Cells were seeded at 120,000 per well in 24-well plates. HA hydrogel was added on 90% confluent cells. Control well contains cells only. Both control and HA hydrogel-covered cells were maintained in an induction media for two days and switched to a maintenance media on Day 3. On Day 5, cells were harvested and CD36, PPAR γ and aP2 mRNA expression levels were determined by qPCR (n= 3, students t-test, ns- non-significant. Error bars one standard deviation).

4.8 Conclusion

This Chapter has demonstrated that *Per2-dLuc* 3T3-L1, CAG-luc-eGFP primary murine adipocytes and primary human adipocytes remained viable when exposed to HA hydrogel. Cell viability and survival investigations were made possible by the construction of a bespoke macro written in FIJI for the analysis of photon emission from bioluminescent cell types.

For *Per2-dLuc* 3T3-L1 cells exposed to HA hydrogel (all conditions), there was a ~15% reduction in photon emission compared to control. As described in Section 4.5.2.1.1, there was already a difference in photon emission from Day 0 ($t = 0$) for *Per2-dLuc* 3T3-L1 cells grown on top of HA hydrogel compared to control (Figure 4.5A). Further investigations will be necessary to elucidate the underlining phenomenon responsible for the apparent difference. For example, growing *Per2-dLuc* 3T3-L1 cells on a semi-permeable membrane inset, which sits on HA hydrogel, compared to *Per2-dLuc* 3T3-L1 cells growing directly on HA hydrogel and control cells without any gel might give insights about the possible mechanical factors causing the immediate reduction in photon emission of *Per2-dLuc* 3T3-L1 cells proliferating directly on HA hydrogel. The insert may prevent cells from falling into ridges/ microscopic holes on the HA hydrogel surface which may impair photon emission.

This effect was not seen, however, for *Per2-dLuc* 3T3-L1 cells grown underneath HA hydrogel, where both intervention *Per2-dLuc* 3T3-L1 cells and control cells emitted the same photon intensity at the start of the experiment when $t = 0$ (Figure 4.6A), and then diverged over the period of several days. As explained in Section 4.5.2.1.2, the difference over several days may be caused by continued hydration of HA hydrogel in media, an effect that was seen in Section 3.4.3. This would cause an increase in weight and size of the HA hydrogel, causing shearing effects on the *Per2-dLuc* 3T3-L1 cells growing beneath HA hydrogel, potentially scraping off cells from their attachments and thus affecting

photon emission. A method to counteract this effect may be to prepare the gel in advance by 2-3 days and expose the HA hydrogel to F12/DMEM media during this time. Thus, the HA hydrogel would be maximally hydrated when added to a layer of adhered cells on plastic, reducing the chance of further change in the gel's physical characteristics. *Per2-dLuc* 3T3-L1 cells under HA hydrogel had no statistically significant difference in the mature adipocyte expression marker PPAR γ compared to control. Coupled with the photon emission findings, HA hydrogel permits proliferation and differentiation of *Per2-dLuc* 3T3-L1 cells exposed to HA hydrogel.

CAG-luc-eGFP primary murine adipocytes demonstrated proliferation and differentiation when exposed to HA hydrogel, with cells mixed in with HA hydrogel demonstrating better photon emission than cells grown on top of gel (Section 4.6). This was reassuring as it satisfied the question of whether primary cells can survive when fully encapsulated in gel, similar to “real life” adipose tissue transfer procedures where cells are implanted in three dimensions, as described in Section 1.3. HA hydrogel did not affect CAG-luc-eGFP primary murine adipocytes in term of gene expression for PPAR γ and CD36, confirming that the gel does not affect CAG-luc-eGFP primary murine adipocyte character.

Finally, primary human adipocytes grown under a layer of HA hydrogel did not show any difference compared to control for adipocyte gene expression markers CD36, PPAR γ and aP2 expression (Section 4.7). This confirms that the HA hydrogel does not impair mature adipocyte characteristics of primary human adipocytes- the same population of cells that is used in adipose tissue transfer reconstruction surgery.

Chapter Five: *In vivo* effects of HA hydrogel on injected adipocytes in a murine model

5.1 Introduction

Chapter 3 focussed on chemical synthesis and rheological characterisation of the novel HA hydrogel, followed by cell viability and gene expression studies *in vitro* with HA hydrogel in Chapter 4. Having firstly determined the optimal HA hydrogel concentration and the best ratio of HA-ALD:HA-HYD gel to maintain its shape, self-healing properties and function; and secondly, demonstrating that 3T3-L1 adipocytes grow and differentiate adequately under, on and mixed in with gel, I next investigated HA hydrogel to optimise adipocyte tissue transfer in an animal model.

5.1.1 Selection of the *in vivo* model

A murine animal model has been used to interrogate *in vivo* survival of lipo-aspirate previously (Thanik et al., 2009, Kirkham et al., 2012). Thanik et al., 2009 developed the first murine model to study the fate of injected adipose tissue and cell populations contained within. The authors injected nude mice with 2 mL of human lipo-aspirate into the dorsal subcutaneous space of recipient mice in a fan-like pattern. The dorsal skin and associated adipose tissue were excised at various timepoints and volumetric analysis performed at the end of an eight week period. Gross analysis of injected lipo-aspirate demonstrated the adipose tissue was healthy, non-fibrotic and well vascularised with a minimal inflammatory or capsular reaction using haematoxylin and eosin analysis.

Using a murine model, Kirkham et al., 2012 injected lipo-aspirate surplus to clinical need from female human patients undergoing elective liposuction, harvested using two aspiration cannular sizes (5 mm and 3 mm diameter). The lipo-aspirate was injected into nude mice using a 14-gauge needle, with excision of the injected adipose tissue after six weeks for histological examination. The authors found human adipose tissue harvested using a 5 mm cannula retained 25% more weight compared to a 3 mm cannula harvest group.

However, as in humans, injected lipo-aspirate has variable graft take in a murine model, with injected adipocytes being subjected to resorption, necrosis and the formation of oil cysts which decreases the volume of adipose tissue retained after injection (Thanik et al., 2009, Kirkham et al., 2012). A murine model was chosen based on a search of the literature and the examples detailed above which set a precedent for the injection of lipo-aspirate into a murine *in vivo* model.

5.2 Chapter aims

In this Chapter, the overarching goals were to demonstrate that murine models were not negatively impacted by injection of HA hydrogel, and that lipo-aspirate survived when it was injected mixed with HA hydrogel.

As described in Section 5.1.1, numerous papers described injection of lipoaspirate in a murine model in a variety of techniques (Thanik et al., 2009, Kirkham et al., 2012). As such, the proliferation of injected adipocytes in previous studies was not a proof of concept that lipoaspirate would survive in this study. Thus, a pilot murine study investigating injection methodology and survival was performed, so that data gathered from this pilot could inform the formulation of learning points to improve and inform a main murine study design. Additionally, in order to track survival of injected lipo-aspirate in a murine model, a reproducible methodology needed to be developed.

After completion of the pilot murine study, a main murine study was designed and implemented with learning points and improvements taken from the pilot murine study. This study aimed to investigate adipocyte survival with HA hydrogel *in vivo*. At the end of the main murine study, gene expression of markers of differentiation were examined in the graft.

5.3 Pilot murine study: design optimisation

The pilot murine study was performed to ensure that methodology could be applied with minimal animal suffering or waste, and to yield a good quality data set for the main murine study.

5.3.1 Methods

5.3.1.1 Whole body luciferase expressing (CAG-luc-eGFP) mice

FVB-Tg (CAG-luc-eGFP)-L2G85Chco/J homozygous mice express firefly luciferase and enhanced green fluorescence protein directed by the human cytomegalovirus immediate early promoter enhancer with chicken beta-actin/rabbit beta-globin hybrid promoter (CAG). Luciferase expression has been confirmed in adipose tissues in this animal model (Gassman et al., 2016).

All mice were 12 weeks old and had *ad libitum* access to food and water. Ambient humidity and temperature were kept at 50% and 21°C, respectively. The mice were culled by cervical dislocation. Further information can be found in Section 2.3.6.4 and 2.3.11.

5.3.1.2 Experimental design

Three-month old male FVB-Tg (CAG-luc-eGFP)-L2G85Chco/J mice were culled by cervical dislocation, and gonadal adipose tissue pads were harvested (Figure 2.1 and Figure 2.2). 1 g of dissected gonadal adipose tissue was placed in 100 mm tissue culture plates containing 10 mL of PBS, supplemented with 1% penicillin/streptomycin (Figure 2.3) and minced into 1-2 mm pieces (see Section 2.3.6.4).

The 6% HA hydrogel in a 1:2 HA-ALD: HA-HYD ratio was synthesised and underwent gelation as described in Section 2.3.2. To reduce the risk of infection, the PBS used to make the HA hydrogel also contained 1% penicillin/streptomycin.

Control female FVB/N mice aged 12 weeks old (Charles River, Wilmington, MA) were used as recipients of lipo-aspirate. The recipient mice were numbered 1 to 5. Mice 1 and 2 received the same intervention, with mouse 5 being a control without any intervention. Interventions for each given mouse are described below. All recipient mice were anaesthetised using isoflurane (Merk Scientific, Kenilworth, NJ). Recipient mice received lipo-aspirate/ gel injections in the subcutaneous plane, using 23 g sterile needles (VWR International, Lutterworth, UK) (see Table 5.1). Mice 1 and 2 received two injections each. The left flank had 500 μ L of CAG-luc-eGFP adipose tissue injected subcutaneously, whilst the right flank received a mixture of 250 μ L 6% 1:2 HA-ALD:HA-HYD ratio HA hydrogel and 250 μ L CAG-luc-eGFP adipose tissue. Further detail on mixing between adipose tissue and HA hydrogel is described in Section 2.3.11. Mouse 3 received 1 mL of CAG-luc-eGFP adipose tissue and mouse 4 was injected with a mixture of 500 μ L CAG-luc-eGFP adipose tissue and 500 μ L 6% 1:2 HA-ALD:HA-HYD ratio HA hydrogel. Mouse 5 received no injection and was labelled as control. Photon emission was used to investigate cell viability, in a similar manner to isolated primary adipocytes harvested for *in vitro* studies described in Chapter 4.6. The rationale in using this method, is that it allowed the cells to be interrogated in real-time without the need to disturb the experiment over its duration. Following the injections, mice were imaged under general anaesthesia on Day 0 and at regular intervals till day 13. Mice underwent an intra-peritoneal injection with 100 μ L of 20 mM luciferin ten minutes before imaging. The time between injection and imaging was to allow luciferin to be absorbed by the murine peritoneum into the bloodstream and to reach peak steady-state at the site of the injected adipose tissue (Khalil et al., 2013).

MOUSE NUMBER	SUBCUTANEOUS INJECTION
1	Left flank: 500 μ L adipose tissue injection Right flank: Mixture of 250 μ L adipose tissue and 250 μ L HA hydrogel injection
2	Left flank: 500 μ L adipose tissue injection Right flank: Mixture of 250 μ L adipose tissue and 250 μ L HA hydrogel injection
3	1 mL adipose tissue injection
4	Mixture of 500 μ L adipose tissue and 500 μ L HA hydrogel injection
5	500 μ L PBS

Table 5.1 Summary of the subcutaneous injections of adipose tissue and HA hydrogel (6% concentration, HA-ALD: HA-HYD 1:2 ratio). The 12-week old female control mice (FVB/N) were injected subcutaneously with the indicated volumes of either adipose tissue alone or adipose tissue mixed with HA hydrogel.

5.3.1.3 Data acquisition and processing

Imaging was then performed using a PhotonImager Optima (Biospace Lab, Nesles-la-Vallée, France). The imager comprised of a photon exclusion chamber, photon multiplier tube and a hyper-sensitive camera cooled to -20°C to limit photon noise, mounted above the imaging platform. The number of photons per square centimetre per second were recorded over ten minutes to provide a heat map of photon density per mouse (Figure 5.1).

Image software M3Vision Optima (Biospace Lab, Nesles-la-Vallée, France) was used to analyse normalised photon heat maps for each mouse over time. A region of interest (ROI) was drawn around each mouse flank to measure photons emitted from left and right flank injections described in Table 5.1. Each ROI was the same size and was drawn around the mouse flank on a single mouse, with a margin of no signal around a photon emitted area. This ROI was then applied to the other mice to ensure standardisation.

A graph with photon density over time was plotted for each mouse ROI, to create an objective and quantitative method for photon emission from a given area. A mean measurement of photon density for each mouse ROI was measured on the plateau section of the graph, which corresponded to the first one minute of data capture. The plateau region of the graph signified a steady-state blood luciferin concentration between absorption from the peritoneum of injected luciferin and excretion/ metabolism causing elimination from the blood stream.

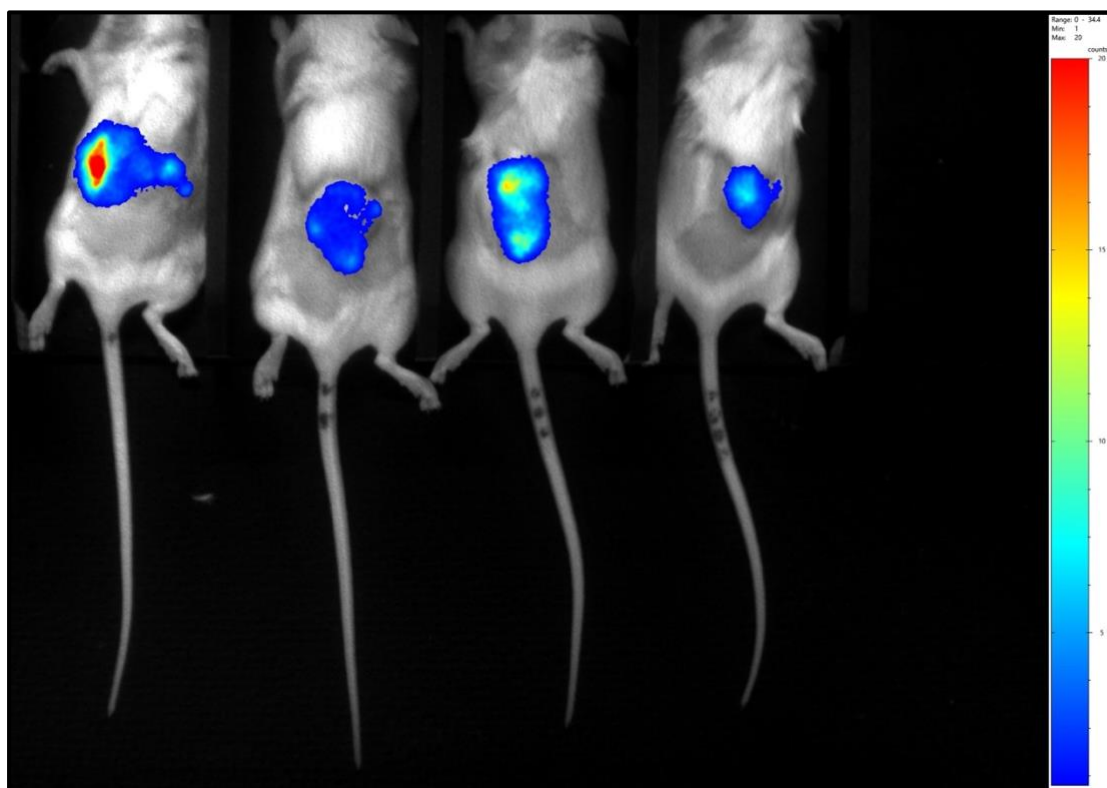


Figure 5.1 Photon density emitted from mice in the PhotonImager Optima. Red areas display areas of high photon density and blue areas low photon density as a spectrum. Image taken on Day 3 over one minute, and ten minutes after intra-peritoneal injection with 100 μ L of 20 mM luciferin.

5.3.2 Pilot results, discussion and improvements to design

Several flaws in the design of the pilot murine study were identified through the course of the experiment. As seen in Figure 5.2A, mouse numbers 1 and 2 had their left and right flank injections merge. This could have been due to the 500 μ L volumes injected to each flank being too large. All mice had no evidence of skin ulceration or any other pathology on visual inspection.

Figure 5.2B shows an Optima image recorded for one minute, ten minutes after an intra-peritoneal injection with 100 μ L of 20 mM luciferin for four mice with ROIs drawn (acquisition and processing described in Section 5.3.1.2). Due to the injected left and right flank injections merging for mouse 1 and mouse 2, which could not be differentiated using the Optima imager, the ROI was amended to include the whole mouse, incorporating both flanks. Mouse 5 (control) with 500 μ L injected PBS and had no signal as expected. Mouse numbers 3 and 4 had clear signals at the site of injection.

Figure 5.3 displays emitted photon density data from all five experimental mice. Mouse numbers 1 and 2 were repeats of each other yet had very different photon density traces over time and started at different photon emission density on Day 1. This could possibly have been due to varying concentrations of luciferin reaching the injection sites.

Mouse 3 had the highest volume of adipose tissue injection and, unsurprisingly, had the highest photon emission at the start of the experiment, decreasing to a plateau on Day 10 till the end of the experiment. The decrease in photon emission may have been due to decreased cell viability which could have been caused by an excessive volume of injected adipose tissue. At 1 mL, mouse 3 had twice the adipose tissue volume of any other mouse at a single location.

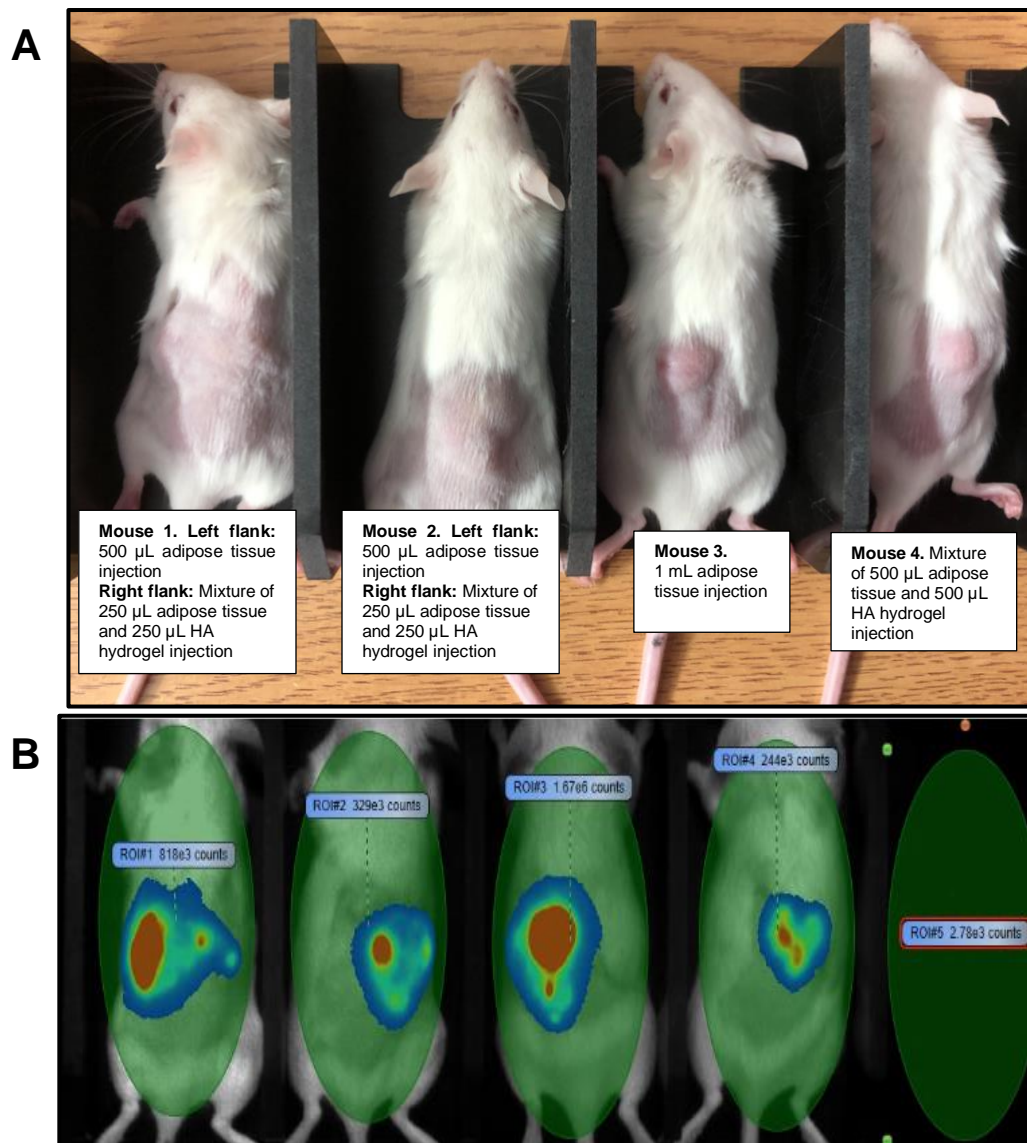


Figure 5.2 Representative images of animals and regions of interest on Day 12 post injection. (A) Pictures of animals under anaesthesia for the indicated volumes of adipose tissue and HA hydrogel in Table 5.1. **(B)** Representative image using PhotonImager Optima showing regions of interest in green. Red areas display areas of high photon density and blue areas low photon density as a spectrum. Image taken over one minute, ten minutes after intra-peritoneal injection with 100 μ L of 20 mM luciferin. Control mouse with 500 μ L PBS injection only not shown.

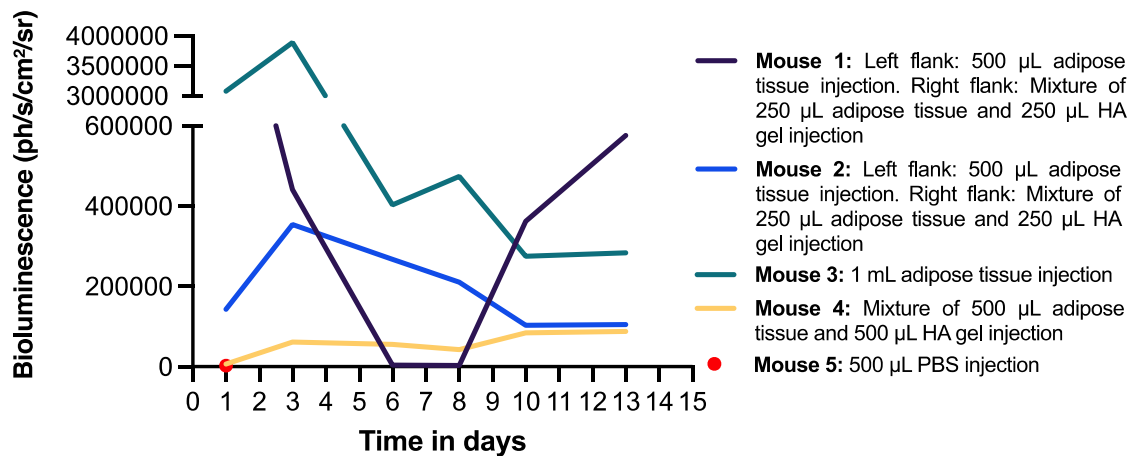


Figure 5.3 Time course of photon emission determined by whole mouse ROIs from Day 1 (first measurement) to Day 13 (experiment end) in indicated mice. Mean photon density measurement taken over one minute, ten minutes after intra-peritoneal injection with 100 μ L of 20 mM luciferin.

Mouse 4 did not display any photon emission at the start of the experiment, with a gradual increase in photon emission till the end of the experiment. This was unusual, as the other mice had the same volume of adipose tissue and had a clear signal at the start of the experiment. It may have perhaps been caused by an intra-bowel injection of luciferin on Day 1, leading to limited absorption and thus no photon emission. Mouse 5 (control) showed no photon emission as expected, being a control without any injected adipose tissue.

A number of improvements were made to the main murine study based on the observations of the pilot study. The 500 μ L volumes used for injection of mouse 1 and mouse 2 were too large - as such, injected volumes were kept at below 250 μ L on each side to limit to reduce the risk of injected left and right flank volumes merging. At least three mice per intervention group was also employed for the main study, as a wide variation photon emission of mouse 1 and mouse 2 was apparent in the pilot study, despite both having the same injected constituents.

One possible explanation for the lack of photon emission of mouse 1 on Day 6 and Day 8 was a mis-placed intra-peritoneal injection of luciferin into the bowel lumen rather than the intra-peritoneal space. Intra-peritoneal luciferin injections for consistent visualisation of target structures can be variable, with some structures not visualised intermittently with intra-peritoneal injection, leading to weak or no photon emission signals. Sub-cutaneous injections have a similar absorption profile to intra-peritoneal injections and a ten-minute delay between injection and Optima imaging was also used to allow blood-stream luciferin to reach a plateau. Furthermore, subcutaneous delivery of luciferin into the bloodstream is more reliable than intra-peritoneal injection for consistent visualisation of target structures (Khalil et al., 2013). As such, sub-cutaneous luciferin injections rather than intra-peritoneal injections were used for the main study.

5.4 Main murine study

5.4.1 Methods

Recipient control female mice were injected with various amounts of adipose tissue isolated from CAG-luc-eGFP mice and HA hydrogel (6% concentration, HA-ALD:HA-HYD 1:2 ratio). Experimental conditions are summarised in Table 5.2. Imaging was performed as described in Section 5.3.1.3. Recipient mice were injected with luciferin (100 μ L of 20 mM subcutaneously), anaesthetised using isoflurane and placed in the Optima imager, ten minutes after luciferin injection. Imaging was performed on Days 3, 5, 7, 11 and 13 post adipose tissue injection.

On Day 13, left and right flank injected adipose tissue or adipose tissue with gel were harvested in order to prepare mRNAs and perform histology studies of the tissues. Body weight was recorded before each imaging session, and the health of each animal inspected (such as the injection site and signs of distress) on a daily basis. As shown in Figure 5.4, there were no changes in total body weight between the two groups of animals suggesting that the animals were not affected by the experiments. Food intake was also not affected (not shown).

Part of the extracted tissues were stored in RNA Later (Thermo Fisher Scientific, Waltham, MA) as per the manufacturers instruction and RNA was later extracted using a RNeasy Plus Micro Kit (Qiagen, Düsseldorf, Germany). qPCR was performed for three gene targets used to interrogate mature adipocyte gene expression: CD36, peroxisome proliferator-activated receptor gamma (PPAR- γ) and fatty acid binding protein 2 (FABP4), normalised to GAPDH.

GROUP NUMBER	SUBCUTANEOUS INJECTION
1	Left Flank: 50 μ L adipose Right Flank: 50 μ L adipose and 50 μ L gel mix
2	Left Flank: 50 μ L adipose Right Flank: 50 μ L adipose and 100 μ L gel mix

Table 5.2 Summary of experimental conditions. Each mouse group (n=3) received 50 μ L of adipose tissue to the left flank and received indicated volumes of adipose tissue mixed with HA hydrogel to the right flank. All injections were subcutaneous.

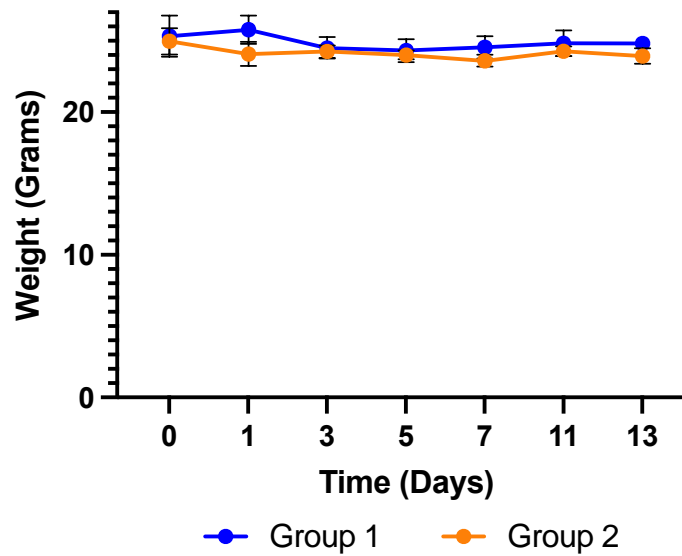


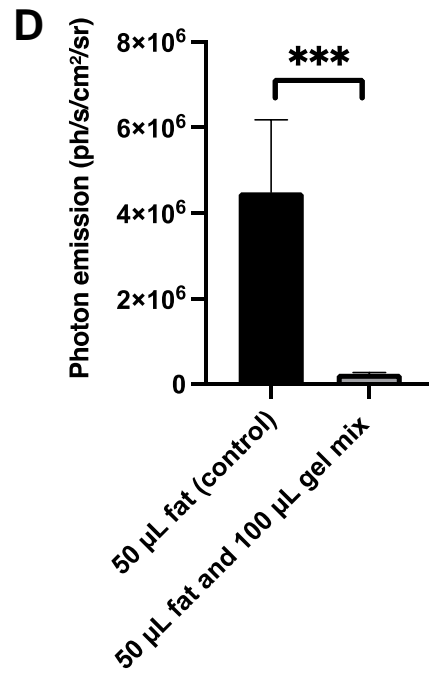
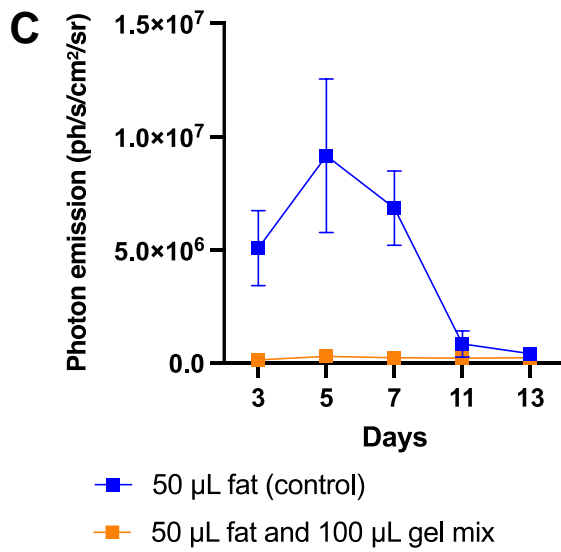
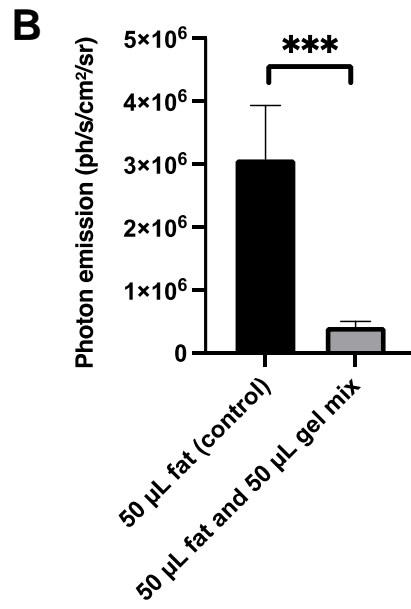
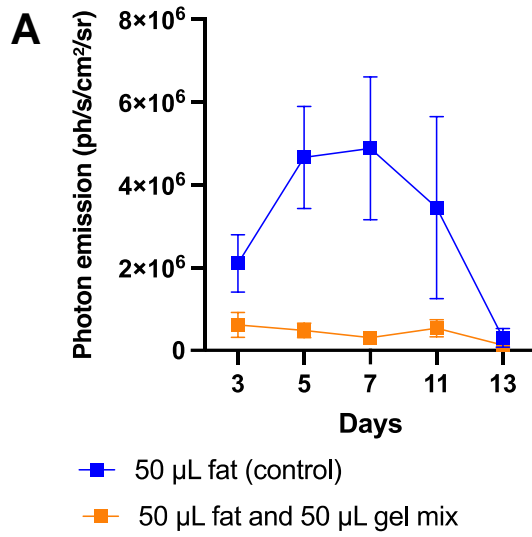
Figure 5.4 Main study animal weights. Total body weights were recorded at the indicated times in Group 1 (blue, right flank subcutaneous injection of 50 μ L CAG-luc-eGFP adipose tissue mixed with 50 μ L HA hydrogel) and Group 2 (orange, 50 μ L CAG-luc-eGFP adipose tissue mixed with 100 μ LHA hydrogel). Duration of study 13 days. Animals weighed every 48 hours (mean \pm s.e.m, n=3 per group).

5.4.2 Results and discussion

Whilst the pilot study suggested that the animals were not negatively impacted by injection of HA hydrogel and adipose tissue, this was confirmed using animal weights for the main study displayed in Figure 5.4. As seen, there was no significant difference in mouse weights between groups, suggesting good animal welfare.

5.4.2.1 Cellular viability of injected CAG-luc-eGFP murine adipose tissue with gel *in vivo*

As seen in Figure 5.5A and C, left flank control only adipose tissue injections follow a similar trend, increasing in photon emission from Day 3 to a peak on Days 5-7, and falling to the end of the experiment on Day 13. This suggested that cell viability peaked at Days 5-7 for control adipose tissue. However, the control starting photon emission in Figure 5.5A was than half that shown in Figure 5.5C. This may have been due to a limitation of the technique—that a volume of 50 μL adipose tissue was injected and not a precise number of cells. Though unlikely, there may have been more cells in one group than the other, with more cells emitting more photons. One method to combat this may be to inject a known number of isolated cells. However, this is not what is done in human adipose tissue transfer, where a known volume of adipose tissue is injected into a region for reconstruction. Group 1 adipose tissue mixed with 50 μL HA hydrogel (Figure 5.5A) was over twice the photon emission of Group 2 adipose tissue mixed with 100 μL HA hydrogel (Figure 5.5C). Figure 5.5E better elucidates this relationship. This could be caused by twice the volume of HA hydrogel in Group 2, interfering with the photons released from adipose tissue to a greater degree. A similar effect was also seen in Section 4.5 *in vitro* for Per 2-dLuc 3T3-L1 adipocytes under HA hydrogel, whereby HA hydrogel seems to impede photons passing through the gel. This effect is further discussed in Chapter 6.



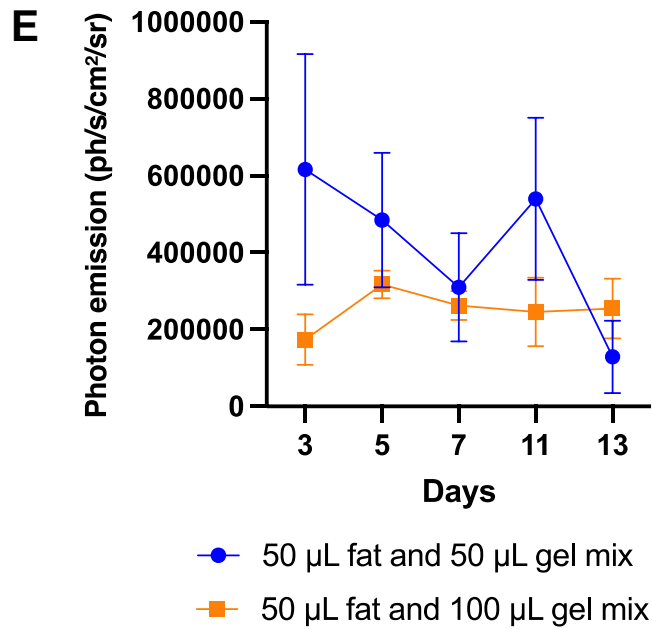


Figure 5.5 Photon emission of murine Groups 1 and 2 (n=3 per Group). The duration of the experiment was to Day 13, with the first measurement on Day 3 and the last on Day 13. **(A and C)** show photon emission of right flank subcutaneous 50 µL CAG-luc-eGFP adipose tissue mixed with 50 µL gel (Group 1) and 50 µL CAG-luc-eGFP adipose tissue mixed with 100 µL gel (Group 2), compared to 50 µL CAG-luc-eGFP adipose tissue control (left flank subcutaneous injections) at each time point. **(B and D)** show cumulative photon emission for each Group compared to control. **(E)** compares photon emission for each of the two Group interventions at each time point (mean +/-s.e.m. ***p<0.001. ANOVA with repeated measures).

As seen in Figure 5.5E, Group 1 adipose tissue with 50 μ L HA hydrogel displayed more variations throughout the time course of the experiment, compared to Group 2 adipose tissue mixed with 100 μ L HA hydrogel, which had a more stable pattern. This may be due to the higher volume HA hydrogel condition protecting cells to a higher degree.

Figures 5.5B and D show a statistically significant difference in photon emission between control and intervention conditions of Groups 1 and 2, respectively. In both groups, HA hydrogel seems to impede passage of photons. As seen in the next Section, mature adipocyte gene expression showed no difference between control and intervention for Groups 1 and 2, which suggests HA hydrogel impedance of emitted photons, rather than the HA hydrogel decreasing cell viability through a potential toxic effect.

5.4.2.2 Gene expression of injected CAG-luc-eGFP murine adipose tissue with gel *in vivo*

As shown in Figure 5.6, there was no difference in the genetic expression of the mature adipocyte markers PPAR- γ , FABP4 and CD36 normalised to GAPDH for control (50 μ L CAG-luc-eGFP adipose tissue) compared to adipose tissue and gel (50 μ L CAG-luc-eGFP adipose tissue mixed with 50 μ L HA hydrogel for Group 1 and 100 μ L HA hydrogel Group 2).

This strongly suggested that the HA hydrogel did not affect primary murine adipocyte gene expression when mixed with varying volumes of HA hydrogel *in vivo*.

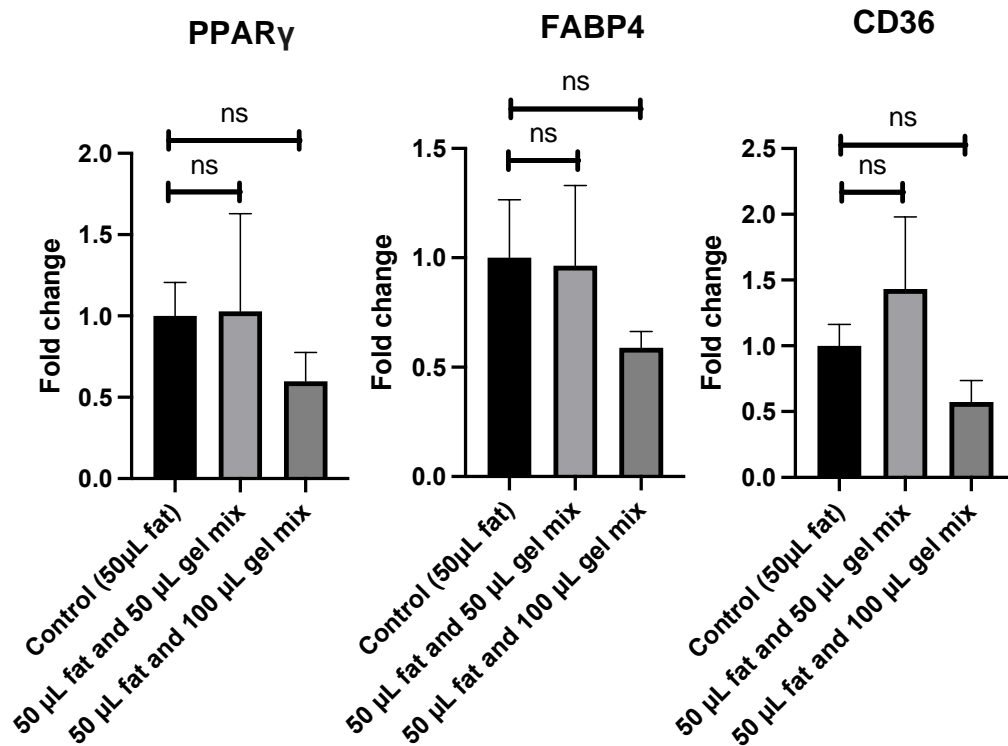


Figure 5.6 Group 1 and 2 gene expression of mature adipocyte markers PPAR γ , FABP4 and CD36 on Day 13 of the main murine *in vivo* study. Expression normalised to housekeeping gene GAPDH as indicated in the Figure. Control (subcutaneously injected 50 μ L CAG-luc-eGFP adipose tissue left flank) black, Group 1 experimental condition (50 μ L CAG-luc-eGFP adipose tissue mixed with 50 μ L HA hydrogel injected subcutaneously into the right flank) light grey, Group 2 experimental condition (50 μ L CAG-luc-eGFP adipose tissue mixed with 100 μ L HA hydrogel injected subcutaneously into the right flank) dark grey (n=3, mean \pm s.e.m. ns= not significant).

5.5 Conclusion

This Chapter demonstrated the appropriate selection of a murine animal model to investigate whether HA hydrogel effects cell viability and gene expression of mature adipocyte markers *in vivo*. A pilot study was performed to optimise the methodology before expansion to more mice in the main study, to limit waste of animals and improve reliability of results. The pilot study found that subcutaneous injected CAG-luc-eGFP adipose tissue that is over 500 μL led to the merging of left and right flank deposits, making discrete photon emission from each side very difficult using the Optima imager. Also, the use of intra-peritoneal injections of luciferin can be unreliable (Khalil et al., 2013), resulting in unusual cessations of photon emission as seen in Figure 5.3. Thus, the route of injection was changed to subcutaneous delivery.

With these improvements from the pilot study, the main study found that CAG-luc-eGFP control adipose tissue mixed with 50 μL and 100 μL HA hydrogel survived *in vivo*. Interestingly, adipose tissue mixed with 100 μL HA hydrogel demonstrated less than half the photon emission as adipose tissue mixed with 50 μL HA hydrogel (Figure 5.5). This is unlikely due to HA hydrogel adipocyte toxicity, as there was no change in expression of mature adipocyte markers for all groups for PPAR- γ , FABP4 and CD36 normalised to GAPDH. This effect is further discussed in Chapter 6.

Chapter Six: General discussion

6.1 Introduction

This study was to investigate the role of an aldehyde and hydrazine side-chain modified hyaluronic acid (HA) hydrogel as a novel agent for the augmentation of adipose tissue transfer, with varying potential applications such as breast reconstruction.

The HA hydrogel was chemically modified by adding hydrazine and aldehyde side chains, conferring the hydrogel unique mechanical properties whilst still being able to be degraded by tissue hyaluronidases. The ability of cells to grow and differentiate within the HA hydrogel was examined in a variety of conditions using a novel method of photon emission quantification using a bespoke macro for analysis. Cell viability was investigated on, under and within HA hydrogel using Per 2-dLuc 3T3-L1 and CAG-luc-eGFP adipocytes expressing luciferase. This allowed a real-time assessment of cell viability after the addition of D-luciferin, and quantification using the bespoke macro to analyse a series of images taken of these cell types over time. Mature adipocyte gene expression markers were also examined to assess the effects of the HA hydrogel on adipocyte differentiation.

Lastly, the HA hydrogel was investigated for *in vivo* toxicity using CAG-luc-eGFP adipose tissue injected subcutaneously into a murine model, with adipocyte viability and mature adipocyte markers interrogated for any changes that the HA hydrogel may have caused.

6.2 Mechanical characteristics: general comments

6.2.1 Synthesis of HA hydrogel modified with aldehyde and hydrazine groups

Synthesis of hyaluronic acid with hydrazine side chain functionalisation was performed as described in Sections 2.3.1 and 3.2. Functionalisation with hydrazine chains usually uses hydroxybenzotriazole dissolved in a DMSO/H₂O mixture as the primary reaction solvent as described in (Wang et al., 2018). The authors describe a yield of ~20% functionalisation of hyaluronic acid using NMR spectroscopy. Improving the primary solution in which the reaction takes place to increase the affinity for hydrazine and hyaluronic acid side chains increases the yield of functionalisation. As such, rather than using hydroxybenzotriazole dissolved in a DMSO/H₂O mixture as the primary reaction solvent, a MES solution was used. This allowed a higher proportion of hydrazine groups to react with hyaluronic acid. This yielded a higher proportion of functionalisation at 77% (Section 3.2.1). A high functionalisation is important for maintaining the properties of HA-ALD and HA-HYD after gelation at a set concentration of gel and ratio between the two constituents. MES is a good solvent for organic molecules and has been demonstrated to allow solution of other extracellular proteins such as proteoglycans (Tang et al., 1979). Low and varying functionalisation of hyaluronic acid may lead to unpredictable hydrogel properties that may affect gel mechanical behaviour and gel interaction (Vasi et al., 2014).

6.2.2 Characterisation of gel with rheology

Rheology was used specifically to determine the viscosity and elasticity of HA hydrogels rather than absolute strength of the material. Hydrogels, as crosslinked, swollen networks typically have a threshold over which they behave in a liquid manner as the limits of their viscosity and elasticity are reached (Rodell et al., 2013).

Gels based on 1.5% and 3% concentrations, compositions did not hold form after gelation, and were therefore not suitable for further interrogation of all HA-ALD:HA-HYD ratios, with only 1.5% 1:1 and 3% 1:1 ratios interrogated (Figure 3.4). Gel ratios based on 6% concentrations were therefore more suitable (Table 3.1), with all 6% ratios not exhibiting liquid flow. Ratios that exhibited flow did not hold their shape after gelation, i.e., were not viscous enough to hold a shape. It is important for hydrogels to be form-stable and resistant to shear forces, as shearing negatively impacts neovascularisation of injected adipose tissue grafts in current practice (Ghavami and Villanueva, 2018). As such, HA hydrogels that hold their shape are more resistant to shearing forces. 6% HA hydrogel concentrations were investigated as they did not exhibit flow.

Panels A-F in Figure 3.6 show the mean G' and G'' frequency sweep traces for 6% gel concentrations for HA-ALD:HA-HYD ratios 1:1, 1.5:1, 1:1.5, 2:1 and 1:2. Here, the frequency force applied to the hydrogel is increasing, with constant amplitude and time points. Graphs of loss factor ($\tan\delta$) in relation to increasing frequency, are displayed also displayed in Figure 3.6 and are used to describe the liquid/ gel transition point. An ideally viscous liquid has a $\tan\delta$ of 100, whilst a solid is ideally elastic if $\tan\delta$ is 0.01 (Anton-Paar, 2021). Importantly, all ratios of 6% displayed in this figure show that the HA-ALD and HA-HYD constituents have a rapid gelation point, which is not seen in any graph as G' is always above G'' when the angular frequency is 0.1, at the start of the frequency sweep. This is especially important in the intra-operative setting, where the shortest duration of general anaesthetic is used for a given procedure. Complications resulting from general anaesthetic are higher as anaesthetic time increases and can include possible life-threatening sequelae such as pneumonia (Brindle and Soliman, 1975). To minimise anaesthetic complications, a hydrogel that takes more than a few minutes to gelate may not be suitable. From mixing of HA-ALD and HA-HYD to initiating given rheological investigations took less than ten seconds. The speed of HA hydrogel gelation suggested that it would be suitable for the operative setting.

Upward trends of G' and G'' traces in Figure 3.6 as the angular frequency approached 100, suggest an evolving ongoing maturation of covalent bonds between HA-ALD and HA-HYD, which results in a stiffer gel as the frequency progresses to the end of the ten-minute study. This suggests that 6% gel becomes more like a solid with increasing frequency (supported by a downward loss factor trend at 100rad/s, Figure 3.6). This may be advantageous, as the gel becomes more resistant to shearing forces as time progresses, potentially allowing a surgeon to inject the gel at a lower viscosity (i.e., immediately after gelation) with the gel maturing in-situ within a reconstructive void after ten minutes, maintaining its shape to a higher degree and resisting shear forces that are damaging to the adipose graft take. Furthermore, a low shear force of injection of adipose grafts has been shown to improve graft survival (Dasiou-Plakida, 2003). A HA hydrogel with a high viscosity may subject adipocytes to high shear forces whilst being extruded from a syringe into a cavity needing reconstruction, reducing overall cell viability (Tirella et al., 2012, Malda et al., 2013). HA hydrogel used immediately after gelation but before covalent bond maturation would have a lower shearing effect (Figure 3.6) and thus higher cell survival.

The above characteristics of HA hydrogel were further described by amplitude sweeps done on the rheometer for varying ratios of HA-ALD:HA-HYD using 6% gel. Amplitude sweeps are best suited to describing the deformation behaviours of materials in a non-destructive range. As shown in Figure 3.7, G' was always above G'' (suggesting a gel had been formed), but most importantly, both G' and G'' were plateaued, suggesting that the gel continued to resist increasing amplitudes applied till the end of the amplitude sweep study. This is of particular importance, as the gel needs to be robust enough not just to resist reformative forced after injection, but also during injection, whilst being extruded out of a syringe.

The last rheological study was a series of time sweeps performed, which evaluated the time-dependent viscoelastic properties of HA hydrogels: oscillatory sweeps performed with shearing under constant dynamic-mechanical conditions (i.e., constant frequency and amplitude). As seen in Figure 3.8, the gelation point was less than two seconds after mixing, further supporting the characteristic of a fast gelation to limit intra-operative anaesthetic and operative time. As suggested by the frequency and amplitude over a fixed time, the gel was robust and maintained its mechanical properties for the duration of the time sweep (ten minutes). This was important to show stability of the 6% gels not changing over time.

6.2.3 HA hydrogel swelling, degradation, and healing

Characterisation of the HA hydrogel for unreacted chemicals after synthesis, hydration of the HA hydrogel product and degradation of the HA hydrogel in a tissue mimicking environment are critical for understanding how the HA hydrogel may behave in both *in vitro* and *in vivo* experiments.

The gel fraction (Section 3.4.1 and equation 2.1A) is useful when describing the proportion of HA hydrogel after functionalisation that is unreacted and has not been removed through serial dialysis steps (Section 2.3.1). Chemicals such as adipic acid and MES used during functionalisation are toxic to cells if not removed before experimentation (Kennedy Jr, 2002). As seen in Section 3.4.1, less than 5% of the total dry weight of both 3% and 6% HA hydrogel was unreacted product. It was important to elucidate that large proportions of unreacted chemicals that are cytotoxic were not present for the experiments in Chapters 4 and 5.

Gel equilibrium water content (EWC) interrogates the proportion of the HA hydrogel that is water (Equation 2.1B). As seen in Figure 3.9, the EWC for 3% and 6% gels was $96.4\% \pm 0.04\%$ and $96.4\% \pm 0.76\%$ respectively. The EWC is

important to determine, as a lower water content may affect the degradation profile of hyaluronidase *in vitro* (Segura et al., 2005). Cross links (such as the dynamic covalent bonds formed between HA-ALD and HA-HYD groups) can also reduce the EWC, which can also affect degradation profiles and mechanical characteristics (Segura et al., 2005). Low EWC (below 50%) can also affect diffusion of small water permeable metabolites to and from cells, affecting cell growth and survival as a high water concentration facilitates diffusion (Dromel et al., 2021).

The HA hydrogel swelling and degradation was critical to demonstrate breakdown of HA hydrogel in a variety of tissue-mimicking scenarios. HA hydrogels were exposed to each of three corresponding solutions: PBS, DMEM/F12 media, and three hyaluronidase solutions (100U/mL, 50U/mL or 10 U/mL in PBS). Hydrogels selected for swelling and degradation studies were 1:1 ratio of 3% and 6% gel, followed by 6% gels in HA-ALD:HA-HYD ratios 1:1.5, 1.5:1, 2:1 and 1:2. A variety of HA hydrogel concentrations and HA-ALD:HA-HYD ratios were used to find a HA hydrogel constituent which lasts more than a week, allowing grafts to experience neovascularisation (starting on Day four) and passing the nutrient diffusion phase of graft take *in vivo* (Peer, 1950) (further described in Section 1.3.4). Degradation using different ratios of HA-ALD:HA-HYD was also interrogated as functionalised side chains may affect the efficacy of hyaluronidase to varying degrees and can be unpredictable in its action (Bulpitt and Aeschlimann, 1999).

As seen in Figure 3.10, 3% 1:1 ratio HA hydrogel had perished by 264 hours under all conditions, whilst 6% gel in PBS and E1 concentration hyaluronidase solution persisted past 264 hours (Figure 3.11). This suggested that a higher concentration of functionalised hyaluronic acid was more robust to degradation. Unlike 3% HA hydrogel, 6% HA hydrogel had an increase in percentage weight before degradation, suggesting that the gel was not fully hydrated prior to the start of the experiment (despite allowing gelation for 30

minutes). This may be caused by molecular relaxation at higher hyaluronic acid concentrations. Hyaluronic acid functionalised with other cross-linking chains in the literature exhibits a phenomenon whereby water diffuses into the molecular construct before the chains have had time to relax. Water diffusion is faster than the relaxation of the molecules and the molecular construct absorbs more water. When the hyaluronic acid chains do relax (from six hours), water is forced out of the hyaluronic acid construct and equilibrium is reached (Collins and Birkinshaw, 2008). Hydrogel integrity is maintained during this relaxation process and has been demonstrated in a variety of hydrogels (Peppas, 1986). HA hydrogel at a 6% concentration and HA-ALD:HA-HYD 1:2 ratio was chosen after PBS HA hydrogel degradation studies for various ratios, as demonstrated in Figure 3.12. As seen, the gel retained the most weight of all the other ratios at the end of the experiment, and showed robust resistance of degradation in PBS to 20 days (Figure 3.13). HA hydrogel at a 6% concentration and HA-ALD:HA-HYD 1:2 ratio was also able to be degraded by hyaluronidase (Figure 3.13), suggesting that a higher proportion of HA-HYD does not affect hyaluronidase activity as can be the case in other functionalised chain hyaluronic acid gels described in the literature (Park et al., 2003).

Self-healing is a critically important HA hydrogel characteristic, as the HA hydrogel will need to be robust to be able to be injected into a patient and self-heal to fill a space during reconstruction. Figure 3.14 shows the self-healing ability of HA hydrogels. Red food dye clearly diffused across the cut interface. This suggests that the dynamic covalent bonds between branches of HA-ALD and HA-HYD have reformed- allowing colour diffusion. This was important to ascertain, as described in Section 3.1; the ability for the HA hydrogel to heal was a key desirable characteristic. This is because of the need for the HA hydrogel to be injected through a needle without losing its eventual mechanical properties, which are restored quickly after HA hydrogel fracture during injection. Other modified hyaluronic acid hydrogels have been manufactured which self-heal (for example by oxidisation and adding thiol groups) and that also exhibit the dynamic covalent

bonds that allow for self-healing (Yang et al., 2021). However, such hydrogels do not demonstrate the robust mechanical characteristics as the HA hydrogel used in this study. Such low-viscous and non-robust HA hydrogels have been used in wound healing, vitreous eye replacement and as vectors for drug release (Qiao et al., 2020, Wang et al., 2021, Yang et al., 2021)

6.3 HA hydrogel *in vitro*: general comments

The extracellular matrix (ECM) has also been shown to affect tissue regeneration, remodelling and the maintenance and differentiation of pre-adipocytes to adipocytes (Flynn et al., 2006). HA is a key constituent of the ECM, and is important for wound healing and the function of tissues and organs (Agren et al., 2000, Highley et al., 2016a). Given the importance of HA, the HA hydrogel was investigated for survival and differentiation into mature adipocytes *in vitro*.

Per2-dLuc 3T3-L1 (expressing luciferase under the *Per2* promoter) and CAG-luc-eGFP (expressing luciferase CAG promoter) primary adipocytes were used in several experiments in this study with HA hydrogel. The light produced from these cells was used as a proxy for cell viability. The cells emitted photons after D-luciferin was added to media. Photons were measured in a reproducible way by taking serial images, as a proxy for alive cell number in the Alligator bioluminescence detector incubator. This method was chosen so that cell viability could be measured in real-time over the course of the experiment, without the cells being disturbed.

6.3.1 Analysis of images taken using a novel automated macro.

A bespoke macro (Figure 4.3) was written in order to analyse and quantify photons emitted from individual wells in a given image, and as a method to analyse the large numbers of photographs taken during the course of the study using FIJI in a high throughput and reliable manner (as described in Section

2.3.9). FIJI is a computer programme for image analysis and has a wide array of applications, from analysing radiographs to images from microscopy (Schneider et al., 2012). A number of studies have described the use of FIJI to analyse images of bioluminescent experiments or photons emitted from cells (Schneider et al., 2012, Wiesmann et al., 2015, Jena et al., 2016). However, no macros have been described in the literature that allow high throughput image processing that is automated when using photons emitted from cells as a proxy for cell viability. The macro identified control versus experiment wells, setting a threshold for the identification of these wells, minimising noise and outputting reliable values.

6.3.2 *Per2-dLuc* 3T3-L1 cell survival on and under HA hydrogel

Per2-dLuc 3T3-L1 cells, which express luciferase under the *per2* promoter, were used in two experiments: cell survival on top of a layer of HA hydrogel (Section 4.5.2.1.1), and cell survival under a layer of HA hydrogel (Section 4.5.2.1.2).

The first set of experiments using *Per2-dLuc* 3T3-L1 cells (described in Section 4.5.2.1.1), allowed gelation of HA hydrogel in wells first on day zero, before the addition of cells, so that the cells sit on a thin layer of HA hydrogel, with serial images taken to measure photon emission till the end of the experiment as a surrogate for cell survival. The rationale of this *in vitro* experiment was the first step in mimicking the environment of adipose tissue transfer in patients, whereby cells would only be in contact with the HA hydrogel. A significant difference in photon emission between control and HA hydrogel cells was present as seen in Figure 4.5A over time. As seen in Figure 4.5B, there was a significant difference in mean photon emission over the course of the experiment. *Per2-dLuc* 3T3-L1 cells grown on a layer of HA hydrogel emitted 15.8% less photons than control, suggesting reduced survival of cells grown on HA hydrogel.

3T3-L1 cells exhibit the ability to proliferate and differentiate to a high degree when grown on plastic (Cao et al., 1991, Zebisch et al., 2012, Kramer et al., 2014). This is due to the ease of cell to cell contact at confluence, which aids differentiation (Zebisch et al., 2012). HA has positive ligands for stromal cell growth such as CD44, RHAMM and ICAM-1, described in Section 1.4 (Agren et al., 2000, Highley et al., 2016a). Such ligands have been shown to be positive proliferation and differentiation factors, regarding 3T3-L1 adipocyte differentiation (Ji et al., 2014). A number of studies have examined the role of other HA hydrogels on *Per2-dLuc* 3T3-L1 cells encapsulated within hydrogels, but not grown on top of HA hydrogel in a two-dimensional layer (Shoham et al., 2013, Chen et al., 2016). Encapsulation of cells within HA hydrogel is further discussed in Section 6.3.3.

However, given that the experiment was designed with HA hydrogelation *in situ*, the HA hydrogel was not as smooth as a plastic well, on top of which the cells were added. The HA hydrogel layer at the bottom of the well could have increased the surface area of the well through small pits and troughs formed during gelation, and thus could delay confluence compared to control, reducing photon emission compared to control and thus the perception of cell survival. This theory, however, is difficult to test. One method to combat this would have been to have numerous experiments of the same type running concurrently, with cell number checked periodically to observe their growth rate.

However, this would not answer the question as to why there was already a difference in photon emission from Day 0 ($t = 0$) for *Per2-dLuc* 3T3-L1 cells grown on top of HA hydrogel compared to control (Figure 4.5A). One method of investigating the reason for this may be to grow *Per2-dLuc* 3T3-L1 cells on a semi-permeable membrane inset, which sits on HA hydrogel, compared to *Per2-dLuc* 3T3-L1 cells growing directly on HA hydrogel and control cells without any gel. The insert may prevent cells from falling into ridges/ microscopic holes on the HA hydrogel surface which may impair photon emission. This effect was not seen,

however, for *Per2-dLuc* 3T3-L1 cells grown underneath HA hydrogel, where both intervention *Per2-dLuc* 3T3-L1 cells and control cells emitted the same photon intensity at the start of the experiment when $t = 0$ (Figure 4.6A).

Regarding cells grown under a layer of HA hydrogel in the second set of experiments, *Per2-dLuc* 3T3-L1 cells were allowed to adhere to plastic and reach 90% confluence before HA hydrogel was added on top of the cells on day one, with serial images taken till the end of the experiment. The experiment was designed in this fashion, as it is well established that 3T3-L1 cells grow and differentiate well on plastic wells, exhibiting normal behaviour before the addition of the HA hydrogel (Kramer et al., 2014).

As shown in Figure 4.6A, there was a significant difference between cells grown in the presence of the HA hydrogel and control cells over the entire course of the experiment, resulting in a 15.2% difference in total photon emission compared to control (Figure 4.6B). This may represent a 15.2% decrease in cell survival under HA hydrogel compared to control, or perhaps a physical effect of the gel impeding photon emission. As shown in Figure 3.4, the HA hydrogel was thought to be transparent to the visible light spectrum. The photon impedance as light passes through large, complex, non-spheroidal and cross-linked hydrogels has yet to be fully described (Rootman et al., 2014) and may be affecting the HA hydrogel in this study causing the 15.2% decrease in photon emission. A slight blueish hue seen after the injection of hyaluronic acid fillers for cosmetic purposes was first described in 2007, hypothesising that shorter wavelengths of lights are scattered preferentially, much in the same manner as the effect the sky seems to appear blue (Hirsch et al., 2007). Hyaluronic acid hydrogels may be susceptible to a similar phenomenon- the Tyndall effect. Physicist John Tyndall observed in the mid 1800s that fine particles in a room reflected light, making them visible to the naked eye, making the further observation that some of these particles created a cone of blue tinged light- postulating the same scattering effect as a blue sky (Gentry, 1997).

The same scattering effect of light was described with larger, complex particles that affects light wavelengths differently depending on a variety of characteristics. Differing scatter of light with larger particles depends on particle size, the refractive index differences between the particle and medium, the wavelength of light and the angle of light (Kinoshita, 2016). As described in Section 1.4.3 and 3.1, hyaluronic acid is a large molecule with extensive cross links in the HA hydrogel used in this study, leading to individual molecules with chain lengths from 300 μm to 700 μm . However, the diameter of individual monomer units is ~ 100 nm (Kablik et al., 2009). The size of the individual HA monomer is less than that of the wavelength of visible light (< 400 nm), suggesting that the Tyndall effect may be in effect when light passes through HA hydrogel. Due to the non-spherical shape of HA molecules and uneven distribution with cross-linking of chains, the photo-optics that HA hydrogel exhibits are less likely to create a cohesive scattering of light to shift the colour of white light that has passed through HA hydrogel to another colour. As such, the scatter HA hydrogel would cause is in a disordered manner, and additionally allowing scatter at the air / gel interface (Rootman et al., 2014). Thus, the photo-optics described in HA hydrogel may have impaired the detection of photons emitted from *Per2-dLuc* 3T3-L1 cells under a layer of HA hydrogel. However, the degree of this effect has not been elucidated and described in the literature. The effects described suggest that the photon difference compared to control may be less than 15.2%.

To investigate whether HA hydrogel has any effect on adipocyte differentiation, markers of differentiation were examined. In this instance, peroxisome proliferator-activated receptor gamma (PPAR- γ) was used, normalised to RPL7 housekeeping gene, as it remains stable through differentiation (Dani et al., 1997, Maeda et al., 1997).

Mean values of gene expression are shown in Figure 4.7 for adipocyte gene PPAR- γ expression normalised to the housekeeping gene RPL7 for *Per2-dLuc* 3T3-L1 cells beneath HA hydrogel. As seen, *Per2-dLuc* 3T3-L1 cells grown under HA hydrogel showed no difference in PPAR- γ expression compared to control. As seen in the next two Sections, primary murine and human cell types also showed no difference when exposed to HA hydrogel (in various conditions) compared to control. Thus, HA hydrogel does not impair the differentiation of pre-adipocytes to mature adipocytes.

Both experiments discussed in this Section yielded a reduction of photon emission in gel experiments versus control of 15.2 to 15.8%. These differences are most likely not due to cell number differences, but rather the effect of the HA hydrogel on photon transmission. This is of particular importance as *Per2-dLuc* 3T3-L1 cells grown under HA hydrogel expressed PPAR- γ with no difference compared to control and were not impaired by the HA hydrogel. Hence, these experiments have shown that 3T3-L1 cells remain viable under and on HA hydrogel.

6.3.3 CAG-luc-eGFP primary murine adipocyte viability on and encapsulated within HA hydrogel.

Using 3T3-L1 cells beneath or on top of HA hydrogel and not mixed/encapsulated within HA hydrogel is not a true simulation, as cells are dispersed within tissues during adipose tissue-transfer in a three-dimensional manner (Section 1.3). CAG-luc-eGFP primary murine cells (which better mimic the cell population harvested in human adipose tissue transfer over 3T3-L1 cells) were mixed into HA hydrogel, so that the cells contacted the HA hydrogel on all surfaces as described in Section 4.6. An experiment was performed comparing CAG-luc-eGFP murine pre-adipocyte survival under three conditions: on a layer of HA hydrogel, cells mixed in with gel and cells without any gel as control.

As seen in Figure 4.9 showing the mean photon emission for the whole experiment, the control cell group had the highest photon emission and therefore survival, followed by the mix of HA hydrogel and cells and lastly, cells grown on top of HA hydrogel. The mixture of cells and HA hydrogel had 17.8% lower photon emission compared to control, whilst cells grown on top of HA hydrogel showed 22.4% lower photon emission compared to control. It is not surprising that cells surrounded by HA hydrogel (with growth ligands described in Section 1.4) in a three-dimensional manner (cells and HA hydrogel mixed group) have a higher photon emission and survival compared to the cells grown on top of HA hydrogel. This may be due to the cells in the mixed group having more points of contact with HA hydrogel's ligands.

In order to investigate whether HA hydrogel has any effect on adipocyte differentiation, markers of differentiation were examined. Two gene targets were used to interrogate mature adipocyte gene expression: CD36 and peroxisome proliferator-activated receptor gamma (PPAR- γ), normalised to the housekeeping gene RPL7. As seen in Figure 4.10, there was no difference in PPAR- γ or CD36 expression between control, cells on HA hydrogel and a HA hydrogel and cell mix at the end of experiment, normalised to RPL7. This finding suggested that HA hydrogel does not influence mature adipocyte gene marker expression for primary murine pre-adipocytes that have contact with HA hydrogel in three dimensions (HA hydrogel and cell mix) and two dimensions (cells on top of HA hydrogel) compared to control.

6.3.4 Mature adipocyte gene expression of primary human cells under HA hydrogel

In addition to cells of murine origin, human primary pre-adipocytes were differentiated in the presence of gel and markers of differentiation examined. Human primary adipocytes and pre-adipocytes were used as they are a constituent of primary adipose tissue transfer reconstructive procedures

described in Chapter 1. Three gene targets were used to interrogate mature adipocyte gene expression: CD36, peroxisome proliferator-activated receptor gamma (PPAR- γ) and adipocyte protein 2 (aP2) in human cells or fatty acid binding protein P4 (FABP4) in murine cells.

The housekeeping gene RPL7 was used as it remained stable throughout differentiation (Dani et al., 1997, Maeda et al., 1997). Primary human adipocytes were grown under a layer of HA hydrogel, identical to the experiment in Section 4.5.2, apart from the use of primary human cells rather than 3T3-L1 cells. Three adipocyte specific genes (aP2, PPAR- γ , and CD36) were normalised to the housekeeping gene RPL7. There was no difference in adipocyte gene expression compared to housekeeping genes of primary human adipocytes grown under a layer of gel compared to control, as seen in Figure 4.12, suggesting that HA hydrogel did not alter primary human adipocyte behaviour.

6.4 HA hydrogel *in vivo*: general comments

A pilot murine study investigating characterisation of injected lipo-aspirate with HA hydrogel versus control animals was designed with the aim to analyse data from this pilot murine study for the formulation of learning points to improve and inform a main murine study design. In order to track survival of injected lipo-aspirate in a murine model, a reproducible methodology needed to be developed. The learning points of this pilot study are discussed in Section 5.3.2.

At the end of the main murine study, gene expression and histology of excised injected adipose tissue was examined.

6.4.1 Main murine study photon emission and cell survival

Six wild-type mice comprised the main murine study with left flanks constituting 50 μ L of subcutaneous CAG-luc-eGFP adipose tissue for all mice as

control. The right flank injections as seen in Table 5.2 injected 50 μL of subcutaneous CAG-luc-eGFP adipose tissue mixed with either 50 μL or 100 μL 6% concentration HA hydrogel in a HA-ALD:HA-HYD 1:2 ratio.

Figure 5.5 shows photon emission for each mouse Group compared to left flank controls. Groups 1 and 2 with 50 μL CAG-luc-eGFP adipose tissue mixed with 50 μL gel and 100 μL gel to the right flanks respectively, had a statistically significant reduction in mean photon emission verses control (Figure 5.5B and D). As described in Section 6.3.3, mature adipocytes are easily damaged through harvest and implantation and are at high risk of being lost soon after injection (Gonzalez et al., 2007). As such, the action of mixing the HA hydrogel and adipose tissue may have injured the cells via the action of the three-way tap (Figure 2.5), leading to a markedly decreased output of photons compared to control seen in Groups 1 and 2. Alternatively, the HA hydrogel may be once more impeding the path of photons emission from cells compared to control (similar to the phenomenon described in Section 6.3.2). This can be evidenced by the starting photon emission in Figure 5.5A (Group 1 50 μL HA hydrogel), being less than half that shown in Figure 5.5C (Group 2, with double the HA hydrogel at 100 μL). As seen in the next Section, mature adipocyte gene expression showed no difference between control and intervention for Groups 1 and 2, which suggests HA hydrogel impedance of emitted photons, rather than the HA hydrogel decreasing cell viability. Alternatively, this relationship may have been due to a limitation of the technique- that a volume of 50 μL adipose tissue was injected, and not a precise number of cells. Though unlikely, there may have been more cells in one Group than the other, with more cells emitting more photons. One method to combat this may be to inject a known number of isolated cells. However, this is not what is done in human adipose tissue transfer, where a known volume of adipose tissue is injected into a region for reconstruction.

As seen in Figure 5.5A and C, experimental right flank photon emission for Groups 1 and 2 demonstrated a steady-state plateau from Day 3 to Day 13. This suggested that a proportion of mature adipocytes survived injection. This is in contrast to Groups 1 and 2 left flank controls, whereby photon emission increased from Day 3 to Day 7 for Group 1 and Day 3 to Day 5 for Group 2, suggesting that cells underwent proliferation until these time points, before photon emission fell to Day 13, with reduced cell survival. It is unclear as to why control adipose tissue injections to the left flank behaved in this manner.

Figure 5.5E shows right flank photon emission of both Groups over time. Group 1 adipose tissue with 50 μ L HA hydrogel mixed with adipose tissue had more variations throughout the time course of the experiment, compared to Group 2 adipose tissue mixed with 100 μ L HA hydrogel which had a more stable pattern. This may be due to the higher volume HA hydrogel condition protecting cells to a higher degree from mechanical trauma suffered from moving animal's normal behaviour, which may not be unsurprising, given that hyaluronic acid is a constituent of the ECM which provides mechanical protection to tissues (Hinz, 2015).

6.4.2 Gene expression of *in vivo* murine experiments

As seen in Figure 5.6, there was no difference in adipocyte gene markers expression for Groups 1 and 2 for PPAR γ , FABP4 and CD36 on Day 13 of the study, normalised to GAPDH. This was important to ascertain and suggests that the HA hydrogel doesn't affect primary murine adipocyte gene expression when exposed to HA hydrogel.

6.5 Future directions

This study has taken the concept of using a novel hyaluronic acid hydrogel as an extracellular matrix with unique properties to augment adipose tissue transfer from the benchtop, through to *in vitro* and *in vivo* experiments.

This study has shown that the HA hydrogel has desirable physical characteristics that resist shearing forces and exhibit self-healing. More so, the HA hydrogel can be degraded by tissue enzymes.

In vitro experiments using murine and human cells, and *in vivo* experiments using a murine model have demonstrated good cell survival and mature adipocyte marker gene expression. This lends to promising future work for human translation to benefit patients.

This project was markedly curtailed by the COVID-19 pandemic in several ways, with best efforts made to limit the impact of laboratory work cessation during the first wave. Whilst the majority of chemical synthesis and physical characterisation of HA gel was performed before the pandemic (Chapter 3), visiting researchers to the Chemistry Department, University of Birmingham, where the HA gel synthesis and characterisation was performed, were not able to access the laboratories for the duration of the pandemic on University regulations. Due to the COVID-19 pandemic, HA-ALD was not characterised due to the drastic reduction of key chemicals commercially available. HA gelation and flow characteristics through a needle with murine or human adipose tissue would have been useful to characterise, with particular attention paid to the homogeneity of mixing of HA gel and adipose tissue. This may have led to development of a delivery system to ensure consistency of mixing between HA hydrogel and adipose tissue. Rheology of fresh adipose tissue would also have been performed, in order to compare the physical properties of HA hydrogel mixed with adipose tissue.

The *in vitro* section of this study (Chapter 4) was also hindered by COVID-19, as the synthesised HA gel from the University of Birmingham could not be attained as easily and relied on collaborators for supply. As a result, *in vitro* experiments were designed to use HA gel sparingly. The *in vivo* section of this study (detailed in Chapter 5) was markedly curtailed by constraints on time caused by the COVID-19 global pandemic through e.g., delays in animal supply. Future work may involve the characterisation of neo-vascularisation *in vivo* of injected adipose tissue with HA hydrogel, to appreciate whether HA hydrogel affects vessel growth and distribution. This may be investigated by using immunohistochemistry for vessel markers of injected adipose tissue with HA hydrogel. Once this further characterisation has taken place, a pilot human *in vivo* study can be designed to examine whether HA hydrogel mixed with adipose tissue is beneficial for reconstruction.

Annex A

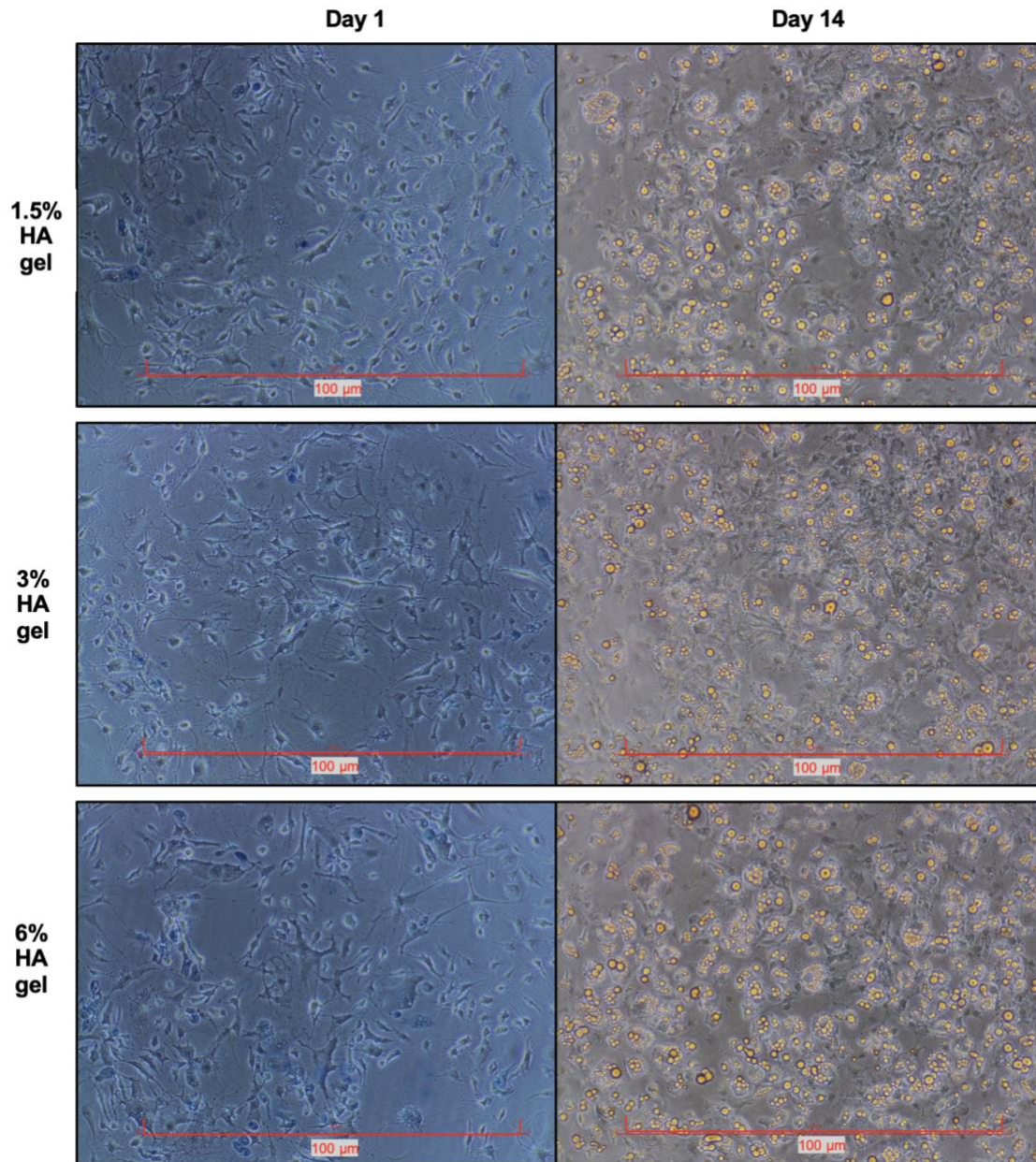


Figure A MCF-7 cell morphology under 1.5%, 3% and 6% gel in a HA-ALD:HA-HYD 1:1 ratio on Day 1 and Day 14. Cells were grown to 80% confluence and 100 μ L HA hydrogel was carefully added on top of the cell layer on Day 1. Cells were stained with Oil Red O on Day 14 after HA hydrogel addition. Pictures are representative images of $n=3$ independent experiments performed in triplicates. Scale (red line) is 100 μ M.

Annex B

```
22 //Segments the wells by thresholding and fitting circles
23 function get_rois(input,filename){
24     open(input+filename);
25     //This must be the same in both functions
26     run("Median...", "radius="+med_rad);
27     run("Duplicate...", "title=Mask");
28     //Q: Is this the right thresholding tool to use?
29     setAutoThreshold("Huang dark");
30     setOption("BlackBackground", false);
31     run("Convert to Mask");
32     run("Analyze Particles...", "size=1000-Infinity show=Nothing add");
33     roi_count=roiManager("count");
34     //Check to see if the number of wells found is what is expected. If not stop, crop region or show error.
35     if (roi_count!=num_wells){
36         Dialog.create("Unexpected number of wells found");
37         Dialog.addMessage(roi_count+" wells found");
38         Dialog.addCheckbox("Do you want to crop this image?", true)
39         Dialog.show();
40         do_crop=Dialog.getCheckbox();
41         if (do_crop) {
42             run("Set Measurements...", "centroid redirect=None decimal=3");
43             roiManager("Measure");
44             setTool("rectangle");
45             waitForUser("Select region containing wells. Click OK when done.");
46             roiManager("Add")
47             roiManager("Select",nResults());
48             for (i = 0; i < nResults(); i++) {
49                 if (selectionContains(getResult("X",i), getResult("Y",i))) {
50                     roiManager("Select",i);
51                     roiManager("Add")
52                     roiManager("Select",nResults());
53                 }
54             }
55             roiManager("Select", Array.getSequence(nResults()+1));
56             roiManager("Delete");
57             selectWindow("Results");
58             run("Close");
59         } else {
60             exit("Unexpected number of wells found. Exiting macro");
61         }
62     }
63 }
64 //Estimate image calibration from row containing largest bounding box
65 roi_list=Array.getSequence(num_wells);
66 roiManager("select",roi_list);
67 run("Set Measurements...", "area bounding redirect=None decimal=3");
68 roiManager("Measure");
69 run("Summarize");
70 //Find well with largest bounding box
71 //getResult counts from 0
72 max_width=getResult("Width",Table.size-1);
73 max_height=getResult("Height",Table.size-1);
74 selectWindow("Results");
75 run("Close");
76 roiManager("Measure");
77 Table.setColumn("Well", roi_list);
78 updateResults();
79 if (max_width>=max_height){
80     Table.sort("Width");
81     column="Width";
82 } else {
83     Table.sort("Height");
84     column="Height";
85 }
86 max_ind_well=getResult("Well",Table.size-1);
87 wells_per_row=num_wells/num_rows;
88 //Find well row containing that bounding box
89 max_well_row=Math.floor(max_ind_well/wells_per_row);
90 roiManager("select",Array.slice(roi_list,max_well_row*wells_per_row,(max_well_row*wells_per_row)+(wells_per_row-1)));
91 selectWindow("Results");
92 run("Close");
93 roiManager("Measure");
94 Well_Diam=getResult(column, "Mean");
95
96 //Estimate how many pixels in well diameter
97 for (i=0;i<num_wells;i++){
98     roiManager("select",i);
99     run("Fit Circle");
100    run("Measure");
101    Diameter=getResult("Height");
102    //Estimated that Well_Diam is approx 15.6 mm
103    run("Enlarge...", "enlarge="+((Well_Diam-Diameter)/2));
104    roiManager("add");
105 }
106 //Clean up temporary rois
107 roiManager("select",roi_list);
108 roiManager("delete");
```

```

110 //Group well rows
111 min_well=0;
112 max_well=num_wells/num_rows;
113 while (max_well<=num_wells) {
114     roiManager("select",Array.slice(roi_list,min_well,max_well));
115     roiManager("Combine");
116     roiManager("Add");
117     min_well=max_well;
118     max_well=max_well+(num_wells/num_rows);
119 }
120 //Clean up temporary rois and results
121 roiManager("select",roi_list);
122 roiManager("delete");
123
124 run("Clear Results");
125 //close("*");
126 }
127
128 //Measures intensity of each group of wells
129 function measure_rois(input,filename){
130     open(input+filename);
131     //This should be the same in both functions
132     run("Median...", "radius="+med_rad);
133     roiManager("Measure");
134     close();
135 }
136
137 //Reformat the results into a table for easy plotting
138 function reformatResults(num_rows,time_step){
139     headings = split(String.getResultsHeadings);
140     Time=Array.getSequence(nResults/num_rows);
141     for (j=0;j<Time.length;j++) {
142         Time[j]*=time_step;
143     }
144     Table.create("Mean Well Intensities Over Time");
145     Table.setColumn("Time",Time);
146     for (n = 0; n < num_rows; n++){
147         for (a=0; a< lengthOf(headings); a++){
148             Table.setColumn(headings[a]+d2s(n+1,0) ,Time);
149         }
150     }
151 }
152 //Get directories for inputs and outputs
153 dir_in=getDirectory("Which folder contains the images?");
154 dir_out=getDirectory("Where should the resulting .csv file be saved?");
155 //Get list of files in input directory
156 list=getFileList(dir_in);
157
158
159 //Create Input Dialog box to get values used in macro
160 Dialog.create("Required Inputs");
161 //What call results file
162 Dialog.addString("Name of results file:", "Results.csv");
163 //What radius to use for the median filter
164 Dialog.addNumber("Median radius:", 3);
165 //How many wells should there be?
166 Dialog.addNumber("Number of wells", 6);
167 Dialog.addNumber("Number of rows", 2);
168 Dialog.addNumber("Time Step", 1);
169 Dialog.show();
170 result_title=Dialog.getString();
171 med_rad=Dialog.getNumber();
172 num_wells=Dialog.getNumber();
173 num_rows=Dialog.getNumber();
174 time_step=Dialog.getNumber();
175
176 if (num_wells%num_rows==0){
177     //Get the position of the wells from first file
178     get_rois(dir_in,list[0]);
179     setBatchMode(true);
180     run("Set Measurements...", "mean standard redirect=None decimal=3");
181     //Measure rois for all images in directory
182     for (i = 0; i < list.length; i++){
183         measure_rois(dir_in, list[i]);
184     }
185 }

```

Code used to analyse Alligator images of experiments using *Per2-dLuc* 3T3-L1 and CAG-luc-eGFP primary mouse pre-adipocytes. Grey numbers on the left confer the numbered line of code. Green text headers are the overall aims of the block code. Pink texts are commands the macro executes.

Code was written in conjunction with Dr Laura Cooper and the CAMDU team, University of Warwick.

Annex C

Published works

A systematic review of the literature and meta-analysis of autologous fat transfer: fat transfer confers a 4.2% incidence of complications.

Janak A Bechar, MBChB BMedSc(Hons) MRCS; Howard Chu, MBBS MRCS; Aakash D Amlani BMBCh MA MRCS; Shervanthi Homer-Vanniasinkam, MD FRCS; Joseph T Hardwicke, PhD FRCS

Status: Accepted pending revision.

Journal: Plastic and Reconstructive Surgery GO.

Bibliography

- ADAMS JR, W. P. 2009. Capsular contracture: what is it? What causes it? How can it be prevented and managed? *Clinics in plastic surgery*, 36, 119-126.
- AGHA, R. A., FOWLER, A. J., PIDGEON, T. E., WELLSTEAD, G., ORGILL, D. P. & GROUP, V. S. 2016. Protocol for the development of a core outcome set for autologous fat grafting to the breast. *Int J Surg*, 31, 104-6.
- AGREN, U., TOLG, C., PAIWAND, F., TURLEY, S., HARRISON, R. & TURLEY, E. 2000. The extracellular matrix receptors CD44 and RHAMMM regulate signalling pathways leading to tumor cell motility and invasion. *New frontiers in Medical Sciences: Redefining Hyaluronan*. Amsterdam: Elsevier, 63-76.
- AHIMA, R. S. & LAZAR, M. A. 2008. Adipokines and the peripheral and neural control of energy balance. *Molecular endocrinology*, 22, 1023-1031.
- AL SUFYANI, M. A., AL HARGAN, A. H., AL SHAMMARI, N. A. & AL SUFYANI, M. A. 2016. Autologous Fat Transfer for Breast Augmentation: A Review. *Dermatol Surg*, 42, 1235-1242.
- AMBROSIO, L., BORZACCHIELLO, A., NETTI, P. & NICOLAIS, L. 1999. Rheological study on hyaluronic acid and its derivative solutions. *Journal of Macromolecular Science—Pure and Applied Chemistry*, 36, 991-1000.
- ANDRE, P. Hyaluronic acid and its use as a "rejuvenation" agent in cosmetic dermatology. *Seminars in cutaneous medicine and surgery*, 2004. 218-222.
- ANTON-PAAR. 2021. 3.3.2. *Storage modulus G' and loss modulus G''* [Online]. Anton-Paar. Available: <https://wiki.anton-paar.com/uk-en/basics-of-rheology/> [Accessed 07/2021 2021].
- ANTRAS, J., HILLIOU, F., REDZINIAK, G. & PAIRAULT, J. 1989. Decreased biosynthesis of actin and cellular fibronectin during adipose conversion of 3T3-F442A cells. Reorganization of the cytoarchitecture and extracellular matrix fibronectin. *Biology of the Cell*, 66, 247-254.
- ANWAR, A., MCTERNAN, P., ANDERSON, L., ASKAA, J., MOODY, C., BARNETT, A., EGGO, M. & KUMAR, S. 2001. Site-specific regulation of oestrogen receptor- α and- β by oestradiol in human adipose tissue. *Diabetes, Obesity and Metabolism*, 3, 338-349.
- AOYAGI, T., SHIMBA, S. & TEZUKA, M. 2005. Characteristics of circadian gene expressions in mice white adipose tissue and 3T3-L1 adipocytes. *Journal of Health Science*, 51, 21-32.
- APOSTOLI, A. J., SKELHORNE-GROSS, G. E., RUBINO, R. E., PETERSON, N. T., DI LENA, M. A., SCHNEIDER, M. M., SENGUPTA, S. K. & NICOL, C. J. 2014. Loss of PPAR γ expression in mammary secretory epithelial cells creates a pro-breast tumorigenic environment. *International journal of cancer*, 134, 1055-1066.
- ARATANI, Y. & KITAGAWA, Y. 1988. Enhanced synthesis and secretion of type IV collagen and entactin during adipose conversion of 3T3-L1 cells and production of unorthodox laminin complex. *Journal of Biological Chemistry*, 263, 16163-16169.

- AU-YONG, I. T., THORN, N., GANATRA, R., PERKINS, A. C. & SYMONDS, M. E. 2009. Brown adipose tissue and seasonal variation in humans. *Diabetes*, 58, 2583-2587.
- BAKER, M., GAUKRODGER, N., MAYOSI, B. M., IMRIE, H., FARRALL, M., WATKINS, H., CONNELL, J. M., AVERY, P. J. & KEAVNEY, B. 2005. Association between common polymorphisms of the proopiomelanocortin gene and body fat distribution: a family study. *Diabetes*, 54, 2492-2496.
- BARBATELLI, G., MURANO, I., MADSEN, L., HAO, Q., JIMENEZ, M., KRISTIANSEN, K., GIACOBINO, J., DE MATTEIS, R. & CINTI, S. 2010. The emergence of cold-induced brown adipocytes in mouse white fat depots is determined predominantly by white to brown adipocyte transdifferentiation. *American Journal of Physiology-Endocrinology and Metabolism*, 298, E1244-E1253.
- BASTARD, J.-P., JARDEL, C., BRUCKERT, E., BLONDY, P., CAPEAU, J., LAVILLE, M., VIDAL, H. & HAINQUE, B. 2000. Elevated levels of interleukin 6 are reduced in serum and subcutaneous adipose tissue of obese women after weight loss. *The Journal of Clinical Endocrinology & Metabolism*, 85, 3338-3342.
- BEAHM, E. K. & WALTON, R. L. 2009. Issues, considerations, and trends in bilateral breast reconstruction. *Plastic and reconstructive surgery*, 124, 1064-1076.
- BENJAMIN, M. A., SCHWARZMAN, G., EIVAZI, M. & ZACHARY, L. 2015. Autologous staged fat tissue transfer in post-traumatic lower extremity reconstruction. *J Surg Case Rep*, 2015.
- BERNLOHR, D. A., ANGUS, C. W., LANE, M. D., BOLANOWSKI, M. A. & KELLY, T. J. 1984. Expression of specific mRNAs during adipose differentiation: identification of an mRNA encoding a homologue of myelin P2 protein. *Proceedings of the National Academy of Sciences*, 81, 5468-5472.
- BJÖRNTORP, P. 1990. " Portal" adipose tissue as a generator of risk factors for cardiovascular disease and diabetes. *Arteriosclerosis: An Official Journal of the American Heart Association, Inc.*, 10, 493-496.
- BLÜHER, M., WILLIAMS, C. J., KLÖTING, N., HSI, A., RUSCHKE, K., OBERBACH, A., FASSHAUER, M., BERNDT, J., SCHÖN, M. R. & WOLK, A. 2007. Gene expression of adiponectin receptors in human visceral and subcutaneous adipose tissue is related to insulin resistance and metabolic parameters and is altered in response to physical training. *Diabetes care*, 30, 3110-3115.
- BODEN, G., CHEN, X., MOZZOLI, M. & RYAN, I. 1996. Effect of fasting on serum leptin in normal human subjects. *The Journal of Clinical Endocrinology & Metabolism*, 81, 3419-3423.
- BORZACCHIELLO, A., MAYOL, L., RAMIRES, P. A., PASTORELLO, A., DI BARTOLO, C., AMBROSIO, L. & MILELLA, E. 2007. Structural and rheological characterization of hyaluronic acid-based scaffolds for adipose tissue engineering. *Biomaterials*, 28, 4399-408.
- BOUCHER, J., KLEINRIDDERS, A. & KAHN, C. R. 2014. Insulin receptor signaling in normal and insulin-resistant states. *Cold Spring Harbor perspectives in biology*, 6, a009191.
- BOUDREAU, N. & WEAVER, V. 2006. Forcing the third dimension. *Cell*, 125, 429-31.

- BRINDLE, G. F. & SOLIMAN, M. G. 1975. Anaesthetic complications in surgical out-patients. *Canadian Anaesthetists' Society Journal*, 22, 613-619.
- BRUUN, J. M., HELGE, J. W., RICHELSEN, B. & STALLKNECHT, B. 2006. Diet and exercise reduce low-grade inflammation and macrophage infiltration in adipose tissue but not in skeletal muscle in severely obese subjects. *American Journal of Physiology-Endocrinology and Metabolism*, 290, E961-E967.
- BULPITT, P. & AESCHLIMANN, D. 1999. New strategy for chemical modification of hyaluronic acid: preparation of functionalized derivatives and their use in the formation of novel biocompatible hydrogels. *Journal of biomedical materials research*, 47, 152-169.
- BURNS, J. W., SKINNER, K., COLT, J., SHEIDLIN, A., BRONSON, R., YAACOBI, Y. & GOLDBERG, E. P. 1995. Prevention of tissue injury and postsurgical adhesions by precoating tissues with hyaluronic acid solutions. *Journal of Surgical Research*, 59, 644-652.
- BUTTERWITH, S. 1994. Molecular events in adipocyte development. *Pharmacology & therapeutics*, 61, 399-411.
- CAMPBELL, G. L., LAUDENSLAGER, N. & NEWMAN, J. 1987. The effect of mechanical stress on adipocyte morphology and metabolism. *The American Journal of Cosmetic Surgery*, 4, 89-94.
- CANCELLO, R. & CLEMENT, K. 2006. Is obesity an inflammatory illness? Role of low-grade inflammation and macrophage infiltration in human white adipose tissue. *BJOG: An International Journal of Obstetrics & Gynaecology*, 113, 1141-1147.
- CANIZARES, O., SCHARFF, C. & NGUYEN, P. 2009. Centrifugation creates unique fractions of lipoaspirate: implications for fat graft survival. *Plast Reconstr Surg*, 126, 75.
- CAO, Y.-A., WAGERS, A. J., BEILHACK, A., DUSICH, J., BACHMANN, M. H., NEGRIN, R. S., WEISSMAN, I. L. & CONTAG, C. H. 2004. Shifting foci of hematopoiesis during reconstitution from single stem cells. *Proceedings of the National Academy of Sciences*, 101, 221-226.
- CAO, Z., UMEK, R. M. & MCKNIGHT, S. L. 1991. Regulated expression of three C/EBP isoforms during adipose conversion of 3T3-L1 cells. *Genes & development*, 5, 1538-1552.
- CAROBBIIO, S., PELLEGRINELLI, V. & VIDAL-PUIG, A. 2017. Adipose tissue function and expandability as determinants of lipotoxicity and the metabolic syndrome. *Obesity and lipotoxicity*, 161-196.
- CHAMBON, F., PETROVIC, Z. S., MACKNIGHT, W. J. & WINTER, H. H. 1986. Rheology of model polyurethanes at the gel point. *Macromolecules*, 19, 2146-2149.
- CHAMRAS, H., ARDASHIAN, A., HEBER, D. & GLASPY, J. A. 2002. Fatty acid modulation of MCF-7 human breast cancer cell proliferation, apoptosis and differentiation. *The Journal of nutritional biochemistry*, 13, 711-716.
- CHEN, Y. S., CHEN, Y. Y., HSUEH, Y. S., TAI, H. C. & LIN, F. H. 2016. Modifying alginate with early embryonic extracellular matrix, laminin, and hyaluronic acid for adipose tissue engineering. *Journal of Biomedical Materials Research Part A*, 104, 669-677.

- CHLOUVERAKIS, C. 1972. Insulin resistance of parabiotic obese-hyperglycemic mice (obob). *Hormone and Metabolic Research*, 4, 143-148.
- CHOI, J. H., GIMBLE, J. M., LEE, K., MARRA, K. G., RUBIN, J. P., YOO, J. J., VUNJAK-NOVAKOVIC, G. & KAPLAN, D. L. 2010. Adipose tissue engineering for soft tissue regeneration. *Tissue Eng Part B Rev*, 16, 413-26.
- CHONDRONIKOLA, M., VOLPI, E., BØRSHEIM, E., CHAO, T., PORTER, C., ANNAMALAI, P., YFANTI, C., LABBE, S. M., HURREN, N. M. & MALAGARIS, I. 2016. Brown adipose tissue is linked to a distinct thermoregulatory response to mild cold in people. *Frontiers in physiology*, 7, 129.
- CHUN, T.-H. 2012. Peri-adipocyte ECM remodeling in obesity and adipose tissue fibrosis. *Adipocyte*, 1, 89-95.
- CINTI, S. 2012. The adipose organ at a glance. *Disease models & mechanisms*, 5, 588-594.
- CINTI, S. 2018. Pink adipocytes. *Trends in Endocrinology & Metabolism*, 29, 651-666.
- CLARK, D. P., HANKE, C. W. & SWANSON, N. A. 1989. Dermal implants: safety of products injected for soft tissue augmentation. *Journal of the American Academy of Dermatology*, 21, 992-998.
- COLEMAN, S. R. 2006. Structural fat grafting: more than a permanent filler. *Plast Reconstr Surg*, 118, 108S-120S.
- COLLINS, M. N. & BIRKINSHAW, C. 2008. Investigation of the swelling behavior of crosslinked hyaluronic acid films and hydrogels produced using homogeneous reactions. *Journal of Applied Polymer Science*, 109, 923-931.
- CONDÉ-GREEN, A., DE AMORIM, N. F. G. & PITANGUY, I. 2010. Influence of decantation, washing and centrifugation on adipocyte and mesenchymal stem cell content of aspirated adipose tissue: a comparative study. *Journal of Plastic, Reconstructive & Aesthetic Surgery*, 63, 1375-1381.
- COOK, K. S., MIN, H. Y., JOHNSON, D., CHAPLINSKY, R. J., FLIER, J. S., HUNT, C. R. & SPIEGELMAN, B. M. 1987. Adipsin: a circulating serine protease homolog secreted by adipose tissue and sciatic nerve. *Science*, 237, 402-405.
- CORONADO-MALAGÓN, M. & TAUFFER-CARRION, L. T. 2012. Jejunal perforation after abdominal liposuction, bilateral breast augmentation and facial fat grafting. *Canadian Journal of Plastic Surgery*, 20, 197-198.
- COUGHLIN, C. C., FINCK, B. N., EAGON, J. C., HALPIN, V. J., MAGKOS, F., MOHAMMED, B. S. & KLEIN, S. 2007. Effect of marked weight loss on adiponectin gene expression and plasma concentrations. *Obesity*, 15, 640-645.
- CRAWFORD, J. L., HUBBARD, B. A., COLBERT, S. H. & PUCKETT, C. L. 2010. Fine tuning lipoaspirate viability for fat grafting. *Plastic and reconstructive surgery*, 126, 1342-1348.
- CROSSNO, J. T., MAJKA, S. M., GRAZIA, T., GILL, R. G. & KLEMM, D. J. 2006. Rosiglitazone promotes development of a novel adipocyte population from bone marrow-derived circulating progenitor cells. *The Journal of clinical investigation*, 116, 3220-3228.

- CROWE JR, J. P., KIM, J. A., YETMAN, R., BANBURY, J., PATRICK, R. J. & BAYNES, D. 2004. Nipple-sparing mastectomy: technique and results of 54 procedures. *Archives of Surgery*, 139, 148-150.
- CRUK. 2020. *Breast cancer statistics* [Online]. Available: <http://www.cancerresearchuk.org/health-professional/cancer-statistics/statistics-by-cancer-type/breast-cancer>. [Accessed 11/2020 2020].
- CYPESS, A. M., LEHMAN, S., WILLIAMS, G., TAL, I., RODMAN, D., GOLDFINE, A. B., KUO, F. C., PALMER, E. L., TSENG, Y.-H. & DORIA, A. 2009. Identification and importance of brown adipose tissue in adult humans. *New England journal of medicine*, 360, 1509-1517.
- DANI, C., SMITH, A., DESSOLIN, S., LEROY, P., STACCINI, L., VILLAGEOIS, P., DARIMONT, C. & AILHAUD, G. 1997. Differentiation of embryonic stem cells into adipocytes in vitro. *Journal of cell science*, 110, 1279-1285.
- DASIOU-PLAKIDA, D. 2003. Fat injections for facial rejuvenation: 17 years experience in 1720 patients. *Journal of cosmetic dermatology*, 2, 119-125.
- DE BOER, M., VAN LEEUWEN, F. E., HAUPTMANN, M., OVERBEEK, L. I., DE BOER, J. P., HIJMERING, N. J., SERNEE, A., KLAZEN, C. A., LOBBES, M. B. & VAN DER HULST, R. R. 2018. Breast implants and the risk of anaplastic large-cell lymphoma in the breast. *JAMA oncology*, 4, 335-341.
- DE SOUZA BATISTA, C. M., YANG, R.-Z., LEE, M.-J., GLYNN, N. M., YU, D.-Z., PRAY, J., NDUBUIZU, K., PATIL, S., SCHWARTZ, A. & KLIGMAN, M. 2007. Omentin plasma levels and gene expression are decreased in obesity. *Diabetes*, 56, 1655-1661.
- DICKER, K. T., GURSKI, L. A., PRADHAN-BHATT, S., WITT, R. L., FARACH-CARSON, M. C. & JIA, X. 2014. Hyaluronan: a simple polysaccharide with diverse biological functions. *Acta biomaterialia*, 10, 1558-1570.
- DRAKE, R. V., A. WAYNE; MITCHELL, ADAM W. M. 2009. *Gray's Anatomy for Students*, London, Churchill Livingstone.
- DROMEL, P. C., SINGH, D., CHRISTOFF-TEMPESTA, T., MARTHESWARAN, T., ALEXANDER-KATZ, A., SPECTOR, M. & YOUNG, M. 2021. Controlling growth factor diffusion by modulating water content in injectable hydrogels. *Tissue Engineering Part A*.
- EDELSTEIN, A. D., TSUCHIDA, M. A., AMODAJ, N., PINKARD, H., VALE, R. D. & STUURMAN, N. 2014. Advanced methods of microscope control using muManager software. *J Biol Methods*, 1.
- EGRO, F. M., ROY, E., RUBIN, J. P. & COLEMAN, S. R. Evolution of the Coleman Technique. *Plastic and Reconstructive Surgery*, 10.1097.
- ELLENBOGEN, R. 1991. Autologous fat injection. *Plastic and reconstructive surgery*, 88, 543-544.
- ERICSSON, J., JACKSON, S. M., KIM, J. B., SPIEGELMAN, B. M. & EDWARDS, P. A. 1997. Identification of glycerol-3-phosphate acyltransferase as an adipocyte determination and differentiation factor 1-and sterol regulatory element-binding protein-responsive gene. *Journal of Biological Chemistry*, 272, 7298-7305.

- FAGRELL, D., ENESTRÖM, S., BERGGREN, A. & KNIOLA, B. 1996. Fat cylinder transplantation: an experimental comparative study of three different kinds of fat transplants. *Plastic and reconstructive surgery*, 98, 90-6; discussion 97.
- FAJAS, L. 2003. Adipogenesis: a cross-talk between cell proliferation and cell differentiation. *Annals of medicine*, 35, 79-85.
- FAJAS, L., FRUCHART, J.-C. & AUWERX, J. 1998. Transcriptional control of adipogenesis. *Current opinion in cell biology*, 10, 165-173.
- FANG, H. & JUDD, R. 2018. Adiponectin regulation and function. *Compr. Physiol.* 8: 1031–1063.
- FERLAY, J., SOERJOMATARAM, I., DIKSHIT, R., ESER, S., MATHERS, C., REBELO, M., PARKIN, D. M., FORMAN, D. & BRAY, F. 2015. Cancer incidence and mortality worldwide: sources, methods and major patterns in GLOBOCAN 2012. *International journal of cancer*, 136, E359-E386.
- FERRARO, G. A., DE FRANCESCO, F., TIRINO, V., CATALDO, C., ROSSANO, F., NICOLETTI, G. & D'ANDREA, F. 2011. Effects of a new centrifugation method on adipose cell viability for autologous fat grafting. *Aesthetic plastic surgery*, 35, 341-348.
- FLYNN, L., SEMPLE, J. L. & WOODHOUSE, K. A. 2006. Decellularized placental matrices for adipose tissue engineering. *Journal of Biomedical Materials Research Part A: An Official Journal of The Society for Biomaterials, The Japanese Society for Biomaterials, and The Australian Society for Biomaterials and the Korean Society for Biomaterials*, 79, 359-369.
- FRAGA, H., FERNANDES, D., NOVOTNY, J., FONTES, R. & ESTEVES DA SILVA, J. 2006. Firefly luciferase produces hydrogen peroxide as a coproduct in dehydroluciferyl adenylate formation. *ChemBioChem*, 7, 929-935.
- FREEDLAND, E. S. 2004. Role of a critical visceral adipose tissue threshold (CVATT) in metabolic syndrome: implications for controlling dietary carbohydrates: a review. *Nutrition & metabolism*, 1, 1-24.
- FREEMAN, D. J., NORRIE, J., CASLAKE, M. J., GAW, A., FORD, I., LOWE, G. D., O'REILLY, D. S. J., PACKARD, C. J., SATTAR, N. & GROUP, W. O. S. C. P. S. 2002. C-reactive protein is an independent predictor of risk for the development of diabetes in the West of Scotland Coronary Prevention Study. *Diabetes*, 51, 1596-1600.
- FRIEDMAN, J. 2016. The long road to leptin. *The Journal of clinical investigation*, 126, 4727-4734.
- FRONTINI, A. & CINTI, S. 2010. Distribution and development of brown adipocytes in the murine and human adipose organ. *Cell metabolism*, 11, 253-256.
- FRÜHBECK, G., BECERRIL, S., SÁINZ, N., GARRASTACHU, P. & GARCÍA-VELLOSO, M. J. 2009. BAT: a new target for human obesity? *Trends Pharmacol Sci*, 30, 387-96.
- FUKAI, F., ISO, T., SEKIGUCHI, K., MIYATAKE, N., TSUGITA, A. & KATAYAMA, T. 1993. An amino-terminal fibronectin fragment stimulates the differentiation of ST-13 preadipocytes. *Biochemistry*, 32, 5746-5751.
- FUNAHASHI, H., YADA, T., SUZUKI, R. & SHIODA, S. 2003. Distribution, function, and properties of leptin receptors in the brain. *International review of cytology*, 224, 1-27.

- GASSMAN, A. A., KAO, K. K., BRADLEY, J. P. & LEE, J. C. 2016. Quantification of adipose transfer viability using a novel, bioluminescent murine model. *Journal of Plastic, Reconstructive & Aesthetic Surgery*, 69, 959-965.
- GAUSE, T. M., KLING, R. E., SIVAK, W. N., MARRA, K. G., RUBIN, J. P. & KOKAI, L. E. 2014. Particle size in fat graft retention: a review on the impact of harvesting technique in lipofilling surgical outcomes. *Adipocyte*, 3, 273-279.
- GENTRY, J. W. 1997. The legacy of John Tyndall in aerosol science. *Journal of aerosol science*, 28, 1365-1372.
- GESTA, S., BLÜHER, M., YAMAMOTO, Y., NORRIS, A. W., BERNDT, J., KRALISCH, S., BOUCHER, J., LEWIS, C. & KAHN, C. R. 2006. Evidence for a role of developmental genes in the origin of obesity and body fat distribution. *Proceedings of the National Academy of Sciences*, 103, 6676-6681.
- GESTA, S., TSENG, Y. H. & KAHN, C. R. 2007. Developmental origin of fat: tracking obesity to its source. *Cell*, 131, 242-56.
- GHABEN, A. L. & SCHERER, P. E. 2019. Adipogenesis and metabolic health. *Nature reviews Molecular cell biology*, 20, 242-258.
- GHAVAMI, A. & VILLANUEVA, N. L. 2018. Gluteal augmentation and contouring with autologous fat transfer: part I. *Clinics in plastic surgery*, 45, 249-259.
- GIORDANO, A., SMORLESI, A., FRONTINI, A., BARBATELLI, G. & CINTI, S. 2014. White, brown and pink adipocytes: the extraordinary plasticity of the adipose organ. *Eur J Endocrinol*, 170, R159-71.
- GIRARD, J., PERDEREAU, D., FOUFELLE, F., PRIP-BUUS, C. & FERRÉ, P. 1994. Regulation of lipogenic enzyme gene expression by nutrients and hormones. *The FASEB Journal*, 8, 36-42.
- GONZALEZ, A. M., LOBOCKI, C., KELLY, C. P. & JACKSON, I. T. 2007. An alternative method for harvest and processing fat grafts: an in vitro study of cell viability and survival. *Plastic and reconstructive surgery*, 120, 285-294.
- GRAVES, R. A., TONONNOZ, P. & SPIEGELMAN, B. M. 1992. Analysis of a tissue-specific enhancer: ARF6 regulates adipogenic gene expression. *Molecular and cellular biology*, 12, 1202-1208.
- GREGOIRE, F. 1998. Smas CM, Sul HS. *Understanding adipocyte differentiation. Physiol Rev*, 78, 783-809.
- GRÉGOIRE, F., DE BROUX, N., HAUSER, N., HEREMANS, H., VAN DAMME, J. & REMACLE, C. 1992. Interferon- γ and interleukin-1 β inhibit adipoconversion in cultured rodent preadipocytes. *Journal of cellular physiology*, 151, 300-309.
- GREGOIRE, F. M. 2001. Adipocyte differentiation: from fibroblast to endocrine cell. *Experimental Biology and Medicine*, 226, 997-1002.
- GUERRA, C., NAVARRO, P., VALVERDE, A. M., ARRIBAS, M., BRÜNING, J., KOZAK, L. P., KAHN, C. R. & BENITO, M. 2001. Brown adipose tissue-specific insulin receptor knockout shows diabetic phenotype without insulin resistance. *The Journal of clinical investigation*, 108, 1205-1213.
- GUSTAFSON, B., HEDJAZIFAR, S., GOGG, S., HAMMARSTEDT, A. & SMITH, U. 2015. Insulin resistance and impaired adipogenesis. *Trends in Endocrinology & Metabolism*, 26, 193-200.

- HAN, C. Y., KARGI, A. Y., OMER, M., CHAN, C. K., WABITSCH, M., O'BRIEN, K. D., WIGHT, T. N. & CHAIT, A. 2010. Differential effect of saturated and unsaturated free fatty acids on the generation of monocyte adhesion and chemotactic factors by adipocytes: dissociation of adipocyte hypertrophy from inflammation. *Diabetes*, 59, 386-396.
- HARCOURT, D. & RUMSEY, N. 2001. Psychological aspects of breast reconstruction: a review of the literature. *Journal of advanced nursing*, 35, 477-487.
- HAUNER, H. & LÖFFLER, G. 1987. Adipose tissue development: The role of precursor cells and adipogenic factors. *Klinische Wochenschrift*, 65, 803-811.
- HAUSMAN, D., DIGIROLAMO, M., BARTNESS, T., HAUSMAN, G. & MARTIN, R. 2001. The biology of white adipocyte proliferation. *Obesity reviews*, 2, 239-254.
- HEILBRONN, L. K. & CAMPBELL, L. V. 2008. Adipose tissue macrophages, low grade inflammation and insulin resistance in human obesity. *Current pharmaceutical design*, 14, 1225-1230.
- HIGHLEY, C. B., PRESTWICH, G. D. & BURDICK, J. A. 2016a. Recent advances in hyaluronic acid hydrogels for biomedical applications. *Current opinion in biotechnology*, 40, 35-40.
- HIGHLEY, C. B., PRESTWICH, G. D. & BURDICK, J. A. 2016b. Recent advances in hyaluronic acid hydrogels for biomedical applications. *Curr Opin Biotechnol*, 40, 35-40.
- HINZ, B. 2015. The extracellular matrix and transforming growth factor- β 1: Tale of a strained relationship. *Matrix biology*, 47, 54-65.
- HIRSCH, R. J., BRODY, H. J. & CARRUTHERS, J. D. 2007. Hyaluronidase in the office: a necessity for every dermatologist that injects hyaluronic acid. *Journal of Cosmetic and Laser Therapy*, 9, 182-185.
- HOLLENBERG, A. N., SUSULIC, V. S., MADURA, J. P., ZHANG, B., MOLLER, D. E., TONONNOZ, P., SARRAF, P., SPIEGELMAN, B. M. & LOWELL, B. B. 1997. Functional antagonism between CCAAT/enhancer binding protein- α and peroxisome proliferator-activated receptor- γ on the leptin promoter. *Journal of Biological Chemistry*, 272, 5283-5290.
- HOLLIDAY, D. L. & SPEIRS, V. 2011. Choosing the right cell line for breast cancer research. *Breast cancer research*, 13, 1-7.
- HUANG, L.-K. & WANG, M.-J. J. 1995. Image thresholding by minimizing the measures of fuzziness. *Pattern recognition*, 28, 41-51.
- HUBE, F., LIETZ, U., IGEL, M., JENSEN, P., TORNQVIST, H., JOOST, H.-G. & HAUNER, H. 1996. Difference in leptin mRNA levels between omental and subcutaneous abdominal adipose tissue from obese humans. *Hormone and metabolic research*, 28, 690-693.
- HUSS, F. R. & KRATZ, G. 2001. Mammary epithelial cell and adipocyte co-culture in a 3-D matrix: the first step towards tissue-engineered human breast tissue. *Cells Tissues Organs*, 169, 361-367.
- IBARBURU, A. S. 2006. Introduction to the structure and properties of polymers-rheology and dynamic viscoelasticity part 1. In: POLYMAT (ed.). University of the Basque Country.

- IBRAHIMI, A., BONINO, F., BARDON, S., AILHAUD, G. & DANI, C. 1992. Essential role of collagens for terminal differentiation of preadipocytes. *Biochemical and biophysical research communications*, 187, 1314-1322.
- IDEALMEDICALSOLUTIONS. 2021. Available: <https://ideal-ms.com/product/filtron/> [Accessed].
- IKEDA, K., MARETICH, P. & KAJIMURA, S. 2018. The common and distinct features of brown and beige adipocytes. *Trends in Endocrinology & Metabolism*, 29, 191-200.
- ILLOUZ, Y.-G., ILLOUZ, Y.-G. & DE VILLERS, Y. T. 1989. *Body sculpturing by lipoplasty*, Churchill Livingstone.
- INOUE, M. & KATAKAMI, C. 1993. The effect of hyaluronic acid on corneal epithelial cell proliferation. *Investigative ophthalmology & visual science*, 34, 2313-2315.
- ITO, T., YEO, Y., HIGHLEY, C. B., BELLAS, E., BENITEZ, C. A. & KOHANE, D. S. 2007. The prevention of peritoneal adhesions by in situ cross-linking hydrogels of hyaluronic acid and cellulose derivatives. *Biomaterials*, 28, 975-983.
- JENA, P. V., SHAMAY, Y., SHAH, J., ROXBURY, D., PAKNEJAD, N. & HELLER, D. A. 2016. Photoluminescent carbon nanotubes interrogate the permeability of multicellular tumor spheroids. *Carbon*, 97, 99-109.
- JESSEN, B. A. & STEVENS, G. J. 2002. Expression profiling during adipocyte differentiation of 3T3-L1 fibroblasts. *Gene*, 299, 95-100.
- JHA, A. K., MALIK, M. S., FARACH-CARSON, M. C., DUNCAN, R. L. & JIA, X. 2010. Hierarchically structured, hyaluronic acid-based hydrogel matrices via the covalent integration of microgels into macroscopic networks. *Soft matter*, 6, 5045-5055.
- JI, E., JUNG, M., PARK, J., KIM, S., SEO, C., PARK, K., LEE, E., YEOM, C. & LEE, S. 2014. Inhibition of adipogenesis in 3T3-L1 cells and suppression of abdominal fat accumulation in high-fat diet-feeding C57BL/6J mice after downregulation of hyaluronic acid. *International journal of obesity*, 38, 1035-1043.
- JOYCE, C. W., JOYCE, K. M., RAHMANI, G., WALSH, S. R., CARROLL, S. M., HUSSEY, A. J. & KELLY, J. L. 2015. Fat grafting: a citation analysis of the seminal articles. *Plast Reconstr Surg Glob Open*, 3, e295.
- KABLIK, J., MONHEIT, G. D., YU, L., CHANG, G. & GERSHKOVICH, J. 2009. Comparative physical properties of hyaluronic acid dermal fillers. *Dermatologic Surgery*, 35, 302-312.
- KAISANLAHTI, A. & GLUMOFF, T. 2019. Browning of white fat: agents and implications for beige adipose tissue to type 2 diabetes. *Journal of physiology and biochemistry*, 75, 1-10.
- KAKAGIA, D. & PALLUA, N. 2014. Autologous fat grafting: in search of the optimal technique. *Surgical innovation*, 21, 327-336.
- KATZ, A. J., LLULL, R., HEDRICK, M. H. & FUTRELL, J. 1999. Emerging approaches to the tissue engineering of fat. *Clinics in plastic surgery*, 26, 587-603.
- KENNEDY JR, G. L. 2002. Toxicity of adipic acid. *Drug and chemical toxicology*, 25, 191-202.

- KHALIL, A. A., JAMESON, M. J., BROADDUS, W. C., CHUNG, T. D., GOLDING, S. E., DEVER, S. M., ROSENBERG, E. & VALERIE, K. 2013. Subcutaneous administration of D-luciferin is an effective alternative to intraperitoneal injection in bioluminescence imaging of xenograft tumors in nude mice. *International Scholarly Research Notices*, 2013.
- KHAN, T., MUISE, E. S., IYENGAR, P., WANG, Z. V., CHANDALIA, M., ABATE, N., ZHANG, B. B., BONALDO, P., CHUA, S. & SCHERER, P. E. 2009. Metabolic dysregulation and adipose tissue fibrosis: role of collagen VI. *Molecular and cellular biology*, 29, 1575-1591.
- KHATER, R., ATANASSOVA, P., ANASTASSOV, Y., PELLERIN, P. & MARTINOT-DUQUENNOY, V. 2009. Clinical and experimental study of autologous fat grafting after processing by centrifugation and serum lavage. *Aesthetic plastic surgery*, 33, 37-43.
- KHOURI, R. K., RIGOTTI, G., CARDOSO, E., KHOURI JR, R. K. & BIGGS, T. M. 2014a. Megavolume autologous fat transfer: part I. Theory and principles. *Plastic and reconstructive surgery*, 133, 550-557.
- KHOURI, R. K., RIGOTTI, G., CARDOSO, E., KHOURI JR, R. K. & BIGGS, T. M. 2014b. Megavolume autologous fat transfer: part II. Practice and techniques. *Plastic and reconstructive surgery*, 133, 1369-1377.
- KIM, J. B., JIN, H. B., SON, J. H. & CHUNG, J. H. 2018. For better fat graft outcome in soft tissue augmentation: systematic review and meta-analysis. *Archives of Aesthetic Plastic Surgery*, 24, 116-127.
- KIM, J. B. & SPIEGELMAN, B. M. 1996. ADD1/SREBP1 promotes adipocyte differentiation and gene expression linked to fatty acid metabolism. *Genes & development*, 10, 1096-1107.
- KIMURA, Y., OZEKI, M., INAMOTO, T. & TABATA, Y. 2003. Adipose tissue engineering based on human preadipocytes combined with gelatin microspheres containing basic fibroblast growth factor. *Biomaterials*, 24, 2513-2521.
- KINOSHITA, S. 2016. Light scattering. *Bionanophotonics*. Jenny Stanford Publishing.
- KIRKHAM, J. C., LEE, J. H., MEDINA, M. A., 3RD, MCCORMACK, M. C., RANDOLPH, M. A. & AUSTEN, W. G., JR. 2012. The impact of liposuction cannula size on adipocyte viability. *Ann Plast Surg*, 69, 479-81.
- KLEIN, J. A. 1993. Tumescence technique for local anesthesia improves safety in large-volume liposuction. *Plastic and reconstructive surgery*, 92, 1085-1085.
- KNUDSON, C. B. & KNUDSON, W. 1993. Hyaluronan-binding proteins in development, tissue homeostasis, and disease. *The FASEB Journal*, 7, 1233-1241.
- KONIECZNY, S. F. & EMERSON JR, C. P. 1984. 5-Azacytidine induction of stable mesodermal stem cell lineages from 10T1/2 cells: evidence for regulatory genes controlling determination. *Cell*, 38, 791-800.
- KRAL, J. G. & CRANDALL, D. L. 1999. Development of a human adipocyte synthetic polymer scaffold. *Plastic and reconstructive surgery*, 104, 1732-1738.
- KRAMER, A. H., JOOS-VANDEWALLE, J., EDKINS, A. L., FROST, C. L. & PRINSLOO, E. 2014. Real-time monitoring of 3T3-L1 preadipocyte differentiation using a

- commercially available electric cell-substrate impedance sensor system. *Biochemical and biophysical research communications*, 443, 1245-1250.
- KRSSAK, M., PETERSEN, K. F., DRESNER, A., DIPIETRO, L., VOGEL, S., ROTHMAN, D., SHULMAN, G. & RODEN, M. 1999. Intramyocellular lipid concentrations are correlated with insulin sensitivity in humans: a ¹H NMR spectroscopy study. *Diabetologia*, 42, 113-116.
- KURITA, M., MATSUMOTO, D., SHIGEURA, T., SATO, K., GONDA, K., HARI, K. & YOSHIMURA, K. 2008. Influences of centrifugation on cells and tissues in liposuction aspirates: optimized centrifugation for lipotransfer and cell isolation. *Plastic and reconstructive surgery*, 121, 1033-1041.
- KWOK, K. H., LAM, K. S. & XU, A. 2016. Heterogeneity of white adipose tissue: molecular basis and clinical implications. *Experimental & molecular medicine*, 48, e215-e215.
- LA CAVA, A. & MATARESE, G. 2004. The weight of leptin in immunity. *Nature Reviews Immunology*, 4, 371-379.
- LAHARRAGUE, P., LARROUY, D., FONTANILLES, A. M., TRUDEL, N., CAMPFIELD, A., TENENBAUM, R., GALITZKY, J., CORBERAND, J. X., PÉNICAUD, L. & CASTEILLA, L. 1998. High expression of leptin by human bone marrow adipocytes in primary culture. *The FASEB journal*, 12, 747-752.
- LAVIK, E. & LANGER, R. 2004. Tissue engineering: current state and perspectives. *Applied microbiology and biotechnology*, 65, 1-8.
- LEVENBERG, S. & LANGER, R. 2004. 5 Advances in Tissue Engineering. *Current topics in developmental biology*, 61, 113-134.
- LEVINE, J. F. & STOCKDALE, F. E. 1984. 3T3-L1 adipocytes promote the growth of mammary epithelium. *Experimental cell research*, 151, 112-122.
- LIU, A. C., WELSH, D. K., KO, C. H., TRAN, H. G., ZHANG, E. E., PRIEST, A. A., BUHR, E. D., SINGER, O., MEEKER, K. & VERMA, I. M. 2007. Intercellular coupling confers robustness against mutations in the SCN circadian clock network. *Cell*, 129, 605-616.
- LOUET, J.-F., COSTE, A., AMAZIT, L., TANNOUR-LOUET, M., WU, R.-C., TSAI, S. Y., TSAI, M.-J., AUWERX, J. & O'MALLEY, B. W. 2006. Oncogenic steroid receptor coactivator-3 is a key regulator of the white adipogenic program. *Proceedings of the National Academy of Sciences*, 103, 17868-17873.
- MA, X., LIU, X., WANG, P., WANG, X., YANG, R., LIU, S., YE, Z. & CHI, B. 2020. Covalently adaptable hydrogel based on hyaluronic acid and poly (γ -Glutamic Acid) for potential load-bearing tissue engineering. *ACS Applied Bio Materials*, 3, 4036-4043.
- MACDOUGALD, O. A. & LANE, M. D. 1995. Transcriptional regulation of gene expression during adipocyte differentiation. *Annual review of biochemistry*, 64, 345-373.
- MAEDA, K., OKUBO, K., SHIMOMURA, I., MIZUNO, K., MATSUZAWA, Y. & MATSUBARA, K. 1997. Analysis of an expression profile of genes in the human adipose tissue. *Gene*, 190, 227-235.

- MALDA, J., VISSER, J., MELCHELS, F. P., JÜNGST, T., HENNINK, W. E., DHERT, W. J., GROLL, J. & HUTMACHER, D. W. 2013. 25th anniversary article: engineering hydrogels for biofabrication. *Advanced materials*, 25, 5011-5028.
- MANDRUP, S. & LANE, M. D. 1997. Regulating adipogenesis. *Journal of Biological Chemistry*, 272, 5367-5370.
- MANDRUP, S., SØRENSEN, R. V., HELLEDIE, T., NØHR, J., BALDURSSON, T., GRAM, C., KNUDSEN, J. & KRISTIANSEN, K. 1998. Inhibition of 3T3-L1 adipocyte differentiation by expression of acyl-CoA-binding protein antisense RNA. *Journal of Biological Chemistry*, 273, 23897-23903.
- MARKEY, A. C. & GLOGAU, R. G. 2000. Autologous fat grafting: comparison of techniques. *Dermatologic surgery*, 26, 1135-1139.
- MCKINNON, D. D., DOMAILLE, D. W., CHA, J. N. & ANSETH, K. S. 2014. Biophysically defined and cytocompatible covalently adaptable networks as viscoelastic 3D cell culture systems. *Advanced materials*, 26, 865-872.
- MEGÍAS M, M. P., POMBAL MA. 2019. *Atlas of Plant and Animal Histology* [Online]. Available: https://mmegias.webs.uvigo.es/02-english/guiada_a_adiposo.php [Accessed 2021].
- MEZZANOTTE, L., MONIEK VAN 'T, R., KARATAS, H., GOUN, E. A. & LÖWIK, C. W. G. M. 2017. In Vivo Molecular Bioluminescence Imaging: New Tools and Applications. *Trends in Biotechnology*, 35, 640-652.
- MILLER JR, W. H., FAUST, I. M. & HIRSCH, J. 1984. Demonstration of de novo production of adipocytes in adult rats by biochemical and radioautographic techniques. *Journal of lipid research*, 25, 336-347.
- MIYAZONO, K., MAEDA, S. & IMAMURA, T. 2005. BMP receptor signaling: transcriptional targets, regulation of signals, and signaling cross-talk. *Cytokine & growth factor reviews*, 16, 251-263.
- MOJALLAL, A. & FOYATIER, J. L. 2004. [The effect of different factors on the survival of transplanted adipocytes]. *Ann Chir Plast Esthet*, 49, 426-36.
- MORI, S., KIUCHI, S., OUCHI, A., HASE, T. & MURASE, T. 2014. Characteristic expression of extracellular matrix in subcutaneous adipose tissue development and adipogenesis; comparison with visceral adipose tissue. *International journal of biological sciences*, 10, 825.
- MOW, V. C., HOLMES, M. H. & LAI, W. M. 1984. Fluid transport and mechanical properties of articular cartilage: a review. *Journal of biomechanics*, 17, 377-394.
- NAPOLITANO, L. M. 1965. Observations on the fine structure of adipose cells. *Annals of the New York Academy of Sciences*, 131, 34-42.
- NEDERGAARD, J., BENGTSSON, T. & CANNON, B. 2007. Unexpected evidence for active brown adipose tissue in adult humans. *American Journal of Physiology-Endocrinology and Metabolism*.
- NEUBER, G. 1910. Asepsis und kunstliche Blutleere. *Verhandl d deutsch Gesellsch F Chir (Berl)*, 22, 159.
- NIEMELÄ, S.-M., MIETTINEN, S., KONTTINEN, Y., WARIS, T., KELLOMÄKI, M., ASHAMMAKHI, N. A. & YLIKOMI, T. 2007. Fat tissue: views on reconstruction and exploitation. *Journal of Craniofacial Surgery*, 18, 325-335.

- NTAMBI, J. M. & YOUNG-CHEUL, K. 2000. Adipocyte differentiation and gene expression. *The Journal of nutrition*, 130, 3122S-3126S.
- ONO, M., ARATANI, Y., KITAGAWA, I. & KITAGAWA, Y. 1990. Ascorbic acid phosphate stimulates type IV collagen synthesis and accelerates adipose conversion of 3T3-L1 cells. *Experimental cell research*, 187, 309-314.
- PALLUA, N., PULSFORT, A. K., SUSCHEK, C. & WOLTER, T. P. 2009. Content of the growth factors bFGF, IGF-1, VEGF, and PDGF-BB in freshly harvested lipoaspirate after centrifugation and incubation. *Plastic and reconstructive surgery*, 123, 826-833.
- PAN, H.-Y., GUO, L. & LI, Q. 2010. Changes of serum omentin-1 levels in normal subjects and in patients with impaired glucose regulation and with newly diagnosed and untreated type 2 diabetes. *Diabetes research and clinical practice*, 88, 29-33.
- PARK, Y. D., TIRELLI, N. & HUBBELL, J. A. 2003. Photopolymerized hyaluronic acid-based hydrogels and interpenetrating networks. *Biomaterials*, 24, 893-900.
- PATRICK JR, C. 2001. Tissue engineering strategies for adipose tissue repair. *The Anatomical Record: An Official Publication of the American Association of Anatomists*, 263, 361-366.
- PATRICK JR, C., CHAUVIN, P., HOBLEY, J. & REECE, G. P. 1999. Preadipocyte seeded PLGA scaffolds for adipose tissue engineering. *Tissue engineering*, 5, 139-151.
- PEER, L. A. 1950. Loss of weight and volume in human fat grafts: with postulation of a "cell survival theory". *Plastic and Reconstructive Surgery*, 5, 217-230.
- PELTONIEMI, H. H., SALMI, A., MIETTINEN, S., MANNERSTRÖM, B., SAARINIEMI, K., MIKKONEN, R., KUOKKANEN, H. & HEROLD, C. 2013. Stem cell enrichment does not warrant a higher graft survival in lipofilling of the breast: a prospective comparative study. *Journal of plastic, reconstructive & aesthetic surgery*, 66, 1494-1503.
- PEPPAS, N. A. 1986. *Hydrogels in medicine and pharmacy*, CRC press Boca Raton, FL.
- PRADHAN, A. D., MANSON, J. E., RIFAI, N., BURING, J. E. & RIDKER, P. M. 2001. C-reactive protein, interleukin 6, and risk of developing type 2 diabetes mellitus. *Jama*, 286, 327-334.
- PRINS, J. B. & O'RAHILLY, S. 1997. Regulation of adipose cell number in man. *Clinical science*, 92, 3-11.
- PU, L. L., CUI, X., FINK, B. F., CIBULL, M. L. & GAO, D. 2005. The viability of fatty tissues within adipose aspirates after conventional liposuction: a comprehensive study. *Annals of plastic surgery*, 54, 288-292.
- PU, L. L. Q., COLEMAN, S. R., CUI, X., FERGUSON, R. E. H., JR. & VASCONEZ, H. C. 2008. Autologous fat grafts harvested and refined by the Coleman technique: a comparative study. *Plast Reconstr Surg*, 122, 932-937.
- QIAO, Y., XU, S., ZHU, T., TANG, N., BAI, X. & ZHENG, C. 2020. Preparation of printable double-network hydrogels with rapid self-healing and high elasticity based on hyaluronic acid for controlled drug release. *Polymer*, 186, 121994.
- QIU, Y., NGUYEN, K. D., ODEGAARD, J. I., CUI, X., TIAN, X., LOCKSLEY, R. M., PALMITER, R. D. & CHAWLA, A. 2014. Eosinophils and type 2 cytokine signaling in

- macrophages orchestrate development of functional beige fat. *Cell*, 157, 1292-1308.
- RAMANATHAN, C., KHAN, S. K., KATHALE, N. D., XU, H. & LIU, A. C. 2012. Monitoring cell-autonomous circadian clock rhythms of gene expression using luciferase bioluminescence reporters. *JoVE (Journal of Visualized Experiments)*, e4234.
- RAMANATHAN, C., XU, H., KHAN, S. K., SHEN, Y., GITIS, P. J., WELSH, D. K., HOGENESCH, J. B. & LIU, A. C. 2014. Cell type-specific functions of period genes revealed by novel adipocyte and hepatocyte circadian clock models. *PLoS genetics*, 10, e1004244.
- REDDY, P., LENT-SCHOCHET, D., RAMAKRISHNAN, N., MCLAUGHLIN, M. & JIALAL, I. 2019. Metabolic syndrome is an inflammatory disorder: A conspiracy between adipose tissue and phagocytes. *Clinica Chimica Acta*, 496, 35-44.
- REUSCH, J. E., COLTON, L. A. & KLEMM, D. J. 2000. CREB activation induces adipogenesis in 3T3-L1 cells. *Molecular and cellular biology*, 20, 1008-1020.
- REYNÉS, B., PALOU, M., RODRÍGUEZ, A. M. & PALOU, A. 2019. Regulation of adaptive thermogenesis and browning by prebiotics and postbiotics. *Frontiers in physiology*, 9, 1908.
- RICHARD, A. J., WHITE, U., ELKS, C. M. & STEPHENS, J. M. 2020. Adipose tissue: physiology to metabolic dysfunction. *Endotext [Internet]*.
- RODELL, C. B., KAMINSKI, A. L. & BURDICK, J. A. 2013. Rational design of network properties in guest–host assembled and shear-thinning hyaluronic acid hydrogels. *Biomacromolecules*, 14, 4125-4134.
- RONDINONE, C. M., BAKER, M. E. & RODBARD, D. 1992. Progesterins stimulate the differentiation of 3T3-L1 preadipocytes. *The Journal of steroid biochemistry and molecular biology*, 42, 795-802.
- ROOTMAN, D. B., LIN, J. L. & GOLDBERG, R. 2014. Does the Tyndall effect describe the blue hue periodically observed in subdermal hyaluronic acid gel placement? *Ophthalmic Plastic & Reconstructive Surgery*, 30, 524-527.
- ROSEN, E. D. & SPIEGELMAN, B. M. 2000. Molecular regulation of adipogenesis. *Annual review of cell and developmental biology*, 16, 145-171.
- ROSEN, E. D., WALKEY, C. J., PUIGSERVER, P. & SPIEGELMAN, B. M. 2000. Transcriptional regulation of adipogenesis. *Genes & development*, 14, 1293-1307.
- SALADIN, R., FAJAS, L., DANA, S., HALVORSEN, Y.-D., AUWERX, J. & BRIGGS, M. 1999. Differential regulation of peroxisome proliferator activated receptor gamma1 (PPARgamma1) and PPARgamma2 messenger RNA expression in the early stages of adipogenesis. *Cell growth & differentiation: the molecular biology journal of the American Association for Cancer Research*, 10, 43-48.
- SALEH, J., AL-WARDY, N., FARHAN, H., AL-KHANBASHI, M. & CIANFLONE, K. 2011. Acylation stimulating protein: a female lipogenic factor? *Obesity Reviews*, 12, 440-448.
- SALGARELLO, M., VISCONTI, G. & RUSCIANI, A. 2011. Breast fat grafting with platelet-rich plasma: a comparative clinical study and current state of the art. *Plastic and reconstructive surgery*, 127, 2176-2185.

- SAMARAS, K., BOTELHO, N. K., CHISHOLM, D. J. & LORD, R. V. 2010. Subcutaneous and visceral adipose tissue gene expression of serum adipokines that predict type 2 diabetes. *Obesity*, 18, 884-889.
- SANTAMARIA-MARTOS, F., BENITEZ, I. D., LATORRE, J., LLUCH, A., MORENO-NAVARRETE, J. M., SABATER, M., RICART, W., DE LA TORRE, M. S., MORA, S. & FERNÁNDEZ-REAL, J. M. 2020. Comparative and functional analysis of plasma membrane-derived extracellular vesicles from obese vs. nonobese women. *Clinical Nutrition*, 39, 1067-1076.
- SCHINDELIN, J., ARGANDA-CARRERAS, I., FRISE, E., KAYNIG, V., LONGAIR, M., PIETZSCH, T., PREIBISCH, S., RUEDEN, C., SAALFELD, S. & SCHMID, B. 2012. Fiji: an open-source platform for biological-image analysis. *Nature methods*, 9, 676-682.
- SCHMIDT, C. E. & BAIER, J. M. 2000. Acellular vascular tissues: natural biomaterials for tissue repair and tissue engineering. *Biomaterials*, 21, 2215-2231.
- SCHNEIDER, C. A., RASBAND, W. S. & ELICEIRI, K. W. 2012. NIH Image to ImageJ: 25 years of image analysis. *Nature methods*, 9, 671-675.
- SEGURA, T., ANDERSON, B. C., CHUNG, P. H., WEBBER, R. E., SHULL, K. R. & SHEA, L. D. 2005. Crosslinked hyaluronic acid hydrogels: a strategy to functionalize and pattern. *Biomaterials*, 26, 359-371.
- SHAN, B., WANG, X., WU, Y., XU, C., XIA, Z., DAI, J., SHAO, M., ZHAO, F., HE, S. & YANG, L. 2017. The metabolic ER stress sensor IRE1 α suppresses alternative activation of macrophages and impairs energy expenditure in obesity. *Nature immunology*, 18, 519-529.
- SHEIKH, A. Y., LIN, S. A., CAO, F., CAO, Y., VAN DER BOGT, K. E., CHU, P., CHANG, C. P., CONTAG, C. H., ROBBINS, R. C. & WU, J. C. 2007. Molecular imaging of bone marrow mononuclear cell homing and engraftment in ischemic myocardium. *Stem cells*, 25, 2677-2684.
- SHERMAN, J. E., FANZIO, P. M., WHITE, H. & LEIFER, D. 2010. Blindness and necrotizing fasciitis after liposuction and fat transfer. *Plastic and reconstructive surgery*, 126, 1358-1363.
- SHOHAM, N., SASSON, A. L., LIN, F.-H., BENAYAHU, D., HAJ-ALI, R. & GEFEN, A. 2013. The mechanics of hyaluronic acid/adipic acid dihydrazide hydrogel: towards developing a vessel for delivery of preadipocytes to native tissues. *Journal of the mechanical behavior of biomedical materials*, 28, 320-331.
- SIMONACCI, F., BERTOZZI, N., GRIECO, M. P., GRIGNAFFINI, E. & RAPOSIO, E. 2017. Procedure, applications, and outcomes of autologous fat grafting. *Ann Med Surg (Lond)*, 20, 49-60.
- SMAS, C. M., CHEN, L., ZHAO, L., LATASA, M.-J. & SUL, H. S. 1999. Transcriptional Repression of pref-1 by Glucocorticoids Promotes 3T3-L1 Adipocyte Differentiation. *Journal of Biological Chemistry*, 274, 12632-12641.
- SOMMER, B. & SATTLER, G. 2000. Current concepts of fat graft survival: histology of aspirated adipose tissue and review of the literature. *Dermatologic Surgery*, 26, 1159-1166.
- SPENCER, M., UNAL, R., ZHU, B., RASOULI, N., MCGEHEE JR, R. E., PETERSON, C. A. & KERN, P. A. 2011. Adipose tissue extracellular matrix and vascular abnormalities

- in obesity and insulin resistance. *The Journal of Clinical Endocrinology & Metabolism*, 96, E1990-E1998.
- SPIEGELMAN, B. M., CHOY, L., HOTAMISLIGIL, G. S., GRAVES, R. A. & TONTONOZ, P. 1993. Regulation of adipocyte gene expression in differentiation and syndromes of obesity/diabetes. *Journal of Biological Chemistry*, 268, 6823-6826.
- SPIEGELMAN, B. M. & GINTY, C. A. 1983. Fibronectin modulation of cell shape and lipogenic gene expression in 3T3-adipocytes. *Cell*, 35, 657-666.
- STERN, R., ASARI, A. A. & SUGAHARA, K. N. 2006. Hyaluronan fragments: an information-rich system. *European journal of cell biology*, 85, 699-715.
- STOLIER, A. J., SULLIVAN, S. K. & DELLACROCE, F. J. 2008. Technical considerations in nipple-sparing mastectomy: 82 consecutive cases without necrosis. *Annals of Surgical Oncology*, 15, 1341-1347.
- STRONG, A. L., CEDERNA, P. S., RUBIN, J. P., COLEMAN, S. R. & LEVI, B. 2015. The current state of fat grafting: a review of harvesting, processing, and injection techniques. *Plastic and reconstructive surgery*, 136, 897.
- SUN, K., KUSMINSKI, C. M. & SCHERER, P. E. 2011. Adipose tissue remodeling and obesity. *The Journal of clinical investigation*, 121, 2094-2101.
- TACHI, M. & YAMADA, A. 2005. Choice of flaps for breast reconstruction. *International journal of clinical oncology*, 10, 289-297.
- TANG, L., ROSENBERG, L., REINER, A. & POOLE, A. 1979. Proteoglycans from bovine nasal cartilage. Properties of a soluble form of link protein. *Journal of Biological Chemistry*, 254, 10523-10531.
- THANIK, V. D., CHANG, C. C., LERMAN, O. Z., ALLEN JR, R. J., NGUYEN, P. D., SAADEH, P. B., WARREN, S. M., LEVINE, J. P., COLEMAN, S. R. & HAZEN, A. 2009. A murine model for studying diffusely injected human fat. *Plastic and reconstructive surgery*, 124, 74-81.
- TIRELLA, A., DE MARIA, C., CRISCENTI, G., VOZZI, G. & AHLUWALIA, A. 2012. The PAM2 system: a multilevel approach for fabrication of complex three-dimensional microstructures. *Rapid Prototyping Journal*.
- TSENG, Y.-H., KRIAUCIUNAS, K. M., KOKKOTOU, E. & KAHN, C. R. 2004. Differential roles of insulin receptor substrates in brown adipocyte differentiation. *Molecular and cellular biology*, 24, 1918-1929.
- TURLEY, E. 1982. Purification of a hyaluronate-binding protein fraction that modifies cell social behavior. *Biochemical and biophysical research communications*, 108, 1016-1024.
- UGAROVA, N. 1989. Luciferase of *Luciola mingrelica* fireflies. Kinetics and regulation mechanism. *Journal of bioluminescence and chemiluminescence*, 4, 406-418.
- ULLMANN, Y., HYAMS, M., RAMON, Y., BEACH, D., PELED, I. J. & LINDENBAUM, E. S. 1998. Enhancing the survival of aspirated human fat injected into nude mice. *Plastic and reconstructive surgery*, 101, 1940-1944.
- UNAMUNO, X., FRÜHBECK, G. & CATALÁN, V. 2018. The Adipose Tissue. *Encyclopedia of Endocrine Diseases (Second Edition)*.
- VARGOVIC, P., MANZ, G. & KVETNANSKY, R. 2016. Continuous cold exposure induces an anti-inflammatory response in mesenteric adipose tissue associated with

- catecholamine production and thermogenin expression in rats. *Endocrine regulations*, 50, 137-144.
- VASI, A.-M., POPA, M. I., BUTNARU, M., DODI, G. & VERESTIUC, L. 2014. Chemical functionalization of hyaluronic acid for drug delivery applications. *Materials Science and Engineering: C*, 38, 177-185.
- WANG, L. L., HIGHLEY, C. B., YEH, Y. C., GALARRAGA, J. H., UMAN, S. & BURDICK, J. A. 2018a. Three-dimensional extrusion bioprinting of single- and double-network hydrogels containing dynamic covalent crosslinks. *J Biomed Mater Res A*, 106, 865-875.
- WANG, L. L., HIGHLEY, C. B., YEH, Y. C., GALARRAGA, J. H., UMAN, S. & BURDICK, J. A. 2018b. Three-dimensional extrusion bioprinting of single-and double-network hydrogels containing dynamic covalent crosslinks. *Journal of Biomedical Materials Research Part A*, 106, 865-875.
- WANG, S., CHI, J., JIANG, Z., HU, H., YANG, C., LIU, W. & HAN, B. 2021. A self-healing and injectable hydrogel based on water-soluble chitosan and hyaluronic acid for vitreous substitute. *Carbohydrate Polymers*, 256, 117519.
- WANG, S., PAN, M.-H., HUNG, W.-L., TUNG, Y.-C. & HO, C.-T. 2019. From white to beige adipocytes: therapeutic potential of dietary molecules against obesity and their molecular mechanisms. *Food & function*, 10, 1263-1279.
- WANG, Y., KIM, K.-A., KIM, J.-H. & SUL, H. S. 2006. Pref-1, a preadipocyte secreted factor that inhibits adipogenesis. *The Journal of nutrition*, 136, 2953-2956.
- WEINER, F. R., SHAH, A., SMITH, P. J., RUBIN, C. S. & ZERN, M. A. 1989. Regulation of collagen gene expression in 3T3-L1 cells. Effects of adipocyte differentiation and tumor necrosis factor. *Biochemistry*, 28, 4094-4099.
- WIESMANN, V., FRANZ, D., HELD, C., MÜNZENMAYER, C., PALMISANO, R. & WITTENBERG, T. 2015. Review of free software tools for image analysis of fluorescence cell micrographs. *Journal of microscopy*, 257, 39-53.
- WU, J., BOSTRÖM, P., SPARKS, L. M., YE, L., CHOI, J. H., GIANG, A.-H., KHANDEKAR, M., VIRTANEN, K. A., NUUTILA, P. & SCHAART, G. 2012. Beige adipocytes are a distinct type of thermogenic fat cell in mouse and human. *Cell*, 150, 366-376.
- WU, Z., BUCHER, N. & FARMER, S. R. 1996. Induction of peroxisome proliferator-activated receptor gamma during the conversion of 3T3 fibroblasts into adipocytes is mediated by C/EBPbeta, C/EBPdelta, and glucocorticoids. *Molecular and cellular biology*, 16, 4128-4136.
- YANG, R., LIU, X., REN, Y., XUE, W., LIU, S., WANG, P., ZHAO, M., XU, H. & CHI, B. 2021. Injectable adaptive self-healing hyaluronic acid/poly (γ -glutamic acid) hydrogel for cutaneous wound healing. *Acta Biomaterialia*, 127, 102-115.
- YEO, Y., HIGHLEY, C. B., BELLAS, E., ITO, T., MARINI, R., LANGER, R. & KOHANE, D. S. 2006. In situ cross-linkable hyaluronic acid hydrogels prevent post-operative abdominal adhesions in a rabbit model. *Biomaterials*, 27, 4698-4705.
- YONESHIRO, T., AITA, S., MATSUSHITA, M., KAYAHARA, T., KAMEYA, T., KAWAI, Y., IWANAGA, T. & SAITO, M. 2013. Recruited brown adipose tissue as an antiobesity agent in humans. *The Journal of clinical investigation*, 123, 3404-3408.

- YU, N. Z., HUANG, J. Z., ZHANG, H., WANG, Y., WANG, X. J., ZHAO, R., BAI, M. & LONG, X. 2015. A systemic review of autologous fat grafting survival rate and related severe complications. *Chin Med J (Engl)*, 128, 1245-51.
- ZEBISCH, K., VOIGT, V., WABITSCH, M. & BRANDSCH, M. 2012. Protocol for effective differentiation of 3T3-L1 cells to adipocytes. *Analytical biochemistry*, 425, 88-90.
- ZHANG, Y., PROENCA, R., MAFFEI, M., BARONE, M., LEOPOLD, L. & FRIEDMAN, J. M. 1994. Positional cloning of the mouse obese gene and its human homologue. *Nature*, 372, 425-432.
- ZHU, Y., QI, C., KORENBERG, J. R., CHEN, X.-N., NOYA, D., RAO, M. S. & REDDY, J. K. 1995. Structural organization of mouse peroxisome proliferator-activated receptor gamma (mPPAR gamma) gene: alternative promoter use and different splicing yield two mPPAR gamma isoforms. *Proceedings of the national academy of sciences*, 92, 7921-7925.